

**Ly49 RECEPTORS:  
REQUIREMENTS FOR LIGAND RECOGNITION  
AND STRUCTURAL ASSEMBLY**

by

Carla Maria Craveiro Salvado

A thesis submitted in partial fulfillment of the requirements for the degree of

Doctor of Philosophy

in

Immunology

Department of Medical Microbiology and Immunology  
University of Alberta

©Carla Maria Craveiro Salvado, 2015

## ABSTRACT

Natural killer (NK) cells in the mouse and rat rely on homodimeric Ly49 receptors to detect virally infected or transformed cells. The identification of altered cells requires the engagement of Ly49 receptors with MHC class I molecules. The engagement requires contact at three specific sites located below the floor of the peptide binding groove of MHC class I by three loop regions located within the ligand-interacting domain of Ly49s, the natural killer domain (NKD). Any alteration within either the MHC class I molecule or the Ly49 receptor could inhibit or disrupt the interaction, affecting the recognition of the ligand by the receptor, ultimately reflected in the functions of the NK cell. This relationship has not been as extensively studied in the rat as compared to the mouse. Given the sequence variability between the mouse and rat Ly49 loop regions, the significance of the loops in rat Ly49 receptors should be explored. Utilizing surface plasmon resonance (SPR), I was able to quantify the binding affinity of the rat Ly49i2 receptor for the MHC class I molecule RT1-A1<sup>c</sup>. Furthermore, I also showed that at least two of the three loop regions are required for RT1-A1<sup>c</sup> recognition by the Ly49i2 receptor. While complete binding between RT1-A1<sup>c</sup> and Ly49i2 was lost with mutated NKD L3 loop regions, only partial binding was lost with a mutated L6 loop, implying that the L6 loop may be required for MHC class I recognition, while the L3 loop may be required for MHC specificity. To assess the practical significance of the Ly49 loop regions, a functional assay is required. The RNK-16 rat leukemic cell line is heavily relied upon for NK cell functional studies. Expression of exogenous genes in RNK-16 cells, however, is difficult and extremely time consuming. I outlined a lentivirus-mediated transduction method that will allow RNK-16 cells to be transfected

rapidly resulting in high transfection efficiency rate. The functional output of NK cells is a result of the signaling induced by the engagement of the MHC class I molecule with the Ly49 homodimer receptor. Utilizing biochemical assays, I demonstrate that Ly49 receptors belonging to the same group can associate as heterodimers. The ability of these receptors to form heterodimers may allow for manipulation of the receptors, altering the function of the NK cell.

## TABLE OF CONTENTS

<b>CHAPTER</b>	<b>PAGE</b>
<b>I. INTRODUCTION</b>	
1.1 General overview: Natural killer cells in the context of innate immunity.....	1
1.1.1 Brief overview of natural killer cell development and maturation.....	1
1.1.2 Functions of NK cells.....	2
1.2 Major histocompatibility complex molecules.....	4
1.3 Natural killer cell surface receptors.....	6
1.3.1 NK cell activation.....	6
1.3.2 NK cell inhibition.....	7
1.3.3 The leukocyte receptor complex.....	8
1.3.4 The natural killer cell complex.....	10
1.3.4.1 The Ly49 receptor family in the mouse and rat.....	14
1.3.4.1.1 The structure of the Ly49 receptors.....	14
1.3.4.1.2 The Ly49 receptor repertoire.....	17
1.4 Ly49 receptor engagement with MHC class I molecules.....	18
1.4.1 Self tolerance and NK cell education.....	19
1.4.2 Ly49 receptor and ligand binding specificity.....	20
1.5 Background and rationale.....	21
<b>II. MATERIALS AND METHODS</b>	
2.1 Cell lines.....	31
2.2 Antibodies.....	31
2.3 Cloning of Ly49 receptors.....	32
2.4 Mutagenesis and gene synthesis.....	33
2.5 Lentivirus packaging and virus titering.....	33
2.6 RNK-16 transduction.....	35
2.7 Flow cytometry.....	35
2.8 Puromycin titration.....	36

2.9 Protein expression, purification, folding, and analysis.....	36
2.10 Surface plasmon resonance.....	37
2.11 Transfection of COS-7 cells.....	38
2.12 Immunoprecipitation and Western blotting.....	38
2.13 Sequence alignments.....	39
2.14 Protein structure analysis.....	39

### **III. STRUCTURAL SPECIFICITY DETERMINANTS OF THE Ly49i2 RECEPTOR FOR ITS COGNATE LIGAND RT1-A1<sup>c</sup>**

3.1 Introduction.....	40
3.2 Results.....	41
3.2.1 Determining the binding interaction of the rat inhibitory receptor Ly49i2 with its cognate ligand, the MHC class I molecule RT1-A1 <sup>c</sup> .....	41
3.2.2 The L6 loop in Ly49i2 may be required for RT1-A1 <sup>c</sup> recognition.....	44
3.2.3 A requirement for the L5 loop of Ly49i2 for RT1-A1 <sup>c</sup> recognition is inconclusive.....	47
3.2.4 The Ly49i2 L3 loop is critical for RT1-A1 <sup>c</sup> recognition.....	50
3.3 Discussion.....	57

### **IV. LENTIVIRAL-MEDIATED EXOGENOUS GENE EXPRESSION IN RNK-16 CELLS**

4.1 Introduction.....	90
4.2 Results.....	92
4.2.1 RNK-16 cells cannot be transduced to express the transgene Ly49i2 under the control of the universal CMV promoter.....	92
4.2.2 Wildtype Ly49i2 is expressed on the surface of RNK-16 cells using a lentivirus transduction system with an elongation factor-1 $\alpha$ promoter for transgene expression....	98
4.3 Discussion.....	101

## **V. DIMERIZATION OF Ly49 RECEPTORS**

<b>5.1</b> Introduction.....	110
<b>5.2</b> Results.....	111
<b>5.2.1</b> The activating Ly49M, Ly49W2, and Ly49P1 receptors associate together, and may form heterodimers.....	111
<b>5.2.2</b> The activating Ly49M and Ly49W2 receptors associate individually with the inhibitory receptor Ly49G2, possibly forming heterodimers.....	117
<b>5.3</b> Discussion.....	123

## **VI. DISCUSSION AND CONCLUSION**

<b>6.1</b> Overview of thesis.....	141
<b>6.2</b> Analysis of thesis studies.....	141
<b>6.2.1</b> Structural specificity determinants of the Ly49i2 receptor for its cognate ligand RT1-A1 <sup>c</sup> .....	142
Summary of contributions.....	142
Discussion and future directions.....	146
<b>6.2.2</b> Lentiviral-mediated exogenous gene expression in RNK-16 cells.....	148
Summary of contributions.....	148
Discussion and future directions.....	150
<b>6.2.3</b> Dimerization of Ly49 receptors.....	151
Summary of contributions.....	151
Discussion and future directions.....	153
<b>6.3</b> Concluding remarks.....	157

<b>BIBLIOGRAPHY.....</b>	<b>160</b>
--------------------------	------------

## LIST OF FIGURES

<b>FIGURE</b>	<b>DESCRIPTION</b>	<b>PAGE</b>
<b>1-1</b>	The genetic organization of the MHC complex in the human (HLA), mouse (H2), and rat (RT1) and the structure of MHC class I molecules.....	25
<b>1-2</b>	The Leukocyte Receptor Complex (LRC).....	26
<b>1-3</b>	The Natural Killer Complex (NKC).....	27
<b>1-4</b>	Inhibitory and activating Ly49 receptors.....	28
<b>1-5</b>	Mouse and rat Ly49 gene alignments of MHC class I interacting regions.....	29
<b>1-6</b>	Co-crystal structures of Ly49A-H-2D <sup>d</sup> and Ly49C-H-2K <sup>b</sup> .....	30
<b>3-1</b>	The mouse Ly49 NKD homodimer.....	64
<b>3-2</b>	The rat MHC class I molecule RT1-A1 <sup>c</sup> .....	65
<b>3-3</b>	Wildtype Ly49i2 receptor and RT1-A1 <sup>c</sup> refolds.....	66
<b>3-4</b>	Ly49i2 <sub>ED</sub> binding interactions with STOK2 Ab and RT1-A1 <sup>c</sup> .....	67
<b>3-5</b>	L6 loop chimeric receptor, Ly49i2.L6.NCDQ <sub>ED</sub> , refold.....	68
<b>3-6</b>	L6 loop chimeric receptor, Ly49i2.L6.NCDQ <sub>ED</sub> , binding interactions with the STOK2 Ab and RT1-A1 <sup>c</sup> .....	69
<b>3-7</b>	L6 loop chimeric receptor, Ly49i2.L6.ACGA <sub>ED</sub> , refold.....	70
<b>3-8</b>	L6 loop chimeric receptor, Ly49i2.L6.ACGA <sub>ED</sub> , binding interactions with the STOK2 Ab and RT1-A1 <sup>c</sup> .....	71
<b>3-9</b>	L5 loop chimeric receptor, Ly49i2.S241A <sub>ED</sub> , refold.....	72
<b>3-10</b>	L5 loop chimeric receptor, Ly49i2.S241A <sub>ED</sub> , binding interactions with the STOK2 Ab and RT1-A1 <sup>c</sup> .....	73
<b>3-11</b>	L5 loop chimeric receptor, Ly49i2.T243A <sub>ED</sub> , refold.....	74
<b>3-12</b>	L5 loop chimeric receptor, Ly49i2.T243A <sub>ED</sub> , binding interactions with the STOK2 Ab and RT1-A1 <sup>c</sup> .....	75
<b>3-13</b>	L5 loop chimeric receptor, Ly49i2.S241A.T243A <sub>ED</sub> , refold.....	76
<b>3-14</b>	L5 loop chimeric receptor, Ly49i2.S241A.T243A <sub>ED</sub> , binding interactions with the STOK2 Ab and RT1-A1 <sup>c</sup> .....	77
<b>3-15</b>	L3 loop chimeric receptor, Ly49i2.L3.s3 <sub>ED</sub> , refold.....	78

<b>3-16</b> L3 loop chimeric receptor, Ly49i2.L3.s3 <sub>ED</sub> , binding interactions with the STOK2 Ab and RT1-A1 <sup>c</sup> .....	79
<b>3-17</b> L3 loop chimeric receptor, Ly49i2.L3.s5 <sub>ED</sub> , refold.....	80
<b>3-18</b> L3 loop chimeric receptor, Ly49i2.L3.s5 <sub>ED</sub> , binding interactions with the STOK2 Ab and RT1-A1 <sup>c</sup> .....	81
<b>3-19</b> L3 loop chimeric receptor, Ly49i2.L3.i5 <sub>ED</sub> , refold.....	82
<b>3-20</b> L3 loop chimeric receptor, Ly49i2.L3.i5 <sub>ED</sub> , binding interactions with the STOK2 Ab and RT1-A1 <sup>c</sup> .....	83
<b>3-21</b> L3 loop chimeric receptor, Ly49i5.L3.i2 <sub>ED</sub> , refold.....	84
<b>3-22</b> L3 loop chimeric receptor, Ly49i5.L3.i2 <sub>ED</sub> , binding interaction with RT1-A1 <sup>c</sup> .....	85
<b>3-23</b> The putative L6 loop structure of the Ly49i2 receptor.....	86
<b>3-24</b> The putative L5 loop structure of the Ly49i2 receptor.....	87
<b>3-25</b> The putative L3 loop structure of the Ly49i2 receptor.....	88
<b>4-1</b> The Gateway® recombinational cloning reaction.....	104
<b>4-2</b> Transfection of COS-7 cells with wildtype Ly49i2.....	105
<b>4-3</b> Transduction of HT1080 cells for lentivirus titering.....	106
<b>4-4</b> Transduction of RNK-16 cells with pLenti plasmids for Ly49i2 cell surface expression.....	107
<b>4-5</b> Transduction of RNK-16 cells with pLEX307 lentivirus plasmid for Ly49i2 cell surface expression.....	108
<b>4-6</b> Generation of stable RNK-16 cell transductants expressing Ly49i2.....	109
<b>5-1</b> Protein sequence alignment for the activating NOD mouse receptors Ly49M and Ly49W2.....	127
<b>5-2</b> Protein sequence alignment for the activating NOD mouse receptors Ly49M and Ly49P1.....	128
<b>5-3</b> Protein sequence alignment for the activating NOD mouse receptors Ly49W2 and Ly49P1.....	129
<b>5-4</b> Transfection of COS-7 cells with activating Ly49 receptors of the NOD mouse....	130

<b>5-5</b> The HA-tagged and FLAG-tagged receptors Ly49M, Ly49W2, and Ly49P1 associate, and may form homodimers.....	131
<b>5-6</b> Transfection of COS-7 cells with activating Ly49 receptors of the NOD mouse....	132
<b>5-7 A</b> The activating NOD mouse receptors Ly49M, Ly49W2, and Ly49P1 associate together, possibly as heterodimers.....	133
<b>5-7 B</b> The activating NOD mouse receptors Ly49M, Ly49W2, and Ly49P1 associate together, possibly as heterodimers.....	134
<b>5-8</b> Protein sequence alignment for the activating NOD mouse receptor Ly49W2 and inhibitory BALB/c receptor Ly49G2.....	135
<b>5-9</b> Protein sequence alignment for the activating NOD mouse receptor Ly49M and inhibitory BALB/c receptor Ly49G2.....	136
<b>5-10</b> Transfection of COS-7 cells with activating and inhibitory mouse receptors.....	137
<b>5-11</b> The inhibitory Ly49G2.HA and Ly49G2.FLAG receptors associate, possibly forming homodimers.....	138
<b>5-12</b> The activating NOD mouse receptors Ly49M and Ly49W2 associate with the inhibitory BALB/c mouse receptor Ly49G2.....	139
<b>5-13</b> Protein sequence alignment of the stalk region and the natural killer domain (NKD) for the activating inhibitory Ly49 receptors.....	140
<b>6-1</b> Lentiviral-mediated exogenous gene expression in RNK-16 cells.....	158
<b>6-2</b> The rat MHC class I molecule RT1-A1 <sup>c</sup> and the putative inhibitory rat Ly49i2 receptor.....	159

**LIST OF TABLES**

<b>TABLE</b>	<b>DESCRIPTION</b>	<b>PAGE</b>
<b>3-1</b>	Binding affinities, $K_D$ ( $\mu\text{M}$ ) between various mouse (M) or human (H) NK cell inhibitory (I) or activating (A) receptors and their ligands.....	89

## **CHAPTER I: INTRODUCTION**

### **1.1 GENERAL OVERVIEW: NATURAL KILLER CELLS IN THE CONTEXT OF INNATE IMMUNITY**

Natural killer (NK) cells are a vital component of the innate immune system. These large granular lymphocytes were first described in the mouse for their innate cytotoxic ability to eliminate tumor cells *in vitro* without priming [1, 2]. Natural killer cells lack the ability to somatically rearrange their cell surface receptor genes, hence their inability to generate antigen specific responses [3]. Therefore, NK cells are effector immune surveyors that broadly target virally infected or transformed target cells [4].

In agreement with their role as innate sentinels, NK cells are found widely distributed. In the mouse and rat, 5 – 10% of circulating lymphocytes are NK cells, where a greater percentage is observed in non-lymphoid tissues such as peripheral blood, liver, and lungs, as compared to their presence in lymphoid tissues such as the lymph nodes and the spleen; the latter in which, the greatest number of NK cells are found [5, 6]. In humans, NK cells represent approximately 5 – 20% of all circulating lymphocytes in peripheral blood, and are also found in the same tissues as in rodents [7].

Typically, cell-surface markers are used to identify NK cells via flow cytometry. Mouse NK cells, depending on the strain, are defined as NK1.1<sup>+</sup>CD3<sup>-</sup> or DX5<sup>+</sup>CD3<sup>-</sup>, whereas human NK cells are identified as CD56<sup>+</sup>CD3<sup>-</sup> [8]. Rat NK cells have an NKR-P1<sup>+</sup>CD3<sup>-</sup> phenotype [9]. Additionally, all mammalian NK cells are further characterized as NKp46<sup>+</sup> [10].

#### **1.1.1 *Brief Overview of Natural Killer Cell Development & Maturation***

Both human and rodent NK cell development and maturation originate from a common lymphoid progenitor (CLP) from bone marrow (BM) derived hematopoietic stem cells (HSCs) [11]. Natural killer cell differentiation downstream of the CLP requires the presentation of interleukin-15 (IL-15) *in trans* to the  $\beta$  chain (CD122) and common  $\gamma$  chain (CD132) subunits of the IL-15 receptor (IL-15R) expressed by NK cell

precursors during intermediate stages of development [12, 13]. The late stages of NK cell development, which result in a mature NK cell, involve the gain of phenotypic and functional characteristics such as the gradual acquisition of various functional cell surface receptors, including the killer cell immunoglobulin-like receptors (KIRs) in humans, and the Ly49 receptors in both the mouse and the rat [14-16]. Survival and homeostasis of the peripheral, mature NK cell is dependent on IL-15 [17, 18].

### ***1.1.2 Functions of Natural Killer Cells***

Natural killer cells perform several crucial functions. Traditionally, these lymphocytes are best known as cytotoxic effectors that, upon engagement and recognition of a virus-infected or cancerous cell, can eliminate the target cell by inducing cell death through the release of the effector molecules, perforin and granzymes [19]. The NK cell can also evoke apoptosis through the engagement of its death ligands, such as Fas ligand (FasL) or the tumor necrosis factor-related apoptosis-inducing ligand (TRAIL), with their respective target cell receptors [20-24]. Furthermore, NK cells have also been shown to eliminate their targets via antibody-dependent cellular cytotoxicity (ADCC). The NK cell surface Fc receptor, Fc $\gamma$ RIII (CD16), can detect antibody-bound target cells through the interaction of CD16 with the Fc region of the antibody [8]. Upon engagement, CD16 activates the NK cell to release effector molecules resulting in target cell death [3].

Apart from the elimination of target cells, NK cells are also tasked with another crucial effector function: the secretion of immunoregulatory cytokines, both proinflammatory and immunosuppressive. NK cells are a major primary source of interferon- $\gamma$  (IFN- $\gamma$ ), a cytokine required for immunity against viral and intracellular bacterial infections, as well as for tumor control [25]. Another proinflammatory cytokine secreted by these cells is tumor necrosis factor-alpha (TNF- $\alpha$ ) [3]. NK cells also produce and secrete anti-inflammatory cytokines, such as IL-10 and IL-13, as well as various growth factors (including granulocyte macrophage colony-stimulating factor (GM-CSF), granulocyte colony-stimulating factor (G-CSF), IL-3, and IL-5), and several chemokines (for example: monocyte chemotactic protein - 1 (MCP-1), macrophage

inflammatory protein - alpha (MIP- $\alpha$ ), MIP- $\beta$ , RANTES (regulated on activation, normal T cell expressed and secreted), lymphotactin (XCL1), and IL-8) [3, 26, 27].

In addition to their contribution in controlling disease, NK cells can also play an important role in transplantation. Specifically, NK cells mediate a unique phenomenon, *hybrid resistance*, first described by Cudkowicz *et al.* [28-31]. Hybrid resistance explains the rejection of homologous parental bone marrow cell (BMC) transplants, from either parent, into irradiated heterozygous F<sub>1</sub> hybrid mice generated from two inbred parental mouse strains [32]. Furthermore, NK cells have also been implicated in the rejection of solid organ transplants in both mice and humans [33-36].

Several reports in recent years have suggested that NK cells, or at least a subset, may require priming for full functionality; a concept contradictory to that which is thought to distinguish these innate cells from their adaptive immunity counterpart, T cells. In human NK cells, priming the cell's effector functions via TLR-2 (toll-like receptor 2) was required for effective control of a human cytomegalovirus (HCMV) infection [37]. A similar phenomenon was observed *in vivo* in a mouse model, where the direct recognition of vaccinia virus by TLR-2 expressed on NK cells led to effective NK cell activation and ultimately control of the virus infection [38]. The specific NK cell subsets that require priming via TLRs, and, if this requirement is limited to certain virus infections only, remains to be determined.

In a further challenge of the conventional view of NKs as innate effectors, various recent studies strongly suggest that some NK cell subsets exhibit a “memory-like” function, similar to its adaptive immunity counterpart, the CD8<sup>+</sup> cytotoxic T cell. This phenomenon was first observed in C57BL/6 mice infected with murine cytomegalovirus (MCMV), resulting in the antigen specific clonal expansion of MCMV receptor-specific NK cells [39, 40]. Additionally, another group showed that consistent with memory immune responses, “memory” NK cells were much more efficient and functionally more adept in mediating host protection from a secondary MCMV infection as compared to the response of naïve NK cells [41]. This notion has also been observed by the activation of NK cells by cytokines resulting in long-lived NK cell populations [42]. Strong supporting evidence for NK cell-mediated memory responses, however, was first provided by studies in *Rag2*<sup>-/-</sup> mice with a model of hapten-induced contact

hypersensitivity [43]. Interestingly, this report also implies that only liver-restricted CXCR6<sup>+</sup> NK cells exhibit the memory phenotype. Since these initial studies, the field of memory NK cells has expanded significantly [44, 45]. Nonetheless, several critical questions, such as the understanding of the requirements for the generation of antigen-specific memory NK cells, remain unknown.

## 1.2 MAJOR HISTOCOMPATIBILITY COMPLEX MOLECULES

MHC molecules are type I transmembrane glycoproteins expressed on the surface of all nucleated cells and are a vital component of the jawed vertebrate immune system [46]. The mammalian MHC is divided into three gene regions, class I, class II, and class III. All three classes are encoded in humans on chromosome 6, referred to as the human leukocyte antigen (*HLA*) genes; the MHC H-2 complex in mice is encoded on chromosome 17; whereas rats encode their MHC RT1 complex on chromosome 20 (Figure 1-1 A) [47].

MHC class I regions contain the classical class I (class Ia) and nonclassical class I (class Ib) molecules. Class Ia proteins are highly polymorphic and well characterized as antigen presentation molecules to CD8<sup>+</sup> T cells, as well as ligands for several NK cell surface receptors (i.e. KIRs in humans and Ly49s in rodents) [48, 49]. Crystal structures of class Ia molecules display a conserved heterotrimeric architecture amongst different species, including humans, mice, and rats (Figure 1-1 B). MHC class Ia is composed of a heavy chain non-covalently associated with the small globular beta-2-microglobulin molecule ( $\beta_2m$ ), and that association is a requirement for proper folding of the MHC as well as cell surface expression. Furthermore, the heavy chain is composed of three domains. The  $\alpha 1$  and  $\alpha 2$  domains, each consisting of four anti-parallel  $\beta$ -strands along with a long  $\alpha$ -helix, associate to form a  $\beta$ -sheet platform surrounded by parallel  $\alpha$ -helices, that result in a groove, allowing for binding of an 8 – 10 amino acid peptide. The  $\alpha 3$  domain is responsible for  $\beta_2m$  contact and is located under the peptide-binding groove and near the plasma membrane [50-53]. Most MHC class I peptides are derived from “self” polypeptides, molecules synthesized in the host cell, which are then digested by proteasomes and transported by the transporter associated with antigen processing (TAP)

into the endoplasmic reticulum (ER), where they are loaded into the peptide-binding groove of MHC class I molecules [54, 55]. These peptide-loaded MHC complexes are then transported to the cell surface for antigen presentation to CD8<sup>+</sup> T cells, or for “self” detection by NK cells [54, 55].

Structurally, MHC class Ib molecules are similar to class Ia, they also have a heavy chain that may or may not associate with  $\beta_2m$ , depending on the molecule; furthermore, some class Ib molecules bind peptides [56]. Unlike class Ia, MHC class Ib molecules are oligomeric and include both MHC-encoded and non-MHC encoded proteins [57]. These proteins display important immunoregulatory roles, including involvement in immunity to bacterial infections. In humans, for example, CD1 is a class Ib molecule that presents bacterial lipid antigens resulting in T cell activation [58-61]. Rat MHC class Ib molecules have also been shown to provide resistance against bacterial infections through their engagement with immune receptors [62-65]. On a different note, the mouse class Ib molecule, H2-M3, has recently been implicated in mediating NK cell licensing through its interaction with NK cell receptors that traditionally recognize class Ia molecules [66].

MHC class II molecules vary structurally and functionally as compared to class I molecules. MHC class II are also expressed at the cell surface, but these heterotrimeric complexes consist of two transmembrane glycoprotein chains,  $\alpha$  and  $\beta$ , that form a binding platform for the peptide of endogenous or exogenous origin of 11–20 amino acids, eventually presented to CD4<sup>+</sup> T cells [67]. Furthermore, MHC class II expression is normally restricted to a subset of antigen presenting cells such as B cells, thymic epithelium, DCs, and macrophages [67].

The last region, MHC class III is different from the other MHC loci as it does not encode genes involved in antigen processing and presentation. The MHC class III gene complex encodes molecules of the innate immune system, such as proteins of the complement system [68, 69].

Although all three MHC classes are crucial mediators of immunity, only the MHC class I molecules serve as ligands to NK cell receptors, such as KIRs in humans and Ly49s in rodents.

### **1.3 NATURAL KILLER CELL SURFACE RECEPTORS**

The functions of NK cells are dependent on the signaling cascade induced by their cell surface receptors. NK cells express a multitude of germline-encoded receptors that can either inhibit or induce NK cell activation, depending on the outcome of the engagement of the NK cell receptor with its respective ligand. These innate cells possess a vast array of cell surface molecules that contribute to the varying NK cell functions. Although NK cell activation can be mediated via cytokines, such as IL-2, the focus of this introduction will be on cell surface receptors that engage non-cytokine ligands on other cells that enhance or inhibit NK cell activation, respectively.

#### **1.3.1 *NK Cell Activation***

Activating receptors at the surface of NK cells can activate them by inducing a signaling cascade in the cells, resulting in elimination of target cells. The first described NK cell surface activation molecules were the Fc receptors Fc $\gamma$ RIII (CD16) [70]. CD16, expressed in most rodent and human NK cells, mediates ADCC by associating non-covalently to the immunoreceptor tyrosine-based activation motif (ITAM)-bearing CD3 $\zeta$  and FcR $\gamma$  signal transduction polypeptides [3]. Upon cross-linking through the bound immunoglobulins, ADCC is induced.

Similar to CD16, activating NK cell surface receptor cytoplasmic tails lack the ability to signal intrinsically. The activating NK cell surface receptors associate non-covalently via their positively charged transmembrane region with adaptor molecules such as DNAX activation protein of 10 or 12 kDa (DAP10 or DAP12, respectively) [71]. These adaptor proteins, as well as CD3 $\zeta$  and FcR $\gamma$ , contain an ITAM motif in their cytoplasmic domains that allows for the activation of the NK cell [71]. The aforementioned adaptor molecules, with the exception of DAP10, contain tyrosines in an ITAM with the consensus sequence YxxL<sub>X(7-12)</sub>YxxL, which, upon receptor-ligand binding become phosphorylated by Src family protein tyrosine kinases [72, 73]. The phosphorylation of both ITAM tyrosines on the adaptor molecule leads to the recruitment of Syk family protein tyrosine kinases, such as Syk, allowing for its SH2 domains to dock on the

phosphorylated tyrosines, inducing cellular activation via a downstream signaling cascade [72, 73].

Alternatively, DAP10, an adaptor protein associated with some NK cell activating receptors such as NKG2D, engages with Grb2 or p85 upon phosphorylation of its tyrosine residue contained in a YxxM motif, allowing for subsequent signaling through phosphatidylinositol-3 kinase (PI3K) [71, 74, 75]. Receptor association with DAP12, but not DAP10, results in cytotoxicity of target cells as well as cytokine production by the NK cell [76, 77].

### ***1.3.2 NK Cell Inhibition***

The array of NK cell surface receptors includes those functionally categorized as inhibitory receptors, capable of overriding, thus blocking activation signals. Inhibitory receptors contain an immunoreceptor tyrosine-based inhibitory motif (ITIM) of consensus sequence (S/I/V/L)xYxx(I/V/L) in their cytoplasmic domain, capable of inducing an intracellular signaling cascade upon phosphorylation of the tyrosine by Src family kinases [72]. Once the ITIM tyrosine residue is phosphorylated as a result of receptor-ligand binding, recruitment of the phosphotyrosine phosphatases SHP-1 and/or SHP-2, or the inositolphosphatase SHIP occurs, resulting in intrinsic signaling cascades that inhibit NK cell activity [78-81].

NK cells are normally held in check by engagement of their inhibitory receptors; however, at any time, this state can be overridden by receptor-ligand engagement at the cell surface, or by cytokine stimulation. The signaling pathways activated by the multitude of cell surface receptors ultimately dictate the outcome of the NK cell, all of which are dependent upon the association of the ligand with the respective NK cell receptor. Due to the focus of my thesis project, the remainder of this introduction will focus on MHC class I recognizing NK cell receptors. Two NK gene complexes encode the inhibitory and activating NK cell receptors of interest: the leukocyte receptor complex (LRC) and the natural killer complex (NKC).

### 1.3.3 *The Leukocyte Receptor Complex*

The leukocyte receptor complex (LRC) encodes NK cell receptors of the immunoglobulin-domain superfamily. The LRC is positioned on human chromosome 19, mouse chromosome 7, and rat chromosome 1 (Figure 1-2) [82-84]. Although the LRC has expanded and diversified much more in some species, such as the primates, there are several conserved receptors amongst humans, mice, and rats.

DAP10 and DAP12, are adaptor proteins (previously described) that engage with NK cell activators, allowing them to trigger cell activation upon ligand binding. Both of these conserved proteins are encoded in the LRC of all three species [85, 86].

LAIR-1, a member of the leukocyte associated Ig-like receptors (LAIRs), is an inhibitory receptor expressed on many immune cells including NK cells in all the aforementioned types of organisms, where human LAIR-1 shares 40% sequence homology with mouse LAIR-1 and 71% with rat LAIR-1 [87-89]. This inhibitory receptor binds collagens as a ligand, implicating a regulatory role for LAIR-1 in cell-to-cell interaction and adhesion [90].

Another example of commonly shared LRC-encoded proteins amongst humans, mice and rats is the highly NK-specific activating receptor NKp46, a member of the natural cytotoxicity receptors (NCRs), a subgroup of LRC transcripts [91-93]. NKp46 is almost exclusively expressed in NK cells; however, this receptor is also found on a very small subset of T-cells, as well as on a mucosal population of NKp46<sup>+</sup> innate lymphoid cells that produce IL-22 and express the transcription factor retinoid-related orphan receptor (ROR)- $\gamma$ t [94]. NKp46 relies on its association with the adaptor molecules CD3 $\zeta$  and Fc $\gamma$ RI for ITAM-dependent signaling upon ligand recognition for NK cell activation [95]. NKp46 plays a role in tumor surveillance *in vivo*, as well as by mediating target cell death of various transformed cells, by recognizing and directly binding to cellular ligands expressed on a wide variety of tumor cell lines [96, 97]. Furthermore, as the main activator for NK cells, NKp46 is also implicated in the elimination of virally infected cells. *In vitro* studies show that influenza virus infections, as well as CMV infections are controlled and reduced by NKp46 [98, 99]. Interestingly, NKp46 has also been implicated in the progression of the autoimmune disease type 1 diabetes in both

humans and mice through its engagement with unknown ligands on pancreatic beta cells [100].

Regardless of the overall synteny in the LRC gene organization of humans, mice and rats, some LRC NK cell receptor genes, through the course of evolution, diverged amongst species. Leukocyte Ig-like receptors (LILRs) in humans and paired Ig-like receptors (PIRs) in mice and rats likely diverged from a common ancestor, due to their sequence homology [101, 102]. Of interest is the inhibitory human receptor LILRB1, the only member of the LILBs to be expressed on NK cells. This receptor, also referred to as ILT2 or LIR-1, broadly recognizes various MHC class I, HLA alleles [103, 104]. LILRB1 also binds the HCMV MHC class I homologue UL18 [105]. PIRs, orthologues to LILRs, include activating receptor, PIR-A, and inhibitory receptor, PIR-B. In mice, PIRs are expressed on B cells and myeloid lineage cells simultaneously as pairs, with no mouse NK cell-expressed PIR receptor yet identified [106]. Mouse PIRs include at least six PIR-A transcripts and only one PIR-B, where the inhibitory receptor has been shown to recognize MHC class I molecules [107]. Interestingly, and regardless of the notable conservation of structural features for mouse and rat PIRs, as well as their extremely close evolutionary relationship, rat PIR-A and PIR-B expression does not display a paired expression pattern as seen in mice; although rat PIR-A is detected on B cells, expression of PIR-B is observed on NK cells [102].

Within the LRC, KIRs make up the largest and most expanded group of NK cell receptors. Furthermore, KIRs are the predominant set of receptors that recognize MHC class I ligands in humans, as well as other primates [108]. Human chromosome 19 encodes up to fourteen polymorphic genes (including two pseudogenes) belonging to the multigene KIR receptor family, expressed as either an inhibitory or activating molecule [101]. KIRs are identified as having either two or three C2-type Ig-like domains in their extracellular region, designated KIR2D or KIR3D, respectively [108]. Inhibitory receptors typically have a longer cytoplasmic tail as compared to activating receptors which typically have shorter cytoplasmic tails, thus *L* is used for identifying long cytoplasmic domains versus *S* for shorter ones [108]. KIR2DL4 is an exception to the latter designation protocol; this receptor is the only activating receptor with a long cytoplasmic region, however it still requires association with an adaptor molecule for

functional output, as is with all other activators [108].

The extensive KIR polymorphism results from mammalian *KIR* genes evolving from a single ancestor through duplication and replication events, perhaps due to evolutionary pressure from the also highly polymorphic MHC class I ligands [109-111]. In rodents, however, *KIRs* have not evolved to be as significant despite the one *KIR* gene located on the rat LRC and two *KIR* genes on the mouse X chromosome, all three of which are non-functional [112, 113]. NK cell cytotoxicity is not regulated by KIRs in rodents; mouse and rat NK cells, therefore, bind with MHC class I ligands on other cells via Ly49 receptors, a functionally analogous, yet structurally different group of proteins than KIRs. Interestingly, the natural killer gene complex (NKC), not the LRC, encodes the rodent Ly49 genes.

#### **1.3.4 The Natural Killer Complex**

Receptors of the natural killer gene complex (NKC) share structural similarities. NKC-encoded genes are members of the C-type lectin receptor superfamily, expressed as type II transmembrane, disulfide linked glycoprotein dimers on the surface of NK cells [114]. The NKC shares several similarities to the LRC. Firstly, NK cell receptors are also located on different chromosomes, depending on the species; the NKC is located on human chromosome 12, mouse chromosome 6, and rat chromosome 4 (Figure 1-3) [115-117]. Secondly, these receptors also exist as inhibitory and activating pairs. Thirdly, The NKC of humans, mice, and rats, although located on different chromosomes, also encodes several receptors common amongst the mentioned species.

The NKR-P1 family of receptors, encoded by the *Klrbl/KLRB1* genes in humans, mice, and rats, was one of the first to be discovered, with the first NKC gene identified being rat *Nkrp1* (also referred to as *Klrbl*) [118, 119]. Although their function is not yet fully understood, this group of receptors recognizes other C-type lectin-related proteins (Clr) as their ligand(s); moreover, the *Clec2/CLEC2* encoded Clr genes are also located in the NKC [120]. In both mice and rats, NKR-P1 receptors are mostly detected on NK cells, with a few receptors identified on natural killer T (NKT) cells [118, 121]. In humans, the inhibitory homolog NKR-P1A (CD161) receptor to the mouse and rat

inhibitory receptors NKR-P1B, is found on NK cell subsets and NKT cells, as well as various T cell subsets, displaying a higher expression in memory T cells [122-126]. In mice, NK1.1 has been identified as an NKR-P1 receptor epitope [127]. Antibody binding to NK1.1 was shown to induce NK cell activation, and the NK1.1 epitope is expressed on NK cells across several mouse strains and thus has become a common marker for NK cell identification via detection by the monoclonal antibody (mAb) PK136 [128-131]. In the rat, mAbs 3.2.3 and 10/78 are used to distinguish rat NK cells (in most strains) via the detection of NKR-P1 [132].

Another conserved molecule amongst mice, rats, and humans is CD69 [133-136]. Following cellular activation, CD69 is expressed on various cell types such as T cells and NK cells, implicating its vital role in killer cell-mediated cytotoxicity and allowing it to be used as an activation marker during functional killer cell studies [137].

*Klrc/KLRC* and *Klr1/KLRD1* gene orthologs, expressed as NKG2 proteins and CD94, respectively, are also found amongst the human, mouse, and rat NKC [139]. NKG2 and CD94 are disulfide-linked subunits, forming a heterodimer at the cell surface for functional output [139]. Human, mouse, and rat encode the ITIM-bearing inhibitory receptor NKG2A, as well as the activators NKG2C and NKG2E, both of which associate with DAP12 for functional activity [140-142]. In addition, alternative splicing results in the receptors NKG2B, NKG2F, and NKG2H, where NKG2B is a splice variant of NKG2A and NKG2H of NKG2E [139]. NKG2F (*KLRC4*), encoded only in humans, is unique in this family. This receptor contains a charged transmembrane region (common amongst activators) and also encodes an ITIM-like motif; however, due to the lack of the ligand interacting C-type lectin-like domain (CTLD), it was not expected to be functional [143]. Interestingly, however, NKG2F expression was detected intracellularly on NK cells, as well as its association with DAP12 [144]. Furthermore, expression of this receptor can be up-regulated upon IL-2 and IL-15 stimulation, yet the function of NKG2F remains unknown [145]. The heterodimeric members of this protein family (NKG2A/CD94, NKG2C/CD94, and NKG2E/CD94) all recognize non-classical MHC class I ligands, specifically HLA-E, Qa-1<sup>b</sup>, and RT-BM1 (or RT1-S3) in humans, mice, and rats, respectively [146-150]. Non-classical MHC class I proteins HLA-E and Qa-1<sup>b</sup> of humans and mice, respectively, present peptides derived from the signal/leader

peptides of classical MHC class I, allowing NK cells to indirectly monitor the expression of the latter proteins, typically down-regulated during viral infections, through the interaction of the NKG2/CD94 heterodimers [114].

The NKG2D receptor, another conserved NKC protein, is an activating receptor and is expressed on all NK cells and encoded by the *KLRK1/Klrk1* genes in humans and mice, respectively, and by the orthologous *Nkrp2* gene in rats [140, 151-153]. Humans also express this receptor on all CD8<sup>+</sup> T cells, whereas mice only express it on activated CD8<sup>+</sup> T cells, as well as activated macrophages [154]. In contrast, the rat NKG2D has been detected on CD4<sup>+</sup> T cells, CD8<sup>+</sup> T cells, and dendritic cells (DCs) [152, 155]. Although similar to the NKG2 family proteins in terminology, NKG2D varies significantly in sequence homology; furthermore, it differs in structure and ligands for functional activation. Activating NKG2D receptors are expressed at the cell surface as homodimers and engage with DAP10 or DAP12, depending on the cell type and NKG2D isoform, for activation signaling [154]. NKG2D-induced NK cell activation requires receptor ligand interaction. Normal, healthy cells do not commonly express NKG2D ligands; however, an up-regulation is detected in malignant tissues, as well as during cellular stress and viral infections [154, 156]. These ligands are structurally homologous to MHC class I molecules, yet they do not serve as T cell antigen presentation vehicles [154]. Intriguingly, the human, mouse, and rat ligands for NKG2D are not orthologs of each other. In humans, the stress-induced ligands include MHC class I-related chains-related proteins A and B (MICA and MICB, respectively), as well as retinoic acid early transcripts-1 (RAET1), also referred to as UL-16 binding proteins (ULBPs) [157-159]. In the mouse, despite the lack of MIC homologs, five isoforms of retinoic acid early inducible gene 1 (RAE-1), three variants of minor histocompatibility protein, H-60, and the murine UL-16 binding protein-like transcript 1 (MULT1) have been identified as NKG2D ligands [153, 160, 161]. The ligands for the rat NKG2D include mouse homologous members of the RAE-1 family of proteins, specifically RAE1L and RAE-1-like transcript (RRLT) [156, 162]. The activator NKG2D expressed on rat DCs, however, recognizes the ligand ischemia-responsive protein 94 (Irp94) for DC-mediated tumor killing [155].

Finally, and of great interest to this body of work, is the NKC encoded Ly49

receptors (Ly49s). MHC class I recognition by rodent NK cells is the main responsibility of the highly polymorphic and multigene Ly49 family, similar to KIRs expressed on human NK cells. Although structurally different, KIRs and Ly49s are functional homologs. Interestingly, these two gene families, albeit from different structural families and encoded on different gene complexes and chromosomes, have several features in common. KIRs and Ly49s, as already mentioned, are the predominant allele specific receptors for recognition of polygenic and polymorphic MHC class I molecules. KIR and Ly49 gene families encode stimulatory and inhibitory receptors, which, upon ligand interaction, rely on similar mechanisms for signal transduction. The remarkable ability of these two gene families to generate similar functional outputs upon engagement with the same (species and allele specific) ligands exemplifies the significant convergent evolutionary path undertaken by KIRs and Ly49s [163, 164]. The human NKC does encode a single Ly49 gene, *Ly49L*, however, it contains a premature stop codon, rendering the putative truncated protein non-functional [165]. The *Ly49L* pseudogene is likely an evolutionary remnant, suggesting that the human *Ly49* gene may have evolved from a Ly49 gene-bearing ancestor, and through evolutionary pressure have lost them allowing for the rise of KIRs in humans [163, 164, 166].

The evolution of both KIR and Ly49 genes is highly similar despite the structural differences. The common ancestor of both primates and rodents probably relied on both sets of receptors for immunity; upon divergence of the two lineages, different NK cell receptors became the major group within each lineage, thus becoming efficient to generate only one type while deleting the other [167]. Both KIRs and Ly49s, as previously mentioned, share common signaling modes, for both their inhibitory and activating receptors, despite the signaling domain of Ly49s located on the amino-terminus, while located at the carboxy-terminus in KIRs [168]. Strikingly, and while occurring independently, the expansion of each receptor family occurred via a series of mutations, deletions, duplications, and recombination events, which also resulted in the formation of activators from the inhibitory receptors [167, 168]. The evolutionary patterns observed for both KIRs and Ly49s further suggest that their evolution, despite having occurred separately, is dependent on their engagement with their ligand, MHC class I molecules [167].

### ***1.3.4.1 The Ly49 Receptor Family in the Mouse and Rat***

In 1989, Ly49 receptors were first identified and described in the mouse as T lymphocyte antigens by two separate groups, and subsequently termed “Ly49” for being a lymphocyte cell-surface molecule [169-172]. Since then, a field of study exploded allowing us to appreciate and further understand Ly49s and their role in NK cell function in the context of innate immunity.

The cell surface expression of Ly49s, specifically inhibitory receptors, has been detected on several immune cells, including CD3<sup>+</sup> cells, NKT cells, intestinal intraepithelial lymphocytes, and several T cell subsets [173-179]. NK cells, however, display the most abundant receptor expression levels, diversity in receptor allele products expressed on the cell surface amongst mouse and rat species, as well as best studied functional outputs by the Ly49s. It is also the NK cell expressing Ly49 receptors that is of interest to this body of work, and thus will remain the focus of this thesis ongoing.

#### ***1.3.4.1.1 The Structure of the Ly49 Receptors***

Ly49s are type II transmembrane glycoproteins expressed at the cell surface as disulfide-linked homodimers (Figure 1-4) [169, 170]. Each 40 – 50kDa monomer is composed of a cytoplasmic tail and a transmembrane region linked via a stalk to the extracellular C-type lectin-like domain (CTLD) [169, 170, 180]. The mouse and rat *Ly49* genes encode both inhibitory and activating forms of the receptors (Figure 1-4). Interestingly, the rat NKC also encodes bifunctional receptors capable of exercising both inhibitory and stimulatory functions in the same receptor [181]. To date, this phenomenon has not been detected in the mouse, yet in humans, a unique MHC class I engaging receptor, KIR2DL4, is also bifunctional [182-185].

The Ly49 CTLD, also known as the natural killer receptor domain (NKD), is similar to the typical carbohydrate recognition domain (CRD) of C-type lectins, however, Ly49s, although capable of recognizing polysaccharides, interact with their ligand, MHC class I, in a carbohydrate-independent manner [186]. Based on mouse Ly49 crystal structures, CTLD folding results in six loop regions and five  $\beta$  strands [187]. Sequence

alignments reveal that some regions appear to be much more conserved between receptors, whereas others appear to be much more polymorphic (Figure 1-5). The mouse Ly49s display significant polymorphism in the L6 loop and very little in the L3 (Figure 1-5 *A*), whereas the opposite is observed in the rat, greater polymorphism in the L3 loop region and greater conservation amongst the L6 loops (Figure 1-5 *B*). The polymorphic differences observed in the loops may be relevant to MHC class I interaction specificity. Despite the lack of a rat Ly49 crystal structure to date, the co-crystal structures of the mouse inhibitory receptors Ly49A and Ly49C bound to their ligands, H-2D<sup>d</sup> and H-2K<sup>b</sup>, respectively, display engagement of the CTLD of the two proteins in a groove below the peptide-binding platform of the MHC class I at three distinct MHC class I locations [188, 189]. This receptor-ligand interaction, in both the mouse and the rat, involves several MHC class I regions ( $\beta_2m$ ,  $\alpha 1/\alpha 2$  and  $\alpha 3$  domains), as well as the Ly49 L3, L5 and L6 loop regions [190-193]. Interestingly, the Ly49-MHC class I co-crystal structures also revealed that ligand association by the receptor involves either a symmetrical or asymmetrical conformation. Ly49A interacts with H-2D<sup>d</sup> in a monovalent manner (Figure 1-6 *A*); the asymmetrical engagement involves both Ly49A monomers binding to one H-2D<sup>d</sup> molecule, where only one subunit interacts in the groove below the peptide-binding area [188, 194]. Ly49C, on the other hand, interacts with H-2K<sup>b</sup> in a bivalent fashion (Figure 1-6 *B*), where both monomers engage with two separate ligands; also in the cavity below the peptide-binding groove, resulting in a symmetrical receptor-ligand association [189, 194]. Based on sequence alignments as well as phylogenetic analysis, all mouse Ly49s can be grouped into either Ly49A-like or Ly49C-like receptors (with the exception of Ly49B and Q) (Figure 1-5) [187, 195]. Based on these analyses, all A-like Ly49s are predicted to engage with their ligands similarly as Ly49A- H-2D<sup>d</sup>, in a monovalent manner; conversely, the bivalent Ly49C- H-2K<sup>b</sup> engagement is the predicted form for all C-like receptors with their respective ligands. Due to the lack of rat Ly49-MHC class I co-crystal structures, it is difficult to predict a symmetrical or asymmetrical association of rat Ly49s with their ligands at this point.

The Ly49 stalk region is comprised of approximately 70 residues and it connects the extracellular domain to the transmembrane and intracellular domains. The long stalk structure is a coiled region interspersed with flexible loops, which, based on Ly49 crystal

structures, is predicted to contain three  $\alpha$ -helix regions ( $\alpha_{1s}$ ,  $\alpha_{2s}$ , and  $\alpha_{3s}$ ) where  $\alpha_{2s}$  links  $\alpha_{1s}$ , which anchors the receptor to the cell membrane, to  $\alpha_{3s}$ , the NKD-binding domain [196]. Because of its structure, the stalk is a flexible component of Ly49s, allowing for either monovalent or bivalent binding of the receptors with their ligand, in either a *cis* or *trans* manner. *Trans* interactions allow the NK cell, via its receptors, to survey the cell surface of other cells by engaging with their ligands expressed at the cell surface of their potential targets; whereas *cis* interactions allow binding of the Ly49 with MHC class I expressed on the same cell [197]. The association of Ly49s and MHC class I molecules in the plane of the same membrane reduce the availability of receptors for *trans* binding, reducing the inhibitory capacity of the Ly49s [197, 198].

While sharing very similar structural architecture in the NKD and stalk, inhibitory and activating receptors differ significantly in their transmembrane and cytoplasmic regions. The transmembrane region of Ly49s stabilizes them at the cell surface. With activators, however, it provides another purpose. Stimulatory receptors are unable to induce intracellular signaling upon ligand engagement at the cell surface, thus activators associate with adaptor molecules via the transmembrane region (outlined in section 1.3.1). Several DAP12 orthologs have been identified in mammals, including humans, mice, and rats; DAP12 is a 12kDa adaptor molecule expressed at the cell surface as a disulfide-linked homodimer with no ligand binding ability [199]. This adaptor, through its negatively charged aspartic acid residue located in its transmembrane, associates non-covalently with Ly49s through their positively charged arginine amino acid, also located in the transmembrane region [199]. Upon ligand engagement by the receptor at the cell surface, the ITAM-bearing DAP12 protein induces cellular signaling upon ITAM-tyrosine phosphorylation recruitment of Syk and ZAP70 which in turn induce phosphorylation of activation substrates such as phospholipase C and c-Cbl, ultimately activating the mitogen-activated protein kinase (MAPK) pathway, resulting in NK cell cytotoxicity and apoptosis of the target cell [200]. The described mechanism is observed upon KIR-DAP12 engagement in humans, and Ly49-DAP12 in mice and rats [73, 201, 202].

The cytoplasmic domain also differs between activators and inhibitory receptors. As already described, stimulators rely on ITAM-bearing DAP12 molecules for their

signaling requirements upon ligand binding at the cell surface. Inhibitory receptors, however, contain an ITIM motif in their cytoplasmic tails (described in section 1.3.2). Upon association and recognition of their ligand at the cell surface, the tyrosines in the ITIM become phosphorylated, resulting in the recruitment of SHP-1, SHP-2, or SHIP that ultimately dephosphorylate NK cell activation substrates, thus blocking NK cell effector functions [200].

#### **1.3.4.1.2 The Ly49 Receptor Repertoire**

Although both mouse and rat express numerous Ly49s, the repertoire in the rat is much more extensive. To date, 34 *Ly49* loci have been identified in the rat, but only 26 are believed to be functional, where 13 encode inhibitory receptors (*Ly49i1* – *Ly49i13*), eight encode activating receptors (*Ly49s1* – *Ly49s8*), and five bifunctional receptor genes (*Ly49si1* – *Ly49si5*) [181]. Until five years ago, only the genome of the Brown Norway rat had been fully sequenced; to date, forty rat strains have been sequenced and only very recently was an analysis of the whole genome sequences performed [203-210]. Once the *Ly49* loci are analyzed and compared, a broader and more precise understanding of the rat NKC receptors can then allow for a complete understanding of the rat Ly49s.

The *Ly49* gene family in mice includes at least twenty-three loci, which include thirteen inhibitory receptor genes (*Ly49a, b, c, e, f, g, i, j, o, q, s, t, v*) and eight stimulatory receptor genes (*Ly49d, h, l, m, p, r, u, w*) [49]. These receptors are encoded by the four most characterized mouse strains; however, each strain contains different *Ly49* loci. The first Ly49 haplotype to be characterized was the one in the C57BL/6 mouse strain, which encodes fifteen genes; whereas the 129 mouse possesses nineteen *Ly49* genes [183, 184, 211-214]. Eight genes make up the smallest cluster of *Ly49* loci, encoded in the BALB/c mouse; on the other hand, the largest cluster, containing twenty-one *Ly49* genes, is found in the NOD/ShiLtJ strain [215, 216].

Such diversity in Ly49 genes, is likely a result of selective pressure resulting from pathogenic evolution and challenges. *Listeria monocytogenes*, a rod-shaped, Gram-positive, facultative intracellular bacterium, is a food borne pathogen that can infect epithelial cells and macrophages in humans [62]. Interestingly, rodents can be carriers of

the bacterium without compromising their own health; the lack of engagement between the mouse adhesion molecule E-cadherin and the *Listeria* surface protein internalin A (required for host entry) can provide rodents with immunity [217, 218]. Furthermore, in rat *Listeria* infection models, an up-regulation of non-classical MHC class I molecules allows the engagement of several activating Ly49s (i.e. Ly49s3, Ly49s4, Ly49s5) with their non-classical ligands, providing bacterial resistance in the rat [62-65]. In another example, the mouse activator Ly49H recognizes the MHC class I “decoy”, m157, encoded by MCMV, conferring C57BL/6 mice resistant to an MCMV viral infection; whereas other strains, such as BALB/c, lack the *Ly49h* gene and thus are highly susceptible to MCMV [219-224]. These are two examples of how Ly49s have possibly evolved in response to potential threats against host cells.

Of great interest to this body of work is the specific engagement of rodent Ly49s with their allele specific ligand, MHC class I molecules. This relationship dictates the functional output upon cell surface ligand interaction by Ly49s based on the recognition of the class I molecules via a mechanism that has not been fully explored.

#### **1.4 Ly49 RECEPTOR ENGAGEMENT WITH MHC CLASS I MOLECULES**

As outlined above, the rodent Ly49 receptor repertoire is extensive, yet expression of inhibitory receptors at the cell surface is variegated and stochastic. Each receptor is expressed in a monoallelic manner, with only a few *Ly49* genes expressed by any one given NK cell, independent of animal strain [225]. MHC class I recognition is usually executed via binding with the inhibitory Ly49s, whereas activating receptors engage with a variety of ligands, including viral proteins, MHC class Ia or Ib molecules, and MHC class I-related molecules induced by cellular stress pathways during a viral infection or transformation [226]. The stochastic expression of inhibitory receptors on NK cell subsets partially coincides with the expression of other MHC class I - specific inhibitory receptors, such as the NKG2/CD94 family of receptors, resulting in a complex repertoire of NK cell specificities, with each individual NK cell expressing its own, variegated and stochastic array of inhibitory receptors aimed at surveying the different MHC class I expression patterns on potential target cells [225]. If a host cell down-

regulates only one MHC class I molecule, a strong NK cell response will be elicited upon the lack of ligand detection by the inhibitory receptors on the subset of NK cells that only recognize that particular class I molecule; whereas a more exuberant response results from a complete loss of MHC class I molecules due to the collective response by all the NK cells [225]. The final functional and stochastic repertoire of receptor expression on the mature NK cell requires an education process involving the engagement of Ly49s with MHC class I alleles expressed by the host. NK cell education involved both the inhibitory and activating receptors expressed by individual NK cells. NK cell education, or “training”, is required to ensure proper NK cell function, while protecting the host cell from NK-mediated autoimmune responses.

#### ***1.4.1 Self Tolerance and NK Cell Education***

The ability of NK cell receptors to detect the lack of MHC class I molecules at the cell surface resulting in the cytotoxicity of the target cell was first described in 1986, leading to the postulation of the “*missing-self*” hypothesis [227]. Specifically, cells lacking MHC class I are referred to as missing the “self” ligand. Subsequently, Kärre *et al.* further proposed that all healthy NK cells required the presence of an inhibitory receptor capable of engaging with MHC class I to prevent NK cell activation (autoimmunity) [228]. The first study to provide evidence for the missing-self hypothesis involved the blocking of NK cell activation upon the recognition of MHC class I by the mouse Ly49A inhibitory receptor [229]. Ensuing studies demonstrated that full effector NK cell function not only requires lack of MHC class I recognition by the inhibitory receptor, but also stimulatory signals resulting from the engagement of activators with their respective ligands [230].

The expression of inhibitory Ly49s on immature NK cells early during development in the bone marrow initiates the process of NK cell education. Initially, two NK cell education mechanisms were proposed. In the *licensing* or *arming* model, NK cells are considered inactive by default and only acquire their full functionality through the engagement and the signaling of an inhibitory receptor with its MHC class I ligand [231-233]. Furthermore, hyporesponsive or anergic peripheral NK cells can result from

the lack of inhibitory receptor engagement with MHC class I molecules [232]. In an opposing view, the *disarming* model proposes that, by default, NK cells are active; hyporesponsive or anergic states result from the continuous stimulation induced by the recognition of endogenous ligands by the stimulatory receptors, a state that can ultimately be altered and overridden by signals of the inhibitory receptors [231]. Both models imply that only NK cells with inhibitory receptors that recognize MHC class I molecules are able to become functional. Recent studies have resulted in the proposal of an updated NK cell education mechanism, the *rheostat* model [234-236]. This model is based on the observation that the NK cell signal strength is based on receptor-ligand interactions: the stronger the inhibitory interactions of an NK cell are, the stronger it responds to activating receptor signals, suggesting that NK cell education is a dynamic process [234-236].

NK cell education requires Ly49 *cis* interactions with their MHC class I ligand for some inhibitory receptors, as recently demonstrated for Ly49A [237, 238]. Interestingly, Ly49A has also been shown to bind to and require the class Ib molecule, H2-M3, for its education process [66]. *Trans* interactions have also been shown to be important for the “training” process of NK cells [239]. The significance of *in trans* binding between the NK cell receptors and their cognate ligands is especially highlighted in the recent concept of NK cell re-education, where NK cells can alter their ligand specific activation through a change in their MHC class I environment [240].

The outlined NK cell education concepts have also been similarly observed in humans [230]. In rats, however, this process has not been reported. Although not fully understood or explored, the education of NK cells during development results in their functionality upon maturation and encounter with ligands on potential target, or self-cells.

#### ***1.4.2 Ly49 Receptor and Ligand Binding Specificity***

Ly49 specificity for MHC class I ligands was first described in 1992 [229]. Since then, a great deal of research has led to the understanding that Ly49 receptors engage with and recognize MHC class I molecules as their ligands in an allele specific manner. Many of the characterized rodent Ly49s may have only one, or several MHC class I

alleles they recognize. To date, the inhibitory receptors, the rat Ly49i2 and the mouse Ly49F, have been shown to only recognize one MHC class I allele, the rat RT1-A1<sup>c</sup> and the mouse H2-D<sup>d</sup>, respectively [241]. In the mouse, we also observe several Ly49s displaying specificity for more than one MHC class I allele. Ly49A, for example, has been shown to recognize the class Ia alleles H2-D<sup>b, d, p, k</sup>, as well as the class Ib allele H2-M3 [66, 242]. Differences in ligand specificities for the same receptor amongst different mouse strains have also been reported. The BALB/c Ly49G (Ly49G<sub>BALB/c</sub>) inhibitory receptor recognizes H2-D<sup>d,k</sup>; the Ly49G2<sub>NOD</sub> recognizes H2-K<sup>d</sup>; Ly49G<sub>C57BL/6</sub> engages with H2-D<sup>b,d</sup>; and Ly49G<sub>129</sub> interacts with H2-D<sup>d,k</sup> and H2-K<sup>d</sup> [241, 243]. Activating Ly49s also display allele specificity. Ly49D<sub>NOD</sub>, for example, recognizes the class Ia molecules H2-D<sup>d,r</sup>, while Ly49H engages and binds to the MCMV MHC class I “decoy” m157 [241].

In the rat, ligand specificities are not as well studied. Nonetheless, several investigations have revealed that although the inhibitory Ly49i2 receptor recognizes a classical MHC class I molecule (RT1-A1<sup>c</sup>), other inhibitory receptors, as well as activators, appear to recognize nonclassical ligands. The activating and inhibitory pair, Ly49s5 and Ly49i5, respectively, bind to ligands from the class Ib MHC region RT1-CE/N/M, as does the activator Ly49s3 [64, 201, 244]. Recently, the activating and inhibitory pair, Ly49s4 and Ly49i4, respectively, reportedly bind the class Ib MHC region RT1-CE [63]. Even though the specific ligands have not been identified for the mentioned rat receptors (with the exception of Ly49i2), these rat ligand studies present a similar association pattern as observed and documented for mouse receptors; Ly49s recognize their MHC class I ligands in an allele specific manner.

## **BACKGROUND AND RATIONALE**

Since their discovery over 25 years ago, a great number of investigative teams, including the Kane lab, have concentrated their efforts into understanding the biology, structure, and functionality of Ly49 receptors, specifically in the mouse and the rat. Both the mouse and rat are commonly used as animal models of human disease to elucidate possible mechanisms of disease, as well as potential treatment or therapy. The immense repertoire of mouse models available target many illnesses including autoimmune

diseases, cancer, neurological disorders such Alzheimer's disease, vaccine development, and even wound healing and repair [245-249]. Rats are also commonly used as models for various human disease or implication studies including renal disease, carcinogenicity testing, type 2 diabetes, obesity, drug development and toxicology, cancer, and autoimmune diseases [250-262]. Therefore, further elucidating the structural assembly requirements, as well as specificity requirements for ligand engagement by Ly49 receptors is of great interest to this body of work. Understanding the functionality of Ly49s is also crucial to fully appreciate the final outcome upon receptor-ligand binding.

Chapter III is dedicated to elucidating the recognition requirements of the rat inhibitory Ly49i2 receptor for its cognate ligand, RT1-A1<sup>c</sup>. Studies involving mouse Ly49s report that recognition of MHC class I by Ly49s is determined by the engagement of the Ly49<sub>NKD</sub> loop L3, loop L5, and loop L6 [187]. Furthermore, based on the co-crystal structures of Ly49A and Ly49C with their respective ligands, these loop regions on the receptor interact with the MHC class I at specific locations below the peptide-binding groove [187-189]. Interestingly, our lab has demonstrated that in the rat, RT1-A1<sup>c</sup> recognition by Ly49i2 concurrently involves Ly49<sub>NKD</sub> interaction at any two of three possible MHC class I locations also located below the peptide-binding groove [192]. Unlike the mouse Ly49s, which display polymorphism in loop L6 and a more conserved loop L3 (Figure 1-5 A), the rat Ly49 exhibits the opposite with greater polymorphism in loop L3 and a more conserved L6 (Figure 1-5 B). In Chapter III, we hypothesize that L3, L5, and L6 loops of Ly49i2 are required to confer ligand recognition during the binding of the receptor, Ly49i2, with RT1-A1<sup>c</sup>. Utilizing surface plasmon resonance (SPR) studies, we were able to show the importance of these loop regions for ligand recognition during Ly49-MHC class I association.

Ly49 receptors are expressed on the cell surface of NK cells, thus to fully grasp the significance of the receptor-ligand engagement and the impact this relationship ultimately bears on the function of the NK cell, a functional assessment system that allows for efficient expression of Ly49s is required. For NK cell functional assessments, many groups, including the Kane lab, have relied on RNK-16 cells (RNK-16s), a spontaneous leukemic rat NK cell line that possesses NK cell function and specificity [263], making them an ideal candidate for expression of many types of cell surface

receptors, including human, mouse or even other rat receptors [191, 264-267]. In spite of this, NK cells are resistant to exogenous gene transfections [268-271]. Expression of exogenous DNA in RNK-16s has traditionally relied on electroporation; however, apart from being extremely time consuming, this method yields very low transfection efficiencies [272, 273]. Virus-based transfections systems, specifically lentiviral transduction approaches, have proven successful in expressing foreign DNA in cells that are difficult to transfect, such as murine NK cells [268]. Given the continued interest we have in exploring NK cell biology and functionality, in Chapter IV, we decided to explore the possibility of transducing RNK-16s with a lentivirus-based approach in an effort to quickly express cell surface Ly49 receptors during functional assays. We hypothesized that a lentivirus vector for the transduction of RNK-16 cells would result in expression of Ly49i2 at the cell surface of RNK-16 cells quickly and efficiently. Our results reported in Chapter IV support our hypothesis, suggesting we have indeed developed a method to express exogenous *Ly49s* in RNK-16s with a much higher transduction yield and in a shorter amount of time as compared to electroporation.

Chapter V is aimed at further understanding the structural requirements of Ly49 receptors. Ly49s are type II transmembrane glycoproteins expressed at the cell surface as disulfide-linked homodimers [169, 170]. A stalk region links the extracellular NKD of each monomer to a cytoplasmic tail and a transmembrane region [169, 170]. To date, no Ly49 heterodimers have been reported. Furthermore, the molecular requirements for Ly49 homodimerization have also not been reported. Interestingly, other NK cell receptors, also encoded in the NKC gene complex, such as the NKG2 family, form heterodimers with other cell surface molecules, such as CD94, for full functional output [139]. Given the existence of NK cell surface heterodimeric receptors, in Chapter V we explored the possibility of different *Ly49* allele products dimerizing. We hypothesize that highly homologous Ly49s are capable of heterodimerization. Our results support the ability of Ly49s, within the same receptor structural family, to dimerize, generating Ly49 heterodimers.

This body of work collectively provides a framework for further exploring some fundamental questions that require additional elucidation. Given the SPR binding affinities determined in Chapter III, further support for Ly49 receptor functional

assessments can now be carried out relying on the gene expression protocol outlined in Chapter IV. Furthermore, the functional relevance of Ly49 heterodimers should be assessed.

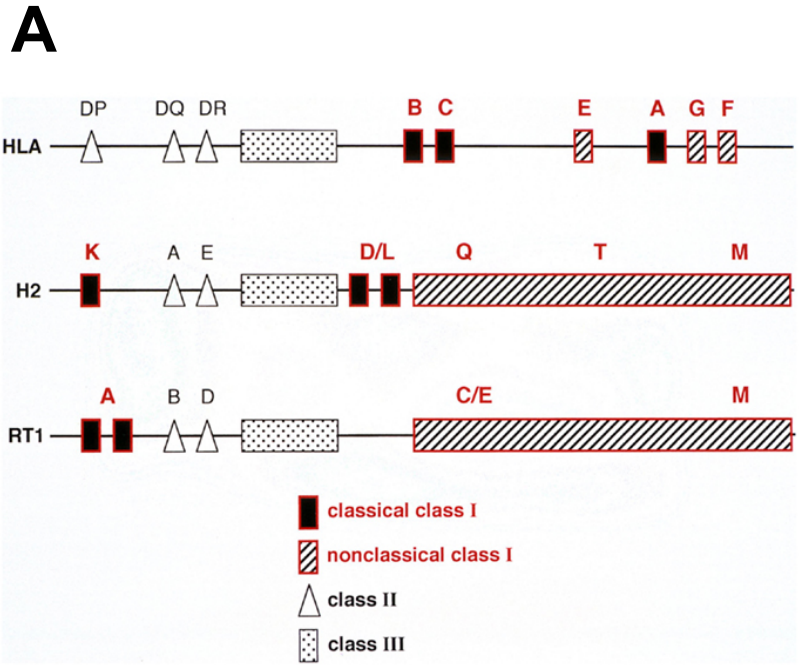
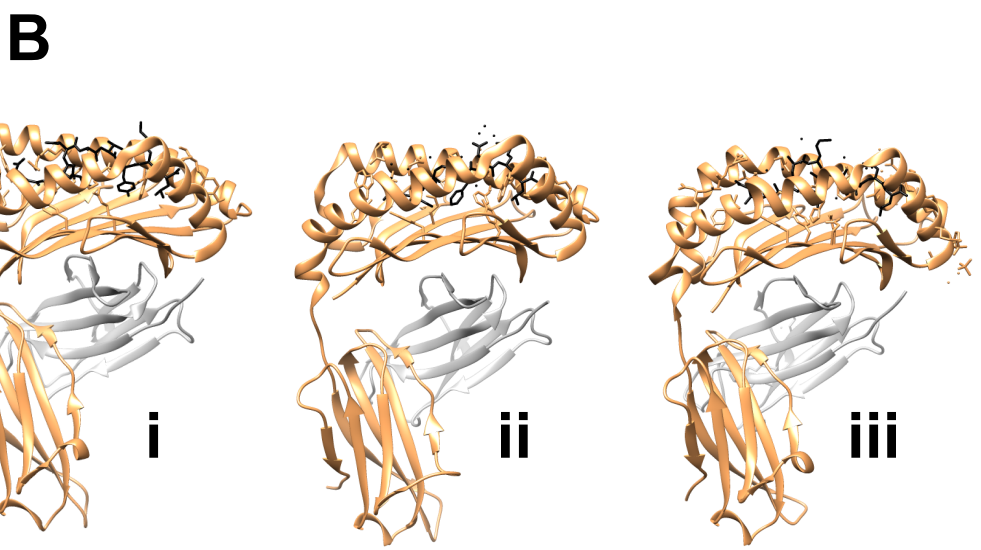
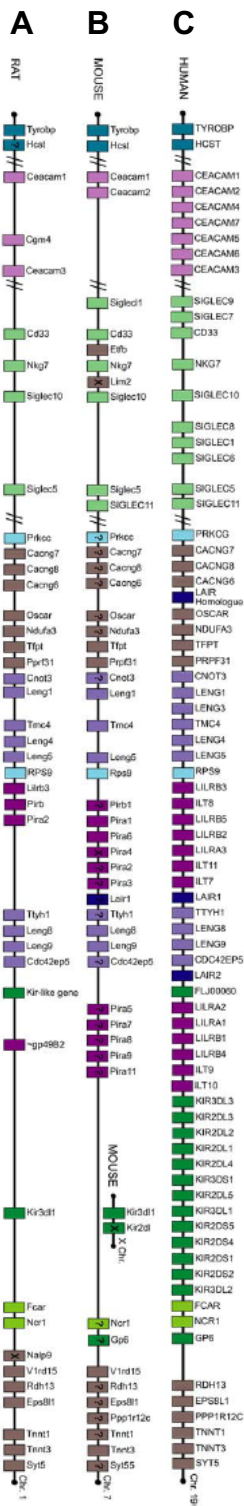


Figure adapted from: [274]



**Figure 1-1: The genetic organization of the MHC complex in the human (HLA), mouse (H2), and rat (RT1) and the structure of MHC class I molecules.** (A) Genes encoding MHC class I, II, and III molecules are displayed in black-filled boxes and striped boxes, open triangles, and dotted boxes, respectively. Non-classical class I (Ib) gene regions are shown in striped boxes. Humans encode the HLA MHC gene complex on chromosome 6, whereas mice (H2) and rats (RT1) encode on chromosomes 17 and 20, respectively. (B) The crystal structure of MHC class I molecules in human (i), mouse (ii), and rat (iii) is displayed. The heavy chain is illustrated in sandy brown;  $\beta_2m$  in grey; bound-peptide in black. PDB ID for *i* is 1QQD; *ii* is 3P9M; and *iii* is 1KJV.



**Figure 1-2: The Leukocyte Receptor Complex (LRC).** NK cell receptors belonging to the immunoglobulin-domain structural superfamily are encoded by the LRC. The LRC is located on human chromosome 19 (A), mouse chromosome 7 (B), and rat chromosome 1 (C). Each family of genes is displayed in a different color, maintaining the same color across the species to display homology. Slash marks represent large distances in the genomic sequence. The illustration is not drawn to scale; however, the linear arrangement of genes is correct. *Figure adapted from: [139]*

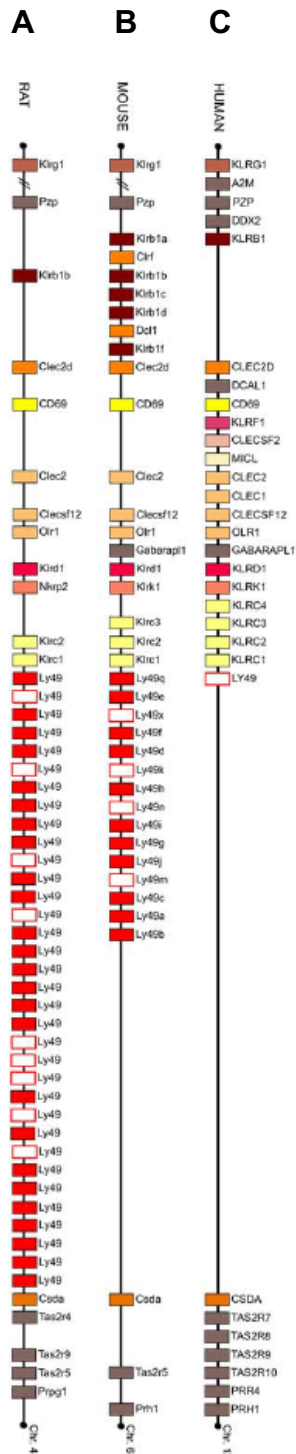


**Figure 1-3: The Natural Killer Complex (NKC).** NK cell receptors belonging to the C-type lectin receptor superfamily are encoded by the NKC, located on human chromosome 12 (A), mouse chromosome 6 (B), and rat chromosome 4 (C). Each family of genes is displayed in a different color, maintaining the same color across the species to display homology. Slash marks represent large distances in the genomic sequence. White boxes mark pseudogenes. The illustration is not drawn to scale; however, the linear arrangement of genes is correct.

Figure adapted from: [139]

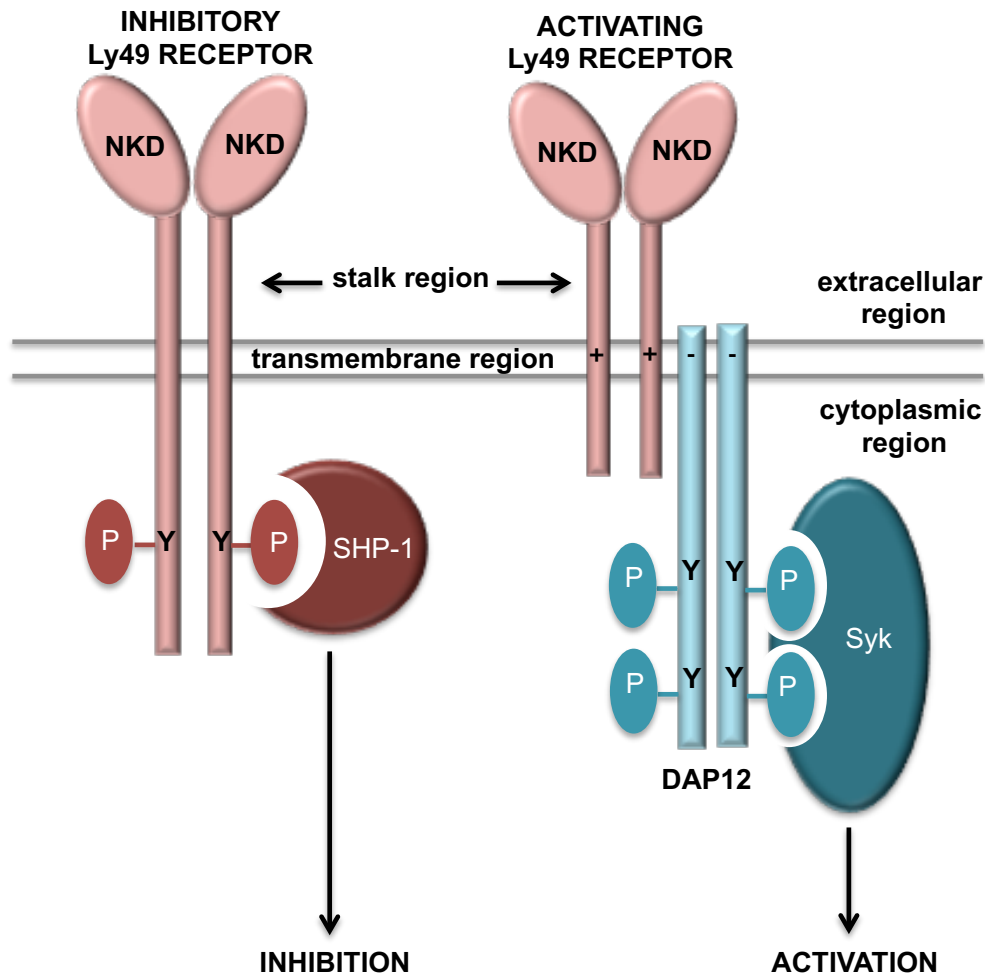


**Figure 1-4: Inhibitory and activating Ly49 receptors.** Ly49 receptors are disulfide-linked homodimeric type II transmembrane glycoproteins expressed at the cell surface of NK cells. Each monomer is composed of a cytoplasmic tail and a transmembrane region linked via a stalk region to the extracellular natural killer receptor domain (NKD). Inhibitory receptors (*left*) contain an ITIM motif in their cytoplasmic tails with tyrosine residues. Upon ligand association with the NKD at the cell surface, the tyrosines in the ITIM become phosphorylated and recruitment of SHP-1, SHP-2, or SHIP occurs resulting in the blocking of NK cell effector functions. Activating receptors (*right*) lack the ability to signal intrinsically. Their positively charged transmembrane region allows them to engage with the adaptor molecule DAP12 via its negatively charged transmembrane domain. Upon binding of the NKD to the ligand, phosphorylation of the tyrosines on DAP12 occurs, followed by the recruitment of Syk kinases resulting in the activation of the NK cell.

**A**

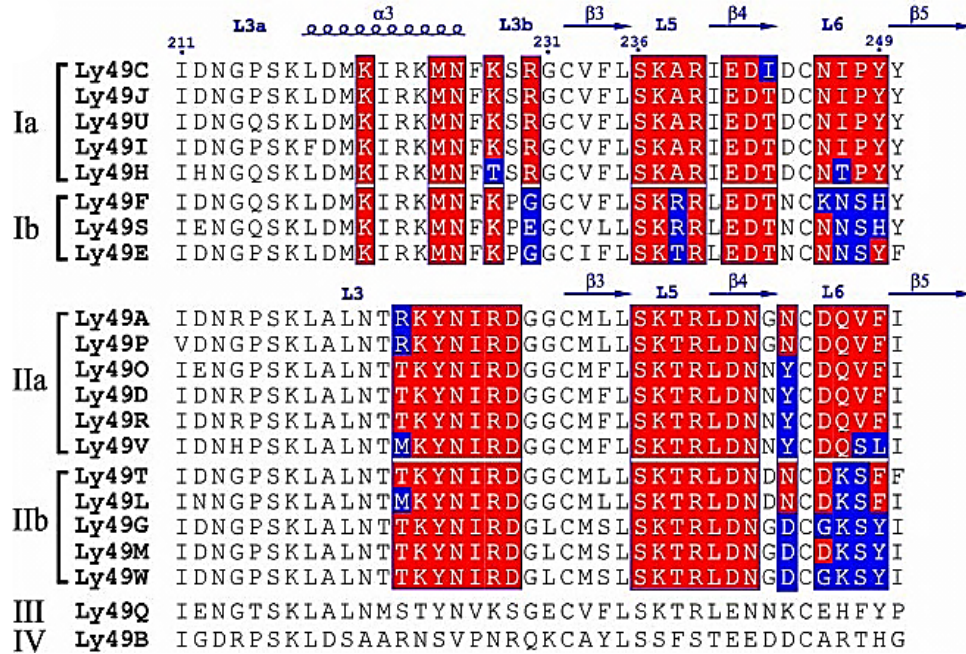
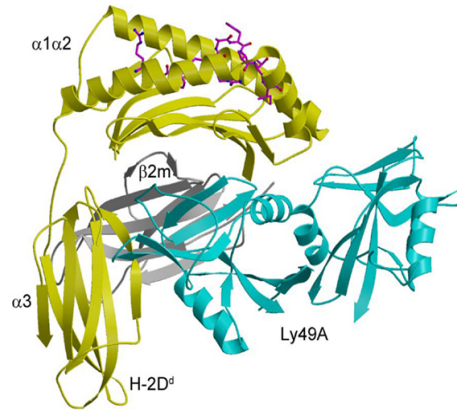
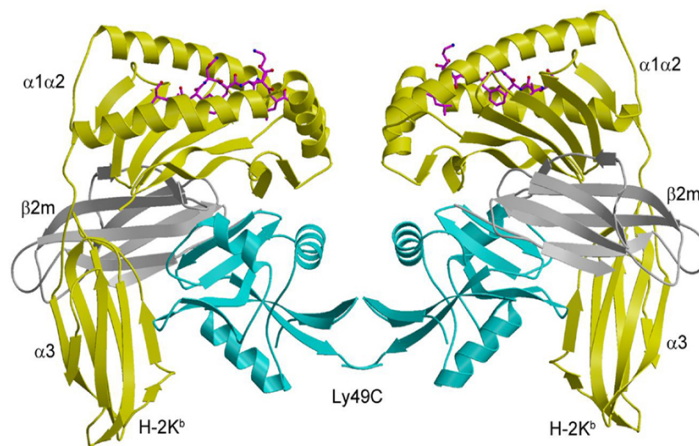


Figure adapted from: [187]

**B**

Ly49i2	WIGLSYNNKKESW	IDNTTLNCDLVAMISLHKTGN	CKYF	SMTG	LHD	D	DCGKRH	LCI	257
Ly49i5	WIGLSYNNIKKESW	IDNSPLNCDL <b>LACKPLQKTGY</b>	CIYF	SMTG	LHY	D	DCGKRH	LCI	254
Ly49s3	WIGSSYNNKKEWAW	IDNSPFDLDFVARTLL <b>RKKTGY</b>	CLYF	SMSG	LHD	D	DCGKRY	LCI	254
Ly49s5	WVGLSYNNIKKESW	IDSSPLNCDL <b>LACKPLQKTGY</b>	CIYF	SMTG	LHY	D	DCGKRH	LCI	254
		Predicted L3		L5	β4		L6		

**Figure 1-5: Mouse and rat Ly49 gene alignments of MHC class I interacting regions.** (A) Mouse Ly49 receptors are classified as members of group I or II based on their predicted structures from sequence alignments with Ly49C (group I) or Ly49A (group II). MHC class I interacting regions are identified in navy blue, highlighting loop L3, L5, L6 and the associated  $\beta$  strands. The major difference between both groups is the presence (group I) or absence (group II) of the  $\alpha 3$  helix in loop L3. Further division in each group is based on the highly polymorphic loop L6 region in group Ib and IIb members (boxed in blue). All residues boxed in red are MHC class I contact residues. Ly49Q and Ly49B are listed as their own group given the substantial sequence divergence between them and all other members listed in either group I or II. (B) The sequence alignment of four rat PVG strain members belonging to the same chromosomal block is shown. The MHC class I interacting regions, the predicted loop L3, loop L5, strand  $\beta 4$ , and loop L6 are in bold navy blue. The pink residues differ in comparison to the inhibitory receptor Ly49i2.

**A****B**

**Figure 1-6: Co-crystal structures of Ly49A-H-2D<sup>d</sup> and Ly49C-H-2K<sup>b</sup>.** The binding of Ly49A with H-2D<sup>d</sup> and Ly49C with H-2K<sup>b</sup> are displayed (*A* and *B*, respectively). The heavy chain of H-2D<sup>d</sup> and H-2K<sup>b</sup> is illustrated in golden yellow; the non-covalently associated  $\beta 2m$  in grey; the bound peptide in magenta; and the Ly49 receptor in cyan. Ly49A associates with H-2D<sup>d</sup> in a monovalent, asymmetrical manner (*A*), whereas Ly49C displays a bivalent, symmetrical association pattern with H-2K<sup>b</sup> (*B*).

*Figure adapted from: [196]*

## **CHAPTER II: MATERIALS AND METHODS**

### ***2.1 Cell Lines***

RNK-16 cells (RNK-16s) are a rat leukemic cell line and have been previously described [263, 272]. RNK-16s were cultured in RNK medium consisting of Roswell Park Memorial Institute 1640 (RPMI 1640) medium supplemented with 10% fetal calf serum (FCS), penicillin, streptomycin, L-glutamine, and 50 $\mu$ M of 2-mercaptoethanol. Ly49i2 expressing RNK-16 transfectants (described below) were cultured in RNK medium and maintained under puromycin selection. COS-7 cells are African green monkey fibroblast-like kidney cells and have been previously described [275, 276]. COS-7 cells were cultured in COS-7 medium composed of Dulbecco's modified Eagle's medium (DMEM) supplemented with 10% FCS, penicillin and streptomycin. 293T cells are a human embryonic kidney cell line and have been previously described [277]. 293T cells were cultured in 293T medium consisting of DMEM supplemented with 10% FCS, L-glutamine, penicillin and streptomycin. 293FT cells (293FTs) are a human embryonic kidney cell line, derived from 293Ts, but grow much faster [278, 279]. 293FTs were included in the pLenti6.3 (and 7.3)/V5-DEST™ Gateway® Vector Kits (Life Technologies™). 293FTs are cultured in 293FT medium composed of DMEM supplemented with 10% FCS, L-glutamine, 1mM sodium pyruvate, 0.1mM non-essential amino acids, penicillin and streptomycin. HT1080 cells are a human fibrosarcoma cell line and have been previously described [280]. HT1080 cells were cultured in Eagle's minimum essential medium (EMEM) supplemented with 10% FCS.

### ***2.2 Antibodies***

The STOK2 antibody (Ab) is a monoclonal antibody of the rat IgG2a isotype and recognizes the rat inhibitory receptor Ly49i2 [281, 282]. The STOK2 hybridoma was generously provided by Dr. John T. Vaage (Oslo University Hospital, Norway). The STOK2 Ab was prepared by ammonium sulfate precipitation and by PBS dialysis of tissue culture supernatants obtained from the culture of the hybridoma in protein-free

hybridoma medium (Life Technologies™). Purified anti-HA tag (IgG isotype), purified 2C16 (anti-HA tag; FITC-conjugated; IgG1 isotype), purified phycoerythrin (PE)-conjugated M2 (anti-DDDK tag; IgG1 isotype), and purified PE-conjugated anti-V5 tag (IgG isotype) were purchased from Abcam® (Toronto, ON). Purified M2 (anti-FLAG®; IgG1 isotype) from Sigma-Aldrich® (St. Louis, MO) was generously provided by Dr. Hanne Ostergaard. Fluorescein isothiocyanate (FITC) coupled secondary mouse anti-rat IgG antibody, anti-mouse and anti-rabbit IgG-HRP (horseradish peroxidase) secondary antibodies were purchased from Jackson ImmunoResearch Laboratories Inc. (Cedarlane; Burlington, ON).

### ***2.3 Cloning of Ly49 Receptors***

The cDNA of the rat wildtype Ly49i2 (Ly49i2<sub>WT</sub>) receptor was previously cloned, in this laboratory, into the BSR $\alpha$ EN expression vector [267]. Ly49i2<sub>WT</sub> was sub-cloned into pENTR/D-TOPO® vector using a pENTR™/D-TOPO® Cloning Kit from Life Technologies™ (Burlington, ON). For lentivirus generation, Ly49i2<sub>WT</sub> was then subcloned into a pLenti6.3, pLenti7.3, or pLEX307 destination vector via recombinational cloning using an LR clonase™ enzyme mix from Life Technologies™ (Burlington, ON), resulting in Ly49i2-pLenti6.3, Ly49i2-pLenti7.3, and pLEX.49i2, respectively. pLenti6.3 and pLenti7.3 are lentivirus plasmids and components of the Gateway® ViraPower™ HiPerform™ Lentiviral Expression System from Life Technologies™ (Burlington, ON). The pLEX307 plasmid was generously provided by Dr. Troy Baldwin (Department of Medical Microbiology & Immunology; University of Alberta) (Addgene plasmid 41392).

The extracellular domain of wildtype Ly49i2 (Ly49i2<sub>ED</sub>) (residues 68 - 280), as well as the loop L6 mutants Ly49i2.L6.NCDQ<sub>ED</sub> and Ly49i2.L6.ACGA<sub>ED</sub>, loop L5 mutants Ly49i2.S241A<sub>ED</sub>, Ly49i2.T243A<sub>ED</sub>, and Ly49i2.S241A.T243A<sub>ED</sub>, loop L3 mutants Ly49i2.L3.i5<sub>ED</sub>, Ly49i2.L3.s5<sub>ED</sub>, and Ly49i2.L3.s3<sub>ED</sub>, Ly49i5.L3.i2<sub>ED</sub> were separately subcloned into the bacterial pET21a+ expression vector (Novagen® from EMD Millipore; Billerica, MA) at the NdeI/BamHI restriction sites for soluble protein generation. The extracellular region of the rat RT1-A1<sup>c</sup> protein (residues 1 - 277) and rat  $\beta_2m$  were

previously cloned separately, by our lab, into the pET21a+ vector [266].

The mouse Ly49W2, Ly49M, Ly49P1, and Ly49G2 receptors, all either HA-tagged or FLAG-tagged, were subcloned into the pCIneo mammalian expression vector at the XhoI/XbaI restriction sites (Promega; Madison, WI). Mouse DAP12 cloned into the pCMV6 mammalian expression vector was purchased from OriGene Technologies (Rockville, MD). All of the described cloning reactions were verified by DNA sequencing analyses (MCLAB; San Francisco, CA).

#### ***2.4 Mutagenesis and Gene Synthesis***

The rat Ly49i2 loop L5 mutants Ly49i2.S241A<sub>ED</sub>, Ly49i2.T243A<sub>ED</sub>, and Ly49i2.S241A.T243A<sub>ED</sub> were generated by site-directed mutagenesis using PCR reactions with primers designed for each specific mutation. The loop L3 mutants (Ly49i2.L3.i5<sub>ED</sub>, Ly49i2.L3.s5<sub>ED</sub>, and Ly49i2.L3.s3<sub>ED</sub>, Ly49i5.L3.i2<sub>ED</sub>) and loop L6 mutants (Ly49i2.L6.NCDQ<sub>ED</sub> and Ly49i2.L6.ACGA<sub>ED</sub>) were ordered from Life Technologies™ (Burlington, ON).

The mouse Ly49W2 and Ly49M receptors has been previously cloned in our laboratory into a BSR $\alpha$ EN expression vector. Through PCR reactions, HA and FLAG tags were added to both receptors separately at the carboxy-terminus, and subsequently subcloned into the pCIneo expression vector. Ly49P1 and Ly49G2 receptors with a carboxy-terminus HA-tag and FLAG-tag, separately, were ordered from GenScript (Piscataway, NJ). All of the described mutants were verified by DNA sequencing analyses (MCLAB; San Francisco, CA).

#### ***2.5 Lentivirus Packaging and Virus Titering***

Infectious lentivirus particles were generated by transfecting 293FT cells via Lipofectamine® 2000 from Life Technologies™ (Burlington, ON). The transient transfection included Ly49i2-pLenti6.3 or Ly49i2-pLenti7.3 along with a plasmid mix containing pLP1, pLP2, and pLP/VSV-G plasmids that encode the HIV *gag/pol* and *rev* genes, and the G glycoprotein gene of the vesicular stomatitis virus (VSV-G),

respectively. The plasmid mix is a component of the Gateway<sup>®</sup> ViraPower<sup>™</sup> HiPerform<sup>™</sup> Lentiviral Expression System from Life Technologies<sup>™</sup> (Burlington, ON). Transfected cells were incubated at 37°C and 5% CO<sub>2</sub> for 16 hours. Cells were then harvested and using an AmiconUltra-15ml centrifugal filter unit with Ultracel-100 kDa membrane, the virus supernatant was concentrated for 3 hours at 5000 rpm, to a final volume of 1ml.

Alternatively, infectious lentivirus particles were generated using a method described by the TRC laboratory available at the RNAi Consortium, Broad Institute website (<https://www.broadinstitute.org/rnai/trc>). In summary, 293T cells were transfected with psPAX2, pMD2.G, and pLEX.49i2 at a ratio of 10:1:10, respectively, using the TransIT<sup>®</sup>-LT1 transfection reagent from Mirus Bio LLC (Cedarlane; Burlington, ON). psPAX2 and pMD2.G are HIV *gag/rev* and VSV-G containing plasmids, respectively, and both were generously provided by Dr. Troy Baldwin (Department of Medical Microbiology & Immunology; University of Alberta) (Addgene plasmids 12260 and 12259, respectively). After an overnight incubation at 37°C and 5% CO<sub>2</sub> for a maximum of 18 hours, the culture medium is replaced with high serum growth medium (293T culture medium supplemented with 30% FCS) and incubated at 37°C and 5% CO<sub>2</sub>. After 24 and 48 hours, the supernatant is collected and pooled together. Upon filtration, the virus supernatant was concentrated also using an AmiconUltra-15ml centrifugal filter unit with an Ultracel-100 kDa membrane, for 3 hours at 5000 rpm, to a final volume of 1ml.

To assess virus titers,  $5 \times 10^5$  HT1080 cells were incubated for 24 hours at 37°C and 5% CO<sub>2</sub> with the concentrated virus supernatant of Ly49i2-pLenti6.3 or Ly49i2-pLenti7.3, at dilution factors of 0,  $10^{-1}$ , and  $10^{-2}$ . As a negative control, HT1080 cells were inoculated with supernatant from an empty vector. Successful Ly49i2 transduction was assessed by flow cytometry. The percentage of gated cells expressing the receptor was used to determine the titer of each lentivirus plasmid using the formula:  $T = (F \times Co/V) \times D$ , where  $T$  is the titer in TU/ml (transducing viral units per milliliter);  $F$  is the frequency of Ly49i2 expressing cells;  $Co$  is the number of target cells used;  $V$  is the volume of inoculum in milliliters (ml); and  $D$  is the dilution factor [283]. For titering virus supernatants containing pLEX.49i2, RNK-16 cells were used (instead of HT1080

cells), following the same method described above.

## ***2.6 RNK-16 Transduction***

For transductions with Ly49i2-pLenti6.3 or Ly49i2-pLenti7.3,  $1 \times 10^6$  RNK-16 cells in a 6-well plate were transduced with concentrated virus supernatants at MOI 1, 5, 10, and 50 and incubated at 37°C and 5% CO<sub>2</sub>. After a minimum of 48 hours, and every 24 hours for 1 week, Ly49i2 expression was assessed via flow cytometry. Mock transductions with an empty lentivirus vector were also performed.

For transductions with pLEX.49i2 virus supernatants,  $1 \times 10^6$  RNK-16 cells were seeded in a 6-well plate 24 hours prior to transduction. The following day, each well was replaced with 1ml of fresh RNK culture medium containing 8µg/ml of polybrene and infectious virus at the desired MOI. Each plate was wrapped with parafilm and placed in a centrifuge at 32°C for 90 minutes at a speed of 2000 rpm. Cells were subsequently incubated for 10 hours at 37°C and 5% CO<sub>2</sub>, with the parafilm removed. After 10 hours, the medium was replaced with fresh RNK culture medium and cells were incubated for 48 hours at 37°C and 5% CO<sub>2</sub>. Ly49i2 expression was assessed via flow cytometry. Mock transductions with an empty lentivirus vector were also performed in the same manner.

## ***2.7 Flow Cytometry***

For all flow cytometric analyses, cells were stained with the primary antibody and incubated at 4°C for 20 minutes. Cells were then subsequently washed and incubated with a fluorescently labeled secondary antibody, also at 4°C for 20 minutes. Cell surface expression of the protein of interest was then assessed with a FACS Canto II cell analyzer (BD Biosciences; Mississauga, ON). Fluorescence-activated cell sorting (FACS) data analyses was carried out using FCS Express from De Novo™ Software (Glendale, CA).

For the assessment of Ly49i2 cell surface expression following lentivirus transduction, HT1080 or RNK-16 cells were stained with the STOK2 antibody, followed by the FITC-conjugated mouse anti-rat IgG secondary antibody. The detection of the

mouse HA-tagged or FLAG-tagged Ly49 receptors was done by staining the COS-7 cells with the 2C16 and PE-conjugated M2 Abs. Prior to all flow cytometric analyses, all stained cells were fixed in 4% formaldehyde fixing solution (containing PBS & 2% FCS).

## **2.8 Puromycin Titration**

RNK-16 cells, non-transduced and transduced to express Ly49i2, were cultured in RNK medium. At 48 hours post-transduction, both groups of cells were incubated with medium containing puromycin ranging in concentration from 0.01 to 10 $\mu$ g/ml. Cell viability was assessed visually through light microscopy. Images were captured with a Hund Wetzlar (Wilovert S) light microscope connected to a Q imaging Retiga 1300 camera. Images were then visualized using Openlab 3.0.9 software.

## **2.9 Protein Expression, Purification, Folding, and Analysis**

All pET21a+ constructs generated (wildtype Ly49i2<sub>ED</sub> and all the loop L6, L5, and L3 mutants, as well as RT1-A1<sup>c</sup> and rat  $\beta_2m$ ) were used to transform *Escherichia coli* strain BL21(DE3) (Agilent Technologies Canada Inc.; Mississauga, ON). The following day, individual colonies for each DNA construct were incubated at 37°C and 250 rpm in an overnight culture of LB broth containing 50 $\mu$ g/ml of ampicillin. Subsequently, 12ml of each culture were used to inoculate 1L of LB broth containing 50 $\mu$ g/ml of ampicillin, for a total of 6L per DNA construct. Inoculated cultures were incubated at 37°C and 250 rpm until reaching an optical density of 0.6 at 600nm. Each culture was then induced with 1mM of isopropyl  $\beta$ -D-1-thiogalactopyranoside (IPTG) and cultured for an additional 4 hours at 37°C and 250 rpm.

Cell pellets were harvested following 20 minutes of centrifugation at 4°C and 5000 rpm. Then, pellets were incubated with 1mg/ml of lysozyme, 5mM of MgCl<sub>2</sub>, 3.5mg/ml DNase, 1% Triton-X 100, and 10mM DTT at 4°C for 30 minutes. Purification of the inclusion bodies further required several rounds of sonication and washing phases until pellets were creamy white and supernatant was clear. For protein solubilization, the pellet for each Ly49i2 construct was dissolved overnight at 4°C in 6M guanidine

hydrochloride. For the pellet of RT1-A1<sup>c</sup> and rat  $\beta_2m$ , each one was separately dissolved in 8M urea for 30 minutes at 4°C.

Refolding of all Ly49i2 constructs was done by rapid injection of each solubilized protein separately into a folding buffer containing 400mM L-arginine, 100mM Tris, 2mM EDTA, 5mM reduced glutathione, and 0.5mM oxidized glutathione. The *in vitro* reaction for the Ly49i2 preparations was carried out for 72 hours at 4°C. Refolding of the RT1-A1<sup>c</sup> was achieved by first injecting dropwise 30mg/L of the commercially synthesized peptide NPRKVTAYL (GenScript; Piscataway, NJ). Then, 1 $\mu$ M of the heavy chain and 2 $\mu$ M of the rat  $\beta_2m$  were forcefully injected. The reaction stirred overnight at 4°C. The next morning, an additional 1 $\mu$ M of the heavy chain was forcefully injected, as well as in the evening. The reaction stirred overnight at 4°C.

After the folding reactions, each preparation was concentrated to a maximum 10 ml volume by ultrafiltration. The concentrate was dialyzed into 100mM Tris/NaCl buffer. The protein sample was further purified by size exclusion chromatography (SEC) on a HiLoad Superdex-75 26/60 prep grade column connected to an ÄKTA FPLC (fast protein liquid chromatography) protein purification system (located in the MBioCore, ADI; University of Alberta). Fractions corresponding to the molecular weight of each protein of interest (i.e.: Ly49i2<sub>ED</sub> or RT1-A1<sup>c</sup>) were then collected and pooled together. Each sample was then analyzed on a reducing 15% SDS-PAGE gel and visualized upon staining with coomassie blue. Protein concentration was determined by measuring absorbance at 280nm using a NanoDrop spectrophotometer (Thermo Scientific; Wilmington, DE).

## **2.10 Surface Plasmon Resonance**

Surface plasmon resonance (SPR) binding assessments of Ly49i2<sub>ED</sub> and of all the mutants with either RT1-A1<sup>c</sup> or STOK2 were determined using a Biacore™ T200 (located in the laboratory of Dr. Michalak; University of Alberta). All SPR studies were executed with HBS-EP+ buffer (GE Healthcare Life Sciences) at 25°C and a flow rate of 30  $\mu$ l/min. 10,000nM of solubilized Ly49i2 dimers (*ligand*) in 10mM sodium acetate at a pH 6.5 was immobilized onto a CM5 biosensor chip via amine coupling (GE Healthcare

Life Sciences) to a target of approximately 1000 resonance units (RUs). STOK2 or RT1-A1<sup>c</sup> (*analyte*) were then injected in a concentration series ranging from 32  $\mu\text{M}$  to 0.125  $\mu\text{M}$  or 64  $\mu\text{M}$  to 0.125  $\mu\text{M}$  in two-fold increments, respectively, flowing over the coupled (bound) Ly49i2. The interaction occurred over 60 seconds. The binding interactions were analyzed using Biacore™ T200 Software (GE Healthcare Life Sciences). Dissociation constants ( $K_D$ ) for each ligand:analyte interaction were determined by 1:1 Langmuir curve fitting.

### **2.11 Transfection of COS-7 Cells**

Transfection of COS-7 cells with various mouse Ly49s (along with DAP12 for the transfections involving activating receptors) was accomplished using the Amaxa® Nucleofector® kit for COS-7 cells (Lonza; Basel, Switzerland). Protocol outlined by the manufacturer was followed. Briefly, per reaction,  $1 \times 10^6$  COS-7 cells in PBS buffer were dispensed into separate microcentrifuge tubes and pelleted at  $500 \times g$  at  $4^\circ\text{C}$  for 10 minutes. The supernatant was removed, and the pellet was resuspended in 50  $\mu\text{l}$  of Nucleofection solution (included in the kit). In separate microcentrifuge tubes, 50  $\mu\text{l}$  of Nucleofection solution along with 5  $\mu\text{g}$  plasmid DNA was added. One tube containing cells and another tube containing the plasmid DNA were combined. Nucleofection required the W-01 program on the Amaxa nucleofector. 500  $\mu\text{l}$  of pre-warmed COS-7 cell culture medium was then added to each tube at room temperature for 10 minutes. Subsequently, nucleofected cells were transferred into 1 ml prewarmed medium in a 6-well plate. Cells were incubated and cultured at  $37^\circ\text{C}$  and 5%  $\text{CO}_2$ . After 24 hours, medium was replaced with fresh culture medium and cells were incubated and cultured for an additional 24 hours at  $37^\circ\text{C}$  and 5%  $\text{CO}_2$ . At 48 hours post-transfection, cells were harvested. Transfection efficiency of Ly49 receptors was assessed by flow cytometry. Harvested cells were also used for immunoprecipitation and Western blotting.

### **2.12 Immunoprecipitation and Western Blotting**

For immunoprecipitation, lysates of  $1 \times 10^6$  cells were incubated with anti-HA Ab for

1 hour on ice. Then, 30 $\mu$ l of Protein A Sepharose beads (GE Healthcare Life Sciences) (from a 50% bead slurry in lysis buffer) were added and to the sample and incubated for 4 hours on a rotator at 4°C. Beads were pelleted and washed three times with lysis buffer at 4°C and 8000 rpm. Beads were then resuspended in 1X reducing sample buffer incubated at 100°C for 10 minutes. Total cell lysates or immunoprecipitates were loaded onto a 15% SDS-PAGE gel, then, transferred to a polyvinylidene difluoride (PVDF) membrane.

Western blots were carried out using anti-HA or M2 primary antibodies, followed by anti-rabbit and anti-mouse HRP-coupled secondary antibodies, respectively. Visualization required ECL (PerkinElmer; Waltham, MA). Sequential Western blots were executed on the same membrane once they were treated with a stripping buffer (consisting of  $\beta$ -mercaptoethanol, SDS and Tris) and incubation of the membrane in a 56°C water bath. The order of the blots in the figures is representative of the order in which the membranes were probed with the corresponding antibodies.

### **2.13 Sequence Alignments**

Sequence alignments were carried out using MAFFT (*multiple alignment using fast fourier transform*), an online resource provided by The European Bioinformatics Institute (EMBL-EBI) (<http://www.ebi.ac.uk/Tools/msa/mafft/>).

### **2.14 Protein Structure Analysis**

Molecular images were generated with the UCSF Chimera package. Chimera is developed by the Resource for Biocomputing, Visualization, and Informatics at the University of California, San Francisco. Chimera is accessed online via the Chimera home page <http://www.cgl.ucsf.edu/chimera/>. Protein Data Bank (PDB) ID codes used are mentioned with each image in the figures section(s).

**CHAPTER III:**  
**STRUCTURAL SPECIFICITY DETERMINANTS OF THE Ly49i2 RECEPTOR**  
**FOR ITS COGNATE LIGAND RT1-A1<sup>c</sup>**

### **3.1 INTRODUCTION**

Rodent Ly49 receptors recognize their MHC class I ligands in an allele specific manner [200, 360]. Rodent (specifically mouse and rat) Ly49 genes are highly polymorphic. The structural and molecular basis of MHC class I recognition and specificity by the Ly49s, although extensively studied, is not yet completely understood. The crystal and co-crystal structure of various mouse Ly49 receptors, whether in complex with MHC class I or not, have been determined [187-189, 197, 361]; these crystal and co-crystal structures provide a significant amount of structural information about Ly49s. Structurally, the MHC class I interacting domain, the Ly49 natural killer domain (Ly49<sub>NKD</sub>) (Figure 3-1), folds into six loop regions and five  $\beta$ -strands [187]. Recognition of the Ly49 ligand, MHC class I, is determined by interactions involving the Ly49<sub>NKD</sub> L3 loop, L5 loop, strand  $\beta$ 4, and L6 loop [187]. These loop and strand regions on the receptor interact with the MHC class I at specific locations below the peptide-binding groove [187-189]. Our laboratory has demonstrated that, similar to mouse Ly49 detection of MHC class I, RT1-A1<sup>c</sup> recognition by Ly49i2 involves Ly49<sub>NKD</sub> interaction at two MHC class I locations in the  $\alpha$ 1- $\alpha$ 2 domains, subsites B and F, and at subsite C, on the  $\alpha$ 3 domain (Figure 3-2) [192].

Sequence alignments reveal that the mouse Ly49 receptors display significant polymorphism in the L6 loop and very little in the L3 loop (Figure 1-5 *A*) [187, 191]. In contrast, rat Ly49s exhibit much greater variability in the L3 loop in comparison to the L6 loop (Figure 1-5 *B*). The rat Ly49 receptors have not been as extensively studied as the mouse receptors. Rats are commonly used as models of human disease [250-257]; thus, given the diversity between mouse and rat Ly49 receptors, it is important to understand the mechanism of ligand recognition as it may vary between the mouse and the rat. The polymorphic differences observed in the various loops may be relevant to MHC class I interaction specificity.

In this chapter, I describe a role for Ly49i2 loop regions in the recognition of its cognate ligand, RT1-A1<sup>c</sup>. By using surface plasmon resonance (SPR) studies, I was able to quantitatively assess the binding interactions between various Ly49i2 chimeric receptors and the MHC class I ligand. These binding interactions allowed me to determine the significance of each loop region in ligand recognition. From my studies in this chapter, I identified the L3 loop as critical for MHC class I recognition by the inhibitory receptor Ly49i2. Furthermore, my results suggest a role for loop L6 during engagement with the receptor. Conversely, however, my data were not conclusive in assessing a role for the L5 loop during ligand:receptor contact.

## **3.2 RESULTS**

### **3.2.1 Determining the binding interaction of the rat inhibitory receptor Ly49i2 with its cognate ligand, the MHC class I molecule RT1-A1<sup>c</sup>**

The mouse Ly49 receptors have been extensively studied, including their interactions with their ligands. Rat Ly49 receptors, however, have not been as well defined, nor their engagement with their respective ligands, specifically MHC class I molecules. Ly49i2, an inhibitory receptor of the PVG rat strain, is one of the first identified rat Ly49 receptors, and it recognizes the MHC class I molecule RT1-A1<sup>c</sup> [281]. Although the specificity of Ly49i2 for RT1-A1<sup>c</sup> has been shown functionally [281], the binding interaction has yet to be characterized. The binding interaction of various NK cell receptors with their respective ligands, including mouse Ly49s, has been reported (Table 3-1). These quantitative assessments relied on surface plasmon resonance (SPR), a technique commonly used to study the binding interaction between two proteins [362]. Given the interest of the Kane laboratory and of this body of work on the association between Ly49i2 and RT1-A1<sup>c</sup>, I assessed the binding interaction between the two proteins by SPR. I hypothesized that the dissociation constant ( $K_D$ ) between the rat inhibitory receptor Ly49i2 and its cognate ligand, RT1-A1<sup>c</sup>, to be lower, thus a higher affinity, as compared to the range reported for the mouse Ly49s (Table 3-1). Our laboratory has previously shown that the interaction between Ly49i2 and RT1-A1<sup>c</sup> is difficult to disrupt with single point mutations on the MHC class I molecule [192], thus

the affinity between Ly49i2 and RT1-A1<sup>c</sup> may be higher as compared to mouse Ly49s and their ligands, resulting in a lower K<sub>D</sub>.

To test my hypothesis, I carried out an SPR analysis using a Biacore™ T200 to perform the binding interaction assay between Ly49i2 and RT1-A1<sup>c</sup> to determine their K<sub>D</sub>. Firstly, I generated soluble protein of the ectodomain (Ly49i2<sub>ED</sub>), which included the functional domain, the NKD, along with the stalk. To do so, I cloned Ly49i2<sub>ED</sub> into a pET21a expression vector and generated the corresponding inclusion bodies in *E. coli* BL21 competent cells. Once purified and solubilized, the protein was folded, concentrated, and dialyzed into a Tris/NaCl buffer. When ready, I purified Ly49i2<sub>ED</sub> by size exclusion chromatography (SEC) using FPLC (fast protein liquid chromatography) (Figure 3-3 A). Prior to SEC, a pre-FPLC sample of the Ly49i2<sub>ED</sub> was collected. The predicted molecular weight of the Ly49i2<sub>ED</sub> monomer is 25.3 KDa, hence the dimers have a predicted molecular weight of 50.6KDa. The SEC fractions corresponding to an approximate molecular weight of 50KDa, likely containing the Ly49i2 dimers (Figure 3-3 A, *grey box*), were collected, pooled, concentrated, and analyzed by SDS-PAGE. I also collected a sample of the protein aggregates (fractions C10 – D11) (Figure 3-3 A). Protein aggregation is usually the result of misfolded proteins that clump together. I ran the sample containing the pooled Ly49i2<sub>ED</sub> dimers along with the other collected samples on a 15% SDS-PAGE reducing gel (Figure 3-3 A, *right panel*). A band at the approximate molecular weight corresponding to the reduced dimers, thus the monomer molecular weight of approximately 25KDa, is detected (Figure 3-3 A, *right panel*). The pre-FPLC sample, as well as the sample for protein aggregates (Figure 3-3 A), also appear to have a band at the same molecular weight. I also produced soluble RT1-A1<sup>c</sup><sub>ED</sub>, folded with rat β<sub>2</sub>m and the peptide NPRKVTAYL. Based on peptide elution studies for RT1-A1<sup>c</sup> [363], a peptide library was created and used in the design of the composite peptide NPRKVTAYL [364]. The identities of each amino acid at each position in peptide sequences were analyzed and the most prominent were selected for the generation of the peptide with the highest affinity for RT1-A1<sup>c</sup> [364]. Subsequently, our laboratory has used the peptide in functional studies [266]. Upon completion of the folding reaction of RT1-A1<sup>c</sup><sub>ED</sub> along with rat β<sub>2</sub>m and the peptide NPRKVTAYL, I purified the RT1-A1<sup>c</sup><sub>ED</sub> complex also by SEC, resulting in a chromatogram that displays

a peak at the expected molecular weight of 47.06 KDa for the MHC class I complex (Figure 3-3 B, *grey box*). The fractions corresponding to RT1-A1<sup>c</sup><sub>ED</sub> were collected, pooled and concentrated. I analyzed the sample by SDS-PAGE under reducing conditions (Figure 3-3 B, *right panel*). The RT1-A1<sup>c</sup><sub>ED</sub> SDS-PAGE analysis resulted in two bands from the SEC sample containing the MHC class I complex (Figure 3-3 B). The first band (gel lane 2) of approximately 34 KDa corresponds to the heavy chain, while the second band (12KDa), also visible in fractions D4 – E1 (gel lane 3), identifies the rat  $\beta_2m$ . I also purified the STOK2 antibody (Ab) from the STOK2 hybridoma, which was generously provided by Dr. John T. Vaage (Oslo University Hospital, Norway). The STOK2 Ab is a monoclonal antibody of the IgG2a isotype that recognizes properly folded Ly49i2 [281, 282]. The STOK2 Ab allowed me to ensure I had properly folded Ly49i2<sub>ED</sub>.

For the binding interaction assessments via SPR, I coupled 10,000nM of Ly49i2<sub>ED</sub> in 10mM sodium acetate pH 6.5 to a CM5 biosensor chip by amine coupling, generating 1100 coupled RUs (resonance units). I then injected the STOK2 Ab as the analyte over the bound receptor in a concentration series ranging from 32 $\mu$ M to 0.125 $\mu$ M in two-fold increments, allowing the two proteins to interact for 60 seconds (Figure 3-4 A, *left panel*), resulting in a  $K_D = 0.77\mu$ M. The equilibrium binding curve (Figure 3-4 A, *right panel*), which measures the binding response at equilibrium ( $R_{eq}$ ), displays an increase in  $R_{eq}$  at each concentration. The detection of a binding interaction between Ly49i2<sub>ED</sub> and the STOK2 Ab implies that Ly49i2<sub>ED</sub> is properly folded. I then assessed the engagement of Ly49i2<sub>ED</sub> with RT1-A1<sup>c</sup><sub>ED</sub>. RT1-A1<sup>c</sup><sub>ED</sub> was injected as the analyte in a concentration series ranging from 64 $\mu$ M to 0.125 $\mu$ M in two-fold increments, allowing the two proteins to interact for 60 seconds. The resulting sensorgram (Figure 3-4 B) displays a different profile as compared to the antibody:receptor profile. Ly49i2<sub>ED</sub> binds to its ligand, RT1-A1<sup>c</sup><sub>ED</sub>, with greater affinity ( $K_D = 0.031\mu$ M) as compared to its binding with the antibody STOK2. The  $R_{eq}$  (Figure 3-4 B, *right panel*) displays an increase in  $R_{eq}$  at each concentration.

The SPR results obtained in this section, specifically the dissociation constants, were used as a reference point for the subsequent interaction assessments in the following sections.

### 3.2.2 The L6 loop in Ly49i2 may be required for RT1-A1<sup>c</sup> recognition

Our laboratory has shown that the L6 loop may have a significant role in MHC class I recognition [190]. This study was the first to validate that a loop region in Ly49 receptors may have a significant role in ligand recognition. The rat inhibitory receptor Ly49i2 recognizes the rat MHC class I molecule RT1-A1<sup>c</sup> [281]. The L6 loop in Ly49i2 contains a conserved sequence, DCGK, also found in mouse Ly49s (Figure 1-5 *A & B*), including Ly49W, a NOD mouse activating receptor (Ly49W<sup>NOD</sup>), and Ly49G, a BALB/c inhibitory receptor (Ly49G<sup>BALB/c</sup>) (Figure 1-5 *A*). We have shown that the rat RT1-A1<sup>c</sup> is a xenogeneic ligand for Ly49W<sup>NOD</sup> and Ly49G<sup>BALB/c</sup> [288]. Ly49P, a NOD mouse activating receptor, has been shown to recognize the mouse MHC class I molecule H-2D<sup>k</sup> when co-expressed with CMV-encoded m04 [365], but not the rat RT1-A1<sup>c</sup> [288]. Ly49P<sup>NOD</sup> contains the sequence NCDQ in the L6 loop, a sequence also found in Ly49A (Figure 1-5 *A*). To further corroborate our initial findings that suggest the importance of the L6 loop in ligand recognition, our laboratory subsequently substituted the L6 loop sequence NCDQ in Ly49P<sup>NOD</sup> for the DCGK sequence in the mouse Ly49W<sup>NOD</sup> receptor and rat Ly49i2 receptor, resulting in the recognition for the xenogeneic ligand RT1-A1<sup>c</sup> by Ly49P<sup>NOD</sup> [288].

Based on our previous findings, we wanted to further characterize the role of the L6 loop in RT1-A1<sup>c</sup> recognition by Ly49i2. Ly49i2, as mentioned, contains the sequence DCGK in the L6 loop, residues 249 – 252 (Figure 1-5 *B*). Furthermore, Ly49i2 residues 249 and 252, D and K, respectively, may interact with the conserved acidic residues 232 and 243 on the  $\alpha$ 3 domain of the rat MHC class I molecule [192]. Therefore, we hypothesize that DCGK are critical to confer MHC class I recognition by rat Ly49s. Given that Ly49P<sup>NOD</sup> gained recognition for RT1-A1<sup>c</sup> upon mutating its NCDQ L6 loop sequence to DCGK, I wanted to assess if Ly49i2 recognition of its ligand would be disrupted if its L6 loop DCGK sequence was mutated to reflect the Ly49P and Ly49A NCDQ sequence (Ly49i2.L6.NCDQ). As another approach, by mutating D and K to alanine residues (Ly49i2.L6.ACGA) the charges should be neutralized, thus potentially disrupting the interaction between the receptor and the ligand. To test my hypothesis, I performed SPR binding interaction studies.

Firstly, I generated soluble protein of the ectodomain of each L6 loop chimeric receptor, Ly49i2.L6.NCDQ<sub>ED</sub> and Ly49i2.L6.ACGA<sub>ED</sub>. I cloned Ly49i2.L6.NCDQ<sub>ED</sub> and Ly49i2.L6.ACGA<sub>ED</sub>, separately, into a pET21a expression vector and generated the corresponding inclusion bodies in *E. coli* BL21 competent cells. Once purified and solubilized, both proteins were folded individually, concentrated and dialyzed into a Tris/NaCl buffer for FPLC. I purified the proteins by size exclusion chromatography (SEC). For Ly49i2.L6.NCDQ<sub>ED</sub>, SEC fractions, corresponding to an approximate molecular weight of 50KDa (Figure 3-5, *grey box*), were collected, pooled, concentrated, and analyzed by SDS-PAGE. I also collected a sample corresponding to SEC fractions C10–D11, which likely correspond to protein aggregates. I ran the sample containing the Ly49i2.L6.NCDQ<sub>ED</sub> dimers along with the other collected sample, as well as a pre-FPLC sample on a 15% SDS-PAGE reducing gel (Figure 3-5, *right panel*). A band at an approximate molecular weight of 25KDa is detected in the lane corresponding to the reduced dimers (Figure 3-5, *right panel*). I then immobilized 1000 RUs of Ly49i2.L6.NCDQ<sub>ED</sub> onto a CM5 chip with 10 mM sodium acetate pH 6.5 in the same manner as executed for Ly49i2<sub>ED</sub>. I injected both the STOK2 Ab and RT1-A1<sup>c</sup><sub>ED</sub> as analytes, separately, for SPR measurements in concentration series ranging from 32μM to 0.125μM or 64μM to 0.125μM in two-fold increments, respectively, and allowed the interaction to occur for 60 seconds. Ly49i2.L6.NCDQ<sub>ED</sub> was not recognized by the STOK2 Ab (Figure 3-6 A, *left panel*); therefore no measurable association could be detected (Figure 3-6 A, *right panel*). Ly49i2.L6.NCDQ<sub>ED</sub> did not associate with the RT1-A1<sup>c</sup><sub>ED</sub> either (Figure 3-6 B, *left panel*). The STOK2 Ab and RT1-A1<sup>c</sup><sub>ED</sub> binding response at equilibrium with Ly49i2.L6.NCDQ<sub>ED</sub> (Figure 3-6 A & B, *right panels, respectively*), support the SPR sensorgram profiles.

I applied the same methodology for the assessment of the engagement of Ly49i2.L6.ACGA<sub>ED</sub> with the STOK2 Ab and RT1-A1<sup>c</sup><sub>ED</sub>. SEC fractions corresponding to an approximate molecular weight of 50KDa (Figure 3-7, *grey box*) were collected, pooled, concentrated, and analyzed by SDS-PAGE. I also collected a sample corresponding to SEC fractions C11–D12, likely corresponding to protein aggregates. I also collected fractions D11–D9. Given the chromatogram profile (Figure 3-7), the peak corresponding to fractions D11–D9 overlaps with the peak that possibly contains the

Ly49 dimers of interest. These fractions, D11–D9, may contain Ly49i2.L6.ACGA<sub>ED</sub> dimers. I ran the collected samples, as well as a pre-FPLC sample on a 15% SDS-PAGE reducing gel (Figure 3-7, *right panel*). A band at an approximate molecular weight of the reduced dimers, 25KDa, is detected in the lane corresponding to fractions D8-D5 (Figure 3-7, *right panel*). The lane containing fractions D11–D9 also has a faint band at approximately 25KDa; however, given the presence of other bands in the same lane, I decided not to use the collected D11–D9 fractions during subsequent SPR analyses. I then proceeded to immobilize 1000 RUs of Ly49i2.L6.ACGA<sub>ED</sub> onto a CM5 chip with 10 mM sodium acetate pH 6.5, as outlined for Ly49i2<sub>ED</sub>. I injected both the STOK2 Ab in a concentration series ranging from 32 $\mu$ M to 0.125 $\mu$ M in two-fold increments, and allowed the interaction to occur for 60 seconds (Figure 3-8 *A*). The interaction between Ly49i2.L6.ACGA<sub>ED</sub> and the STOK2 Ab resulted in a  $K_D = 0.318\mu$ M, an affinity of approximately double of that observed for Ly49i2<sub>ED</sub> with STOK2 (Figure 3-4 *A*). The binding response at equilibrium ( $R_{eq}$ ) displays an increase in  $R_{eq}$  at each concentration (Figure 3-8 *A, right panel*). Successively, I then injected both RT1-A1<sup>c</sup><sub>ED</sub> as the analyte for SPR measurements in a concentration series ranging from 64 $\mu$ M to 0.125 $\mu$ M in two-fold increments and allowed the interaction to occur for 60 seconds. The interaction with RT1-A1<sup>c</sup><sub>ED</sub> and Ly49i2.L6.ACGA<sub>ED</sub> generated a  $K_D = 6.96 \mu$ M (Figure 3-8 *B*), approximately a 224-fold difference when compared to Ly49i2<sub>ED</sub>.

The results in this section show that the STOK2 Ab recognized Ly49i2.L6.ACGA<sub>ED</sub> with similar affinity as Ly49i2<sub>ED</sub>, implying that the mutant likely folded properly. Interestingly, however, was the observed 224-fold difference in the binding of RT1-A1<sup>c</sup><sub>ED</sub> by Ly49i2.L6.ACGA<sub>ED</sub> and Ly49i2<sub>ED</sub>. The affinity of the wildtype receptor was much greater as compared to the L6 loop mutant Ly49i2.L6.ACGA<sub>ED</sub>, suggesting that neutralized residues at positions at 249 and 252, in the substitution of D and K for A, respectively, interrupt the interaction with the MHC class I molecule RT1-A1<sup>c</sup>, thus are important in conferring ligand recognition by the Ly49i2 receptor. The other L6 loop mutant did not engage with either the antibody or the ligand. The lack of association between Ly49i2.L6.NCDQ<sub>ED</sub> and the STOK2 Ab limits the interpretation of the results obtained from the interaction between Ly49i2.L6.NCDQ<sub>ED</sub> and RT1-A1<sup>c</sup><sub>ED</sub>. Nonetheless, the SPR results from the engagement

of Ly49i2.L6.ACGA<sub>ED</sub> with RT1-A1<sup>c</sup> suggest that the L6 loop may be required for ligand recognition.

### **3.2.3 A requirement for the L5 loop of Ly49i2 for RT1-A1<sup>c</sup> recognition is inconclusive**

Most rat Ly49 receptors, including Ly49i2, along with all mouse group II Ly49 receptors (Ly49A-like members), conserve two residues on the L5 loop, S241 and T243 in Ly49i2 and S236 and T238 in Ly49A (Figure 1-5). In addition, the only member of mouse Ly49 group III, Ly49Q, also conserves S236 and T238 (Figure 1-5 A). Ly49Q is not found on NK cells; this inhibitory receptor is expressed on macrophage cells and subsets of dendritic cells [366, 367]. The conserved L5 residues in mouse NK cell receptors are critical for MHC class I recognition [187]. Given the conservation of these two residues in the same loop region in two related rodent species, we hypothesize that S241 and T243 on the rat L5 loop of Ly49i2 makes a contribution to MHC class I detection.

To assess the role of the L5 loop in rat ligand specificity, I mutated the serine and threonine at position 241 and 243, respectively, to an alanine residue, resulting in three mutant receptors: Ly49i2.S241A, Ly49i2.T243A, and Ly49i2.S241A.T243A. Generating a Ly49i2 mutant with only one altered residue allowed me to assess the contribution made by each residue to ligand recognition by Ly49i2. The double mutant, Ly49i2.S241A.T243A, will help assess if both residues are required in concert for ligand detection. Relying on the same methodology outlined in section 4.2.1 for wildtype Ly49i2, I investigated the importance of the L5 loop in Ly49i2 recognition of its MHC class I ligand, RT1-A1<sup>c</sup>, using SPR kinetic analyses. I produced soluble proteins by first cloning the ectodomain of the three mutants, Ly49i2.S241A<sub>ED</sub>, Ly49i2.T243A<sub>ED</sub>, and Ly49i2.S241A.T243A<sub>ED</sub>, into a pET21a vector, individually, for BL21 *E. coli* competent cell transformation, which resulted in the generation of inclusion bodies. Once purified and solubilized, all three soluble proteins were folded separately, concentrated and dialyzed for protein purification by SEC. For Ly49i2.S241A<sub>ED</sub>, the SEC fractions consistent with an approximate molecular weight of 50KDa, likely corresponding to Ly49i2.S241A<sub>ED</sub> dimers, were collected (Figure 3-9, *grey box*). I also collected fractions

C11-D12, likely corresponding to protein aggregates, as well as fractions D12-D9 (Figure 3-9). The latter fractions were collected because the SEC chromatogram displays a peak that overlaps with fractions D8-D6, the fractions of interest, thus D12-D9 may contain the protein of interest, Ly49i2.S241A<sub>ED</sub> dimers. I then pooled, concentrated, and analyzed the fractions by SDS-PAGE (Figure 3-9, *right panel*). A band of approximate molecular weight 25KDa is visible on the reducing gel in the lane containing fractions D8-D6. Given the predicted molecular weight of the Ly49i2.S241A<sub>ED</sub> dimers to be 50.6KDa, the band likely reflect the reduced dimers, thus the monomer molecular weight of 25KDa (Figure 3-9, *right panel*). The other two samples collected, including the pre-FPLC sample include multiple bands. The D12-D9 fractions will not be used for SPR as the lane displays several bands that are not of interest to this study (Figure 3-9, *right panel*). Subsequently, I immobilized 1000 RUs of the Ly49i2.S241A<sub>ED</sub> receptor onto a CM5 chip with 10 mM sodium acetate pH 6.5, following the same method I carried out for Ly49i2<sub>ED</sub>. I first injected the STOK2 Ab, followed by RT1-A1<sup>c</sup><sub>ED</sub>, separately, as analytes for SPR analyses in concentration series ranging from 32μM to 0.125μM or 64μM to 0.125μM in two-fold increments, respectively, and allowed the interaction to occur for 60 seconds in a Biacore™ T200. Ly49i2.S241A<sub>ED</sub> was not recognized by the STOK2 Ab (Figure 3-10 A, *left panel*), thus the binding response at equilibrium ( $R_{eq}$ ), where an increase in RUs at each concentration level results from the interaction of two proteins, did not display any interaction either (Figure 3-10 A, *right panel*). Due to the lack of interaction between Ly49i2.S241A<sub>ED</sub> and the STOK2 Ab, no measureable dissociation constant ( $K_D$ ) resulted. The same outcome was observed for the binding assessment between RT1-A1<sup>c</sup><sub>ED</sub> with Ly49i2.S241A<sub>ED</sub> (Figure 3-10 B, *left panel*), a result supported by the binding response at equilibrium, resulting in no measureable  $K_D$  (Figure 3-10 B, *right panel*).

To determine the significance of the Ly49i2 T243 residue during receptor-ligand interaction, I carried out the same procedure for Ly49i2.T243A<sub>ED</sub> as outlined for Ly49i2.S241A<sub>ED</sub>. After separation by FPLC, I collected the SEC fractions consistent with an approximate molecular weight of 50KDa that likely correspond to Ly49i2.T243A<sub>ED</sub> dimers (Figure 3-11, *grey box*). I also collected fractions C9-D12, corresponding to protein aggregates (Figure 3-11). After pooling and concentrating the

samples separately, I analyzed them SDS-PAGE (Figure 3-11, *right panel*). A band of approximate molecular weight 25KDa is visible on the reducing gel in the lane containing the fractions of interest, D11-D6. These fractions likely contain the Ly49i2.T243A<sub>ED</sub> dimers, thus upon being subjected to reducing conditions, the band likely reflects the reduced dimers, thus the monomer molecular weight of 25KDa (Figure 3-11, *right panel*). The other collected sample, including the pre-FPLC sample, display multiple bands (Figure 3-11, *right panel*). I then immobilized 1000 RUs of Ly49i2.T243A<sub>ED</sub> onto a CM5 chip with 10 mM sodium acetate pH 6.5, following the same procedure I executed for Ly49i2<sub>ED</sub>. Firstly, I injected the STOK2 Ab in a concentration series ranging from 32μM to 0.125μM in two-fold increments, allowing the interaction to occur for 60 seconds. Ly49i2.T243A<sub>ED</sub> did not interact with the STOK2 Ab (Figure 3-12 A, *left panel*), thus the binding response at equilibrium did not display an interaction either at any of the concentrations (Figure 3-12 A, *right panel*). RT1-A1<sup>c</sup><sub>ED</sub> was then introduced as the analyte for SPR analysis in a concentration series ranging from 64μM to 0.125μM in two-fold increments for 60 seconds. This interaction between Ly49i2.T243A<sub>ED</sub> and RT1-A1<sup>c</sup><sub>ED</sub> is slightly detected at two highest RT1-A1<sup>c</sup><sub>ED</sub> concentrations (Figure 3-12 B, *left panel*), an observation supported by the binding response curve at equilibrium (Figure 3-12 B, *right panel*); however, the interaction was not sufficient to result in a measureable dissociation constant ( $K_D$ ).

Lastly, I assessed the importance of S241 and T243, together, for RT1-A1<sup>c</sup> recognition by Ly49i2. Once the Ly49i2.S241A.T243A<sub>ED</sub> preparation had been separated by FPLC, I collected the SEC fractions corresponding to an approximate molecular weight of 50KDa that likely correspond to Ly49i2.S241A.T243A<sub>ED</sub> dimers (Figure 3-13, *grey box*). I also collected fractions C11-D12, likely corresponding to protein aggregates (Figure 3-13). After pooling and concentrating the samples separately, I analyzed them by SDS-PAGE (Figure 3-13, *right panel*). A band at the approximate molecular weight of 25KDa is visible on the reducing gel in the lane containing fractions D11-D7. These fractions likely contain the Ly49i2.S241A.T243A<sub>ED</sub> dimers, thus upon being reduced, the band likely reflects the reduced dimers, equivalent to the monomer molecular weight of 25KDa (Figure 3-13, *right panel*). The other collected fractions, including the pre-FPLC sample, display multiple bands that are not of interest to this study (Figure 3-13, *right*

*panel*). Subsequently, I immobilized 1000 RUs of the Ly49i2.S241A.T243A<sub>ED</sub> onto a CM5 chip with 10 mM sodium acetate pH 6.5, following the same method I carried out for Ly49i2<sub>ED</sub>. Then, I injected the STOK2 Ab, and in a separate set up, RT1-A1<sup>c</sup><sub>ED</sub>, as analytes for SPR analyses in concentration series ranging from 32μM to 0.125μM or 64μM to 0.125μM in two-fold increments, respectively, and allowed the interaction to occur for 60 seconds. The STOK2 Ab did not bind with Ly49i2.S241A.T243A<sub>ED</sub> (Figure 3-14 A, *left panel*), an observation supported by the binding response at equilibrium graph that did not display any interaction either (Figure 3-14 A, *right panel*). The SPR sensorgram for the interaction between Ly49i2.S241A.T243A<sub>ED</sub> and RT1-A1<sup>c</sup><sub>ED</sub> also did not display any binding between the two proteins (Figure 3-14 B, *left panel*). The binding response at equilibrium plot did not display any increase in RUs at the various concentrations either (Figure 3-14 B, *right panel*), a result consistent with the SPR sensorgram. As a result of the lack of interaction between the Ly49i2.S241A.T243A<sub>ED</sub> with the STOK2 Ab and RT1-A1<sup>c</sup><sub>ED</sub>, no measureable dissociation constants ( $K_D$ ) resulted, respectively.

The results in this section are inconclusive. The lack of recognition of each of the L5 loop Ly49i2 mutant receptors by the STOK2 Ab suggests the possibility that each protein may not have been folded properly, thus potentially inhibiting the binding of the antibody to the epitope on the Ly49i2 mutant receptors. Another possibility is that the L5 loop mutants are properly folded, but cannot be recognized by the STOK2 Ab as the epitope for the antibody may be within the L5 loop. As a result, the lack of interaction of each mutant receptor with the cognate ligand, RT1-A1<sup>c</sup>, cannot be interpreted. Further studies are required to determine if indeed the L5 loop is required for ligand recognition by the receptor.

### **3.2.4 The Ly49i2 L3 loop is critical for RT1-A1<sup>c</sup> recognition**

The rat genome encodes at least 26 functional Ly49 genes [181]. To date, only the rat PVG strain inhibitory receptor, Ly49i2, has been shown to distinguish MHC class I in an allele specific manner, recognizing RT-1A1<sup>c</sup> as its cognate ligand [281]. Ly49i2 is an inhibitory receptor and a member of block II of three Ly49 gene blocks [181]. The

ligand interacting loop regions in the NKD of Ly49i2 display closely related protein sequences with other block II members, including other PVG strain Ly49s, such as the inhibitory Ly49i5 receptor, and the activating receptors Ly49s5 and Ly49s3 (Figure 1-5 B). Despite the close proximity in protein sequence alignment, Ly49i5, Ly49s5, and Ly49s3 have been shown to recognize undefined non-classical MHC class Ib molecule(s). Ly49i5 and Ly49s5 both recognize similar allogeneic RT1-CE MHC class Ib ligands encoded by the *u* rat haplotype, while Ly49i5 further recognizes the *l* rat haplotype [244]. Furthermore, unlike the traditional NK cell response against virally infected or transformed target cells, Ly49s5 has been shown to play a role in stimulating innate immune responses due to an upregulation of MHC class Ib molecules resulting from *Listeria monocytogenes* infections of intestinal epithelial cells [64, 65]. Although Ly49s3 has also been shown to identify non-classical MHC class I molecules, its specificity is for the *n*, *av1*, *lv1* and *c* haplotypes [201].

An amino acid sequence alignment of the rat Ly49i2, Ly49i5, Ly49s5, and Ly49s3 reveals that the L3 loop residues are highly variable compared to those in the mouse and between these rat Ly49 receptors, while the L5 and L6 loops are highly conserved in these rat receptors (Figure 1-5). Intriguingly, all four rat Ly49s exhibit different MHC specificities. I hypothesize that the variable L3 loop dictates ligand recognition by the rat Ly49 receptors. Specifically, the L3 loop residues dictate specificity for the Ly49i2 cognate ligand, RT1-A1<sup>c</sup>. To test my hypothesis, I used the same methodology outlined in the previous sections. Briefly, the binding kinetics between various mutants of Ly49i2 with RT1-A1<sup>c</sup> were determined using a Biacore™ T200 for SPR studies. Firstly, I replaced the L3 loop residues in the ectodomain of the Ly49i2 receptor with the L3 loop sequence of Ly49i5, Ly49s5, and Ly49s3, individually, resulting in the chimeras Ly49i2.L3.i5<sub>ED</sub>, Ly49i2.L3.s5<sub>ED</sub>, and Ly49i2.L3.s3<sub>ED</sub>, respectively. Then, I cloned all three chimeras into pET21a, separately, followed by BL21 transformation for the generation of inclusion bodies. Next, I purified and solubilized each individual mutant protein for individual folding reactions, followed by buffer exchange for further protein purification via FPLC.

The Ly49i2.L3.s3<sub>ED</sub> SEC fractions corresponding to an approximate molecular weight of 50KDa were collected, pooled, and concentrated (Figure 3-15, *grey box*).

These fractions, D11-D7, likely contain the Ly49i2.L3.s3<sub>ED</sub> dimers since the predicted molecular weight of the chimeric receptor is approximately 50KDa. I also collected, pooled and concentrated fractions C10-D12, which probably contain protein aggregates (Figure 3-15). Both collected samples were analyzed for protein content via SDS-PAGE. The lane used to run the SEC fractions D11-D7, which likely contain the Ly49i2.L3.s3<sub>ED</sub> dimers, displays a band at an approximate molecular weight of 25KDa (Figure 3-15, *right panel*), consistent with reduced Ly49i2 dimers, the molecular weight of a Ly49i2 monomer. I then immobilized approximately 1000 RUs of Ly49i2.L3.s3<sub>ED</sub> onto a CM5 chip with 10 mM sodium acetate pH 6.5, following the same method I carried out for Ly49i2<sub>ED</sub>. I injected the STOK2 Ab as the analyte in a concentration series ranging from 32 $\mu$ M to 0.125 $\mu$ M in two-fold increments, and allowed the interaction to occur for 60 seconds. The STOK2 Ab bound with Ly49i2.L3.s3<sub>ED</sub> resulted in the sensorgram profile displayed (Figure 3-16 A, *left panel*). The binding response at equilibrium ( $R_{eq}$ ) displays an increase in RUs at each concentration level, with the exception of highest concentration (32 $\mu$ M) of the antibody which resulted in similar RUs as the second highest concentration of the STOK2 Ab used, 16 $\mu$ M (Figure 3-16 A, *right panel*). The binding interactions between Ly49i2.L3.s3<sub>ED</sub> and the STOK2 Ab resulted in a  $K_D = 0.11\mu$ M (Figure 3-16 A, *right panel*). Ly49i2.L3.s3<sub>ED</sub> was also subjected to RT1-A1<sup>c</sup><sub>ED</sub> as the analyte, injected in a concentration series ranging from 64 $\mu$ M to 0.125 $\mu$ M in two-fold increments, and allowed to interact for 60 seconds. The resulting SPR sensorgram did not display any interaction between the two proteins (Figure 3-16 B, *left panel*). The binding response at equilibrium also did not display an increase in RUs at each concentration level (Figure 3-16 B, *right panel*). Hence, the lack of binding between Ly49i2.L3.s3<sub>ED</sub> and RT1-A1<sup>c</sup><sub>ED</sub> did not result in a measureable  $K_D$  (Figure 3-16 B, *right panel*).

For the Ly49i2.L3.s5<sub>ED</sub> chimeric receptor, after solubilization, I also further purified it by FPLC. I collected the SEC fractions corresponding to an approximate molecular weight of 50KDa (Figure 3-17, *grey box*), pooled, and concentrated them. These fractions, D11-D8, likely contain the Ly49i2.L3.s5<sub>ED</sub> dimers given the predicted molecular weight of the chimeric receptor to be around 50KDa. I also collected, pooled and concentrated fractions C11-D12, likely containing protein aggregates (Figure 3-17).

Both collected samples, along with a pre-FPLC sample, were analyzed for protein content via SDS-PAGE. The lane used to run the SEC fractions D11-D7, which likely contain the Ly49i2.L3.s<sub>ED</sub> dimers, displays a band at an approximate molecular weight of 25KDa (Figure 3-17, *right panel*), consistent with reduced Ly49i2 dimers, the molecular weight of a Ly49i2 monomer. For SPR analysis, I immobilized roughly 1000 RUs of Ly49i2.L3.s<sub>ED</sub> onto a CM5 chip with 10 mM sodium acetate pH 6.5, following the same method I executed for Ly49i2<sub>ED</sub>. I injected the STOK2 Ab as the analyte in a concentration series ranging from 32μM to 0.125μM in two-fold increments, and allowed the interaction to occur for 60 seconds. The binding interaction between the STOK2 Ab and Ly49i2.L3.s<sub>ED</sub> was detected (Figure 3-18 *A, left panel*). The binding response at equilibrium displays an increase in RUs at each concentration level, with the exception of the three highest concentrations of the antibody, 8μM, 16μM, and 32μM, which resulted in similar RUs (Figure 3-18 *A, right panel*). The binding interactions between Ly49i2.L3.s<sub>ED</sub> and the STOK2 Ab resulted in a  $K_D = 0.37\mu\text{M}$  (Figure 3-18 *A, right panel*). Ly49i2.L3.s<sub>ED</sub> was also subjected to RT1-A1<sup>c</sup><sub>ED</sub> as the analyte, injected in a concentration series ranging from 64μM to 0.125μM in two-fold increments, and allowed to interact for 60 seconds. The interaction between Ly49i2.L3.s<sub>ED</sub> and RT1-A1<sup>c</sup><sub>ED</sub> is slightly detected at the highest RT1-A1<sup>c</sup><sub>ED</sub> concentration (Figure 3-18 *B, left panel*), an observation supported by the binding response curve at equilibrium (Figure 3-18 *B, right panel*); however, the interaction was not sufficient to result in a measureable dissociation constant ( $K_D$ ).

In continuing to assess the role of the L3 loop of Ly49i2 during engagement with RT1-A1<sup>c</sup>, I also assessed the Ly49i2.L3.i<sub>ED</sub> mutant for its ability to recognize the MHC class I molecule. Once I had purified the inclusion bodies and solubilized the protein, I further purified it by SEC using FPLC. As previously described for the other Ly49i2 mutants, I collected the SEC fractions corresponding to an approximate molecular weight of 50KDa (Figure 3-19, *grey box*), pooled, and concentrated them. These fractions, D11-D5, possibly contain the Ly49i2.L3.i<sub>ED</sub> dimers given the predicted molecular weight of the chimeric receptor to be around 50KDa. I also collected, pooled and concentrated the protein aggregates fractions, C10-D12 (Figure 3-19, *left panel*). Both collected samples, along with a pre-FPLC sample, were analyzed for protein content by

SDS-PAGE. The lane with the SEC fractions D11-D5, which likely contain the Ly49i2.L3.i5<sub>ED</sub> dimers, displays a band at an approximate molecular weight of 25KDa (Figure 3-19, *right panel*), consistent with reduced Ly49i2 dimers, the molecular weight of a Ly49i2 monomer. The band is very faint, but is present. Then, I immobilized approximately 1000 RUs of Ly49i2.L3.i5<sub>ED</sub> onto a CM5 chip with 10 mM sodium acetate pH 6.5, following the same method I carried out for Ly49i2<sub>ED</sub>. I injected the STOK2 Ab as the analyte in concentration series ranging from 32 $\mu$ M to 0.125 $\mu$ M in two-fold increments, and allowed the interaction to occur over 60 seconds in a Biacore<sup>TM</sup> T200. Consistent with the other L3 loop mutants, the STOK2 Ab bound with Ly49i2.L3.i5<sub>ED</sub> (Figure 3-20, *left panel*). The binding response at equilibrium ( $R_{eq}$ ) displays an increase in RUs at each concentration level, with the exception of highest concentration (32 $\mu$ M) of the antibody which resulted in similar RUs as the second highest concentration of the STOK2 Ab used, 16 $\mu$ M (Figure 3-20 *A, right panel*). The interaction between these two proteins, Ly49i2.L3.i5<sub>ED</sub> and the STOK2 Ab, resulted in  $K_D = 0.26 \mu\text{M}$  (Figure 3-20 *A, right panel*). Subsequently, Ly49i2.L3.i5<sub>ED</sub> was also subjected to RT1-A1<sup>c</sup><sub>ED</sub> as the analyte, injected in a concentration series ranging from 64 $\mu$ M to 0.125 $\mu$ M in two-fold increments, and allowed to interact for 60 seconds. The interaction between Ly49i2.L3.i5<sub>ED</sub> and RT1-A1<sup>c</sup><sub>ED</sub> was not detected (Figure 3-20 *B, left panel*), a result supported by the binding response curve at equilibrium (Figure 3-20 *B, right panel*). Due to the lack of binding between Ly49i2.L3.i5<sub>ED</sub> and RT1-A1<sup>c</sup><sub>ED</sub>, the dissociation constant ( $K_D$ ) could not be determined (Figure 3-20 *B, right panel*).

To corroborate the findings described above, I decided to further test the significance of the L3 loop of Ly49i2 for granting RT1-A1<sup>c</sup> recognition by exchanging the L3 loop region of Ly49i2 and insert it into the L3 loop region of the Ly49i5 receptor, generating the mutant receptor Ly49i5.L3.i2. Upon careful examination of the L3 loop sequences between Ly49i2, Ly49i5, Ly49s5, and Ly49s3 (Figure 1-5 *B*), Ly49i2 and Ly49i5 share the most amino acid identity. If the L3 loop is indeed required for ligand recognition, the molecular requirements are likely within the non-conserved amino acids within the L3 loop of the receptors (Figure 1-5 *B*). Ly49i2, as described above, recognizes the MHC class Ia molecule RT1-A1<sup>c</sup> [281], whereas Ly49i5 has been shown to recognize allogeneic RT1-CE MHC class Ib ligands encoded by the *u* and *l* rat

haplotype [244]. Given the different ligand specificities, I hypothesized that Ly49i5.L3.i2 could only recognize RT1-A1<sup>c</sup> if the L3 loop is required for ligand recognition upon engagement with the Ly49i2 receptor. To test my hypothesis, I performed the same methodology as described for Ly49i2<sub>ED</sub>, including all of the various loop mutants. I performed an SPR analysis using a Biacore<sup>TM</sup> T200 to assess the binding interaction between Ly49i5.L3.i2 and RT1-A1<sup>c</sup> and determine their dissociation constant ( $K_D$ ). Firstly, I generated soluble protein of the ectodomain of the mutant protein by cloning Ly49i5.L3.i2<sub>ED</sub> into a pET21a expression vector and generated inclusion bodies in *E. coli* BL21 competent cells. Once purified and solubilized, I folded the protein, concentrated it, and dialyzed it into a Tris/NaCl buffer. I purified Ly49i5.L3.i2<sub>ED</sub> by SEC using FPLC (Figure 3-21). The predicted molecular weight of the Ly49i5.L3.i2<sub>ED</sub> monomer is 16.5KDa, hence the dimers have a predicted molecular weight of 33KDa. The SEC fractions corresponding to an approximate molecular weight of 33KDa, likely containing the Ly49i5.L3.i2<sub>ED</sub> dimers (Figure 3-21, *grey box*), were collected, pooled, concentrated, and analyzed by SDS-PAGE. I ran the sample containing the pooled Ly49i5.L3.i2<sub>ED</sub> dimers along with a pre-FPLC sample on a 15% SDS-PAGE reducing gel (Figure 3-21, *right panel*). A band at the approximate molecular weight corresponding to the reduced dimers, the monomer molecular weight of approximately 16.5KDa, is detected (Figure 3-21, *right panel*). For the binding interaction assessment via SPR, I coupled 10,000nM of Ly49i5.L3.i2<sub>ED</sub> in 10mM sodium acetate pH 6.5 to a CM5 biosensor chip by amine coupling, generating around 1000 coupled RUs. I then injected RT1-A1<sup>c</sup><sub>ED</sub> as the analyte in a concentration series ranging from 64 $\mu$ M to 0.125 $\mu$ M in two-fold increments, allowing the two proteins to interact for 60 seconds. The resulting sensorgram (Figure 3-22, *left panel*) displays a binding interaction similar to the profile resultant from the interaction between Ly49i2<sub>ED</sub> and RT1-A1<sup>c</sup><sub>ED</sub>. The binding response curve at equilibrium,  $R_{eq}$ , supports the sensorgram with an increase in RUs at each RT1-A1<sup>c</sup><sub>ED</sub> concentration (Figure 3-22, *right panel*). The binding of Ly49i5.L3.i2<sub>ED</sub> with RT1-A1<sup>c</sup><sub>ED</sub> resulted in  $K_D = 2.77\mu$ M, a 90-fold increase in  $K_D$ , thus a 90-fold decrease in affinity, as compared to Ly49i2<sub>ED</sub> and RT1-A1<sup>c</sup><sub>ED</sub>. Nonetheless, a partial restoration of binding was observed, and although the affinity is 90-fold less as compared to Ly49i2<sub>ED</sub> and RT1-A1<sup>c</sup><sub>ED</sub>, the  $K_D$  obtained is comparable to mouse Ly49s for their MHC class I

ligands (Table 3-1).

The STOK2 Ab only recognizes properly folded Ly49i2 [281, 282]; therefore, I could not use the antibody to verify the folding of Ly49i5.L3.i2<sub>ED</sub>. Furthermore, the Ly49i2 L3 loop mutants were all recognized by the STOK2 Ab; therefore, the epitope for the Ab is likely not within the L3 loop. Hence, the Ly49i5 receptor, even with the L3 loop of Ly49i2, would likely not be recognized by the STOK2 Ab. In addition, a commercial antibody for Ly49i5 is not available; thus, I was unable to verify the folding of Ly49i5.L3.i2<sub>ED</sub>. The partial restoration of binding between Ly49i5 chimeric receptor and RT1-A1<sup>c</sup> implies the possibility of properly folded Ly49i5.L3.i2. Our lab has previously shown that contact by Ly49i2 at a minimum of two subsites on the MHC class I molecule (Figure 3-2) is required for ligand recognition [192]. The MHC class I subsites B, F, and C interact with the L3, L5, and L6 loops of Ly49i2, respectively (Figure 4-2). Sequence alignment of Ly49i2 and Ly49i5 shows 100% amino acid sequence identity between both receptors in the L5 and L6 loops (Figure 1-5 B). Taken together, the observed partial restoration of binding to RT1-A1<sup>c</sup> by Ly49i5.L3.i2 likely resulted from the proper folding of the chimeric receptor.

The outcomes in this section display a binding profile and K<sub>D</sub> of the Ly49i2 L3 loop mutant receptors with the STOK2 Ab similar to the wildtype Ly49i2 receptor. Intriguingly, however, the SPR data resultant from the interactions between the Ly49i2 L3 loop mutants and RT1-A1<sup>c</sup> did not result in the same binding profile as compared to the wildtype receptor. In fact, all three mutants, Ly49i2.L3.i5<sub>ED</sub>, Ly49i2.L3.s5<sub>ED</sub>, and Ly49i2.L3.s3<sub>ED</sub> did not bind with the ligand, thus no K<sub>D</sub> could be obtained. Furthermore, the reverse mutant, Ly49i5.L3.i2<sub>ED</sub> recognized RT1-A1<sup>c</sup>, albeit a 90-fold decrease in affinity as compared to wildtype Ly49i2, but within the range for mouse Ly49 and their respective ligands (Table 3-1). Taken together, these results strongly suggest a critical role for the L3 loop residues in the recognition of the MHC class I molecule, RT1-A1<sup>c</sup>, by the inhibitory rat receptor Ly49i2.

### 3.3 DISCUSSION

Effective NK cell function requires the regulation of the balance of signals resulting from the engagement of its cell surface receptors with their respective cognate ligands. Various receptors, such as Ly49s in rodents, and the KIR family in humans, recognize their ligand in an allele specific manner, resulting from an interaction between various structural components on both the target cell ligand and effector cell receptor. The precise molecular determinants of this interaction have been extensively studied in humans and mice, but not in rats.

Surface plasmon resonance (SPR) is a technique that allows for the detection and kinetic assessment of the molecular interactions between two proteins in real time [368]. The ability to assess the engagement of two protein without any labels or tags, relying on simply binding one molecule (termed the ligand) onto a surface via amine coupling, one of the most common covalent immobilization methods, and allowing a second protein (termed the analyte) to flow over and interact with the ligand, allows for quantitative assessments to be determined, such as the dissociation constant ( $K_D$ ), a measure of binding affinity [369].

In this report, I assessed various structural loop regions for their significance in MHC class I recognition by the rat inhibitory receptor, Ly49i2. Upon purifying and solubilizing the various Ly49 mutants, I was able to examine their interaction with MHC class I molecule, RT1-A1<sup>c</sup> via SPR. By generating mutants for each Ly49 loop region being tested, I was able to approach the role of each structural loop for its contribution to ligand recognition. I proposed that the L6, L5 and L3 loops all play a role in ligand detection by the receptor. Using SPR technology, I was able to determine that the L6 loop may be important for detection of the ligand during its engagement with the receptor. I was not able to ascertain the role of the L5 loop, however. Interestingly, the experimental outcomes demonstrate a critical role for the L3 loop in recognition of the rat MHC class I molecule, RT1-A1<sup>c</sup>, by the rat inhibitory receptor Ly49i2.

The binding assessment of any rat Ly49 receptor with its ligand has yet to be reported. Ly49i2 is the first rat inhibitory receptor to be identified along with its associated ligand, the MHC class I molecule, RT1-A1<sup>c</sup> [281]. STOK2 is a monoclonal

antibody that specifically recognizes properly folded Ly49i2, although the exact epitope has not been mapped [281, 282]. In this study, I assessed and reported the binding affinity for wildtype Ly49i2, as well as various Ly49i2 mutants upon engagement with RT1-A1<sup>c</sup> and the STOK2 Ab, individually. The experiments in this chapter required the generation of many chimeric receptors, thus using the STOK2 Ab as an SPR analyte provided the study with a means of assessing properly folded Ly49i2 proteins. For the Ly49i5.L3.i2 mutant, however, I was unable to do the same. The STOK2 Ab only recognizes Ly49i2, and, with no commercial antibodies available, I was unable to assess the folding of the Ly49i5 mutant. Nonetheless, Ly49i5.L3.i3 was likely folded properly, as suggested by the partial restoration of binding observed between the Ly49i5.L3.i2 chimeric receptor and RT1-A1<sup>c</sup>. The Ly49i2 L3 loop mutants were all recognized by the STOK2 Ab, implying that the epitope for the Ab is likely not within the L3 loop. Furthermore, our laboratory has previously shown that contact by Ly49i2 at a minimum of two subsites on the MHC class I molecule (Figure 3-2) is required for ligand recognition [192]. The MHC class I subsites B, F, and C interact with the L3, L5, and L6 loops of Ly49i2, respectively (Figure 3-2). In addition, the sequence alignment of Ly49i2 and Ly49i5 shows 100% amino acid sequence identity between Ly49i2 and Ly49i5 in the L5 and L6 loops (Figure 1-5 *B*). The SPR data involving the Ly49i2 L3 loop mutants did not result in a binding interaction, suggesting that the L3 loop is required for recognition of the ligand. Therefore, Ly49i5.L3.i2 was likely properly folded.

Various mouse Ly49s have been studied for their binding affinities to their respective ligands. Dissociation constants ( $K_D$ ) for the interaction between the inhibitory mouse Ly49A receptor and H-2D<sup>d</sup> have been reported to range between 1.8 – 4.4 $\mu$ M (Table 3-1) [187, 370]. On the other hand, Ly49C association with either H-2K<sup>b</sup> or H-2D<sup>d</sup> has resulted in  $K_D$  values of 80 – 102 $\mu$ M and 136  $\mu$ M, respectively (Table 3-1) [189]. In this chapter, the Ly49i2  $K_D$  values for its interaction with the STOK2 Ab is 0.77  $\mu$ M, and 0.031  $\mu$ M for its engagement with RT1-A1<sup>c</sup>. These results suggest that the rat inhibitory receptor Ly49i2 has a stronger binding affinity for its MHC class I ligand as compared to its mouse counterparts, Ly49A and Ly49C for their MHC class I partners. Furthermore, Ly49i2 appears to associate with RT1-A1<sup>c</sup> with greater affinity than with its

specific antibody. Other studies assessing the binding interaction between additional mouse Ly49s, such as Ly49G and Ly49W, an inhibitory and activating receptor shown to recognize the same ligands, H-2D<sup>d</sup> and H-2D<sup>k</sup>, have reported K<sub>D</sub> ranging from 46.1 - 48.3 μM and 13.6 – 22.9 μM, respectively (Table 3-1) [371]. These values are comparable to other mouse Ly49:MHC class I engagement K<sub>D</sub> values, such as the ones identified for Ly49A and Ly49C. Both mouse and rat lineage divergence occurred from a common ancestor at approximately the same time [372]. Phylogenetic studies suggest that the common ancestor already possessed various *Ly49* genes that simply expanded post divergence [167]. Thus, there is no evolutionary evidence to suggest a lower K<sub>D</sub>, thus higher affinity, for rat Ly49:MHC class I interactions as compared to its mouse counterpart. KIRs, human NK cell receptors functionally analogous to Ly49s, engage their ligands with affinities ranging from 0.015 - 7.2μM (Table 3-1) [373-375]. Ly49i2 binds its ligand, RT1-A1<sup>c</sup>, with an affinity comparable to KIR and HLA-C interactions (Table 3-1) [374]. Additionally, other NK cell receptors, the heterodimers CD94/NKG2A/C/E, have been shown to engage HLA-E with binding affinities of 0.53 – 56.6μM, 3.8 – 120.0μM, and 0.72 – 22.9μM, respectively (Table 3-1) [376, 377]. CD94/NKG2 display lower affinities for their ligands as compared to the K<sub>D</sub> reported in this chapter for Ly49i2 and RT1-A1<sup>c</sup>. The rat Ly49 receptor displays a much stronger affinity for its ligand as compared to various other NK cell receptors, with the exception of KIR for HLA-C. Further studies are required to assess if the K<sub>D</sub> observed for Ly49i2 and RT1-A1<sup>c</sup> is similar amongst other inhibitory rat receptors and their ligands.

To define the structural requirements of ligand recognition by the receptor, several Ly49i2 chimeras were generated, intended to test reduction or full disruption of the interaction between Ly49i2:RT1-A1<sup>c</sup>. The Ly49i2 L6 loop contains the DCGK sequence that is highly conserved in rodent Ly49s (Figure 1-5). Our laboratory has previously shown that recognition of the rat MHC class I ligand, RT1-A1<sup>c</sup>, was conferred onto a non-RT1-A1<sup>c</sup> recognizing mouse receptor, Ly49P, by simply substituting the Ly49P L6 loop sequence, NCDQ, for the Ly49i2 L6 loop sequence DCGK [288]. In the current study, the opposite was executed, the Ly49i2 L6 loop sequence DCGK was mutated to reflect the Ly49P L6 loop NCDQ sequence (Ly49i2.L6.NCDQ<sub>ED</sub>). Furthermore, the mutant Ly49i2.L6.ACGA<sub>ED</sub> was also generated to assess the

significance of the MHC class I associating residues D and K of the L6 loop conserved sequence. SPR analysis of Ly49i2.L6.NCDQ<sub>ED</sub> with the STOK2 Ab and RT1-A1<sup>c</sup> did not reveal any association between the mutant receptor and the antibody or the ligand. The lack of binding between the mutant and the ligand could indicate the requirement of DCGK for RT1-A1<sup>c</sup> recognition by the receptor; however, given no association of Ly49i2 with the STOK2 Ab, no interpretation is possible at this point. By mutating the Ly49i2 L6 loop conserved sequence DCGK to NCDQ, I did expect an interruption in the binding between the receptor and the ligand. The change in residues alters the loop configuration (Figure 3-23 *A & B*), which may have resulted in the hypothesized disruption. The lack of interaction with the Ab STOK2 could be indicative of poorly folded protein, thus affecting the binding of the antibody to Ly49i2. Alternatively, Ly49i2.L6.NCDQ<sub>ED</sub> could possess its correct structure. The epitope for the STOK2 Ab has not been defined, thus, it is possible that the mutant is indeed folded correctly but, the mutated L6 loop region has affected the STOK2 binding site, resulting in a lack of epitope recognition. Given that no other antibodies are available for Ly49i2 detection, alternative folding assessments would have to be considered. Once the mutant is confirmed to be correctly folded, the SPR result for Ly49i2.L6.NCDQ<sub>ED</sub>:RT1-A1<sup>c</sup> interaction could then be evaluated. Ly49i2.L6.ACGA<sub>ED</sub>, on the other hand, did interact with the STOK2 Ab, resulting in an SPR sensorgram profile somewhat different as compared to Ly49i2<sub>ED</sub> and its STOK2 Ab binding profile. Ly49i2.L6.ACGA<sub>ED</sub>:STOK2 Ab engagement resulted in a  $K_D=0.318\mu\text{M}$ , comparable to the result observed for Ly49i2<sub>ED</sub>. This interaction suggests that the mutant may have folded in such a way that revealed the epitope enough for STOK2 Ab binding but altered enough to slightly disrupt the contact sites. This may have been the reason for the different SPR sensorgram profile for the Ly49i2.L6.ACGA<sub>ED</sub>:STOK2 binding, as compared to the Ly49i2<sub>ED</sub>:STOK2 interaction. The binding of Ly49i2.L6.ACGA<sub>ED</sub> with the STOK2 Ab, nonetheless, allows me to interpret the Ly49i2.L6.ACGA<sub>ED</sub>:RT1-A1<sup>c</sup> interaction. The mutant receptor Ly49i2.L6.ACGA<sub>ED</sub> and RT1-A1<sup>c</sup><sub>ED</sub> associated, resulting in  $K_D = 6.96 \mu\text{M}$ . The dissociation constant is 224-fold higher as compared to wildtype Ly49i2 and RT1-A1<sup>c</sup> engagement, suggesting that the interaction between the mutant receptor and the ligand was diminished, resulting in less binding affinity. Asp249 and Lys252 in the Ly49i2

DCGK conserved sequence may interact with conserved acidic residues Glu232 and Lys243 on the  $\alpha 3$  domain of the RT1-A1<sup>c</sup> [192]. Mutating D249A and K252A alters the L6 loop structure (Figure 3-23 A & C). Furthermore, D at position 249 on the Ly49i2 L6 loop is a larger residue, compared to A, and is also negatively charged. By eliminating the charge at this position, the interaction with the positively charged K243 on the  $\alpha 3$  domain of the RT1-A1<sup>c</sup> is likely interrupted. Similarly, the engagement between the negatively charged E at position 232 on the  $\alpha 3$  domain of the ligand may be disrupted by neutralizing position 252 on the L6 loop of Ly49i2 through the placement of A instead of the positively charged K residue. A complete loss in binding was not observed when Ly49i2.L6.ACGA<sub>ED</sub> and RT1-A1<sup>c</sup><sub>ED</sub> associated during SPR analysis; however, the large 224-fold difference may be due to the neutralized 249 and 252 positions on the L6 loop of the receptor. This result implies a role for loop L6 in RT1-A1<sup>c</sup> recognition by the Ly49i2 receptor. Further studies would have to be conducted to support the findings outlined in this section of the chapter.

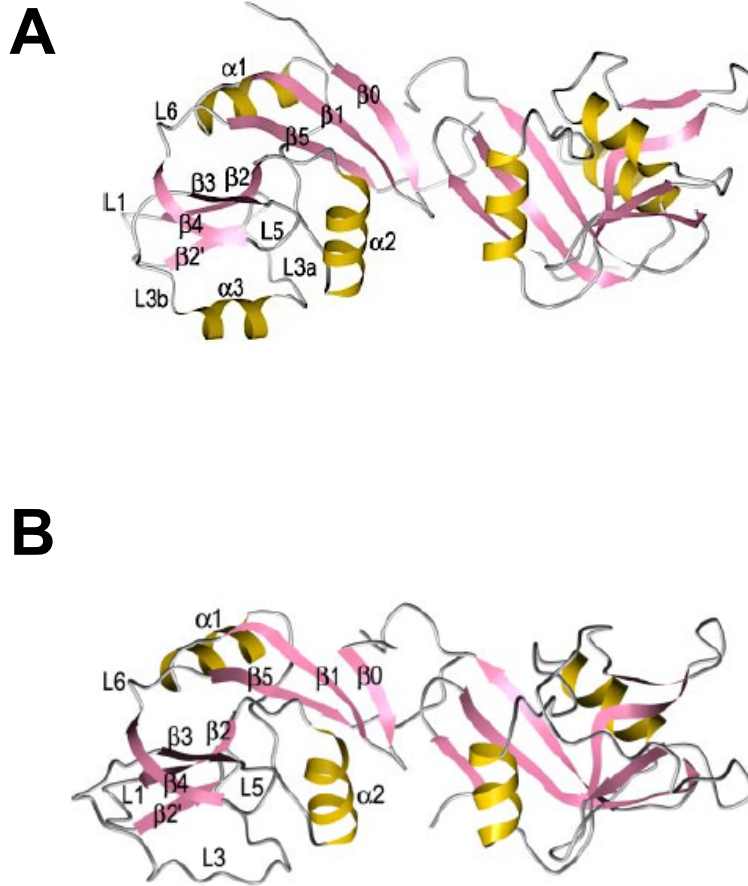
The Ly49i2 S241 and T243 residues are highly conserved residues in both rat and group II mouse Ly49s. These residues located on the L5 loop were assessed in this report for their importance in RT1-A1<sup>c</sup> recognition. Both residues were mutated individually, as well as together, generating the three mutant receptors Ly49i2.S241A<sub>ED</sub>, Ly49i2.T243A<sub>ED</sub>, and Ly49i2.S241A.T243A<sub>ED</sub>. None of the mutants generated SPR binding profiles with RT1-A1<sup>c</sup>, with the exception of Ly49i2.T243A<sub>ED</sub>, which displays a slight interaction at the two highest concentrations of the ligand, 32 $\mu$ M and 64 $\mu$ M, but this association was not sufficient for K<sub>D</sub> determination. Compared to the results from the wildtype Ly49i2 SPR assessment with the MHC class I molecule, the results could indicate a complete disruption in ligand recognition by the ligand. However, the lack of binding by the L5 loop mutants with the STOK2 Ab do not allow for such a conclusion. The utilization of the STOK2 Ab serves to assess correctly folded Ly49i2. On account of the loss of recognition by the STOK2 Ab of the L5 loop mutants, two interpretations are possible. The loop L5 mutants may have all been misfolded, thus resulting in the improper recognition by the antibody STOK2. Alternatively, the mutants may have assumed their proper form; however, due to the unknown location of the STOK2 Ab epitope on Ly49i2, the mutations may be located either at, or near the antibody site of

attachment, resulting in the hindrance of L5 loop mutant recognition by the STOK2 Ab. Either way, the SPR data resulting from the interaction of the loop L5 chimeras and RT1-A1<sup>c</sup> cannot be interpreted and the results in this section are inconclusive. Both S and T are uncharged, polar residues, thus hydrophilic in nature. By mutating the residues, either individually or at the same time, to A, a hydrophobic residue, the L5 loop alters its shape (Figure 3-24). I expected some disruption during contact between the L5 loop mutant receptors and RT1-A1<sup>c</sup>. Further investigation is required to confirm folding of the Ly49i2 mutants before the role of L5 loop can be assessed via SPR.

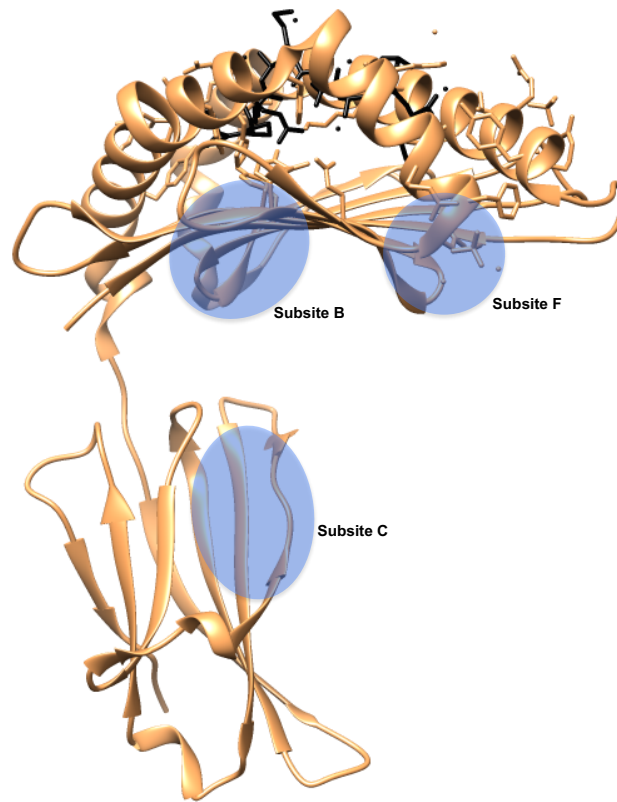
The polymorphic L3 loop in rat Ly49s may dictate ligand specificity. This chapter also tackled defining the significance of the L3 loop region in ligand recognition by the inhibitory receptor Ly49i2. Three other members of the PVG strain and chromosomal block II, Ly49i5, Ly49s5, and Ly49s3, display significant residue differences in the L3 loop, while conserving several other residues. The entire L3 loop region of Ly49i2 was replaced by the L3 loop residues of the other Ly49s, resulting in Ly49i2.L3.i5<sub>ED</sub>, Ly49i2.L3.s5<sub>ED</sub>, and Ly49i2.L3.s3<sub>ED</sub> mutant receptors. These L3 loop mutants were assessed for their ability to recognize and bind to the STOK2 Ab and RT1-A1<sup>c</sup> by SPR. Binding interactions were detected between the L3 loop mutants and the STOK2 Ab, resulting in  $K_D = 0.26\mu\text{M}$ ,  $0.37\mu\text{M}$ , and  $0.11\mu\text{M}$  for Ly49i2.L3.i5<sub>ED</sub>, Ly49i2.L3.s5<sub>ED</sub>, and Ly49i2.L3.s3<sub>ED</sub>, respectively, values comparable to the  $K_D=0.77\mu\text{M}$  resultant from Ly49i2<sub>ED</sub> and the STOK2 Ab association. The SPR sensorgrams display a binding profile similar to the Ly49i2<sub>ED</sub>:STOK2 Ab SPR sensorgram. These results suggest that all three mutants assumed their correct conformation. Interestingly, the interaction of the L3 loop chimeric receptors Ly49i2.L3.i5<sub>ED</sub> and Ly49i2.L3.s3<sub>ED</sub> with RT1-A1<sup>c</sup> did not generate an SPR binding profile nor any measureable  $K_D$ . These results suggest that engagement of the receptor with the ligand was disrupted, thus preventing Ly49i2 from recognizing RT1-A1<sup>c</sup>. Ly49i2.L3.s5<sub>ED</sub>, unlike the other mutants, did have a slight interaction with the MHC class I ligand, but only at the highest concentrations, however no measureable  $K_D$  resulted. To further support these results, I also generated another L3 loop mutant. The L3 loop sequence alignment between Ly49i2, Ly49i5, Ly49s5, and Ly49s3 (Figure 1-5 B) reveals that Ly49i2 and Ly49i5 share the most amino acids sequence identity. Nonetheless, the Ly49i5 L3 loop (when present in the Ly49i2

receptor) did not allow for RT1-A1<sup>c</sup> recognition. I exchanged the L3 loop of Ly49i5 for the Ly49i2 L3 loop (Ly49i5.L3.i2) to determine if recognition of RT1-A1<sup>c</sup> would be restored. SPR analysis revealed that partial recognition of RT1-A1<sup>c</sup> was gained, resulting in  $K_D=2.77\mu\text{M}$ . Although the  $K_D$  is 90-fold higher, thus 90-fold lower in affinity, compared to Ly49i2<sub>ED</sub>: RT1-A1<sup>c</sup>, it is still comparable to the  $K_D$  of many other NK cell receptors and their ligands (Table 3-1). The L3 loop region is twenty-one amino acids in length. With only 62% amino acid sequence identity between the L3 loop of Ly49i2 and Ly49i5, the structure of the loop is predicted to be different (Figure 3-25). The putative L3 loop of Ly49i5 appears to fold inward, with the terminal residues oriented differently as compared to Ly49i2 (Figure 3-25). Given an even lower sequence identity between Ly49i2 with Ly49s5 and Ly49s3, altered conformations are also predicted between the two sets of L3 loop regions. The L3 loop of Ly49s5, when superimposed with the L3 loop of Ly49i2 appears to be significantly different at each terminus. On the one hand, the terminus residues that superimpose the closest to Ly49i2, are orientated differently. As well, the other end of the loop is folded inward almost forming a complete loop, differently than Ly49i2 (Figure 3-25). The putative L3 loop of Ly49s3 also displays a different conformation with one terminus folding inward and orientated differently as compared to the L3 loop of Ly49i2. These altered structures may contribute to the different ligand specificities between each of the receptors [201, 244, 281], as well as elucidate the results reported in this section of the chapter. All together, the results in this section strongly indicate a critical role for L3 loop in ligand recognition by the Ly49i2 receptor.

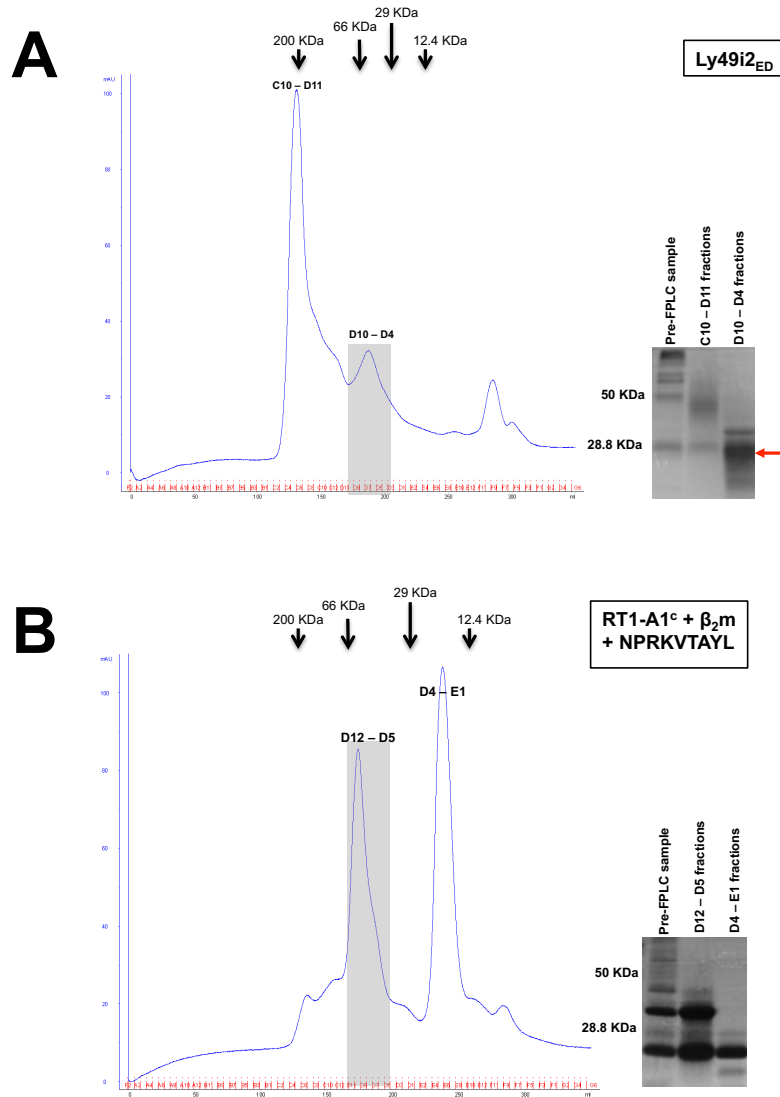
Recognition by Ly49i2 of its cognate ligand RT1-A1<sup>c</sup> was shown, by our laboratory, to require the interaction of Ly49i2 and RT1-A1<sup>c</sup> at the three MHC class I subsites B, F, and C by RT1-A1<sup>c</sup> mutagenesis [192], putative engagement locations for the Ly49 loop regions L3, L5, and L6, respectively. Our studies in this chapter define a role for the loop regions of Ly49i2 during the engagement and identification of self-molecules. Specifically, the results presented in this section, although indeterminate for the L5 loop, suggest a role for the L6 loop in ligand recognition. Furthermore, the results demonstrate that the L3 loop is vital and required for the interaction, and ultimately the recognition of RT1-A1<sup>c</sup> by Ly49i2.



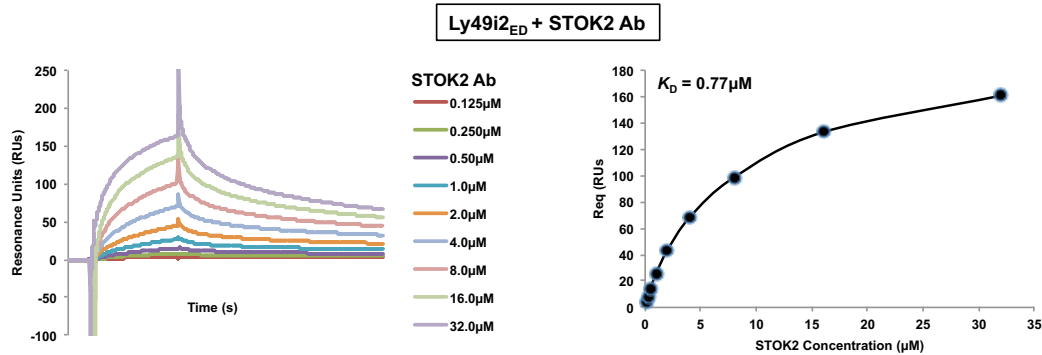
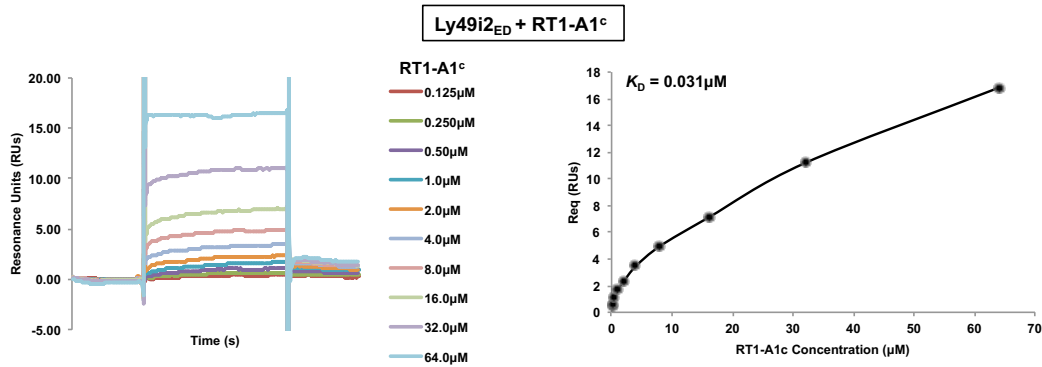
**Figure 3-1: The mouse Ly49 NKD homodimer.** The crystal structure of the Ly49 NKD homodimer reveals that the folding of the protein results in six loops and five  $\beta$ -strands. The  $\alpha$ 3 helix in loop L3 of the NKD, a distinguishing characteristic of group I mouse Ly49s, is seen in Ly49C (A). Ly49G (B), a member of group II mouse Ly49s, lacks the  $\alpha$ 3 helix in loop L3, as do all members of the group. *Figure adapted from: [187]*



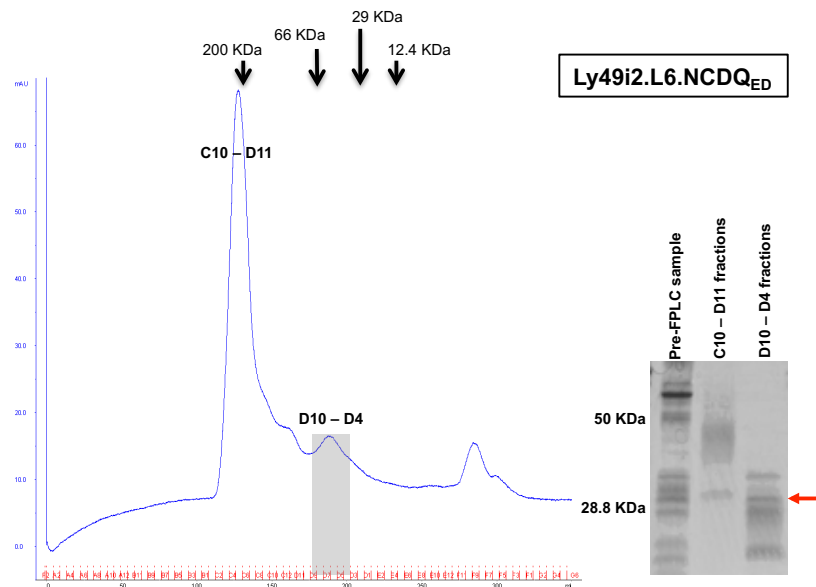
**Figure 3-2: The rat MHC class I molecule RT1-A1<sup>c</sup>.** The rat inhibitory Ly49i2 receptor recognizes the MHC class I molecule, RT1-A1<sup>c</sup>, as its cognate ligand. Putative MHC class I interaction sites with the Ly49i2 L3, L5, and L6 loop regions are outlined in blue and designated as subsites B, F, and C, respectively. (PDB ID: 1KJV)



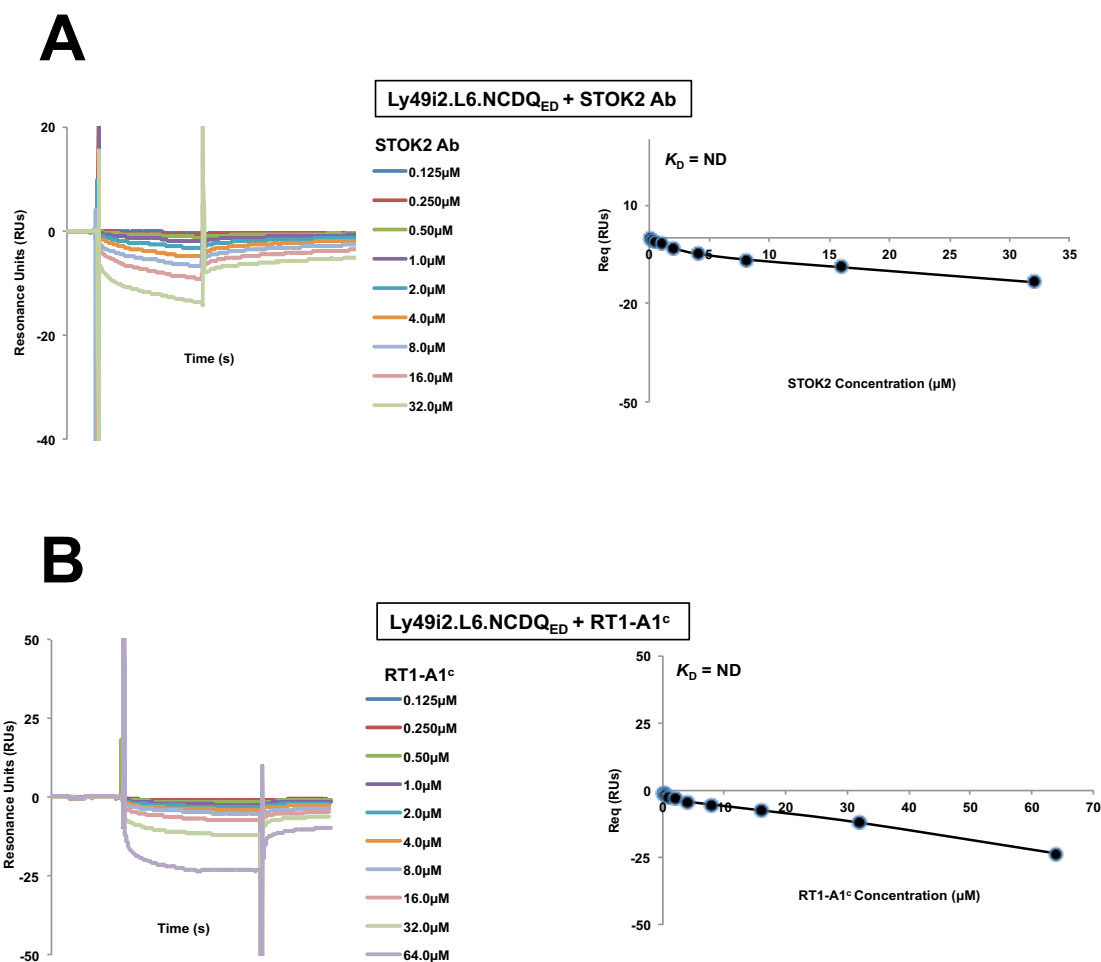
**Figure 3-3: Wildtype Ly49i2 receptor and RT1-A1<sup>c</sup> refolds.** The ectodomains of wildtype Ly49i2 (*A*), as well as RT1-A1<sup>c</sup> and rat  $\beta_2m$  (*B*) were cloned individually into a pET21a vector and expressed as inclusion bodies in *E. coli* BL21 competent cells. Once purified, the inclusion bodies were solubilized in 6M G. HCl. Wildtype Ly49i2 was refolded in 400mM L-Arginine buffer. RT1-A1<sup>c</sup> was also refolded with rat  $\beta_2m$  and the peptide NPRKVTAYL. Upon concentration and dialysis into a 100mM Tris/NaCl pH 8.5 buffer, the proteins were purified by size exclusion chromatography, generating the above chromatograms. The gray-shaded areas correspond to the fractions of the refolded wildtype Ly49i2 (*A*) and RT1-A1<sup>c</sup> (*B*), respectively, which were then pooled and concentrated. The corresponding molecular weights at each fraction are identified above each panel. Purified wildtype Ly49i2 (*A, right*) and RT1-A1<sup>c</sup> (*B, right*) were also analyzed by SDS-PAGE, respectively. A sample of each protein along with various other samples corresponding to the isolated fractions (as illustrated) were run on a 15% SDS-PAGE reducing gel and stained with Coomassie Blue for visualization. The red arrow indicates the band corresponding to the reduced Ly49i2<sub>ED</sub> dimer fractions.

**A****B**

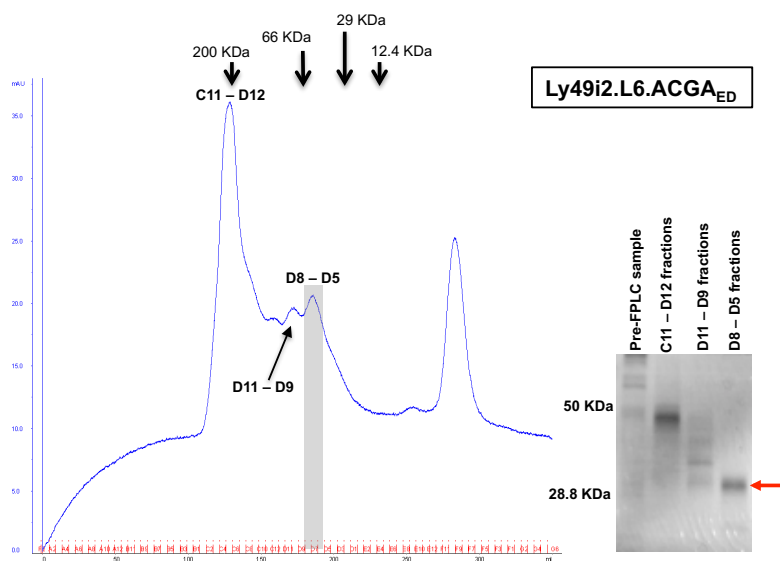
**Figure 3-4: Ly49i2<sub>ED</sub> binding interactions with STOK2 Ab and RT1-A1<sup>c</sup>.** (A) STOK2 Ab was injected at various concentrations ranging from 0.125 μM to 32 μM in two-fold increments over 1100 RU of immobilized Ly49i2<sub>ED</sub> on a CM5 biosensor chip, while (B) RT1-A1<sup>c</sup><sub>ED</sub> was injected, also in two-fold increments, with concentrations varying from 0.125 μM to 64 μM. SPR for each interaction was measured using a Biacore™ T200. Contact between Ly49i2<sub>ED</sub> and STOK2 Ab (A, left panel) or RT1-A1<sup>c</sup><sub>ED</sub> (C, left panel) occurred with HBS-EP+ buffer at 25°C and a flow rate of 30 μl/min. Interactions for each concentration series were measured three times, all resulting in similar data results. The binding response at equilibrium (R<sub>eq</sub>) for the STOK2 Ab and RT1-A1<sup>c</sup><sub>ED</sub> with Ly49i2<sub>ED</sub> resulted in the equilibrium binding curves shown, (A, right panel) and (B, right panel), respectively, where R<sub>eq</sub> for each analyte was plotted against concentration. Dissociation constants (K<sub>D</sub>) for each ligand:analyte interaction was determined by 1:1 Langmuir curve fitting and presented at the top left corner of (A, left panel) and (B, left panel), respectively.



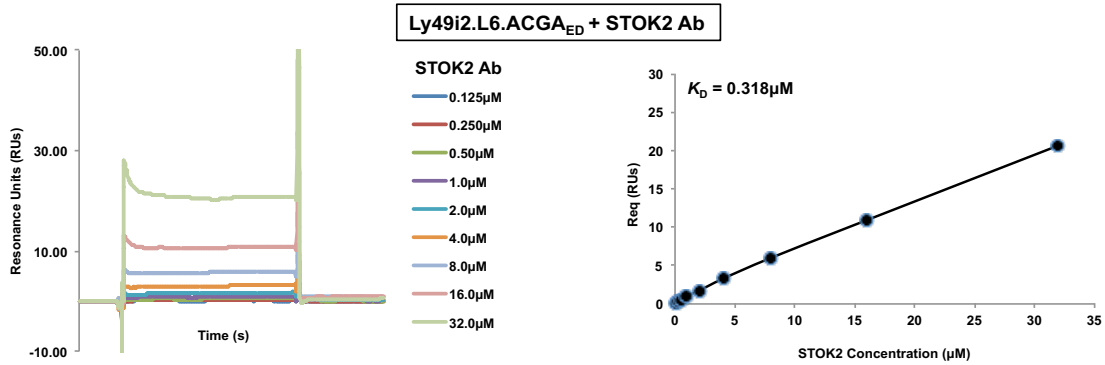
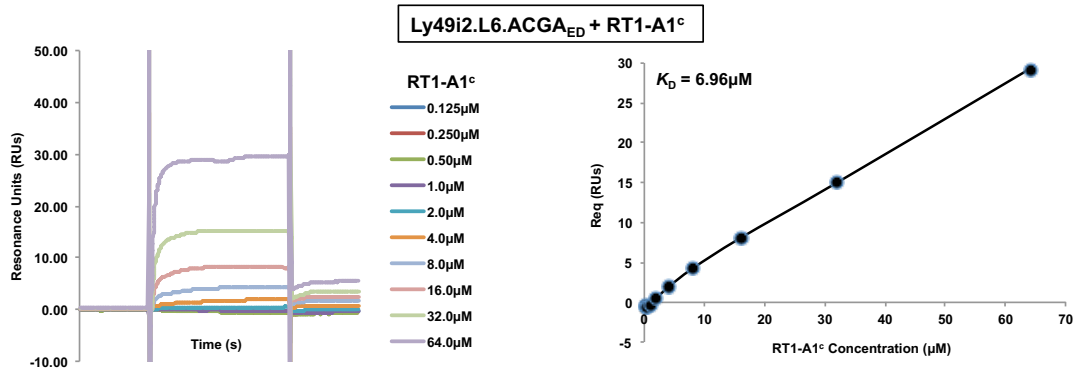
**Figure 3-5: L6 loop chimeric receptor, Ly49i2.L6.NCDQ<sub>ED</sub>, refold.** The ectodomain of Ly49i2.L6.NCDQ was cloned into a pET21a vector and expressed as inclusion bodies in *E. coli* BL21 competent cells. Once purified, the inclusion bodies were solubilized in 6M G. HCl and refolded in 400mM L-Arginine buffer. Upon concentration and dialysis into a 100mM Tris/NaCl pH 8.5 buffer, the proteins were purified by size exclusion chromatography, generating the chromatogram shown (*left*). The gray-shaded area corresponds to the fractions of the refolded Ly49i2.L6.NCDQ<sub>ED</sub> receptor, which were then pooled and concentrated. The corresponding molecular weights at each fraction are identified above the top panel. Purified Ly49i2.L6.NCDQ<sub>ED</sub> was analyzed by SDS-PAGE (*right*). A sample of the protein along with other samples corresponding to the isolated fractions (as illustrated) were run on a 15% SDS-PAGE reducing gel and stained with Coomassie Blue for visualization. The red arrow indicates the band corresponding to the reduced Ly49i2.L6.NCDQ<sub>ED</sub> dimer fractions.



**Figure 3-6: L6 loop chimeric receptor, Ly49i2.L6.NCDQ<sub>ED</sub>, binding interactions with the STOK2 Ab and RT1-A1<sup>c</sup>.** (A, left panel) The STOK2 Ab was injected at various concentrations ranging from 0.125 $\mu$ M to 32 $\mu$ M in two-fold increments over 1000 RU of immobilized Ly49i2.L6.NCDQ<sub>ED</sub> on a CM5 biosensor chip, while (B, left panel) RT1-A1<sup>c</sup><sub>ED</sub> was injected, also in two-fold increments, with concentrations varying from 0.125 $\mu$ M to 64 $\mu$ M also over Ly49i2.L6.NCDQ<sub>ED</sub>. SPR for each interaction was measured using a Biacore<sup>TM</sup> T200. Contact between both chimeric receptors and both analytes occurred with HBS-EP+ buffer at 25 $^{\circ}$ C and a flow rate of 30 $\mu$ l/min. Interactions for each concentration series were measured three times, all resulting in similar data results. The binding response at equilibrium ( $R_{eq}$ ) of the STOK2 Ab and RT1-A1<sup>c</sup><sub>ED</sub> with Ly49i2.L6.NCDQ<sub>ED</sub>, respectively, resulted in the equilibrium binding curves shown, (A, right panel & B right panel), respectively, where  $R_{eq}$  for each analyte was plotted against concentration. Dissociation constants ( $K_D$ ) for each ligand:analyte interaction was determined by 1:1 Langmuir curve fitting and presented at the top left corner (A, right panel & B, right panel). ND = non-determinable



**Figure 3-7: L6 loop chimeric receptor, Ly49i2.L6.ACGA<sub>ED</sub>, refold.** The ectodomain of Ly49i2.L6.ACGA was cloned into a pET21a vector and expressed as inclusion bodies in *E. coli* BL21 competent cells. Once purified, the inclusion bodies were solubilized in 6M G. HCl and refolded in 400mM L-Arginine buffer. Upon concentration and dialysis into a 100mM Tris/NaCl pH 8.5 buffer, the proteins were purified by size exclusion chromatography, generating the chromatogram shown (*left*). The gray-shaded area corresponds to the fractions of the refolded Ly49i2.L6.ACGA<sub>ED</sub> receptor, which were then pooled and concentrated. The corresponding molecular weights at each fraction are identified above the top panel. Purified Ly49i2.L6.ACGA<sub>ED</sub> was analyzed by SDS-PAGE (*right*). A sample of the protein along with other samples corresponding to the isolated fractions (as illustrated) were run on a 15% SDS-PAGE reducing gel and stained with Coomassie Blue for visualization. The red arrow indicates the band corresponding to the reduced Ly49i2.L6.ACGA<sub>ED</sub> dimer fractions.

**A****B**

**Figure 3-8: L6 loop chimeric receptor, Ly49i2.L6.ACGA<sub>ED</sub>, binding interactions with the STOK2 Ab and RT1-A1<sup>c</sup>.** (A, left panel) The STOK2 Ab was injected at various concentrations ranging from 0.125 μM to 32 μM in two-fold increments over 1000 RU of immobilized Ly49i2.L6.ACGA<sub>ED</sub> on a CM5 biosensor chip, while (B, left panel) RT1-A1<sup>c</sup><sub>ED</sub> was injected, also in two-fold increments, with concentrations varying from 0.125 μM to 64 μM also over Ly49i2.L6.ACGA<sub>ED</sub>. SPR for each interaction was measured using a Biacore™ T200. Contact between both chimeric receptors and both analytes occurred with HBS-EP+ buffer at 25°C and a flow rate of 30 μl/min. Interactions for each concentration series were measured three times, all resulting in similar data results. The binding response at equilibrium ( $R_{eq}$ ) of the STOK2 Ab and RT1-A1<sup>c</sup><sub>ED</sub> with Ly49i2.L6.ACGA<sub>ED</sub>, respectively, resulted in the equilibrium binding curves shown, (A, right panel & B right panel), respectively, where  $R_{eq}$  for each analyte was plotted against concentration. Dissociation constants ( $K_D$ ) for each ligand:analyte interaction was determined by 1:1 Langmuir curve fitting and presented at the top left corner (A, right panel & B, right panel).

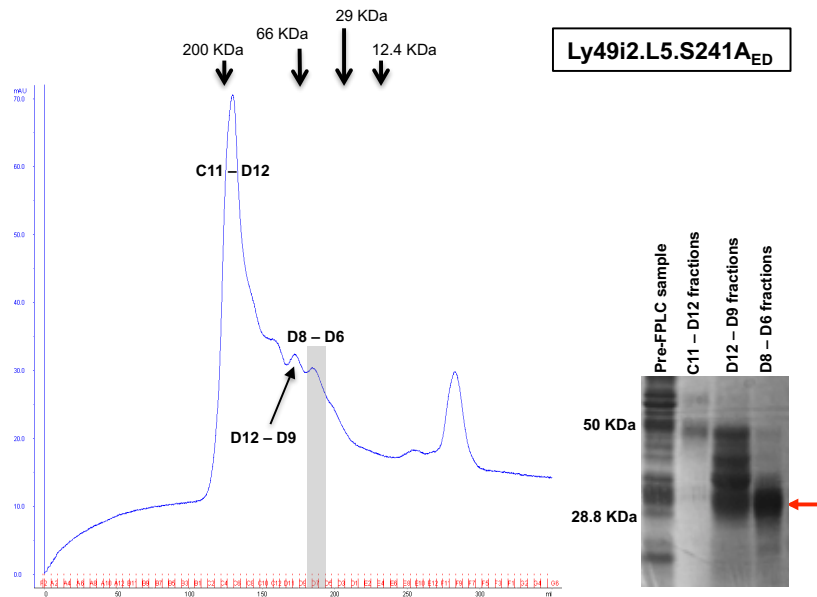


**Figure 3-9: L5 loop chimeric receptor, Ly49i2.S241A<sub>ED</sub>, refold.** The ectodomain of Ly49i2.S241A was cloned into a pET21a vector and expressed as inclusion bodies in *E. coli* BL21 competent cells. Once purified, the inclusion bodies were solubilized in 6M G. HCl and refolded in 400mM L-Arginine buffer. Upon concentration and dialysis into a 100mM Tris/NaCl pH 8.5 buffer, the proteins were purified by size exclusion chromatography, generating the chromatogram shown (*left*). The gray-shaded area corresponds to the fractions of the refolded Ly49i2.S241A receptor, which were then pooled and concentrated. The corresponding molecular weights at each fraction are identified above the top panel. Purified Ly49i2.S241A<sub>ED</sub> was analyzed by SDS-PAGE (*right*). A sample of the protein along with other samples corresponding to the isolated fractions (as illustrated) were run on a 15% SDS-PAGE reducing gel and stained with Coomassie Blue for visualization. The red arrow indicates the band corresponding to the reduced Ly49i2.S241A<sub>ED</sub> dimer fractions.

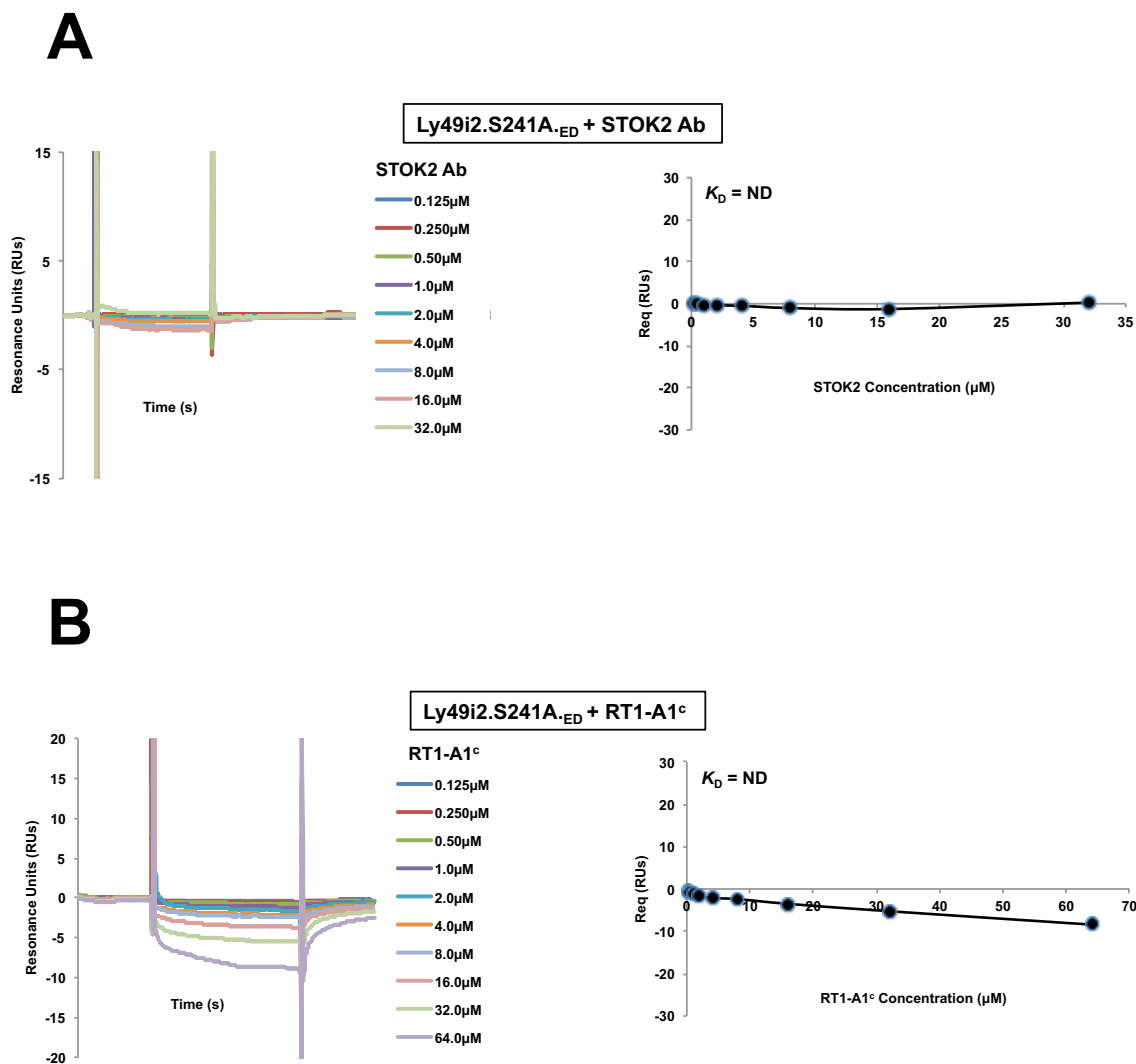


**Figure 3-10: L5 loop chimeric receptor, Ly49i2.S241A<sub>ED</sub>, binding interactions with the STOK2 Ab and RT1-A1<sup>c</sup>.** (A, left panel) The STOK2 Ab was injected at various concentrations ranging from 0.125 μM to 32 μM in two-fold increments over 1000 RU of immobilized Ly49i2.S241A<sub>ED</sub> on a CM5 biosensor chip, while (B, left panel) RT1-A1<sup>c</sup><sub>ED</sub> was injected, also in two-fold increments, with concentrations varying from 0.125 μM to 64 μM also over Ly49i2.S241A<sub>ED</sub>. SPR for each interaction was measured using a Biacore™ T200. Contact between both chimeric receptors and both analytes occurred with HBS-EP+ buffer at 25°C and a flow rate of 30 μl/min. Interactions for each concentration series were measured three times, all resulting in similar data results. The binding response at equilibrium ( $R_{eq}$ ) of the STOK2 Ab and RT1-A1<sup>c</sup><sub>ED</sub> with Ly49i2.S241A<sub>ED</sub>, respectively, resulted in the equilibrium binding curves shown, (A, right panel & B right panel), respectively, where  $R_{eq}$  for each analyte was plotted against concentration. Dissociation constants ( $K_D$ ) for each ligand:analyte interaction was determined by 1:1 Langmuir curve fitting and presented at the top left corner (A, right panel & B, right panel). ND = non-determinable

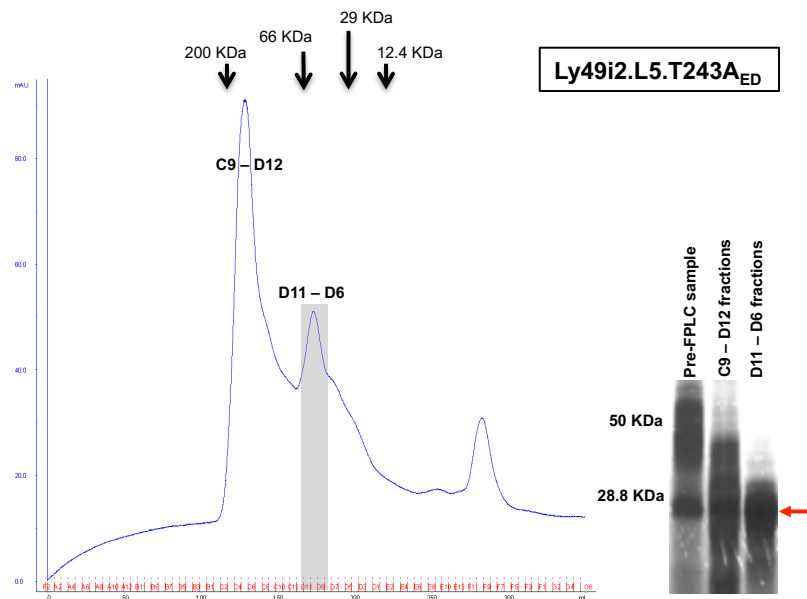


**Figure 3-11: L5 loop chimeric receptor, Ly49i2.T243A<sub>ED</sub>, refold.** The ectodomain of Ly49i2.T243A was cloned into a pET21a vector and expressed as inclusion bodies in *E. coli* BL21 competent cells. Once purified, the inclusion bodies were solubilized in 6M G. HCl and refolded in 400mM L-Arginine buffer. Upon concentration and dialysis into a 100mM Tris/NaCl pH 8.5 buffer, the proteins were purified by size exclusion chromatography, generating the chromatogram shown (*left*). The gray-shaded area corresponds to the fractions of the refolded Ly49i2.T243A receptor, which were then pooled and concentrated. The corresponding molecular weights at each fraction are identified above the top panel. Purified Ly49i2.T243A<sub>ED</sub> was analyzed by SDS-PAGE (*right*). A sample of the protein along with other samples corresponding to the isolated fractions (as illustrated) were run on a 15% SDS-PAGE reducing gel and stained with Coomassie Blue for visualization. The red arrow indicates the band corresponding to the reduced Ly49i2.T243A<sub>ED</sub> dimer fractions.

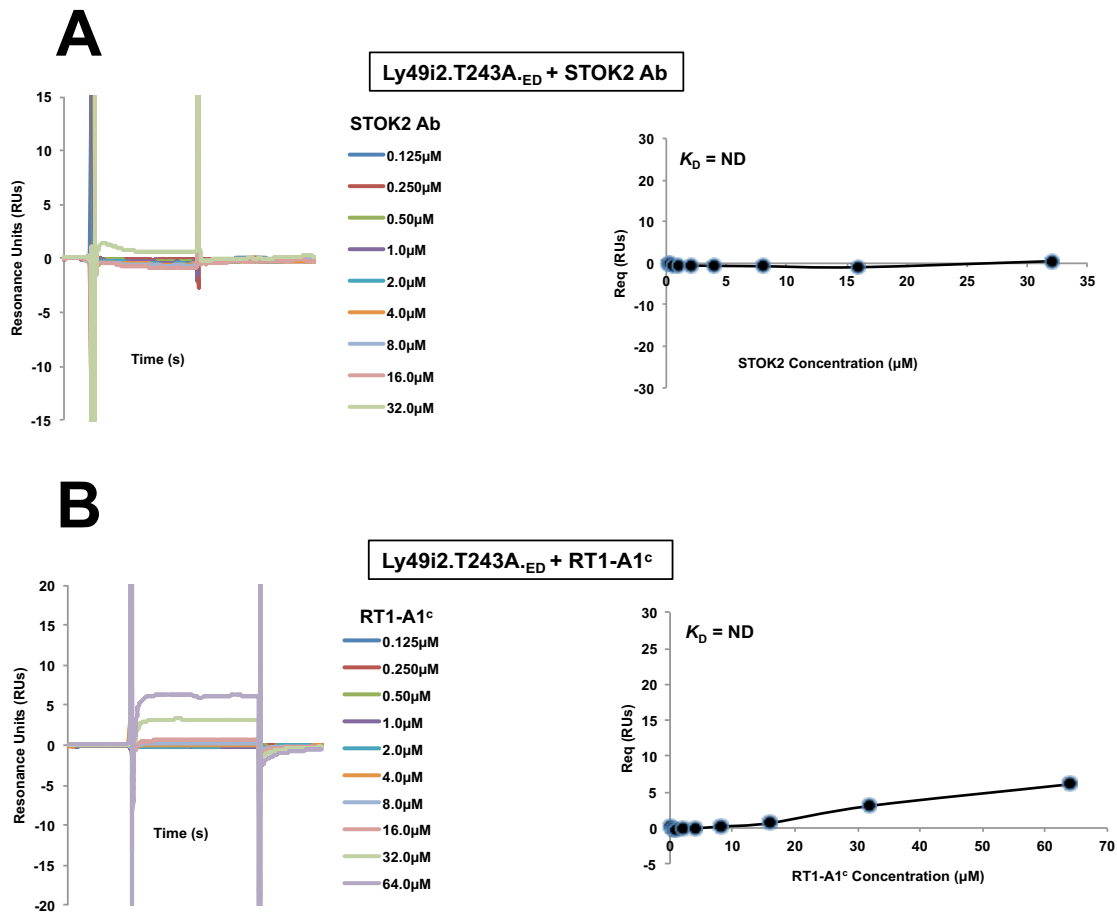


**Figure 3-12: L5 loop chimeric receptor, Ly49i2.T243A<sub>ED</sub>, binding interactions with the STOK2 Ab and RT1-A1<sup>c</sup>.** (A, left panel) The STOK2 Ab was injected at various concentrations ranging from 0.125 μM to 32 μM in two-fold increments over 1000 RU of immobilized Ly49i2.T243A<sub>ED</sub> on a CM5 biosensor chip, while (B, left panel) RT1-A1<sup>c</sup> was injected, also in two-fold increments, with concentrations varying from 0.125 μM to 64 μM also over Ly49i2.T243A<sub>ED</sub>. SPR for each interaction was measured using a Biacore<sup>TM</sup> T200. Contact between both chimeric receptors and both analytes occurred with HBS-EP+ buffer at 25°C and a flow rate of 30 μl/min. Interactions for each concentration series were measured three times, all resulting in similar data results. The binding response at equilibrium ( $R_{eq}$ ) of the STOK2 Ab and RT1-A1<sup>c</sup> with Ly49i2.T243A<sub>ED</sub>, respectively, resulted in the equilibrium binding curves shown, (A, right panel & B right panel), respectively, where  $R_{eq}$  for each analyte was plotted against concentration. Dissociation constants ( $K_D$ ) for each ligand:analyte interaction was determined by 1:1 Langmuir curve fitting and presented at the top left corner (A, right panel & B, right panel). ND = non-determinable

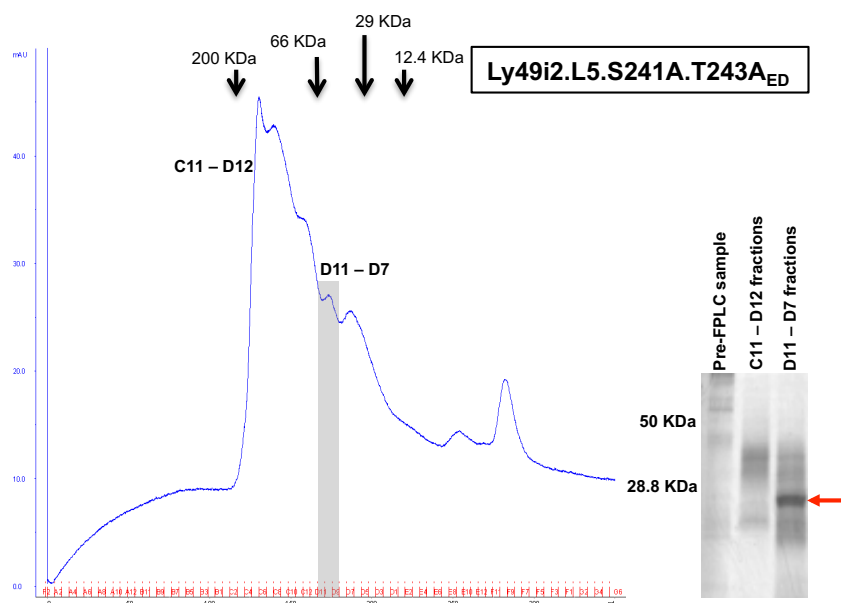


**Figure 3-13: L5 loop chimeric receptor, Ly49i2.S241A.T243A<sub>ED</sub>, refold.** The ectodomain of Ly49i2.S241A.T243A was cloned into a pET21a vector and expressed as inclusion bodies in *E. coli* BL21 competent cells. Once purified, the inclusion bodies were solubilized in 6M G. HCl and refolded in 400mM L-Arginine buffer. Upon concentration and dialysis into a 100mM Tris/NaCl pH 8.5 buffer, the proteins were purified by size exclusion chromatography, generating the chromatogram shown (*left*). The gray-shaded area corresponds to the fractions of the refolded Ly49i2.S241A.T243A receptor, which were then pooled and concentrated. The corresponding molecular weights at each fraction are identified above the top panel. Purified Ly49i2.S241A.T243A<sub>ED</sub> was analyzed by SDS-PAGE (*right*). A sample of the protein along with other samples corresponding to the isolated fractions (as illustrated) were run on a 15% SDS-PAGE reducing gel and stained with Coomassie Blue for visualization. The red arrow indicates the band corresponding to the reduced Ly49i2.S241A.T243A<sub>ED</sub> dimer fractions.

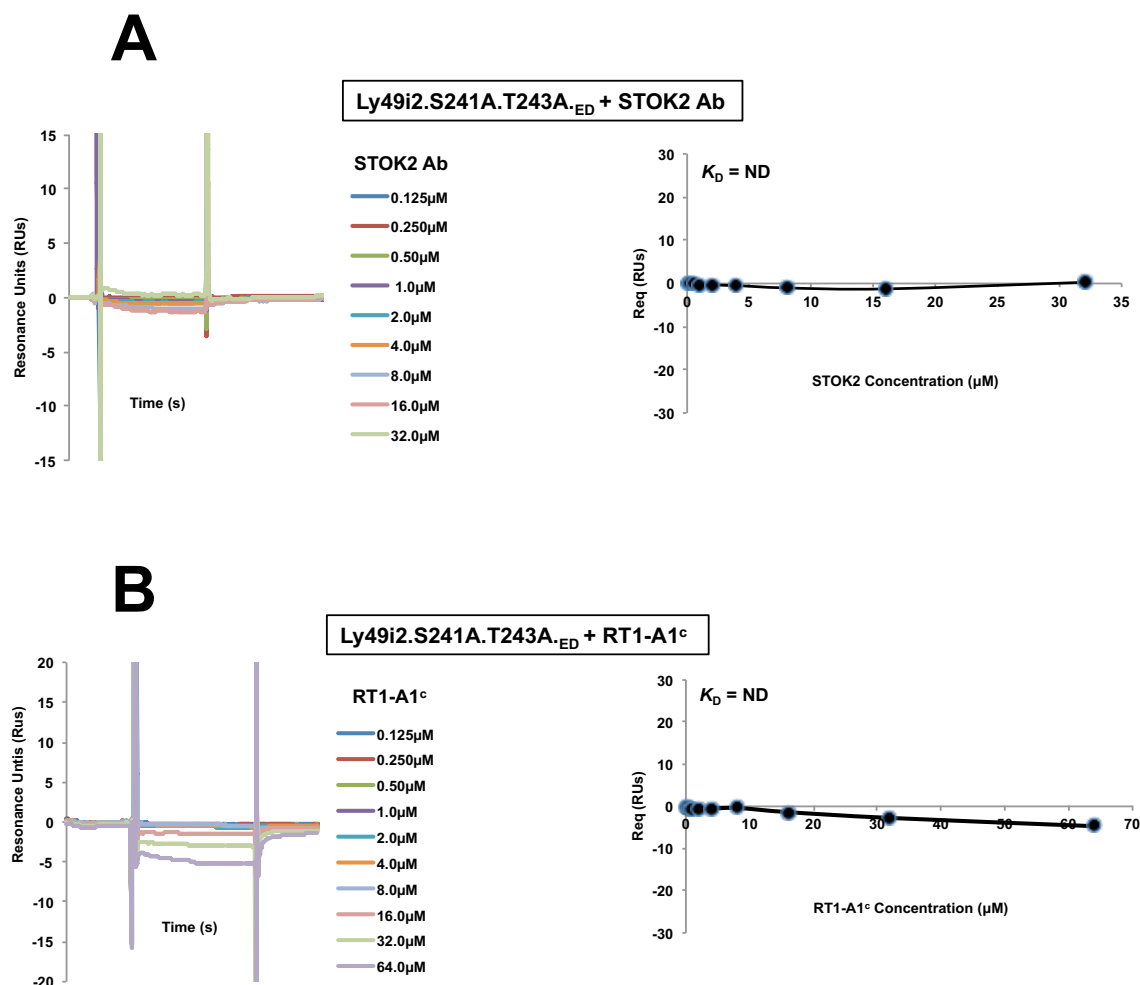


**Figure 3-14: L5 loop chimeric receptor, Ly49i2.S241A.T243A<sub>ED</sub>, binding interactions with the STOK2 Ab and RT1-A1<sup>c</sup>.** (A, left panel) The STOK2 Ab was injected at various concentrations ranging from 0.125  $\mu\text{M}$  to 32  $\mu\text{M}$  in two-fold increments over 1000 RU of immobilized Ly49i2.S241A.T243A<sub>ED</sub> on a CM5 biosensor chip, while (B, left panel) RT1-A1<sup>c</sup><sub>ED</sub> was injected, also in two-fold increments, with concentrations varying from 0.125  $\mu\text{M}$  to 64  $\mu\text{M}$  also over Ly49i2.S241A.T243A<sub>ED</sub>. SPR for each interaction was measured using a Biacore™ T200. Contact between both chimeric receptors and both analytes occurred with HBS-EP+ buffer at 25°C and a flow rate of 30  $\mu\text{l}/\text{min}$ . Interactions for each concentration series were measured three times, all resulting in similar data results. The binding response at equilibrium ( $R_{\text{eq}}$ ) of the STOK2 Ab and RT1-A1<sup>c</sup><sub>ED</sub> with Ly49i2.S241A.T243A<sub>ED</sub>, respectively, resulted in the equilibrium binding curves shown, (A, right panel & B right panel), respectively, where  $R_{\text{eq}}$  for each analyte was plotted against concentration. Dissociation constants ( $K_D$ ) for each ligand:analyte interaction was determined by 1:1 Langmuir curve fitting and presented at the top left corner (A, right panel & B, right panel). ND = non-determinable

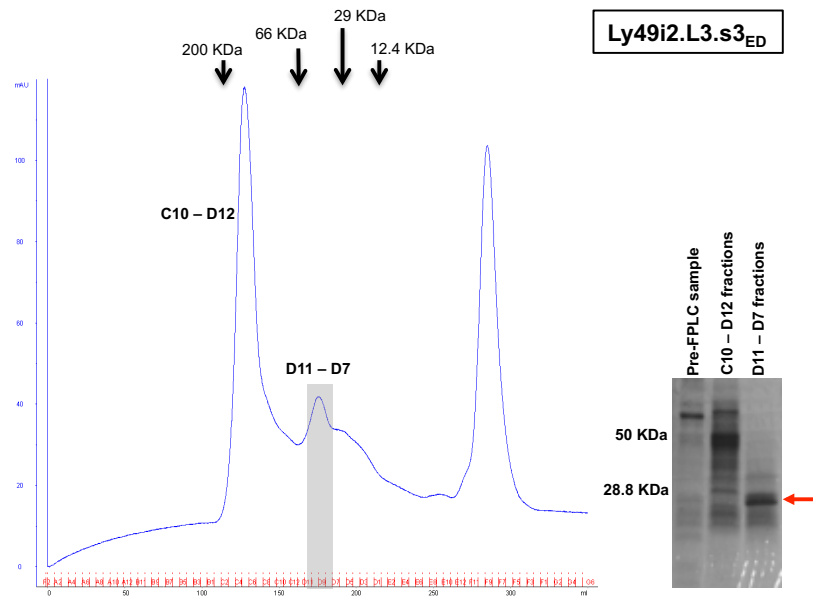


**Figure 3-15: L3 loop chimeric receptor, Ly49i2.L3.s3<sub>ED</sub>, refold.** The ectodomain of Ly49i2.L3.s3 was cloned into a pET21a vector and expressed as inclusion bodies in *E. coli* BL21 competent cells. Once purified, the inclusion bodies were solubilized in 6M G. HCl and refolded in 400mM L-Arginine buffer. Upon concentration and dialysis into a 100mM Tris/NaCl pH 8.5 buffer, the proteins were purified by size exclusion chromatography, generating the chromatogram shown (*left*). The gray-shaded area corresponds to the fractions of the refolded Ly49i2.L3.s3<sub>ED</sub> receptor, which were then pooled and concentrated. The corresponding molecular weights at each fraction are identified above the top panel. Purified Ly49i2.L3.s3<sub>ED</sub> was analyzed by SDS-PAGE (*right*). A sample of the protein along with other samples corresponding to the isolated fractions (as illustrated) were run on a 15% SDS-PAGE reducing gel and stained with Coomassie Blue for visualization. The red arrow indicates the band corresponding to the reduced Ly49i2.L3.s3<sub>ED</sub> dimer fractions.

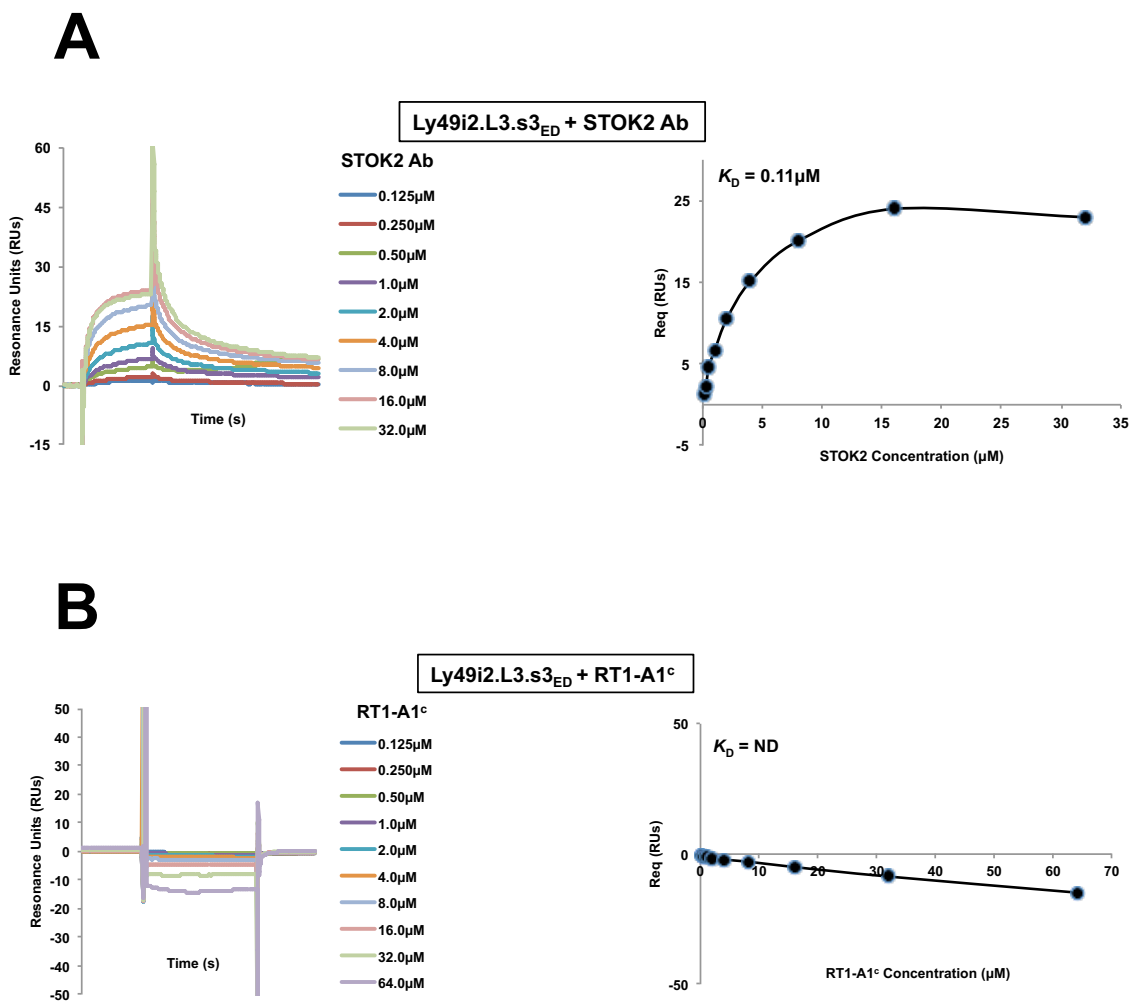


**Figure 3-16: L3 loop chimeric receptor, Ly49i2.L3.s3<sub>ED</sub>, binding interactions with the STOK2 Ab and RT1-A1<sup>c</sup>.** (A, left panel) The STOK2 Ab was injected at various concentrations ranging from 0.125 μM to 32 μM in two-fold increments over 1000 RU of immobilized Ly49i2.L3.s3<sub>ED</sub> on a CM5 biosensor chip, while (B, left panel) RT1-A1<sup>c</sup><sub>ED</sub> was injected, also in two-fold increments, with concentrations varying from 0.125 μM to 64 μM also over Ly49i2.L3.s3<sub>ED</sub>. SPR for each interaction was measured using a Biacore™ T200. Contact between both chimeric receptors and both analytes occurred with HBS-EP+ buffer at 25°C and a flow rate of 30 μl/min. Interactions for each concentration series were measured three times, all resulting in similar data results. The binding response at equilibrium ( $R_{eq}$ ) of the STOK2 Ab and RT1-A1<sup>c</sup><sub>ED</sub> with Ly49i2.L3.s3<sub>ED</sub>, respectively, resulted in the equilibrium binding curves shown, (A, right panel & B right panel), respectively, where  $R_{eq}$  for each analyte was plotted against concentration. Dissociation constants ( $K_D$ ) for each ligand:analyte interaction was determined by 1:1 Langmuir curve fitting and presented at the top left corner (A, right panel & B, right panel). ND = non-determinable

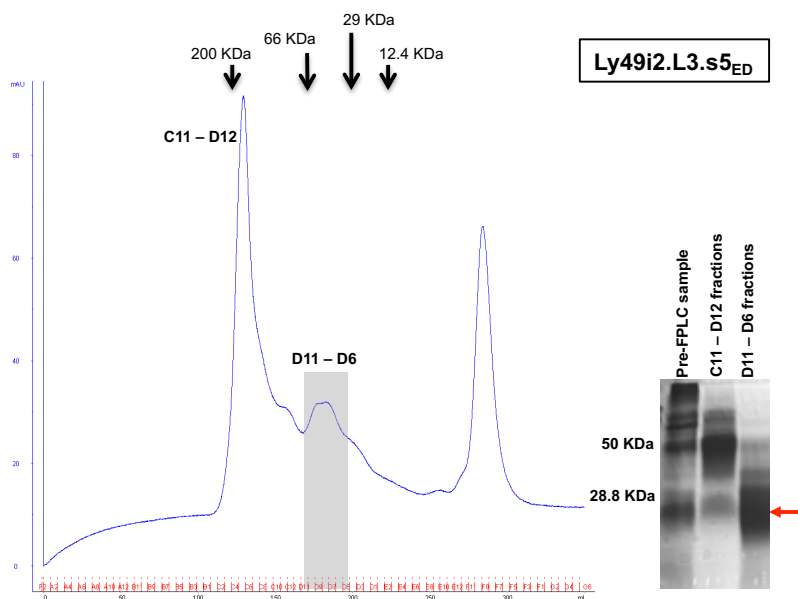


**Figure 3-17: L3 loop chimeric receptor, Ly49i2.L3.s5<sub>ED</sub>, refold.** The ectodomain of Ly49i2.L3.s5 was cloned into a pET21a vector and expressed as inclusion bodies in *E. coli* BL21 competent cells. Once purified, the inclusion bodies were solubilized in 6M G. HCl and refolded in 400mM L-Arginine buffer. Upon concentration and dialysis into a 100mM Tris/NaCl pH 8.5 buffer, the proteins were purified by size exclusion chromatography, generating the chromatogram shown (*left*). The gray-shaded area corresponds to the fractions of the refolded Ly49i2.L3.s5<sub>ED</sub> receptor, which were then pooled and concentrated. The corresponding molecular weights at each fraction are identified above the top panel. Purified Ly49i2.L3.s5<sub>ED</sub> was analyzed by SDS-PAGE (*right*). A sample of the protein along with other samples corresponding to the isolated fractions (as illustrated) were run on a 15% SDS-PAGE reducing gel and stained with Coomassie Blue for visualization. The red arrow indicates the band corresponding to the reduced Ly49i2.L3.s5<sub>ED</sub> dimer fractions.

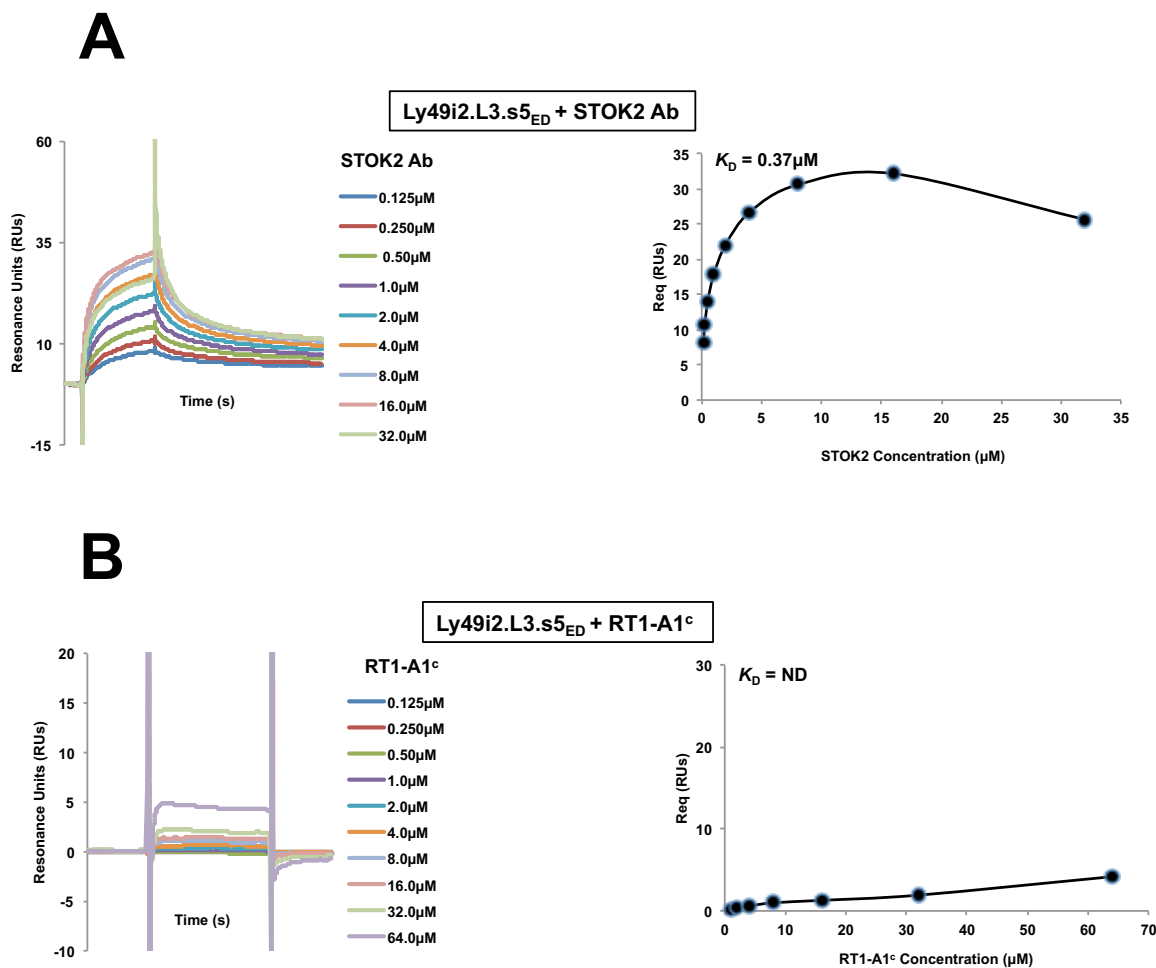


**Figure 3-18: L3 loop chimeric receptor, Ly49i2.L3.s5<sub>ED</sub>, binding interactions with the STOK2 Ab and RT1-A1<sup>c</sup>.** (A, left panel) The STOK2 Ab was injected at various concentrations ranging from 0.125 $\mu$ M to 32 $\mu$ M in two-fold increments over 1000 RU of immobilized Ly49i2.L3.s5<sub>ED</sub> on a CM5 biosensor chip, while (B, left panel) RT1-A1<sup>c</sup><sub>ED</sub> was injected, also in two-fold increments, with concentrations varying from 0.125 $\mu$ M to 64 $\mu$ M also over Ly49i2.L3.s5<sub>ED</sub>. SPR for each interaction was measured using a Biacore<sup>TM</sup> T200. Contact between both chimeric receptors and both analytes occurred with HBS-EP+ buffer at 25 $^{\circ}$ C and a flow rate of 30 $\mu$ l/min. Interactions for each concentration series were measured three times, all resulting in similar data results. The binding response at equilibrium ( $R_{eq}$ ) of the STOK2 Ab and RT1-A1<sup>c</sup><sub>ED</sub> with Ly49i2.L3.s5<sub>ED</sub>, respectively, resulted in the equilibrium binding curves shown, (A, right panel & B right panel), respectively, where  $R_{eq}$  for each analyte was plotted against concentration. Dissociation constants ( $K_D$ ) for each ligand:analyte interaction was determined by 1:1 Langmuir curve fitting and presented at the top left corner (A, right panel & B, right panel). ND = non-determinable

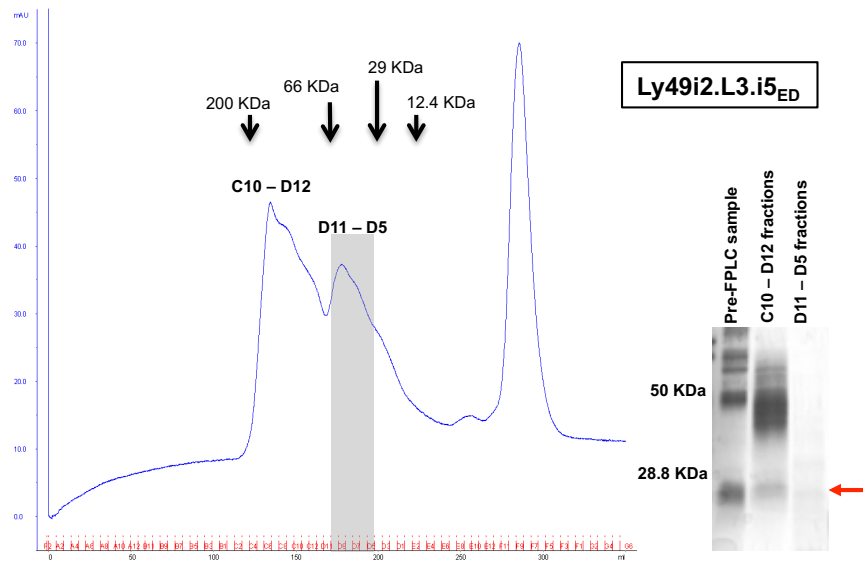


**Figure 3-19: L3 loop chimeric receptor, Ly49i2.L3.i5<sub>ED</sub>, refold.** The ectodomain of Ly49i2.L3.i5 was cloned into a pET21a vector and expressed as inclusion bodies in *E. coli* BL21 competent cells. Once purified, the inclusion bodies were solubilized in 6M G. HCl and refolded in 400mM L-Arginine buffer. Upon concentration and dialysis into a 100mM Tris/NaCl pH 8.5 buffer, the proteins were purified by size exclusion chromatography, generating the chromatogram shown (*left*). The gray-shaded area corresponds to the fractions of the refolded Ly49i2.L3.i5<sub>ED</sub> receptor, which were then pooled and concentrated. The corresponding molecular weights at each fraction are identified above the top panel. Purified Ly49i2.L3.i5<sub>ED</sub> was analyzed by SDS-PAGE (*right*). A sample of the protein along with other samples corresponding to the isolated fractions (as illustrated) were run on a 15% SDS-PAGE reducing gel and stained with Coomassie Blue for visualization. The red arrow indicates the band corresponding to the reduced Ly49i2.L3.i5<sub>ED</sub> dimer fractions.

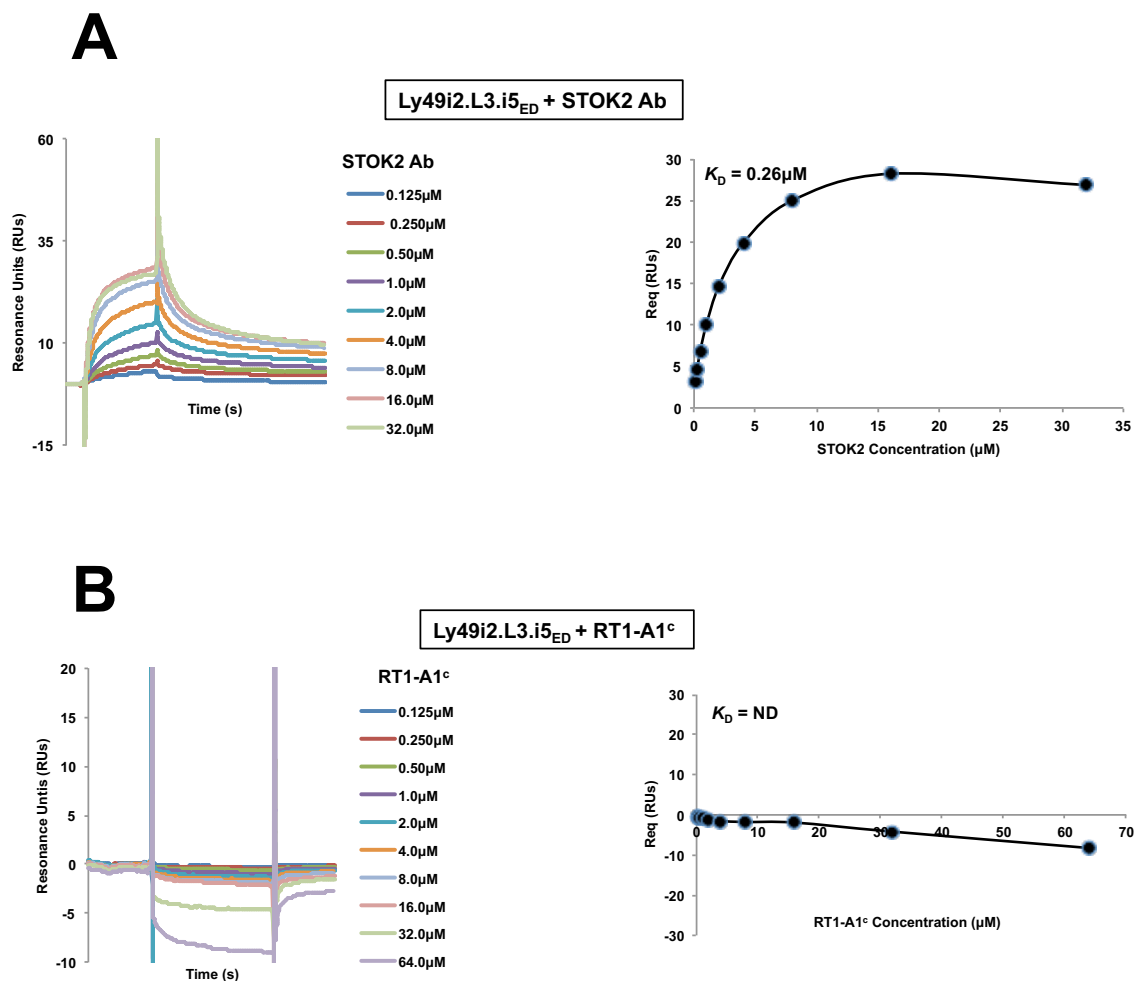


**Figure 3-20: L3 loop chimeric receptor, Ly49i2.L3.i5<sub>ED</sub>, binding interactions with the STOK2 Ab and RT1-A1<sup>c</sup>.** (A, left panel) The STOK2 Ab was injected at various concentrations ranging from 0.125 $\mu$ M to 32 $\mu$ M in two-fold increments over 1000 RU of immobilized Ly49i2.L3.i5<sub>ED</sub> on a CM5 biosensor chip, while (B, left panel) RT1-A1<sup>c</sup><sub>ED</sub> was injected, also in two-fold increments, with concentrations varying from 0.125 $\mu$ M to 64 $\mu$ M also over Ly49i2.L3.i5<sub>ED</sub>. SPR for each interaction was measured using a Biacore<sup>TM</sup> T200. Contact between both chimeric receptors and both analytes occurred with HBS-EP+ buffer at 25°C and a flow rate of 30 $\mu$ l/min. Interactions for each concentration series were measured three times, all resulting in similar data results. The binding response at equilibrium ( $R_{eq}$ ) of the STOK2 Ab and RT1-A1<sup>c</sup><sub>ED</sub> with Ly49i2.L3.i5<sub>ED</sub>, respectively, resulted in the equilibrium binding curves shown, (A, right panel & B right panel), respectively, where  $R_{eq}$  for each analyte was plotted against concentration. Dissociation constants ( $K_D$ ) for each ligand:analyte interaction was determined by 1:1 Langmuir curve fitting and presented at the top left corner (A, right panel & B, right panel). ND = non-determinable

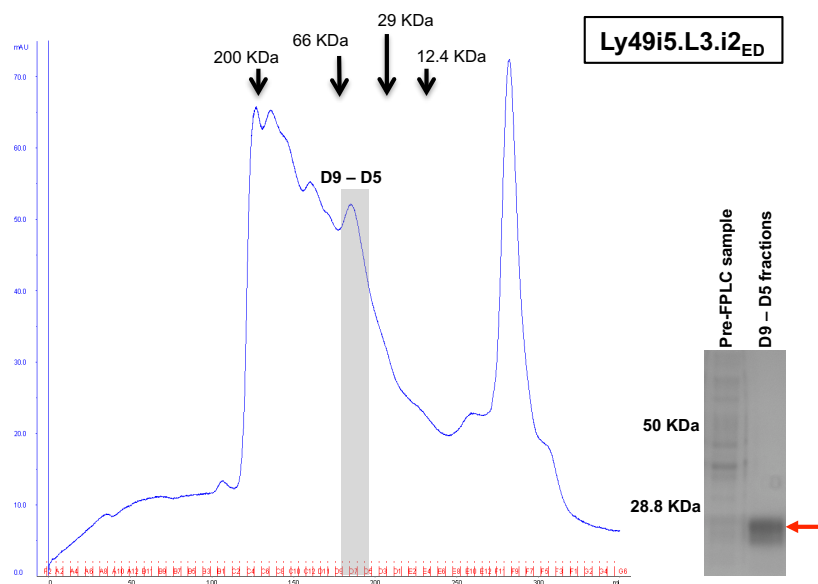


**Figure 3-21: L3 loop chimeric receptor, Ly49i5.L3.i2<sub>ED</sub>, refold.** The ectodomain of Ly49i5.L3.i2 was cloned into a pET21a vector and expressed as inclusion bodies in *E. coli* BL21 competent cells. Once purified, the inclusion bodies were solubilized in 6M G. HCl and refolded in 400mM L-Arginine buffer. Upon concentration and dialysis into a 100mM Tris/NaCl pH 8.5 buffer, the proteins were purified by size exclusion chromatography, generating the chromatogram shown (*left*). The gray-shaded area corresponds to the fractions of the refolded Ly49i5.L3.i2<sub>ED</sub> receptor, which were then pooled and concentrated. The corresponding molecular weights at each fraction are identified above the top panel. Purified Ly49i5.L3.i2<sub>ED</sub> was analyzed by SDS-PAGE (*right*). A sample of the protein along with other samples corresponding to the isolated fractions (as illustrated) were run on a 15% SDS-PAGE reducing gel and stained with Coomassie Blue for visualization. The red arrow indicates the band corresponding to the reduced Ly49i5.L3.i2<sub>ED</sub> dimer fractions.

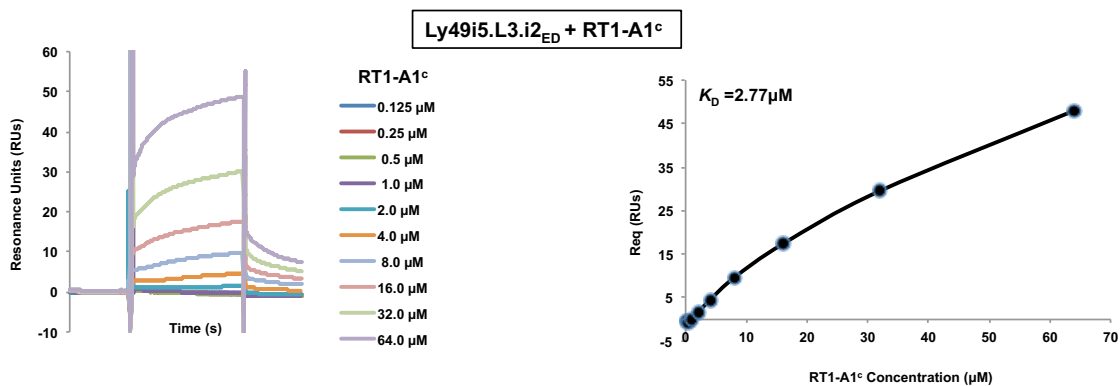


**Figure 3-22: L3 loop chimeric receptor, Ly49i5.L3.i2<sub>ED</sub>, binding interaction with RT1-A1<sup>c</sup>.** RT1-A1<sup>c</sup><sub>ED</sub> was injected at various concentrations ranging from 0.125 μM to 64 μM in two-fold increments over 1000 RU of immobilized Ly49i5.L3.i2<sub>ED</sub> on a CM5 biosensor chip. SPR for each interaction was measured using a Biacore<sup>TM</sup> T200 (*left panel*). Contact between the receptor, Ly49i5.L3.i2<sub>ED</sub>, and the analyte, RT1-A1<sup>c</sup><sub>ED</sub>, occurred with HBS-EP+ buffer at 25°C and a flow rate of 30 μl/min. The interaction for each concentration was measured three times, resulting in similar data results. The binding response at equilibrium ( $R_{eq}$ ) of RT1-A1<sup>c</sup><sub>ED</sub> with Ly49i5.L3.i2<sub>ED</sub> resulted in the equilibrium binding curves shown, (*right panel*), where  $R_{eq}$  for the analyte was plotted against concentration. The dissociation constant ( $K_D$ ) for the ligand:analyte interaction was determined by 1:1 Langmuir curve fitting and presented at the top left corner (*right panel*).

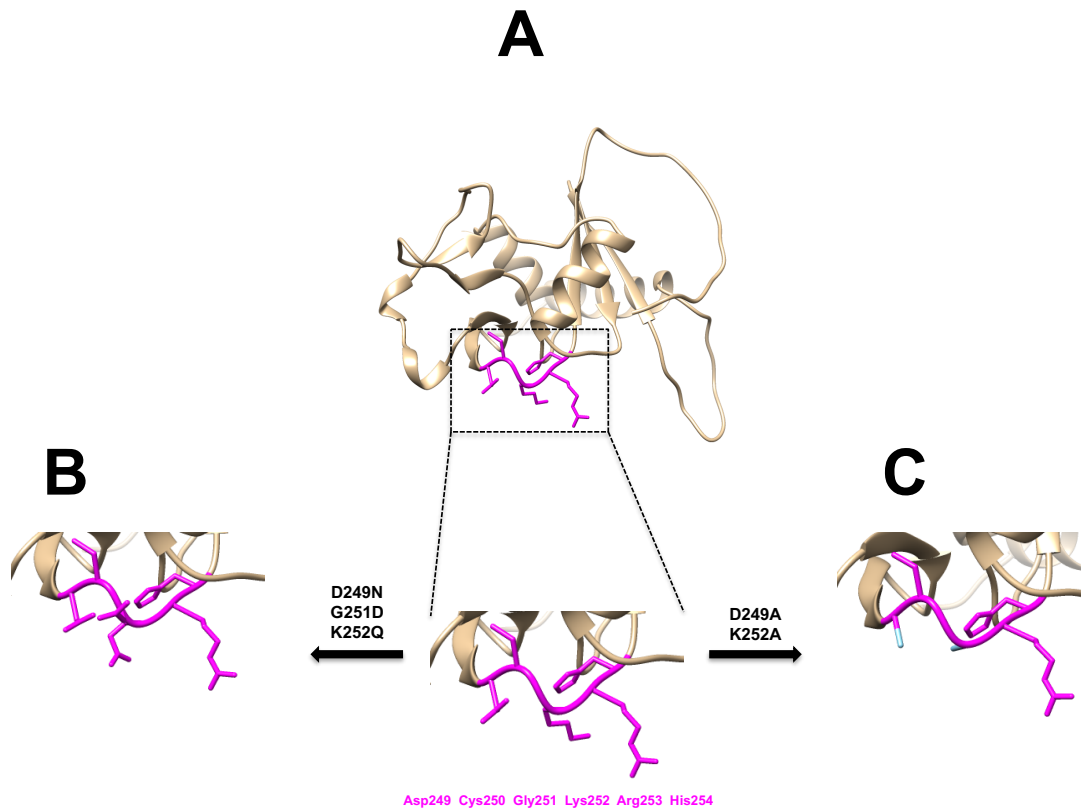


**Figure 3-23: The putative L6 loop structure of the Ly49i2 receptor.** The putative structure of the inhibitory rat Ly49i2 receptor was predicted using the molecular modeling system Chimera (<http://www.cgl.ucsf.edu/chimera/>) with the graphical interface to Modeller (<http://www.salilab.org/modeller/>), relying on the structure of the mouse activating receptor Ly49L (PDB ID: 3G8L). (A) The putative Ly49i2 structure is displayed in tan, with the L6 loop region (DCGKRH) highlighted in magenta. An amplified view of the L6 loop is also illustrated. (B) The putative L6 loop region with the NCDQRH sequence displayed in magenta. (C) The putative L6 loop region with the ACGARH sequence displayed in magenta.

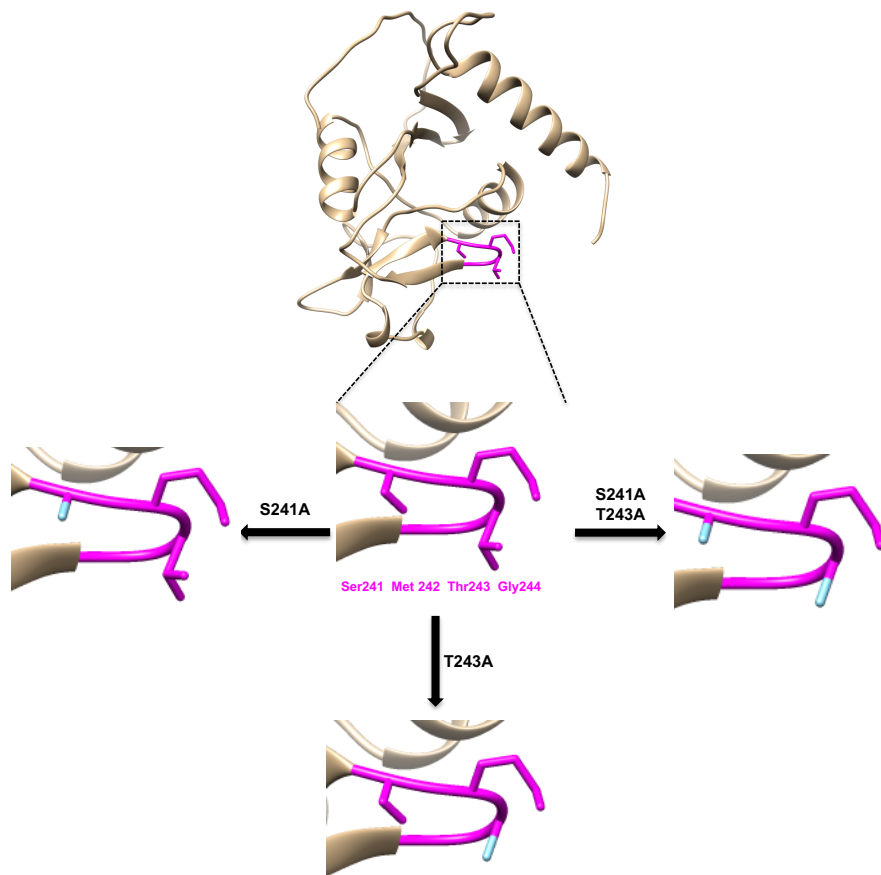


**Figure 3-24: The putative L5 loop structure of the Ly49i2 receptor.** The putative structure of the inhibitory rat Ly49i2 receptor was predicted using the molecular modeling system Chimera (<http://www.cgl.ucsf.edu/chimera/>) with the graphical interface to Modeller (<http://www.salilab.org/modeller/>), relying on the structure of the mouse activating receptor Ly49L (PDB ID: 3G8L). The putative Ly49i2 structure is displayed in tan, with the L5 loop region (SMTG) highlighted in magenta. An amplified view of the L5 loop is also illustrated. The putative L5 loop region with the AMTG sequence, the SMAG sequence, and AMAG sequences are also displayed in magenta.

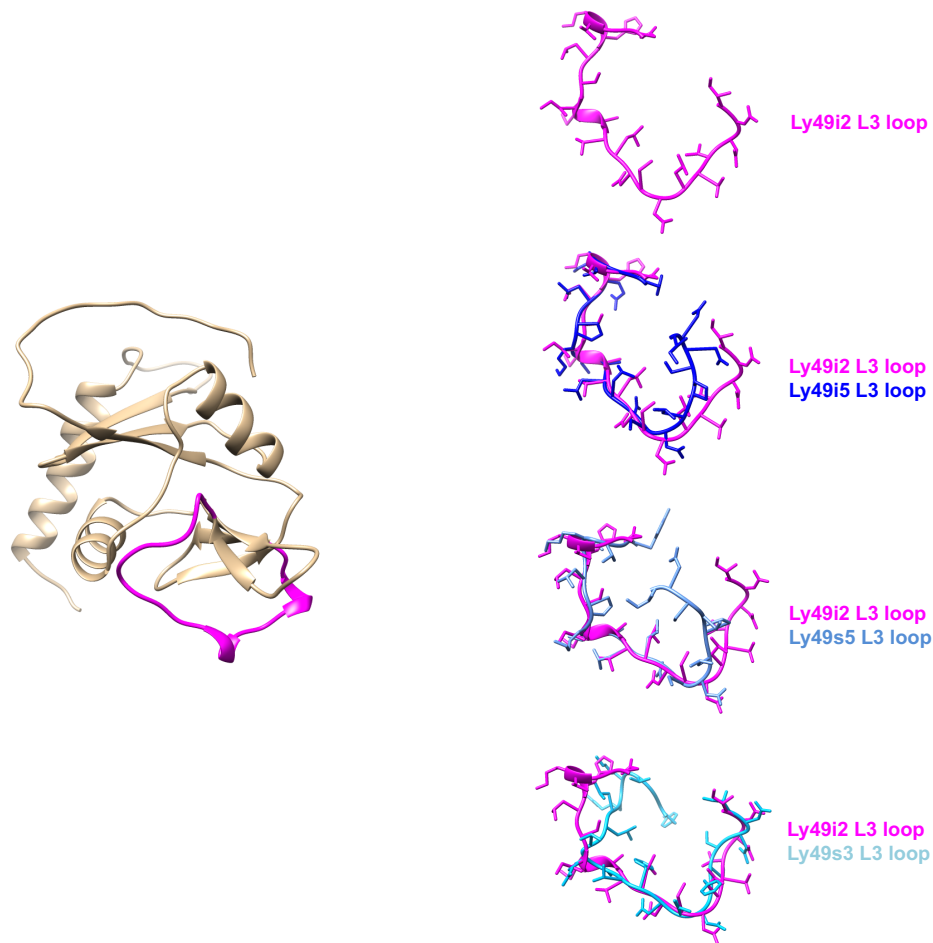


**Figure 3-25: The putative L3 loop structure of the Ly49i2 receptor.** The putative structure of the inhibitory rat Ly49i2 receptor was predicted using the molecular modeling system Chimera (<http://www.cgl.ucsf.edu/chimera/>) with the graphical interface to Modeller (<http://www.salilab.org/modeller/>), relying on the structure of the mouse activating receptor Ly49L (PDB ID: 3G8L). The putative Ly49i2 structure is displayed in tan, with the L3 loop region highlighted in magenta (*left*). An overlap of the Ly49i2 L3 loop (magenta) with the Ly49i5 L3 loop (dark blue), Ly49s5 (medium blue), and Ly49s3 (light blue) is illustrated (*right*).

**Table 3-1:** Binding affinities,  $K_D$  ( $\mu\text{M}$ ) between various mouse (M) or human (H) NK cell inhibitory (I) or activating (A) receptors and their ligands.

Receptor:Ligand	Host	Receptor Type	$K_D$ ( $\mu\text{M}$ )	Reference
Ly49G <sup>BALB/c</sup> :H-2D <sup>d</sup>	M	I	46.1	[371]
Ly49G <sup>BALB/c</sup> :H-2D <sup>k</sup>	M	I	22.9	[371]
Ly49W <sup>NOD</sup> :H-2D <sup>k</sup>	M	A	13.6	[371]
Ly49W <sup>NOD</sup> :H-2D <sup>d</sup>	M	A	48.3	[371]
Ly49A:H-2D <sup>d</sup>	M	I	1.8 – 4.4	[187, 370]
Ly49C:H-2K <sup>b</sup>	M	I	80 - 102	[187, 189]
Ly49C:H-2D <sup>d</sup>	M	I	136	[187]
Ly49I <sup>129/J</sup> :m157	M	I	0.166	[222]
Ly49H:m157	M	A	0.936	[222]
KIR2DL1:HLA-Cw4	M	I	7.2	[373]
KIR2DL2:HLA-C*03:04	H	I	0.015 – 0.036	[374]
KIR2DL3:HLA-C*03:04	H	I	0.03 – 5.6	[374]
KIR3DS1:HLA-B2705	H	A	6.95	[375]
CD94/NKG2-A:HLA-E	H	I	0.53 – 56.6	[376, 377]
CD94/NKG2-C:HLA-E	H	A	3.8 – 120.0	[376, 377]
CD94/NKG2-E:HLA-E	H	A	0.72 – 22.9	[377]

*Table adapted from: [371]*

**CHAPTER IV:  
LENTIVIRAL-MEDIATED EXOGENOUS GENE EXPRESSION  
IN RNK-16 CELLS**

**4.1 INTRODUCTION**

Understanding and defining the function of natural killer (NK) cells during target cell engagement, specifically the contributions made by NK cell specific receptors, requires a functional assessment system that allows for efficient expression of the protein of interest. Traditionally, our lab has relied on RNK-16 cells for NK cell functional studies, as they are commonly used for NK cell activation studies [272]. RNK-16 cells were first described in 1983 as a spontaneous leukemic NK cell line of the F344 rat, possessing NK cell function and specificity [263], and like other NK cells (as described in Chapter I), are NKR-P1<sup>+</sup>CD45<sup>+</sup>CD3<sup>-</sup> [272, 284, 285]. Furthermore, RNK-16s express a variety of other rat specific cell surface receptors; however, the latter are rat strain specific, thus expression of human, mouse or even other rat strain receptors has been shown to be possible on RNK-16 cells, generating receptor specific functional outcomes [191, 264-267]. These cells readily recognize NK cell tumor targets such as rat YB2/0 cells and rapidly kill them, making the RNK-16:YB2/0 combination an effective system for functional NK cell studies [263, 272].

NK cells, however, are resistant to exogenous gene transfers [268-271]. Expression of exogenous genes in RNK-16 cells typically results from electroporation, relying on gene expression driven by the BSR $\alpha$ EN vector, a method first described by Ryan et al in 2000, then updated by the Kane lab [272, 273]. Electroporation of RNK-16s has been extensively used by others and our lab, resulting in successful expression of foreign cell surface proteins, such as Ly49 molecules [190-192, 243, 264-267, 273, 286-291]. Electroporation of RNK-16 cells, however, is extremely time consuming and always results in very low transfection efficiency. On average, one protein of interest may require 3-8 electroporation attempts, and may require a growth period, under antibiotic selection, of 2 – 3 months before the functional assay can be carried out. With a deep investment in defining and understanding NK cell receptor functions, we decided

to explore an alternative expression method for RNK-16 cells.

Several groups have explored alternative NK cell transfection methods. Non-viral methods, such as calcium phosphate, lipofections, electroporation, or particle-mediated gene transfer, if at all successful in exogenous gene expression, they yield low transfection efficiencies [269, 270, 292-295]. A more popular non-viral method, nucleofection, has also been explored. Nucleofection, a Lonza company trademark, was developed as an electroporation type protocol with cell type specific reagents and machinery, and although this costly method has resulted in positive NK cell transfection outcomes, transfection efficiency is still low [295-297]. Furthermore, nucleofections are limited to the cell type kits available; rat NK cells, whether primary or cell lines, are not yet able to express exogenous DNA via this method.

Viral-based transfection approaches have also been considered as possibilities for cells that are difficult to transfect. Several of these options, however, have only reported limited success, while others are not viable at all. Adenoviruses have been used to transduce IL-2 activated NK cells, however, transgene expression is transient to a maximum of 96 hours [298, 299]. The biggest limitation of transduction with adenoviral vectors is the lack of the adenovirus attachment and viral host cell entry receptors, coxsackievirus and adenovirus receptor (CAR) and  $\alpha V$  integrins, on NK cells [300]. Although this limitation can be overcome with chimeric adenoviral vectors that bind CD46, a protein ubiquitously expressed on all nucleated cells [301], the adenovirus chimeras are still unable to generate long term transient or stable transductants [300]. Transductions with vaccinia virus based vectors have also been tested. Although the vaccinia virus is capable of infecting NK cells successfully, the integrity of the NK cell phenotype, functional output, and survival are compromised [302, 303]. Retroviruses are capable of integrating in the host genome, resulting in stable exogenous gene expression on the transduced cells. In spite of this, exogenous gene delivery by retroviral vectors appears to only be effective in primary NK cells activated prior to the transduction, as well as requiring repeated rounds of infection [14, 304, 305].

Lentivirus transduction systems have proven the most successful option for transgene expression in cells difficult to transfect, such as primary mouse NK cells [268]. Furthermore, lentiviruses distinguish themselves from other retrovirus family members

by their ability to also infect non-dividing cells [306, 307]. Most impressively, NK cell transduction by lentiviral vectors appears to sustain the viability, the function, and the phenotype of NK cells [268].

In this chapter, I describe a method for successfully transducing RNK-16 cells with a lentiviral vector system. Furthermore, this protocol allows for efficient high transgene expression in RNK-16 cells in a much shorter time frame than electroporation, the traditional exogenous gene transfer process for RNK-16 cells.

## **4.2 RESULTS**

### **4.2.1 RNK-16 cells cannot be transduced to express the transgene Ly49i2 under the control of the universal CMV promoter**

The functionality of Ly49 receptors has always been of great research interest to the Kane lab. Specific to my research focus, I intend on further elucidating the function of rat Ly49 receptors, specifically the structural specificity requirements of MHC class I recognition by the inhibitory Ly49i2 receptor. As previously mentioned, NK cell functional assays in the Kane lab have traditionally relied on the use of Ly49 transgene expressing RNK-16 cells. To investigate the structural requirements for ligand recognition by Ly49i2, I require a system that effectively allows me to express Ly49i2 and several mutants of the same receptor in a quick, efficient manner to allow for relatively rapid functional assessment.

To date, RNK-16 cells have not been transduced, thus no pre-existing lentivirus systems are obtainable. Due to the abundance of lentiviral systems available, we researched the various options and decided to attempt and optimize RNK-16 cell transduction using commercially available lentiviral kits, specifically, two possibilities available through Life Technologies™. The options selected result in a replication-deficient HIV-1 based lentivirus for the delivery and cell surface expression of our gene of interest, Ly49i2, in RNK-16 cells. Both kits allow for expression of the gene of interest (GOI) through a Gateway® cloning system. The gene is cloned into an entry vector to allow for subcloning into a lentivirus destination vector, which will allow for the expression of the gene product in the transduced cells. Gateway® cloning technology

does not involve traditional gene cloning into a restriction enzyme cloning site, instead, it is based on recombinational cloning, relying on the site-specific recombination system utilized by the bacteriophage lambda ( $\lambda$ ) [308-310].

The GOI is first cloned into a TOPO® entry vector via “TOPO® cloning”. The TOPO® cloning system is available through Life Technologies™. It bypasses traditional cloning methods by relying on the vaccinia virus topoisomerase I to function as both a restriction enzyme and a ligase [311]. Topoisomerase I, which is attached to the ends of commercially available linearized TOPO® vectors, recognizes the sequence (T/C)CCTT that has been previously added to the ends of the PCR-amplified GOI [311]. Cloning the GOI is achieved by simply mixing the TOPO® vector and the GOI together. The entry vector also contains *attL* sequences that flank the gene and allow for its effective transfer to a secondary vector, the destination vector, containing *attR* sequences via recombinational cloning (Figure 4-1) [308, 309, 312]. Recombinational cloning is based on the integration mechanism employed by  $\lambda$  upon infecting its target host, *Escherichia coli* [313, 314]. Integration of the  $\lambda$  genome within the genome of *E. coli* requires reciprocal recombination between specific DNA regions called attachment sites (*att*) where a crossover occurs between the specific site on the  $\lambda$  DNA (*attP*) and the specific site on the bacterial DNA (*attB*); once integrated, the prophage (the integrated  $\lambda$  DNA), is bound by hybrid DNA sequences termed *attL* and *attR* [314]. The reverse reciprocal recombination event of the *attL* and *attR* sites can restore the *attP* and *attB* sites once again [314]. These crossover events require two  $\lambda$ -encoded proteins, integrase (Int) and excisionase (Xis), as well as an *E. coli*-encoded protein, the integration host factor (IHF) [309]. Int is a DNA topoisomerase that acts within the core of the *att* sites for DNA breakage and rejoining during crossover [314]. Xis controls the directionality of the recombination event, as well as binds to specific sequences and bends the DNA allowing reciprocal recombination to occur [315]. IHF is a DNA binding protein that, upon recognizing three specific DNA regions in the *att* sites, induces a sharp bend in the DNA at each *att* site allowing the crossover-specific DNA sites to be in close proximity with each other [316]. The described  $\lambda$  recombination events have been extensively studied and adapted as molecular biology tools, and are the basis for the Gateway® recombinational cloning system [309, 312].

Once the GOI is cloned in an entry vector, the Gateway® cloning system mediates the relocation of the gene into the destination vector. The crossover between the entry vector and the destination vector requires an *in vitro* reaction where the entry vector *attL* sequences recombine with the destination vector *attR* sequences (Figure 4-1) in the presence of the enzymes Int, IHF, and Xis (termed the LR clonase™ enzyme mix) [308-310, 312]. Within the destination vector, the *attR* sequences flank the F-plasmid *ccdB* gene (Figure 4-1), responsible for inhibiting the growth of *E. coli* [317], hence it is used for selection of the destination vector after the successful recombination reaction [308]. Furthermore, the entry plasmid is kanamycin resistant (kan<sup>r</sup>) whereas the destination plasmid is ampicillin resistant (amp<sup>r</sup>); therefore, this second method of selection following *E. coli* transformation with the *in vitro* recombination reaction products ensures only destination vectors with successfully transferred GOIs survive (Figure 4-1) [308]. Both commercial lentivirus vectors chosen, pLenti6.3 and pLenti7.3, rely on the universal human cytomegalovirus (CMV) immediate early promoter for expression of the gene of interest. Transgene expression in mammalian cells driven by the human CMV immediate early promoter has been shown to be effective, resulting in high gene expression levels [318]. In addition, both destination vectors add a V5 epitope tag to the C-terminus of the protein for easy identification. The V5 epitope, of protein sequence GKPIPPLLGLDST, is derived from a small epitope present on the P and V proteins of the paramyxovirus of simian virus 5 [319]. The first selected option, pLenti6.3/V5-DEST™ Gateway® Vector Kit, contains a Blasticidin resistance gene allowing for the generation and selection of stably transduced cells. Our other selected option, pLenti7.3/V5-DEST™ Gateway® Vector Kit, contains the emerald green fluorescent protein (EmGFP) as a reporter gene, that is not fused to the GOI (Ly49i2), to allow for quick and easy detection of gene expression. Based on the description of the technology offered by the vector systems, we decided to use both the pLenti6.3 and pLenti7.3 lentivirus plasmids along with their respective kits to express Ly49i2 on the surface of RNK-16 cells.

Once I cloned the wildtype Ly49i2 into the pENTR™/D-TOPO entry vector and confirmed it by sequencing, I set up a recombination reaction with the LR clonase™ enzyme mix, and the entry vector, bearing the Ly49i2 gene, along with either pLenti6.3

(Ly49i2-pLenti6.3) or pLenti7.3 (Ly49i2-pLenti7.3) destination vectors. Upon confirmation of the successful recombination sequencing, I tested the pLenti plasmids by transfecting COS-7 cells via Lipofectamine® 2000 to assess Ly49i2 expression (Figure 4-2). I assessed Ly49i2 surface expression on COS-7 cells by staining them with STOK2, a Ly49i2 recognizing monoclonal antibody of the IgG2a isotype [281, 282]. I also measured the expression of Ly49i2 indirectly by detecting the V5 epitope through staining the transfected COS-7 cells with an anti-V5 antibody. COS-7 cells transfected with Ly49i2-pLenti6.3 resulted in approximately 22% of transfected cells expressing Ly49i2 with a mean fluorescence intensity (MFI) of just under 450 and the V5 epitope was detected on around 15% of transfected cells with an MFI of almost 420 (Figure 4-2 A). Similar results were obtained with COS-7 cells transfected with Ly49i2-pLenti7.3. Almost 14% of COS-7 transfected cells express Ly49i2 (MFI around 340) and over 16% express the V5 epitope, thus Ly49i2, with an MFI of approximately 380 (Figure 4-2 B). As a negative control, I transfected COS-7 cells with “empty” pLenti6.3 and pLenti7.3 plasmids (Figure 4-2 A & B, *right panels*). Given the result obtained with the COS-7 cell transfection verification step with both destination vectors, I proceeded with the generation of infectious lentivirus for RNK-16 cell transduction for the cell surface expression of wildtype Ly49i2.

As previously mentioned, pLenti6.3 & pLenti7.3 are part of a commercially available transduction system (Life Technologies™). For transduction of the RNK-16 cells, I generated viral stocks of both Ly49i2-pLenti6.3 and Ly49i2-pLenti7.3 following the manufacturer’s suggested protocol. In general, viral stocks are generated by transfecting a producer cell line with several plasmids, each containing different genes. The producer cell line is easily transfected and secretes the replication-deficient virus product containing the necessary elements for transduction. The transduction system offered in the selected kits is based on third-generation HIV-1-derived lentivirus vector delivery systems [278]. Third-generation lentivirus systems offer significant biosafety advantages. Although the HIV-1 genome encodes nine viral protein products, only two structural genes, *gag* and *pol*, and one regulatory element, *rev*, are required for one round of infection in cells of interest [278, 320, 321]. Furthermore, to overcome the limited host-cell range of HIV-1 and typical low retroviral titers, the lentivirus is “pseudotyped”,

where the HIV-1 *env* gene has been replaced with the G glycoprotein gene of the vesicular stomatitis virus (VSV-G); the resultant lentivirus encodes a pseudotyped envelope with broad tropism while yielding high viral titers [322, 323]. The HIV-1 *gag*, *pol* and *rev* genes, along with the VSV-G gene are separated into different plasmids and 293T cells, the common producer cell line, is co-transfected with all the plasmids along with the lentivirus vector containing the gene of interest, resulting in infectious viral particles [278, 320]. I generated infectious viral particles with Ly49i2-pLenti6.3 and Ly49i2-pLenti7.3 by transient transfection of 293FT cells with a plasmid mix containing pLP1, pLP2, and pLP/VSV-G plasmids that encoded *gag/pol*, *rev*, and VSV-G, respectively. 293FT cells are a human embryonic kidney cell line, derived from 293Ts, that expresses the SV40 large T antigen that results in high virus production [278, 279]. Once I harvested and concentrated the viral supernatant from the transfected 293FT cells, I determined the viral titer using HT1080 cells, a human fibrosarcoma cell line [280], commonly used for titering lentivirus. I transduced  $5 \times 10^5$  HT1080 cells with either the concentrated virus supernatant of Ly49i2-pLenti6.3 or Ly49i2-pLenti7.3, both at dilution factors of 0,  $10^{-1}$ , and  $10^{-2}$ , with a mock transduction negative control where HT1080 cells were inoculated with supernatant from an empty vector (Figure 4-3). For each dilution, I determined the Ly49i2 expression via flow cytometry by staining the cells with STOK2 antibody and gating on live cells. I then used the percentage of gated cells expressing the receptor to determine the titer of each Ly49i2-lentivirus plasmid using the formula:  $T = (F \times Co/V) \times D$ , where  $T$  is the titer in TU/ml (transducing viral units per milliliter);  $F$  is the frequency of Ly49i2 expressing cells;  $Co$  is the number of target cells used;  $V$  is the volume of inoculum in milliliters (ml); and  $D$  is the dilution factor [283]. Once I assessed the titer for both Ly49i2-pLenti6.3 and Ly49i2-pLenti7.3 at each dilution factor, I averaged the values obtained for the dilution factors 0,  $10^{-1}$ , and  $10^{-2}$  resulting in a titer of  $4.78 \times 10^6$  TU/ml for Ly49i2-pLenti6.3, and  $4.39 \times 10^6$  TU/ml for Ly49i2-pLenti7.3.

Once I had determined the titers for each viral supernatant stock, I proceeded with the transduction of RNK-16 cells. For cell surface expression of wildtype Ly49i2, I infected RNK-16 cells at MOIs of 1, 5, 10, and 50, as well as a mock infection of supernatant generated from an empty vector, and incubated for 16 hours. After the

overnight incubation, I replaced the virus containing media with fresh complete culture media and assessed for Ly49i2 expression every 24 hours from days 2 till 6 post-transduction. The flow cytometry data obtained at 72 hours post-transduction, displayed in Figure 4-4, is representative of the data obtained for all other days I assessed for Ly49i2 expression. None of the transductions with viral stock of either pLenti construct, Ly49i2-pLenti6.3 or Ly49i2-pLenti7.3, resulted in Ly49i2 expression (Figure 4-4). In summary, my attempts to detect Ly49i2 at the cell surface of RNK-16 cells by staining the cells with STOK2 antibody every 24 hours from 48-hours post-transduction to 144-hours post-transduction were unsuccessful. Given the positive outcome observed with the transduction of HT1080 cells (Figure 4-3), I expected successful transduction of the RNK-16 cells. I persisted to attempt the transduction of RNK-16 cells with the same viral constructs, but altering various conditions such as the MOI, the incubation period, or the addition of polybrene, a cationic polymer commonly used in transductions to increase the efficiency of virus infectivity through the neutralization of the charge repulsion between the virus particles and the target cell surface [324]. None of the alterations resulted in the transduction of the RNK-16 cells for Ly49i2 cell surface expression.

The selected commercial lentivirus transduction systems are capable of transducing some cell types, such as HT1080s, resulting in the cell surface expression of wildtype Ly49i2, as seen in Figure 4-3; however, they were unsuccessful in the transduction of RNK-16 cells for cell surface expression of the same receptor (Figure 4-4). This phenomenon has been observed in human NK cells [295] and in human hematopoietic cells [325]. NK cells, of all the cell types of hematopoietic origin, may be the most difficult cells in which to express exogenous gene delivery [271]. The universal CMV promoter may not be able to induce transgene expression in RNK-16 cells, as the activity of the promoter may be diminished or even completely abrogated in these cells. My results imply that an alternative transduction system may be required for transgene expression under the control of an alternate promoter for cell surface expression of wildtype Ly49i2 in RNK-16 cells.

#### **4.2.2 Wildtype Ly49i2 is expressed on the surface of RNK-16 cells using a lentivirus transduction system with an elongation factor-1 $\alpha$ promoter for transgene expression**

Ly49 receptor functional analysis during its engagement with its cognate ligand, MHC class I, is a significant research focus in the Kane lab. The ability to rapidly express various receptor mutants on RNK-16 cells for functional assessments is of great importance to us. HIV-1 based lentivirus vector systems are able to stably transduce almost all cell types, including non-dividing cells and cells difficult to transfect both *in vitro* and *in vivo* without altering cell viability, function, or phenotype [326-331]. Furthermore, the efficiency of lentivirus systems has also been shown to be successful in transient transgene expression, where the integration of the exogenous gene into the host genome is avoided [332]. Given the benefits and flexibility of lentivirus transduction systems, yet despite the results I reported in section 4.2.1, I decided to continue to search for an alternative transduction system that allows for transgene expression, under the control of an alternate promoter, on the cell surface of RNK-16 cells.

Elongation factor-1-alpha (EF-1 $\alpha$ ), which catalyzes the binding of charged tRNAs to ribosomes in a GTP-dependent manner, is one of the most common prokaryotic and eukaryotic proteins, and is ubiquitously expressed in most mammalian cells, resulting in the characterization of the EF-1 $\alpha$  promoter as being robust and constitutive [333-337]. The EF-1 $\alpha$  promoter has become commonly used for transgene expression in many cell types characterized as difficult to transfect, non-dividing or in cell types where the CMV promoter has been less successful [325, 338-342].

For RNK-16 transgene transduction, I chose to explore the lentiviral vector, pLEX307, which expresses the gene of interest under the control of the EF1 $\alpha$  promoter, and allows for cloning the gene of interest via Gateway® recombination, as outlined in section 4.2.1. The gateway lentiviral destination plasmid pLEX307, along with the packaging plasmid psPAX2 and VSV-G envelope plasmid pMD2.G, were generously provided by Dr. Troy Baldwin (Department of Medical Microbiology & Immunology; University of Alberta). Once I cloned the wildtype Ly49i2 inhibitory rat receptor into pLEX307 (pLEX.49i2), I proceeded to generate infectious virus using the method described by The RNAi Consortium (TRC) laboratory protocol available at The RNAi Consortium, Broad Institute online website (<https://www.broadinstitute.org/rnai/trc>).

Briefly, I transfected 293T packaging cells with psPAX2, pMD2.G, and pLEX.49i2 at a ratio of 10:1:10, respectively, using the TransIT-LT1 transfection reagent. The recommended ratio of each plasmid has been optimized to ensure optimal production of infectious lentivirus is generated. Upon overnight incubation with the transfectants, I replaced the culture media of the 293T cells with high serum growth medium. After 24 and 48 hours, I harvested, pooled, concentrated, and titered the viral supernatants.

Given that the lentivirus system selected was not commercially available in a kit format with optimized protocols recommended, I needed to devise a method for successful RNK-16 transduction using the pLEX307 lentivirus plasmid. After I tested and explored several alternatives and options, I was able to successfully transduce RNK-16 cells to express the Ly49i2 transgene. Through the various trials, I determined that the most efficient transduction method for RNK-16 cells requires a spinfection step where the cells are incubated with culture media containing polybrene, along with the concentrated virus stock at a MOI 50. The introduction of polybrene and a spinfection step dramatically increased the transduction efficiency of RNK-16 cells, as detected after 48 hours post-transduction (Figure 4-5 *A*). At 48 hours post-transduction, the addition of polybrene only (with no spinfection step) along with the infectious virus at an MOI 50 resulted in the expression of Ly49i2 by approximately 15% of RNK-16 cells, whereas a spinfection only (with no polybrene) after the addition of virus at the same MOI resulted in over 50% of RNK-16 cells expressing the receptor (Figure 4-5 *A*). With both polybrene and a spinfection step, along with an MOI 50 resulted in almost 90% of RNK-16 cells expressing the transgene Ly49i2 at 48 hours post-transduction (Figure 4-5 *A*). Given the promising result, I continued growing the transduced cells for 1 week post-transduction to ensure cell viability and transgene expression. Following RNK-16 transduction with pLEX307 cloned with wildtype Ly49i2, almost 85% of the cells continued to express the receptor after 1 week post-transduction (Figure 4-5 *B*). For all transductions with the pLEX307 plasmid, I also performed mock transductions of the RNK-16s with the empty vector only, as a negative control (Figure 4-5 *A & B*).

Given the successful transduction of RNK-16 cells with the lentivirus pLEX307 plasmid and the protocol outlined above, I then proceeded to establish stable Ly49i2-expressing RNK-16 transductants. Stable transductants can be stored and used for future

experiments such as functional assays. For the establishment of stable exogenous gene expressing RNK-16 cells, I transduced RNK-16 cells once again (as outlined above) and at 48 hours post-transduction I replaced the culture medium with growth medium containing puromycin, the selection antibiotic of pLEX307. To determine the appropriate puromycin concentration, I incubated transduced and non-transduced RNK-16 cells with growth medium containing various concentrations of puromycin ranging from 0.01 to 10 $\mu$ g/ml and assessed the survival of transduced RNK-16 cells in the presence of puromycin as compared to non-transduced RNK-16s (Figure 4-6 A). For both groups, transduced and non-transduced RNK-16 cells, the cells were not able to survive in puromycin concentrations ranging from 0.5 - 10  $\mu$ g/ml. Both groups of cells were able to survive at 0.1 $\mu$ g/ml; however, at 0.25  $\mu$ g/ml, only the majority of the transduced RNK-16 cells were able to survive (Figure 4-6 A). Based on these observations, I determined the appropriate puromycin concentration for RNK-16 cells transduced with pLEX.49i2 is 0.25 $\mu$ g/ml. Upon determining the appropriate antibiotic concentration, I replaced the culture medium of RNK-16 cells transduced with pLEX.49i2 at 48 hours post-transduction and allowed them to grow for 1 week in the presence of 0.25 $\mu$ g/ml of puromycin, after which I stained the cells with the STOK2 antibody for Ly49i2 expression via flow cytometry (Figure 4-6 B). After 1 week post-transduction, approximately 75% of the gated cells expressed Ly49i2 (Figure 4-6 B).

The results in this section allowed me to develop a protocol that results in the generation of stable transduced RNK-16 cells expressing an exogenous gene of interest. Throughout this section, I transduced RNK-16 cells with a lentivirus plasmid that drives the expression of the transgene of interest with an EF-1 $\alpha$  promoter. This promoter has been shown to be successful in transgene expression where the universal CMV promoter failed [325, 338-342]. The experimental procedure I developed resulted from testing different parameters at different stages until I reached a lentivirus transduction protocol where the majority of the cells express the exogenous gene, Ly49i2 in this case, without jeopardizing cell viability.

### 4.3 DISCUSSION

The research efforts of the Kane lab are concentrated on further elucidating the specific molecular requirements that dictate ligand recognition by the rodent NK cell receptor family Ly49s. To this purpose, rapid and efficient transgene expression on RNK-16 cells for functional assays is therefore a priority. In this chapter, I describe such a method.

NK cell function and activation studies are commonly executed with RNK-16 cells [272]; however, these cells, like all other NK cells, are difficult to transfect [271]. To date, exogenous gene expression in RNK-16 cells has only been reported with electroporation, a method that allows for foreign DNA entry into a cell through the transiently increased permeability of the cell membrane as a result of an applied electric field [343, 344]. This method, although successful in transgene expression, is extremely time consuming and yields low transfection efficiency, especially with RNK-16 cells. We have relied on this method for many of our studies in the Kane lab; however, due to the limitations outlined, we decided to search for an alternative transfection technique.

Replication-deficient HIV-1 based lentivirus vectors used for transgene delivery and cell surface expression are remarkable in their ability to transduce dividing and non-dividing cells, as well as cells difficult to transfect [306, 307]. Furthermore, lentivirus transduction systems are thus far the most versatile mammalian cell transfection technique available [345-347]. Understanding NK cells and their functional requirements is at the centre of our research focus, therefore the use of NK cells for such studies is a definite prerequisite. NK cells, however, resist exogenous gene transfers [271]; consequently, I opted to investigate a lentivirus vector system to overcome this challenge.

In this chapter, I first presented an attempt at transducing RNK-16 cells using commercially available lentivirus transduction kits. Both kits relied on the universal CMV promoter for transgene expression. The CMV promoter is one of the strongest promoters available for *in vitro* and *in vivo* exogenous gene expression in mammalian cells [348, 349]. Given the use of a lentivirus vector with a transgene CMV promoter, I expected that my gene of interest, Ly49i2, would be expressed in RNK-16 cells. Both of the selected vectors, pLenti6.3 and pLenti7.3, once cloned with my gene of interest,

Ly49i2, were able to transfect COS-7 cells and transduce HT1080 cells with Ly49i2. Conversely, the ultimate goal, transduction of RNK-16 cells for Ly49i2 cell surface expression, was not achieved with these lentivirus vectors. Regardless of the attempts and method modifications, the same outcome always resulted, no cell surface expression of Ly49i2 on RNK-16 cells.

The potency of the CMV promoter has allowed for successful transgene expression in a broad range of cells [349]. However, in both *in vitro* and *in vivo* settings, the CMV promoter has been shown to be sensitive to methylation, thus rendering this promoter unpredictable for transgene expression [348, 350]. The DNA region of the CMV promoter is comprised of four different types of repeat sequences located upstream of the transcriptional start site [351] that bind several positive and negative transcription regulators, as well as methylated DNA binding proteins [348]. Through binding, the methylated DNA binding proteins may block access to the DNA, thus interfere with transcription [352]. Although the exact silencing mechanism is unknown, DNA methylation and histone deacetylation are believed to cooperate and silence the promoter in human and rodent cells both *in vitro* and *in vivo* [348, 350, 353, 354]. Furthermore, the phenomenon of CMV promoter silencing is further supported by the gain of function by the re-activated CMV promoter upon the inhibition of both DNA methylation and histone deacetylation [349, 355, 356]. Interestingly, the CMV promoter of a lentivirus vector was successful in transgene expression in both human and primary mouse NK cells; however, both types of cells required cytokine stimulation [268, 271]. In contrast, another group reported the CMV promoter as poorly active in human hematopoietic cells [325] and non-active in a human leukemic NK cell line [295]. Nonetheless, I also was unable to express Ly49i2 in RNK-16 cells under the regulation of the CMV promoter. Although not yet reported, the CMV promoter is likely silenced in the cytotoxic RNK-16 cells, thus unable to express transgenes in these cells.

Given the versatility of lentivirus vectors and numerous promoter options available, I decided to test RNK-16 transduction with the EF-1 $\alpha$  promoter for transgene expression. The EF-1 $\alpha$  promoter is a non-viral promoter with a vital role in all mammalian cells, thus likely to be immune to transcription silencing and unaffected by cell type [335, 357, 358]. Furthermore, when comparing transgene expression in various

cell types, the EF-1 $\alpha$  promoter displays much more robust results as compared to viral counterparts, such as the CMV promoter [335, 341, 358, 359]. Here, I report the first successful transduction of RNK-16 cells with transgene expression under the control of the EF-1 $\alpha$  promoter. I wanted to continue relying on gateway cloning for the generation of my expression clone (the destination vector cloned with my GOI, Ly49i2), so after considering the available options, I opted to investigate the transduction potential of pLEX307. This destination vector was a generous gift from Dr. Troy Baldwin, but it is also available through a plasmid repository, thus it is not supplied with optimized methods for transgene expression. I therefore sought to develop a protocol for efficient and rapid transduction of RNK-16s. I generated infectious virus following a recommended protocol from the TRC laboratory available at the RNAi Consortium, Broad Institute online website. From there, various transduction conditions were tested and ultimately I was able to transduce RNK-16 cells. My protocol resulted in the majority of RNK-16s expressing Ly49i2 at their cell surface with a high MFI at only 48-hours post-transduction. This efficiency rate persisted to 1 week post-transduction. At this stage, the results I report allow for the transient transduction of RNK-16 cells for short-term assays. In fact, the transduced RNK-16 cells may likely be stable. This allows for functional assays to be carried out in an appropriate length of time. For the generation of stable transductants, I cultured the transduced RNK-16s in the presence of puromycin. This will allow for future assays with the same transduced cells. Others reported the efficiency of the EF-1 $\alpha$  promoter in other cell types (outlined above). In this chapter, I also found the EF-1 $\alpha$  promoter effectively expressed Ly49i2 at the cell surface of the RNK-16 cells, a task that the CMV promoter failed to accomplish.

In this chapter, I report the first method for efficient and rapid transduction of RNK-16 cells. We, and others, rely on these cells for functional assessments. We are interested in assessing and comparing various Ly49 mutants (described in Chapter III) for recognition of their cognate ligand via the functional  $^{51}\text{Cr}$  (chromium 51) release assay. The development of the outlined protocol for transgene expression in RNK-16 cells will allow us to further explore these and other NK cell receptor:ligand interactions in a much faster and proficient manner.

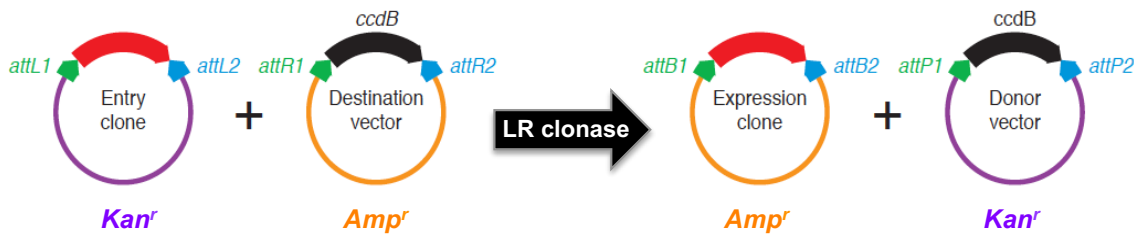


**Figure 4-1: The Gateway® recombinational cloning reaction.** The gene of interest (GOI), represented by the red arrow, is first cloned into the entry clone, or entry vector, and becomes flanked by *attL* sequences, part of the site-specific recombination system utilized by the bacteriophage lambda ( $\lambda$ ). The recombination sequences allow for the effective transfer of the GOI to a secondary plasmid, the destination vector, containing *attR* sequences. The recombination of the *attL* and *attR* sequences occurs in an *in vitro* reaction in the presence of the  $\lambda$  recombinases: integrase, integration host factor, and excisionase (termed LR clonase) resulting in an expression clone, or expression vector, with the GOI, and the original entry clone, the donor vector, bearing the F-plasmid *ccdB* gene. The entry clone is kanamycin resistant ( $Kan^r$ ) which allows for further selection of the expression clone, which is ampicillin resistant ( $Amp^r$ ). [308-310, 312, 317]. *Figure adapted from: [309]*

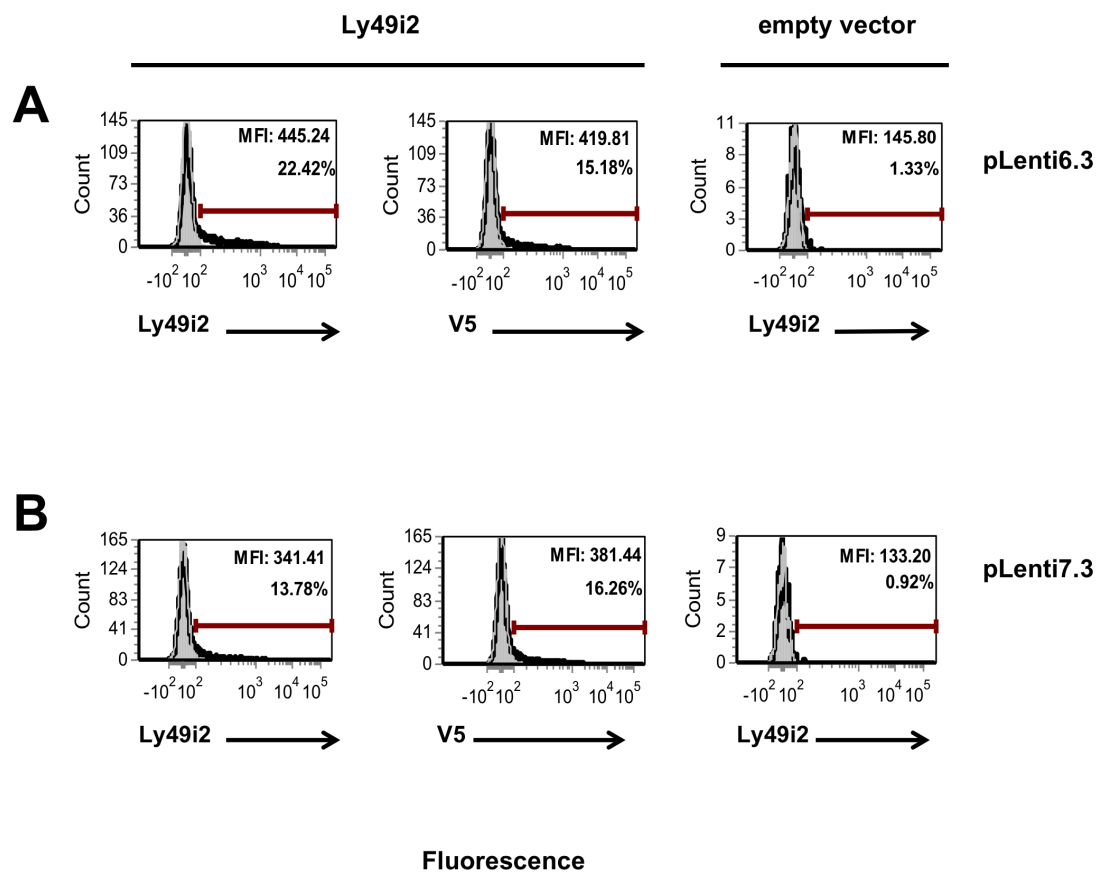


**Figure 4-2: Transfection of COS-7 cells with wildtype Ly49i2.** COS-7 cells were transfected via lipofectamine with wildtype Ly49i2 cloned into either pLenti6.3 (*panel A*) or pLenti7.3 (*panel B*) destination vector. Receptor expression was assessed via flow cytometry where Ly49i2 was stained with STOK2 antibody (*right and left panels*). Ly49i2 expression was further validated by staining for the presence of the V5 epitope with an anti-V5 epitope antibody (*middle panels*). Isotype controls are shown in grey histograms. As a negative control, COS-7 cells were also transfected with empty pLenti6.3 or pLenti7.3 vectors (*right panels*). The mean fluorescence intensity (MFI) for each profiled histogram is presented at the top right-hand corner of each histogram and the percentage of gated cells expressing Ly49i2 or the V5 epitope (%) is displayed just below the MFI. Data are representative of three independent experiments.

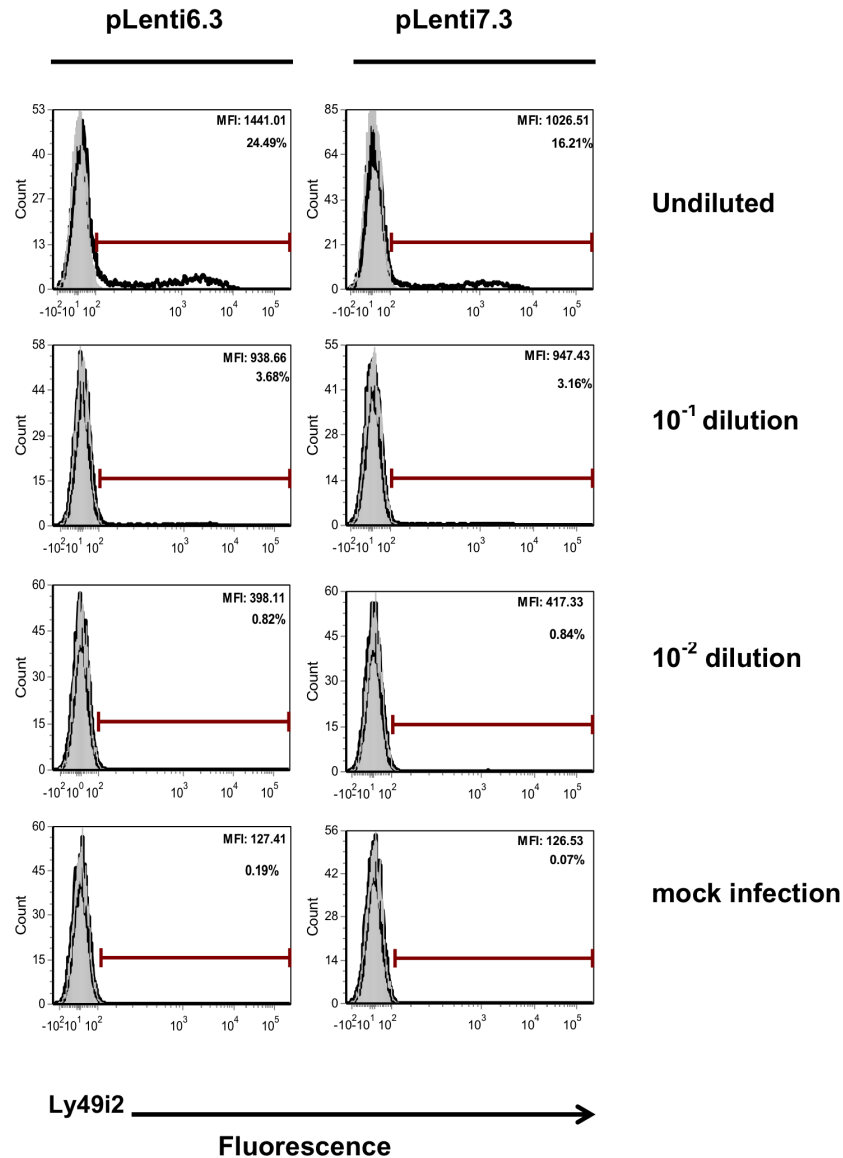


**Figure 4-3: Transduction of HT1080 cells for lentivirus titering.** HT1080 cells were transduced with wildtype Ly49i2 cloned into either pLenti6.3 or pLenti7.3. Receptor expression was assessed via flow cytometry where Ly49i2 was stained with STOK2 antibody. A 10-fold serial dilution was carried out and results for 10<sup>-1</sup> and 10<sup>-2</sup> dilutions are shown, along with the undiluted samples. The percentage of Ly49i2 expressing cells at each dilution was used to determine the titer for both Ly49i2-pLenti6.3 and Ly49i2-pLenti7.3. As a negative control, mock infections with an empty vector were also executed and the results are displayed. Isotype controls are shown in grey histograms. The mean fluorescence intensity (MFI) for each profile is presented at the top right-hand corner of each histogram and the percentage of gated cells expressing Ly49i2 (%) is displayed just below the MFI. Data are representative of three independent experiments.

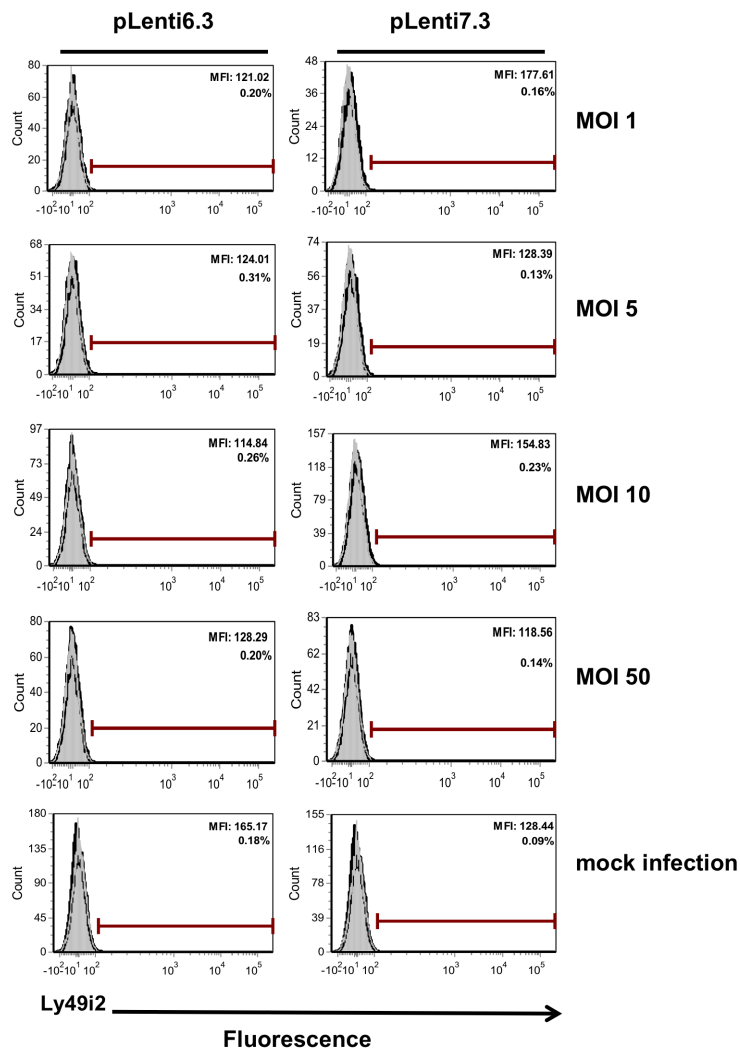


**Figure 4-4: Transduction of RNK-16 cells with pLenti plasmids for Ly49i2 cell surface expression.** RNK-16 cells were transduced with wildtype Ly49i2 cloned into either pLenti6.3 or pLenti7.3 at different MOIs ranging from 1 - 50, as illustrated. Receptor expression was assessed 72 hours post-transduction via flow cytometry where RNK-16 cells were stained with STOK2 antibody for Ly49i2 cell surface expression. As a negative control, mock infections with an empty vector were also executed and the results are displayed. Isotype controls are shown in grey histograms. The mean fluorescence intensity (MFI) for each profile is presented at the top right-hand corner of each histogram and the percentage of gated cells expressing Ly49i2 (%) is displayed just below the MFI. Data are representative of three independent experiments.

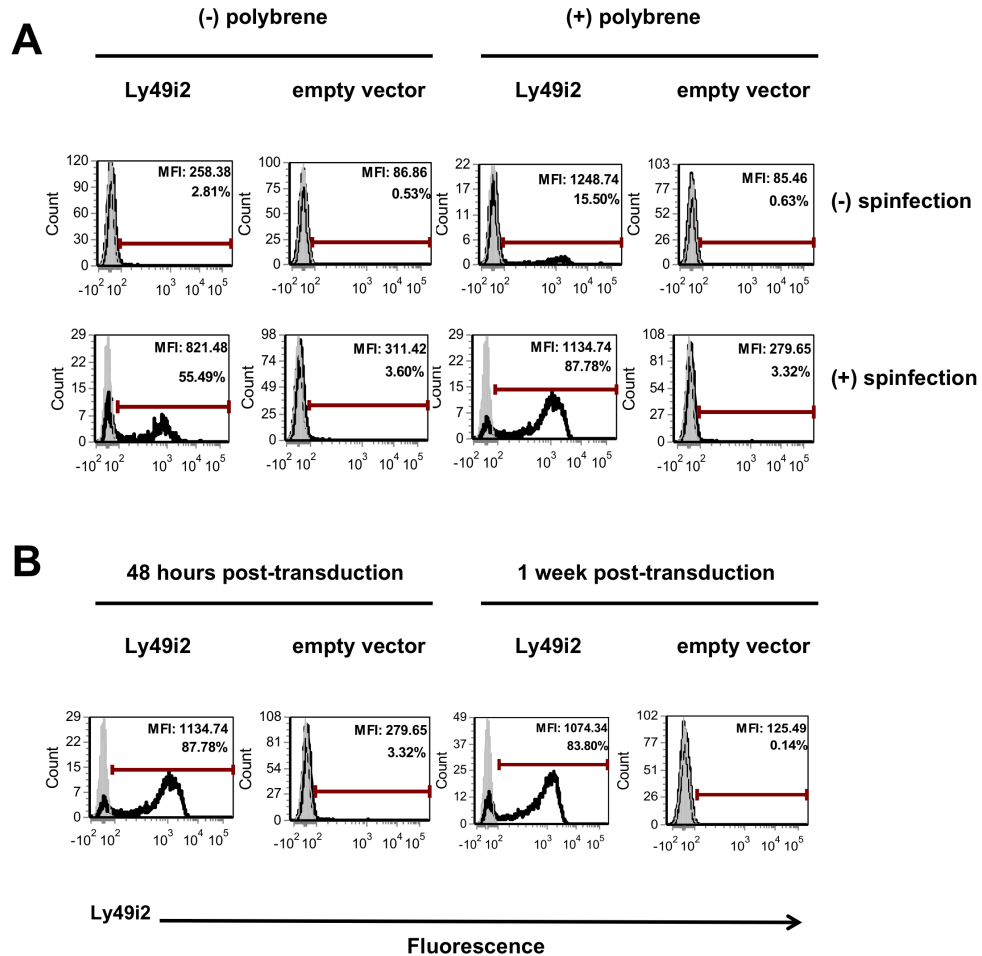


**Figure 4-5: Transduction of RNK-16 cells with pLEX307 lentivirus plasmid for Ly49i2 cell surface expression.** RNK-16 cells were transduced at a MOI 50 with wildtype Ly49i2 cloned into pLEX307. Receptor expression was assessed 48-hours (*A* & *B*) and 1 week post-transduction (*B*) via flow cytometry where RNK-16 cells were stained with STOK2 antibody for Ly49i2 expression. As a negative control, mock transductions with an empty pLEX307 vector were also performed and the results are displayed. Isotype controls are shown in grey histograms. The mean fluorescence intensity (MFI) for each profile is presented at the top right-hand corner of each histogram and the percentage of gated cells expressing Ly49i2 (%) is displayed just below the MFI. (*A*) RNK-16 cell transduction efficiency with or without polybrene and/or a spinfection step. (*B*) Transduction of RNK-16 cells with the addition of polybrene and a spinfection step for Ly49i2 cell surface expression at 48 hours and 1 week post-transduction. Data are representative of three independent experiments.

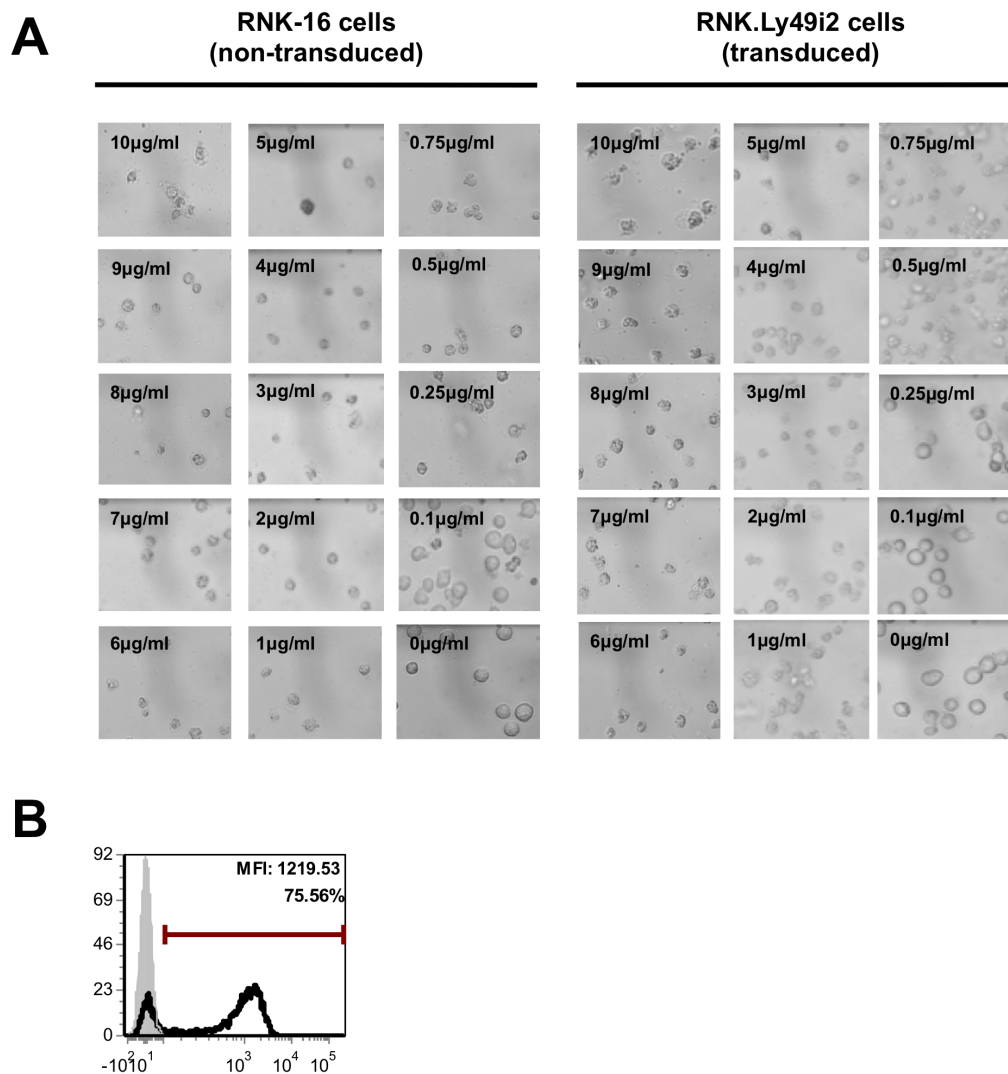


**Figure 4-6: Generation of stable RNK-16 cell transductants expressing Ly49i2.** RNK-16 cells were transduced at MOI 50 with wildtype Ly49i2 cloned into pLEX307. A viability assay was performed to determine the appropriate puromycin concentration for the generation of stable RNK-16 transductants with pLEX307 lentivirus constructs. At 48-hours post-transduction, both transduced and non-transduced RNK-16 cells were cultured with medium containing concentrations of puromycin ranging from 0.01 to 10µg/ml for a total of 1 week. (A) Light microscopy images are representative of non-transduced and transduced RNK-16 cells at the various puromycin concentrations displayed in the top left-hand corner of each image. (B) Transduced RNK-16 cells, cultured in medium containing 0.25µg/ml puromycin, are assessed for Ly49i2 expression via flow cytometry at 1-week post-transduction. Isotype control is shown in the grey histogram. The mean fluorescence intensity (MFI) is presented at the top right-hand corner and the percentage of gated cells expressing Ly49i2 (%) is displayed just below the MFI. Data are representative of three independent experiments.

## **CHAPTER V: DIMERIZATION OF Ly49 RECEPTORS**

### **5.1 INTRODUCTION**

Several cells of the immune system express cell surface proteins composed of subunits that together are required for effective functional activity of the cell surface molecule. Natural killer (NK) cells possess a vast array of homodimeric, as well as some heterodimeric receptors on their surface, such as Ly49 and NKG2/CD94 receptors, respectively [71]. Ly49 proteins, as previously described (*section 1.3.4.1.1*), are disulfide-linked homodimers [169, 170]. Ly49s engage with their ligands in a MHC allele specific manner, an interaction that ultimately dictates the functional response of the NK cell. To fully understand the functional capacity of Ly49s, it is necessary to explore the requirements and limits of Ly49 dimerization. To date, only Ly49 homodimers have been identified, although interest in the possibility of Ly49 heterodimers has been reported [378, 379]. Given the diversity of Ly49s in mice and rats, as well as their MHC allele specificity, it is of importance to understand the fundamental requirements for Ly49 homodimerization. Furthermore, assessing the possibility of Ly49 heterodimerization will contribute to the elucidation of the nature of these vital receptors in the innate immune system of several organisms, including mice and rats, in their resistance to virally infected and/or transformed cells.

The Ly49 receptor interaction with MHC class I can be symmetrical, as viewed in the co-crystal structure of Ly49C engaging with H-2K<sup>b</sup>, where each of the natural killer domain (NKD) monomers (Figure 1-4) engages with a single ligand molecule [189]. Ly49A, on the other hand, engages with its ligand, H-2D<sup>d</sup>, in an asymmetrical manner requiring both NKD monomers to interact with one CI molecule [188]. These two types of ligand-interactions described are based on the homodimeric assembly of Ly49s. If heterodimeric formation amongst Ly49 monomers is possible, our understanding of ligand specificity requirements by these receptors could be further challenged. Thus, if two different *Ly49* monomers heterodimerize, new ligand specificity may be gained, or existing specificity may be enhanced. Given the stochastic and variegated expression of

*Ly49* genes, increased avidity may also result. These and other possibilities are of great interest to this body of work.

In this report, I explore the possibility of *Ly49* receptors heterodimerizing. Using flow cytometry and biochemical assays, I provide evidence for the association between subunits of different activating *Ly49* mouse receptors, possibly forming heterodimers. In addition, my studies also suggest that inhibitory and activating receptors associate together.

## 5.2 RESULTS

### 5.2.1 The activating *Ly49M*, *Ly49W2*, and *Ly49P1* receptors associate together, and may form heterodimers

An interest in the possibility of *Ly49*s forming heterodimers has been reported [378, 379]. Brennan *et al.* attempted to form heterodimers between *Ly49A* and *Ly49C*; however, they were unsuccessful [379]. Both *Ly49A* and *Ly49C* belong to different *Ly49* receptor groups (Figure 1-5 A). Furthermore, the interaction modes with their respective MHC class I ligands exhibited by both receptors is also different [188, 189]. Understanding the requirements of homodimerization and exploring the possibility of *Ly49* heterodimers may lead to control and manipulation of *Ly49* receptors in new ways that could alter NK cell functions.

Mouse *Ly49*s display substantial receptor diversity [183, 184, 216]. A phylogenetic analysis of the *Ly49* ligand interacting domain, the C-type lectin-like domain (CTLD), was first reported by our lab. The study concluded that most *Ly49*s, with the exception of *Ly49B* and *Ly49Q*, diverged from two *Ly49* groups, the *Ly49C*-like and *Ly49A*-like families [195]. Another group found similar results by analyzing sequence alignments of mouse *Ly49*s [187]. Based on the findings of these two studies, mouse *Ly49* receptors are divided into groups (Figure 1-5 A). Group I members are predicted to be *Ly49C*-like proteins. Of interest to this chapter are group II members, proposed to be *Ly49A*-like molecules. Group II members are further divided into subgroups IIa and IIb, based on conserved residues in the CTLD.

To begin understanding the nature of *Ly49* dimerization, I selected *Ly49*

members of the same receptor group, given that a previous attempt to dimerize Ly49 monomers of the two different groups failed to result in the formation of heterodimers [379]. Firstly, I wanted to assess dimerization amongst two members of the same Ly49 subgroup, as well as between subgroups, but within the same group (Group II). Ly49M, Ly49W2, and Ly49P1 are activating NK cell receptors of the non-obese diabetic (NOD) mouse [216]. Both Ly49M and Ly49W2 are members of subgroup IIb mouse receptors, whereas Ly49P1 belongs to subgroup IIa (Figure 1-5 A). I first aligned the sequences of Ly49M, Ly49W2, and Ly49P1 to understand their sequence homology. Ly49M and Ly49W2 share the closest protein sequence identity amongst all Ly49s, at approximately 95% (Figure 5-1). Ly49M and Ly49P1 only share approximately 79% amino acid sequence identity (Figure 5-2), similarly Ly49W2 and Ly49P1 display 76% amino acid sequence identity (Figure 5-3). Given that all three receptors are members of the same group but vary in subgroup, I wanted to assess their ability to form heterodimers. I hypothesized that Ly49M and Ly49W2 would associate together to form Ly49 heterodimers. These two receptors not only belong to the same Ly49 subgroup, they share a high degree of amino acid sequence identity (Figure 5-1). Furthermore, these receptors likely arose from a tandem duplication event [216], thus may be excellent candidates for Ly49 heterodimer formation, should it occur. Moreover, I hypothesized that Ly49M and Ly49W2 would not associate with Ly49P1, based on the relatively low sequence identity observed (Figures 5-2 and 5-3, respectively). Additionally, these receptors belong to different Ly49 subgroups and thus may not associate and form heterodimers.

To test my hypotheses, and all subsequent hypotheses outlined in this chapter, I transfected COS-7 cells and assessed the association of the Ly49 receptors via a combination of flow cytometry and biochemical assays. The COS-7 cell line is derived from the kidney of the African Green Monkey, *Cercopithecus aethiops*, through transformation with a Simian Vacuolating Virus 40 (SV40), which codes for the large T-antigen [276]. The cDNA of each of the receptors used in this chapter was cloned into the pCIneo vector. The pCIneo vector encompasses the SV40 early promoter which, when transfected into COS-7 cells, relies on the SV40 large T antigen expressed in the COS-7 cells for large scale replication of the gene of interest [276]. These characteristics

make COS-7 cells an ideal choice for the transfections required in this chapter. Furthermore, we have previously used COS-7 cells to successfully express Ly49s whose cDNA were cloned into a pCIneo vector [289]. As a result, I decided to proceed with COS-7 cells for the transient transfections required to express the Ly49 cell surface receptors used in this chapter. Each of the receptors used throughout the chapter is also fused with either an influenza hemagglutinin (HA)-tag or a FLAG-tag at the C-terminus for effective identification of each protein in each of the assays performed. Activating Ly49 receptors require DAP12 for cell surface expression [49, 202]. Furthermore, DAP12 association with activating Ly49 receptors is required for functional activity by the NK cell [380]. All of the COS-7 cell transfections with activating Ly49s described in this chapter were in the presence of co-expressed mouse DAP12 (mDAP12). After transfection, I assessed the expression of the receptors at the surface of the COS-7 cells via flow cytometry, specifically for cells that expressed two receptors simultaneously. Then, after generating whole cell lysates (WCL) post-transfection, I immunoprecipitated (IP) one receptor followed by Western blot (WB) analysis for both transfected receptors.

Firstly, to ensure the fused HA and FLAG tags did not interfere with dimerization of each Ly49, as well as to confirm that each Ly49 receptor used in this study is capable of dimer formation, I carried out a positive control study. To start, I transfected COS-7 cells with mDAP12 along with Ly49M tagged with HA and FLAG (Ly49M.HA and Ly49M.FLAG, respectively), another set of COS-7 cells with mDAP12 and Ly49W2 also tagged with HA and FLAG (Ly49W2.HA and Ly49W2.FLAG, respectively), and lastly, a separate set of COS-7 cells with mDAP12 and Ly49P1 also tagged with HA and FLAG (Ly49P1.HA and Ly49P1.FLAG, respectively). As negative controls, I transfected COS-7 cells with only mDAP12 as well as with empty pCIneo vector. At 48-hours post-transfection I assessed the cell surface expression of all receptor combinations via flow cytometry by staining for the detection of the HA-tagged proteins and the FLAG-tagged proteins (Figure 5-4). Between 20–30% of the gated cells expressed Ly49M.HA and Ly49M.FLAG, or Ly49W2.HA and Ly49W2.FLAG, or Ly49P1.HA and Ly49P1.FLAG (Figure 5-4 A). As expected, there was no detection of cell surface tags when COS-7 cells were transfected with only mDAP12 or the empty vector (Figure 5-4 B). Although I observed the expressed Ly49s on the same cells, I wanted to then determine if each pair

of receptors was associating together on the cell surface. For this, I immunoprecipitated the HA-tagged proteins from WCL 48-hours post-transfection and assessed their association with the FLAG-tagged proteins by SDS-PAGE and WB. In parallel, an immunoprecipitate with an isotype control was also carried out. Moreover, non-immunoprecipitated WCL samples were also used. A dense band corresponding to the HA-tag immunoprecipitate was detected upon probing for both HA and FLAG in the samples containing Ly49M.HA:Ly49M.FLAG, Ly49W2.HA:Ly49W2.FLAG, or Ly49P1.HA:Ly49P1.FLAG (Figure 5-5, *top two panels, lanes 4-6, respectively*). Furthermore, the reverse IP, where FLAG-tagged proteins were first immunoprecipitated followed by immunoblotting for FLAG-tagged proteins and subsequently for HA-tagged proteins, also generated a thick band for all three Ly49 receptor combinations (Figure 5-5, *bottom two panels, lanes 4-6, respectively*). The predicted molecular weights for Ly49M, Ly49W2, and Ly49P1 are 30.73 kDa, 30.44 kDa, and 30.56kDa, respectively, so the bands for the reduced dimers migrated to the expected location (Figure 5-5). All of the lanes for the non-immunoprecipitated WCL samples display a band of the predicted mass for Ly49M, LY49W2, and Ly49P1, respectively, that migrated to the same location as seen in the IP blots, but not in the lanes for the IP isotype controls (Figure 5-5). Taken together, these results imply that HA-tagged and FLAG-tagged Ly49M, as well as HA-tagged and FLAG-tagged Ly49W2, and HA-tagged and FLAG-tagged Ly49P1 are associating with each other, potentially as homodimers, without the interference of the fusion tags HA or FLAG.

I had hypothesized that Ly49M and Ly49W2 would associate, yet Ly49M and Ly49W2 would not engage with Ly49P1, individually. To assess my predictions, I followed the methodology outlined above. I transfected different groups of COS-7 cells with mDAP12 along with the following combinations (Ly49M.HA with Ly49W2.FLAG; Ly49M.FLAG with Ly49W2.HA; Ly49M.HA with Ly49P1.FLAG; Ly49M.FLAG with Ly49P1.HA; Ly49W2.HA with Ly49P1.FLAG; and Ly49W2.FLAG with Ly49P1.HA). At 48-hours post-transfection I assessed the cell surface expression of the receptor combinations via flow cytometry by staining for the detection of the HA-tagged proteins and the FLAG-tagged proteins (Figure 5-6). Almost 20% of the gated cells, for each pair of receptors, expressed both the HA-tagged and FLAG-tagged proteins (Figure 5-6).

After I immunoprecipitated the HA-tagged Ly49M receptor, followed by a Western blot for Ly49M.HA and subsequently for the Ly49P1.FLAG, I detected a band in the HA IP, as well as in the non-immunoprecipitated WCL (Figure 5-7 A, *top two panels, lanes 5 & 8, respectively*). Furthermore, the reverse IP revealed the same result, a band in the FLAG IP after probing for the FLAG tagged receptor and sequentially for the HA-tagged receptor, as well as in the non-immunoprecipitated WCL (Figure 5-7 A, *bottom two panels, lanes 5 & 8, respectively*). These data suggest an association between Ly49M with Ly49P1. Furthermore, detection of the HA-tag and FLAG-tag for both IP further implies the possibility of heterodimer association between the paired receptors. To further support these results, I reversed the tags on the same Ly49s. Ly49M.FLAG and Ly49P1.HA, after transfected into COS-7 cells, resulted in the same IP/WB and non-immunoprecipitated WCL result as observed for Ly49M.HA and Ly49P1.FLAG (Figure 5-7 B, *lanes 5 & 8, respectively*). The only exception is the faint band observed for the immunoblot of Ly49M.FLAG following HA IP (Figure 5-7 B, *2<sup>nd</sup> panel, lane 5*); nonetheless, a band is present. No band is observed in the IP isotype control lanes (Figure 5-7 B, *lane 2*). By reversing the tags and generating the same results is strong evidence that Ly49M and Ly49P1 associate as heterodimers.

Similar results were observed for the biochemical analyses of Ly49W2 and Ly49P1. Following the IP for HA-tagged Ly49W2 or for FLAG-tagged Ly49P1, the immunoblot for Ly49W2.HA and subsequent probing for Ly49P1.FLAG, as well as the WB for Ly49P1.FLAG followed by WB for Ly49W2.HA, respectively, resulted in a band for both IPs, as well as the non-immunoprecipitated WCL (Figure 5-7 A, *lanes 6 & 9, respectively*). No band resulted in the IP for the isotype controls (Figure 5-7 A, *lane 3*). These data suggest an association between Ly49W2 with Ly49P1, likely as heterodimers. The analyses of the reverse tagged proteins, Ly49W2.FLAG and Ly49P1.HA, generated a similar outcome. After the HA IP, a band is visible for the HA immunoblot, but not for the FLAG immunoblot, including the WCL (Figure 5-7 B, *top two panels, lanes 6 & 9, respectively*). When the IP for FLAG was carried out, the WB for FLAG-tagged Ly49P1 followed by WB for HA-tagged Ly49W2 did reveal a band for both immunoblots, as well as the non-immunoprecipitated WCL (Figure 5-7 B, *bottom two panels, lanes 6 & 9, respectively*). The band for the WB probing for FLAG,

following the IP for FLAG, is visible but the detection required long exposure to reveal the faint band in the non-immunoprecipitated WCL sample (Figure 5-7 B, 3<sup>rd</sup> panel, lane 9). The flow cytometry data, although it reveals that approximately 18% of the transfected COS-7 cells expressed Ly49W2.FLAG and Ly49P1.HA (Figure 5-6 C, bottom plot), it may not have been sufficient to be detected by the immunoblot for FLAG, nor in the non-immunoprecipitated WCL (Figure 5-7 B, 2<sup>nd</sup> panel, lanes 6 & 9, respectively). Taken together, the data suggest that Ly49W2 and Ly49P1 associate possibly as heterodimers.

The data in this section also imply that Ly49M and Ly49W2 associate, as hypothesized. A dense band is visible for the IP of the Ly49M.HA receptor, followed by the WB for the HA-tag (Figure 5-7 A, top panel, lane 4). The non-immunoprecipitated WCL also revealed a band (Figure 5-7 A, top panel, lane 7). When subsequently probing for the FLAG-tagged Ly49W2 receptor, a faint band is seen in the IP for HA, as well as in the non-immunoprecipitated WCL ((Figure 5-7 A, 2<sup>nd</sup> panel, lanes 4 & 7, respectively). The reverse IP resulted in a similar outcome. The IP for the Ly49W2.FLAG protein, then the sequential immunoblots for FLAG and HA, resulted in a band for both, including the non-immunoprecipitated WCL (Figure 5-7 A, bottom two panels, lanes 4 & 7, respectively). These data suggest a heterodimeric association between Ly49M and Ly49W2. After reversing the tags, the data from the biochemical assays for Ly49M.FLAG and Ly49W2.HA are parallel to the data observed for Ly49M.HA and Ly49W2.FLAG, with one exception. Following the IP for the HA-tagged protein, the probe for the FLAG-tagged Ly49 did not result in a band (Figure 5-7 B, 2<sup>nd</sup> panel, lane 4). The anti-FLAG antibody may not have been able to detect small quantities of FLAG-tagged proteins. A very faint band is visible in the non-immunoprecipitated WCL (Figure 5-7 B, 2<sup>nd</sup> panel, lane 7). A double band resulted from the IP for the FLAG-tagged Ly49M followed by the WB for the HA-tagged Ly49W2.HA (Figure 5-7 B, 4<sup>th</sup> panel, lane 4). The doublet may be due to an alteration in post-translational modifications, such as glycosylation. None of the isotype control IPs in this section display a band (Figure 5-7 A & B, lanes 1-3). The migration of the receptors tested in this section is within the correct molecular weight range (Figure 5-7 A & B).

Taken together, the data presented in this section revealed interesting results.

Ly49M and Ly49W2 associated with Ly49P1, individually, implying the possibility of the formation of heterodimers between Ly49M and Ly49P1, as well as between Ly49W2 and Ly49P1. Because Ly49P1 belongs to a different Ly49 receptor subgroup, IIa, and Ly49M and Ly49W2 both belong to subgroup IIb (Figure 1-5 A), I did not expect the observed outcome. On the other hand, I had predicted that Ly49M and Ly49W2 would associate together and the data presented supports my hypothesis. In this section, I demonstrated for the first time that activating receptors within the same receptor family, group II, specifically Ly49M and Ly49W2, Ly49M and Ly49P1, as well as Ly49W2 and Ly49P1 associate together, possibly forming heterodimers.

### **5.2.2 The activating Ly49M and Ly49W2 receptors associate individually with the inhibitory receptor Ly49G2, possibly forming heterodimers**

Mouse Ly49 receptors exist in both activating and inhibitory forms. Although structurally similar, the main difference between activating and inhibitory Ly49s is the ability of inhibitory receptors to prevent NK cell activation, while activating receptors stimulate the NK cell resulting in cytotoxicity. In general, inhibitory mouse Ly49 receptors engage with MHC class I molecules; an interaction that has been extensively studied [49]. Activating receptors, on the other hand, are not as well characterized. A few Ly49 activating receptors have been shown to also distinguish MHC class I ligands [242]. Our lab has demonstrated that the NOD mouse activator Ly49W recognizes the MHC class I molecules H-2D<sup>d</sup> and H-2K<sup>k</sup> [289]. These MHC class I molecules are also recognized by the BALB/c inhibitory receptor Ly49G2 [243, 289, 381]. Furthermore, we have also demonstrated that both the activating Ly49W2 and inhibitory Ly49G2 recognize H-2D<sup>d</sup> and H-2K<sup>k</sup> with similar binding affinities [371]. Upon sequence alignment analysis of Ly49W2 and Ly49G2, I observed that they share 82% amino acid sequence identity (Figure 5-8). Given the 95% amino acid sequence identity between Ly49M and Ly49W2 (Figure 5-1), I also assessed the sequence identity between Ly49M and Ly49G2. Ly49M and Ly49G2 also share 82% identity in their protein sequence (Figure 5-9). Despite the degree of sequence identity, Ly49G2 differs the most from Ly49M and Ly49W2 in their cytoplasmic domains and transmembrane regions. Ly49G2 contains an ITIM motif near the N-terminus of the cytoplasmic tail, whereas Ly49W2

and Ly49M lack the ITIM consensus sequence (Figures 5-8 and 5-9), both typical of inhibitory and activating NK cell receptors, respectively [72]. The Ly49G2 cytoplasmic domain C-terminus also contains three extra residues, KYS, making it longer than the Ly49W2 and Ly49M receptors (Figures 5-8 and 5-9). The most noteworthy difference in the transmembrane regions, apart from the low sequence identity, is the presence of an arginine residue in only Ly49W2 and Ly49M, a charged residue typically required by activating receptors for engagement with adaptor molecules, such as DAP12, for functional output [71]. The stalk region of Ly49W2 and the stalk of Ly49M display approximately 85% identity in their protein sequence with Ly49G2 (Figures 5-8 and 5-9). Interestingly, Ly49W2 and Ly49G2 share 98% identity in their amino acid sequence in their ligand interacting region, the natural killer domain (NKD), differing by only three residues (Figure 5-8). Ly49M and Ly49G2 display 94% protein sequence identity in their NKD (Figure 5-9). Furthermore, all three receptors, Ly49W2, Ly49M, and Ly49G2, belong to the same receptor family, group II, and subgroup IIb (Figure 1-5). Therefore, I hypothesized that Ly49W2 and Ly49G2, as well as Ly49M and Ly49G2 would associate together. To test my hypotheses, I relied on the same methodology as described in section 5.2.1; hence, Ly49M, Ly49W2, and Ly49G2 were all tagged with HA and FLAG, separately.

Firstly, to ensure that the tags did not interfere with dimer formation of Ly49G2 (as previously examined for Ly49M and Ly49W2), I transfected COS-7 cells with Ly49G2.HA and Ly49G2.FLAG; mDAP12 was not used in the transfections given that Ly49G2 is an inhibitory receptor. At 48-hours post-transfection I assessed the cell surface expression of Ly49G2.HA and Ly49G2.FLAG via flow cytometry (Figure 5-10 A). Approximately 25% of the gated cells expressed the Ly49G2 receptors on the surface of the same transfected cells (Figure 5-10 A). Subsequently, I immunoprecipitated the HA-tagged Ly49G2 proteins from WCL 48-hours post-transfection and assessed their association with the FLAG-tagged Ly49G2 molecules by SDS-PAGE and WB. In parallel, an immunoprecipitate with an isotype control was also carried out. Additionally, non-immunoprecipitated WCL samples were also collected. A band corresponding to the HA-tag IP was detected upon probing for both HA and FLAG, but not in the immunoprecipitated isotype control (Figure 5-11, *top two panels, lanes 2 & 1*,

*respectively*). A band was also detected in the non-immunoprecipitated WCL (Figure 5-11, *top two panels, lane 3*). Moreover, the same result was observed upon performing the reverse IP for the FLAG proteins, followed by WB analysis for FLAG-tagged protein, and sequential probing of HA-tagged protein (Figure 5-11, *bottom two panels, lane 2*). The predicted molecular weight for Ly49G2 is 31.21kDa, thus the observed bands migrated as expected. These results indicate that Ly49G2.HA and Ly49G2. FLAG associate, potentially form homodimers, without restriction from the fusion tags, HA or FLAG.

To assess the ability of the inhibitory Ly49G2 receptor linking with the activating Ly49W2 and Ly49M receptors, individually, conceivably forming heterodimers, I once again followed the same protocols as outlined previously. Flow cytometry analysis of COS-7 cells transfected with Ly49W2.FLAG, Ly49G2.HA and mDAP12 revealed that around 16% of the gated cells expressed both the Ly49 receptors (Figure 5-10 *B*). From the biochemical assays, I was able to detect a band once I performed the IP for the HA-tagged protein, Ly49G2, and the immunoblot for Ly49G2.HA, then for Ly49W2.FLAG (Figure 5-12, *top panel, lane 8*). The isotype control did not result in a band, whereas the non-immunoprecipitated WCL did result in a band (Figure 5-12, *top panel, lanes 1 & 9, respectively*). A band was also detected for the WB of the FLAG-tagged protein, Ly49W2, as well as the non-immunoprecipitated WCL, although both bands are quite faint (Figure 5-12, *2<sup>nd</sup> panel, lanes 8 & 12, respectively*). The faint bands are likely a result of the low expression of Ly49W2.FLAG detected by flow cytometry (Figure 5-10 *B*), and possible low affinity of the antibody for the FLAG epitope. I then completed the reverse IP, where I immunoprecipitated for FLAG-tagged Ly49W2, followed by the WB for the FLAG-tag and subsequent WB for the HA-tagged Ly49G2 receptors. I observed bands for both blots, as well as for the non-immunoprecipitated WCL, but not for the isotype controls (Figure 5-12, *bottom two panels, lanes 8, 12, & 4, respectively*). The data implies an association between the activating receptor Ly49W2 with the inhibitory receptor Ly49G2; Ly49W2 and Ly49G2 are likely engaging as heterodimers.

Similar results were observed when Ly49G2 was again tagged with HA and probed for an association with FLAG tagged Ly49M. The flow cytometry data revealed that approximately 22% of the gated cells expressed both of the receptors (Figure 5-10 *B*);

an expression level slightly higher to that observed with Ly49G2.HA and Ly49W2.FLAG. After the IP for the HA tagged receptor, Ly49G2, the WB for Ly49G2 revealed a band; however, no band was detected in the isotype control, nor in the non-immunoprecipitated WCL (Figure 5-12, *top panel, lanes 6, 2, & 10, respectively*). The lack of a band in the isotype control lane is expected as it demonstrates that the anti-HA antibody does not bind non-specifically. The lack of a band in the non-immunoprecipitated WCL may be a result of insufficient levels of HA-tagged Ly49G2 for detection during WB. The WB for FLAG-tagged Ly49M receptors did positively result in a band, albeit faint, in the HA IP, as well as for the non-immunoprecipitated WCL (Figure 5-12, *2<sup>nd</sup> panel, lanes 6 & 10, respectively*). The faint bands may be a result of low antibody affinity for the FLAG epitope. The IP for the isotype control did not result in a band (Figure 5-12, *2<sup>nd</sup> panel, lane 2*). In the reverse IP, a thick, dense band was detected for the Ly49W2.FLAG IP followed by the WB for the FLAG-tag, as well as in the non-immunoprecipitated WCL (Figure 5-12, *3<sup>rd</sup> panel, lanes 6 & 10, respectively*). Although faint, a band was also detected in the subsequent WB for HA-tagged Ly49G2, in both the FLAG IP and non-immunoprecipitated WCL (Figure 5-12, *4<sup>th</sup> panel, lanes 6 & 10, respectively*). As expected, the isotype control did not result in any bands (Figure 5-12, *bottom two panels, lane 2*). After the IP for FLAG, the dense bands resultant of the FLAG WB and faint bands resultant from the HA WB may suggest that although by flow cytometry around 20% of the gated cells expressed both receptors, not all of the Ly49G2 and Ly49M receptors were associating together. If the association rate is low, then the subsequent WB may result in a faint band to reflect the low rate of association. Thus far, the results suggest that the inhibitory Ly49G2 can associate with Ly49W2 and with Ly49M. The specificity of the IP for the targeted tag, followed by equal specificity of the WB for the tag being probed provides strong evidence that the Ly49 receptors are associating as heterodimers.

To corroborate these results, I reversed the tags where Ly49G2.FLAG was assessed for its ability to associate with Ly49M.HA, in addition to Ly49W2.HA. The transfection of the COS-7 cells with Ly49G2.FLAG and Ly49M.HA, however, did not result in expression levels similar to Ly49G2.HA and Ly49M.FLAG. Only approximately 4% of the gated cells expressed both Ly49G2.FLAG and Ly49M.HA on the same cells

(Figure 5-10 A). Still, a dense band for the HA-tagged Ly49M receptor, after an IP for HA followed by the WB for the HA-tag, is observed, as well as for the non-immunoprecipitated WCL (Figure 5-12, *top panel, lanes 5 & 9, respectively*). Unfortunately, the WB for FLAG-tagged Ly49G2 receptors did not result in a detectable band for the HA IP, nor in the non-immunoprecipitated WCL (Figure 5-12, *second panel, lanes 5 & 9, respectively*). The Ly49M.HA receptors were captured and concentrated during the HA IP, as evidenced by the resultant dense band. If, however, the association rate between Ly49M and Ly49G2 is minimal, given the low cell surface expression levels of both receptors on the same cell (Figure 5-10 A), the amount of FLAG-tagged protein available for detection may not be sufficient for detection by the anti-FLAG antibody used for WB. The affinity of the anti-FLAG antibody may also be lower, as compared to the anti-HA antibody. Coupled with the potential low affinity of the anti-FLAG antibody for the FLAG-tagged Ly49 receptors, this may also justify the faint band observed after the immunoblot for FLAG during the reserve IP for the FLAG-tag, and lack of visible band in the non-immunoprecipitated WCL (Figure 5-12, *3<sup>rd</sup> panel, lanes 5 & 9, respectively*). Following the HA probe, a band is detected, as well as in the non-immunoprecipitated WCL (Figure 5-12, *4<sup>th</sup> panel, lanes 5 & 9, respectively*). No band was observed in the isotype controls (Figure 5-12, *lane 1*). The presence of a band in the HA WB following an IP for FLAG is indicative of an association between the FLAG-tagged Ly49 and HA-tagged Ly49. Even with the faint band detected for the Ly49G2.FLAG WB following the FLAG IP, enough protein must have been concentrated and remained associated with Ly49M.HA for the detection of the latter during the HA WB. Although the results from the HA IP are inconclusive due to the lack of detection of Ly49G2.FLAG, the reverse IP for FLAG followed by the WB for FLAG and HA imply that Ly49M and Ly49G2 are associating. This association is likely in the form of heterodimers.

Parallel results were also observed for Ly49G2.FLAG and Ly49W2.HA. Firstly, the flow cytometry data resulted in only roughly 2% of the gated cells expressing both Ly49G2.FLAG and Ly49W2.HA (Figure 5-10 A). Despite the low expression level, I proceeded with the biochemical assessments. Following the IP for HA-tagged Ly49W2 receptors, I immunoblotted for the HA tag, and sequentially for the FLAG tag. A band is detected for the HA WB, as well as in the non-immunoprecipitated WCL (Figure 5-12, *top*

*panel, lanes 7 & 11, respectively*). However, no band for the FLAG probe was observed, nor detected in the non-immunoprecipitated WCL (Figure 5-12, *2<sup>nd</sup> panel, lanes 7 & 11, respectively*). Given the low expression levels of Ly49W2 and Ly49G2 detected by flow cytometry (Figure 5-10 *A*), the amount of Ly49G2.FLAG receptors that associated with Ly49W2 may not have been sufficient for WB detection. Following the reverse IP for the FLAG-tagged Ly49G2, the immunoblot for FLAG resulted in an extremely faint band, however, no band was visible in the non-immunoprecipitated WCL (Figure 5-12, *3<sup>rd</sup> panel, lanes 7 & 11, respectively*). The extremely faint band may be a result of the low cell surface expression levels detected by flow cytometry (Figure 5-10 *A*). A band was detected for the FLAG IP and non-immunoprecipitated WCL after I probed for HA-tagged Ly49W2 (Figure 5-12, *4<sup>th</sup> panel, lanes 7 & 11, respectively*). No band was observed in the isotype controls (Figure 5-12, *lane 3*). The detection of the band in the HA WB probe following the barely detected band for the FLAG probe suggests that Ly49W2 and Ly49G2 may be associating. These results require further corroboration.

In this section, the transfection of the COS-7 cells with Ly49G2.FLAG along with either Ly49M.HA or Ly49W2.HA resulted in very low expression levels of both receptors on the same cells. Regardless of the low expression levels, all immunoblots of the HA-tagged proteins resulted in a detectable band that migrated to the correct molecular weight range, following either an IP for the mHA-tag or the FLAG-tag. The same results, however, were not observed for the FLAG immunoblots. The COS-7 transfections resultant in over 15% expression levels for both Ly49s, the FLAG-tagged proteins could be detected, albeit weakly. The lysates from the transfections that resulted in low expression levels, no FLAG-tagged proteins were detected in the biochemical assays, with the exception of Ly49G2.FLAG co-transfected with Ly49W2.HA (Figure 5-12, *3<sup>rd</sup> panel, lane 7*). Taken together, the data imply that the inhibitory receptor Ly49G2 can associate with the activating receptor Ly49M, or the activator Ly49W2. The association is likely in the form of heterodimers.

### 5.3 DISCUSSION

The function of NK cells is dependent on the engagement of the cell surface receptors with their cognate ligands. Many of the NK cell receptor proteins are structurally assembled as dimeric molecules for effective functional output. Such proteins include the Ly49 homodimers found in various organisms including rats and mice. Ly49s recognize their ligand in an allele specific manner and both monomers are required for the receptor-ligand interaction. Understanding the precise monomer assembly requirements has yet to be determined. Moreover, no Ly49 heterodimers have been reported to date. The ability of these receptors to form heterodimers may imply an altered specificity for their respective ligands.

In this body of work, I report the association between different Ly49 receptors, possibly as heterodimers. Flow cytometry allowed me to detect the cell surface expression of the receptors on transfected COS-7 cells. Then, by concentrating one of the receptors by targeting the fused tag via an immunoprecipitation (IP), I was then able to assess the association of the receptors by Western blot (WB) analysis. If a band is detected for both fused tags, HA and FLAG, from the same IP, then both receptors are associating together, likely as dimers. The cell surface expression levels were valuable in assessing the outcomes in the biochemical assays performed. Overall, a higher expression level (roughly 20-30%) usually was sufficient for WB detection of the receptor of interest, following an IP. On the other hand, low cell surface expression of a pair of receptors (approximately 15% or less) usually translated into low detection of the same receptors by WB analysis following immunoprecipitation. At times, extremely faint bands resulted, or even no band at all. Furthermore, the anti-FLAG M2 antibody used for WB analyses may not have the same affinity for the FLAG epitope as the anti-HA antibody does for the HA epitope. Most of the bands observed following WB for HA, overall appeared with greater prominence, whereas the bands resultant from FLAG WB were less prominent. Nonetheless, the resultant data in this chapter does allow for further interpretation.

Firstly, I assessed the possibility of activating Ly49 receptors associating and potentially forming heterodimers. Specifically, I selected three activating NOD mouse

receptors belonging to Ly49 receptor group II. I predicted that the two receptors of the same receptor subgroup, Ly49M and Ly49W2, would associate together. Furthermore, I hypothesized that Ly49M and Ly49W2, would not separately associate with Ly49P1, a Ly49 from another receptor subgroup. The data obtained suggest that all three activating receptors do associate, and possibly may form heterodimers. The structural resolution of the only Ly49 receptor with the NKD and stalk region is Ly49L [197]. The structure revealed that the  $\alpha 3_S$  and  $L_S$  regions of the stalk are crucial for the stability of the Ly49L homodimer through their interactions with the NKD dimer [197]. Upon further analysis of the Ly49M, Ly49W2, and Ly49P1 sequences, the  $\alpha 3_S$ ,  $L_S$ , and NKD regions, despite some differences, share several stalk:NKD contact residues (Figure 5-13). Based on the NKD and stalk crystal structure of Ly49L, there are a total of 44 putative contact residues between the NKD and stalk, eight of which are conserved amongst all Ly49s. Of the remaining 36, Ly49M, Ly49W2, and Ly49P1 share 20 contact residues within the  $\alpha 3_S$ ,  $L_S$ , and NKD; these include E<sup>118</sup>, S<sup>119</sup>, Q<sup>124</sup>, R<sup>126</sup>, Y<sup>128</sup>, K<sup>132</sup>, T<sup>133</sup>, D<sup>136</sup>, Q<sup>139</sup>, R<sup>143</sup>, G<sup>144</sup>, Y<sup>148</sup>, F<sup>150</sup>, G<sup>153</sup>, M<sup>161</sup>, D<sup>153</sup>, E<sup>186</sup>, D<sup>187</sup>, P<sup>197</sup>, and K<sup>223</sup> (Figure 5-13). Furthermore, the interface of the two NKD monomers is a result of the interaction between seven residues on the  $\beta 0$  strand of each subunit, creating an antiparallel  $\beta$  sheet [197]. Of the seven  $\beta 0$  strand residues, Ly49M, Ly49W2, and Ly49P1 differ only by one (Figure 5-13). Taken together, these shared residues may have favored the association of Ly49P1 with Ly49M, as well as with Ly49W. In addition, Ly49M and Ly49W2 differ at only three contact residues between the stalk and the NKD, at positions 121, 154, and 185; and at position 135, a conservative substitution is observed where Ly49W2 has S<sup>135</sup> and Ly49M has T<sup>135</sup> (Figure 5-13). All of the seven  $\beta 0$  strand residues are shared between Ly49M and Ly49W2. Given the high degree of sequence homology between these two receptors, it is not surprising Ly49M and Ly49W2 associating together, and potentially even form heterodimers.

In this chapter, I also assessed the possibility of association between inhibitory and activating receptors. Precisely, I had hypothesized that the inhibitory Ly49G2 receptor would associate with the activating Ly49M and the activating Ly49W2 receptors, separately. Given the high degree of sequence identity between the three receptors, the observed association of Ly49G2 with Ly49M, as well as with Ly49W2,

was expected. Analysis of the stalk and NKD protein sequence alignment of the three receptors reveals that Ly49G2 displays the same amino acid identity at all stalk and NKD contact residues as do Ly49M and Ly49W2 (Figure 5-13). Hence, all three Ly49s differ only by three residues at positions 121, 154, and 185; moreover, both Ly49W2 and Ly49G2 share S<sup>135</sup>, whereas Ly49M displays the conservative substitution of T<sup>135</sup> (Figure 5-13). Furthermore, superimposition of the crystal structures of the inhibitory Ly49A, Ly49C, and the activating Ly49L receptors reveals that structurally, the Ly49L is more structurally similar to Ly49A than Ly49A is to Ly49C [188, 189, 197]. This concept fits with the data presented in this section, where the inhibitory Ly49G2 receptor associated with Ly49M and with Ly49W2, and may form heterodimers.

Despite the close sequence identity between all of the receptors used in this study, I did not expect all of the transfected pairs to associate, hence the lack of an additional negative control in this study. Ly49A is the parent member of the group II receptors (Figure 1-5 A), thus all members are predicted to be structurally similar to Ly49A. In fact, crystal structure data of the group II members, Ly49A, Ly49G2, and Ly49L, as well as group I members, Ly49C, Ly49I, and Ly49H, support this concept [187-189, 197, 361, 382]. Ly49C and Ly49H are members of group I. Sequence alignments of the stalk and NKD regions of Ly49C and Ly49H with members of group II, reveal several differences (Figure 5-13). Furthermore, given the lack of association previously reported for Ly49A and Ly49C [379], Ly49C, as well as Ly49H, would likely not associate with Ly49M, Ly49W2, Ly49P1, or Ly49G2, thus any attempt to do so, would serve as a negative control.

The formation of Ly49 dimers is likely the responsibility of the stalk region and the NKD as they interact. Several hydrogen and van der Waals bonds are formed along the NKD interface between the  $\beta_0$  strand residues, as well as between the NKD and the  $\alpha_{3S}$  and  $L_S$  regions of the stalk [187-189, 197, 361, 382]. Furthermore, the stalk monomers do not contact each other, with the exception of the conserved Cys<sup>110</sup>-Cys<sup>110</sup> disulfide bond at the N-terminus of the  $\alpha_{3S}$  helices, and another putative disulfide bond at the N-terminus of the  $\alpha_{2S}$  helices [197]. A previous attempt to heterodimerize Ly49A and Ly49C, inhibitory receptors of different receptor groups, was unsuccessful [379]. Protein sequence alignment analysis of both group I members (Ly49C, Ly49I, and

Ly49H) and group II members (Ly49L, Ly49A, Ly49P1, Ly49W2, Ly49M, and Ly49G2) reveals that within the  $\alpha 3_S$  helix, at position 125, group I members encode either Asp or Glu, negatively charged residues; whereas, group II members encode Asn or Lys (Figure 5-13). Although Asn is not charged, it is a polar residue, and Lys is a positively charged residue, both with opposite properties in comparison to Asp and Glu. Furthermore, within the  $L_S$  loop, at position 140, group I members contain Asp, a negatively charged amino acid, and group II members contain the positively charged His amino acid (Figure 5-13). These opposing charges between the two groups may be what dictates heterodimer assembly within a group, but not between groups.

Overall, the data in this chapter support the association between different Ly49 monomers. Furthermore, the observed associations between the various Ly49s may likely be a result of the formation of heterodimers. To fully understand the nature of dimer assembly, it is of great importance to determine what domains are responsible for the association between the subunits. Furthermore, it is also necessary to determine the residues that contribute to the molecular specificity of homodimer assembly. The activating Ly49M and Ly49W2 receptors are both found in the NOD mouse and share the closest proteins sequence identity of all Ly49s. Although I was able to show their association in this body of work, the heterodimer association of these two receptors in the NOD mouse has not been reported, but also not investigated. Thus, determining the Ly49 regions required for dimer assembly, as well as the molecular determinants for the specificity required for homodimer formation, would elucidate a fundamental biological question that may allow for the control and manipulation of Ly49 receptors, possibly altering NK cell function.

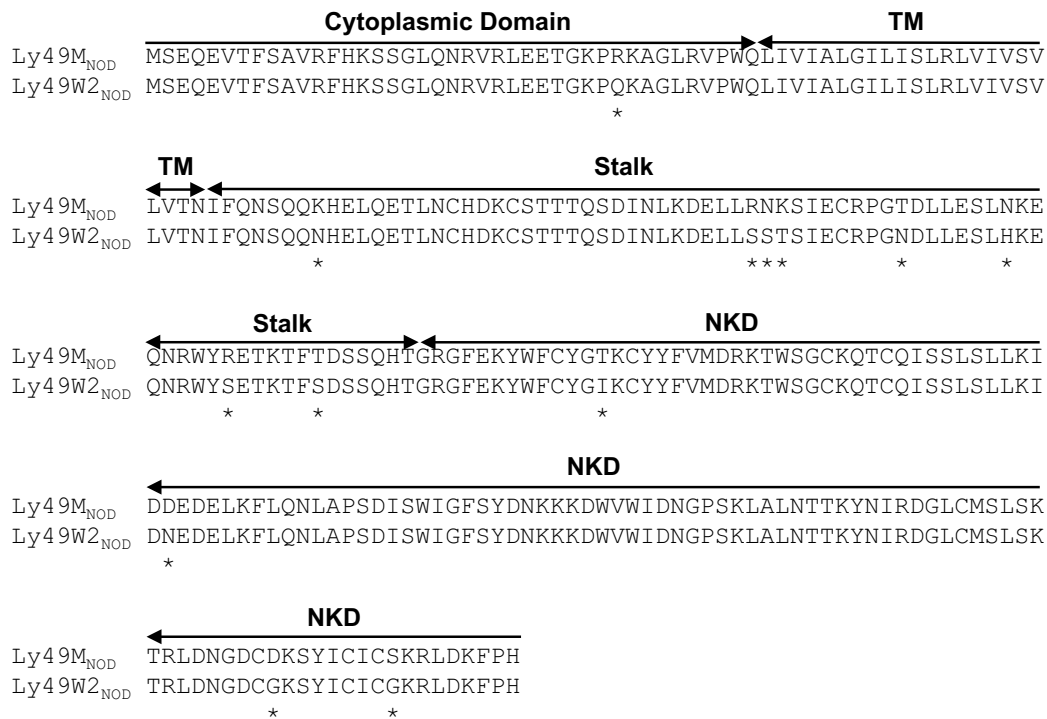


**Figure 5-1: Protein sequence alignment for the activating NOD mouse receptors Ly49M and Ly49W2.** The protein sequence alignment for Ly49M and Ly49W2 (GI n<sup>o</sup>. 13021834 and 9965815, respectively) was executed using the online MAFFT sequence alignment tool (<http://www.ebi.ac.uk/Tools/msa/mafft/>). The various Ly49 structural domains are outlined (NOTE: *TM*=transmembrane domain; *NKD*=natural killer domain). An asterisk (\*) below the alignment denotes a different amino acid at the same location in both proteins.

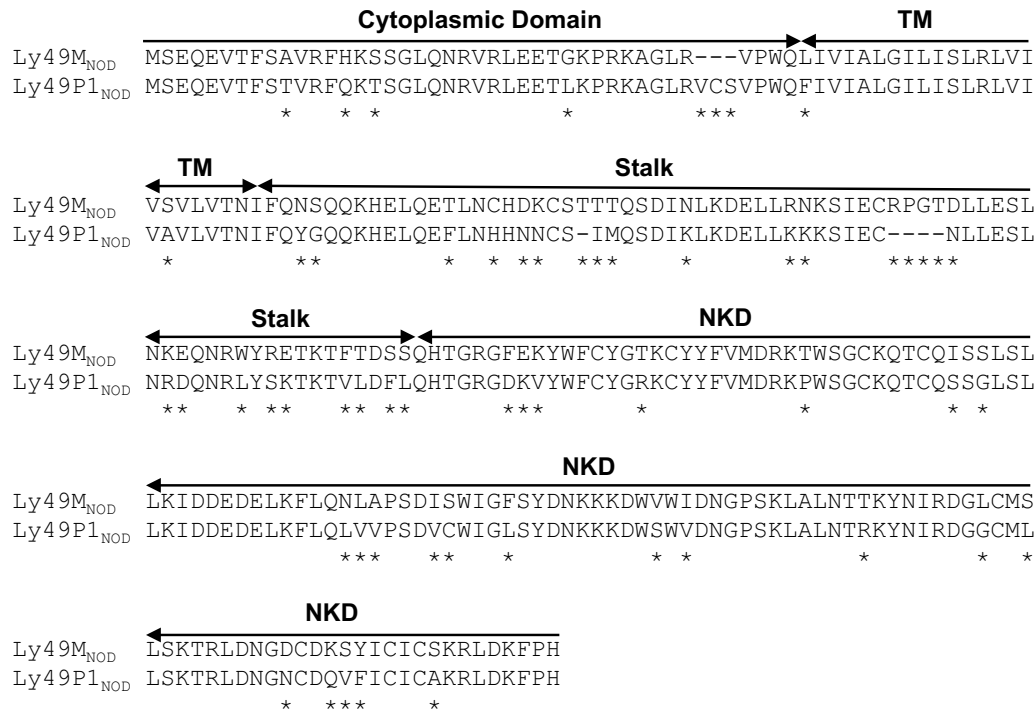


**Figure 5-2: Protein sequence alignment for the activating NOD mouse receptors Ly49M and Ly49P1.** The protein sequence alignment for Ly49M and Ly49P1 (GI n<sup>o</sup>. 13021834 and 9801839, respectively) was executed using the online MAFFT sequence alignment tool (<http://www.ebi.ac.uk/Tools/msa/mafft/>). The various Ly49 structural domains are outlined (NOTE: *TM*=transmembrane domain; *NKD*=natural killer domain). An asterisk (\*) below the alignment denotes a different amino acid at the same location in both proteins. A dash (-) within a protein sequence denotes absent amino acids in the sequence at the particular location in comparison to the other receptor.

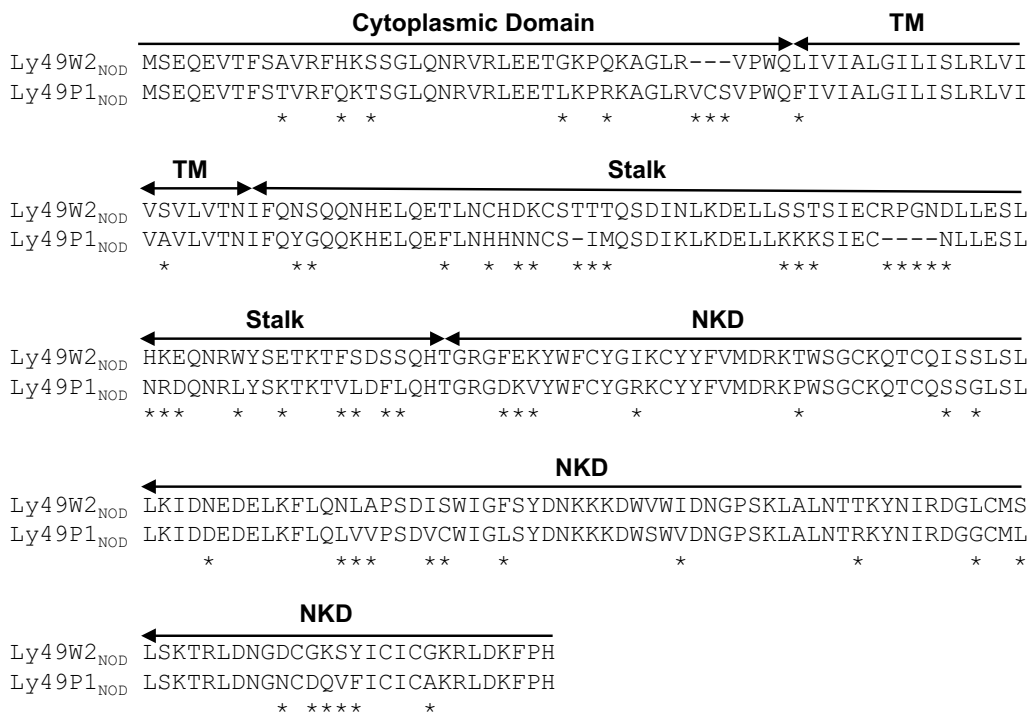


**Figure 5-3: Protein sequence alignment for the activating NOD mouse receptors Ly49W2 and Ly49P1.** The protein sequence alignment for Ly49W2 and Ly49P1 (GI n<sup>o</sup>. 9965815 and 9801839, respectively) was executed using the online MAFFT sequence alignment tool (<http://www.ebi.ac.uk/Tools/msa/mafft/>). The various Ly49 structural domains are outlined (NOTE: *TM*=transmembrane domain; *NKD*=natural killer domain). An asterisk (\*) below the alignment denotes a different amino acid at the same location in both proteins. A dash (-) within a protein sequence denotes absent amino acids in the sequence at the particular location in comparison to the other receptor.

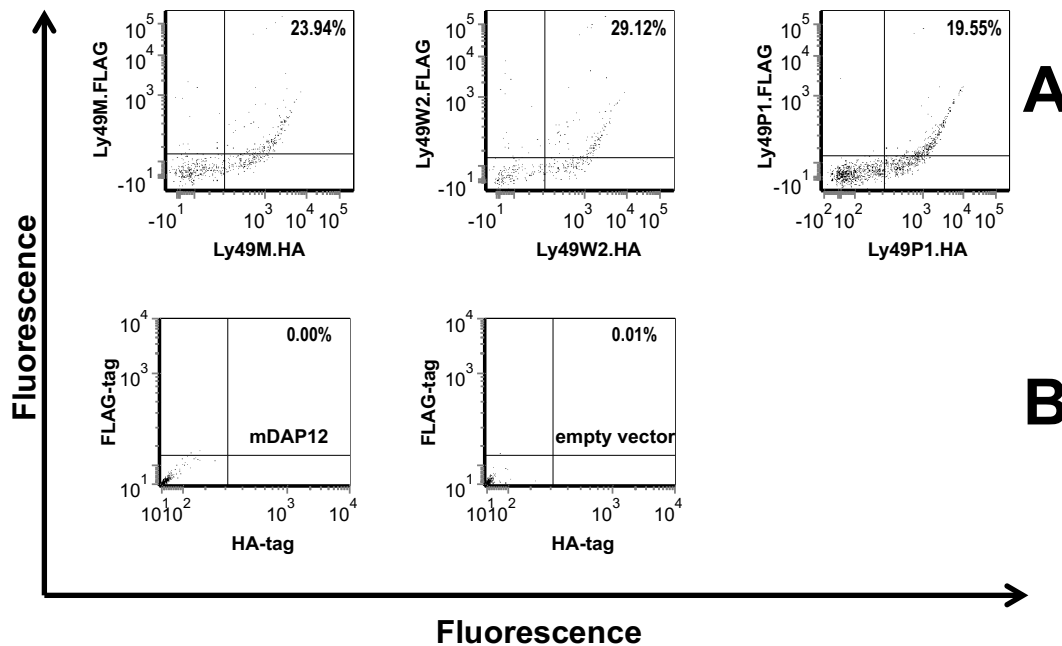


**Figure 5-4: Transfection of COS-7 cells with activating Ly49 receptors of the NOD mouse.**  $1 \times 10^6$  COS-7 cells were transfected with different combinations of Ly49 receptors along with mouse DAP12 (mDAP12) using the Amaxa<sup>®</sup> Nucleofector<sup>®</sup> kit for COS-7 cells. For each plot, the Ly49 receptors (and their respective tags – HA or FLAG) used for the transfection are displayed on the x-axis and y-axis (A). At 48-hours post transfection, receptor expression was assessed via flow cytometry. The analysis is gated on live cells. The percentage of gated cells expressing both of the receptors outlined for each plot is displayed at the top right hand corner. As negative controls, COS-7 cells were also transfected with mDAP12 only or empty vector (B). Data is representative of two independent experiments.

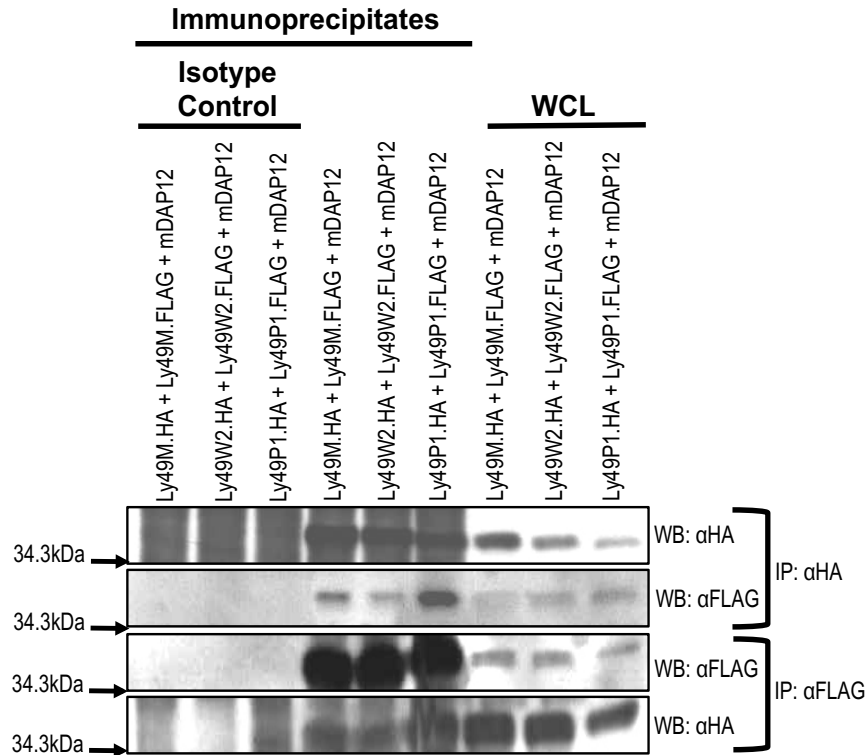


**Figure 5-5: The HA-tagged and FLAG-tagged receptors Ly49M, Ly49W2, and Ly49P1 associate, and may form homodimers.** Whole cell lysates of transfected COS-7 cells with the following combinations (Ly49M.HA, Ly49M.FLAG, and mDAP12; Ly49W2.HA, Ly49W2.FLAG, and mDAP12; Ly49P1.HA, Ly49P1.FLAG, and mDAP12) were immunoprecipitated (IP) with anti-HA antibody or with an isotype control antibody (*top 2 blot panels*) and ran on a 15% reducing SDS-PAGE gel. Immunoblotting (WB) for HA-tagged receptors was executed (*first panel*), followed by sequential probing for FLAG-tagged Ly49s (*second panel*). The reverse immunoprecipitation of FLAG-tagged Ly49 receptors, as well as for the respective isotype control, was also performed in parallel (*bottom two panels*). Immunoblotting for FLAG-tagged Ly49 receptors (*third panel*), followed by probing for HA-tagged receptors (*fourth panel*) was carried out. Non-immunoprecipitated WCL samples of each transfection reaction are also displayed. Data is representative of two independent experiments.

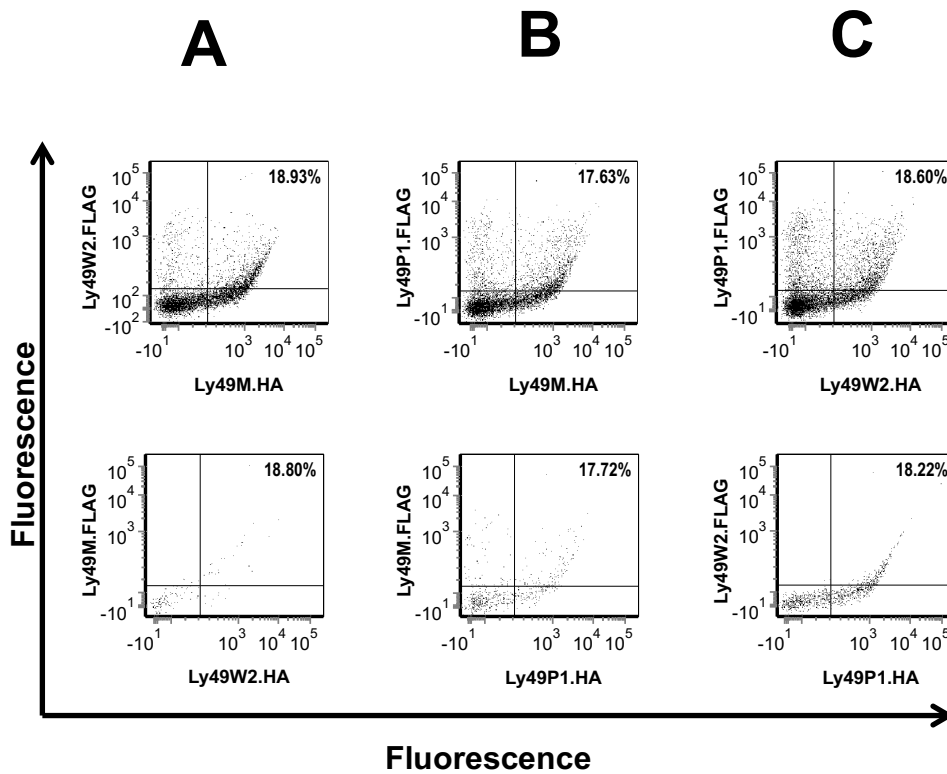


**Figure 5-6: Transfection of COS-7 cells with activating Ly49 receptors of the NOD mouse.**  $1 \times 10^6$  COS-7 cells were transfected with different combinations of Ly49 receptors along with mouse DAP12 (mDAP12) using the Amaxa<sup>®</sup> Nucleofector<sup>®</sup> kit for COS-7 cells. For each plot, the Ly49 receptors (and their respective tags – HA or FLAG) used for the transfection are displayed on the x-axis and y-axis. At 48-hours post transfection, receptor expression was assessed via flow cytometry. The analysis is gated on live cells. The percentage of gated cells expressing both of the receptors outlined for each plot is displayed at the top right hand corner. Data is representative of two independent experiments.

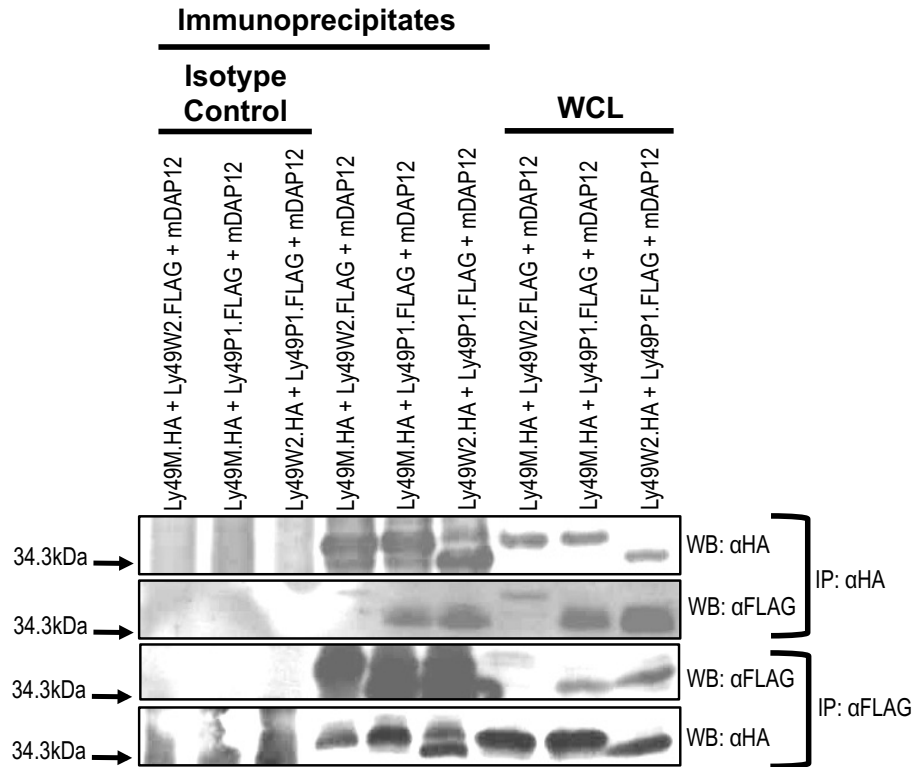


**Figure 5-7 A: The activating NOD mouse receptors Ly49M, Ly49W2, and Ly49P1 associate together, possibly as heterodimers.** Whole cell lysates of transfected COS-7 cells with the following combinations (Ly49M.HA, Ly49W2.FLAG, and mDAP12; Ly49M.HA, Ly49P1.FLAG, and mDAP12; Ly49W2.HA, Ly49P1.FLAG, and mDAP12) were immunoprecipitated (IP) with anti-HA antibody or with an isotype control antibody (*top 2 blot panels*) and ran on a 15% reducing SDS-PAGE gel. Immunoblotting (WB) for HA-tagged receptors was executed (*first panel*), followed by sequential probing for FLAG-tagged Ly49s (*second panel*). The reverse immunoprecipitation of FLAG-tagged Ly49 receptors, as well as for the respective isotype control, was also performed in parallel (*bottom two panels*). Immunoblotting for FLAG-tagged Ly49 receptors (*third panel*), followed by probing for HA-tagged receptors (*fourth panel*) was carried out. Non-immunoprecipitated WCL samples of each transfection reaction are also displayed. Data is representative of two independent experiments.

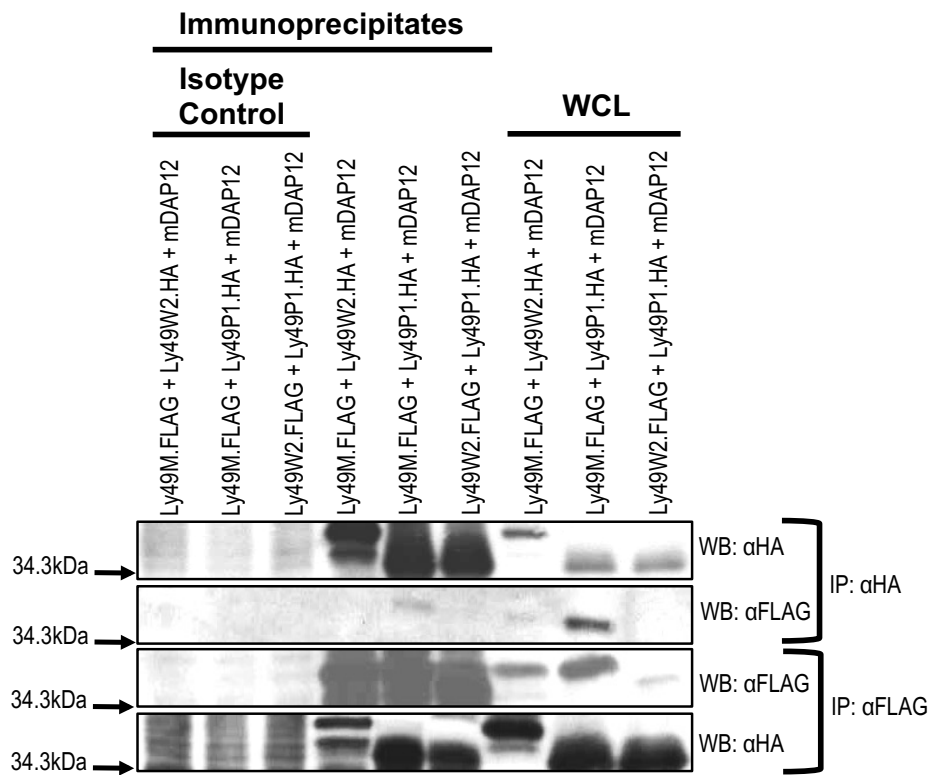


**Figure 5-7 B: The activating NOD mouse receptors Ly49M, Ly49W2, and Ly49P1 associate together, possibly as heterodimers.** Whole cell lysates of transfected COS-7 cells with the following combinations (Ly49M.FLAG, Ly49W2.HA, and mDAP12; Ly49M.FLAG, Ly49P1.HA, and mDAP12; Ly49W2.FLAG, Ly49P1.HA, and mDAP12) were immunoprecipitated (IP) with anti-HA antibody or with an isotype control antibody (*top 2 blot panels*) and ran on a 15% reducing SDS-PAGE gel. Immunoblotting (WB) for HA-tagged receptors was executed (*first panel*), followed by sequential probing for FLAG-tagged Ly49s (*second panel*). The reverse immunoprecipitation of FLAG-tagged Ly49 receptors, as well as for the respective isotype control, was also performed in parallel (*bottom two panels*). Immunoblotting for FLAG-tagged Ly49 receptors (*third panel*), followed by probing for HA-tagged receptors (*fourth panel*) was carried out. Non-immunoprecipitated WCL samples of each transfection reaction are also displayed. Data is representative of two independent experiments.

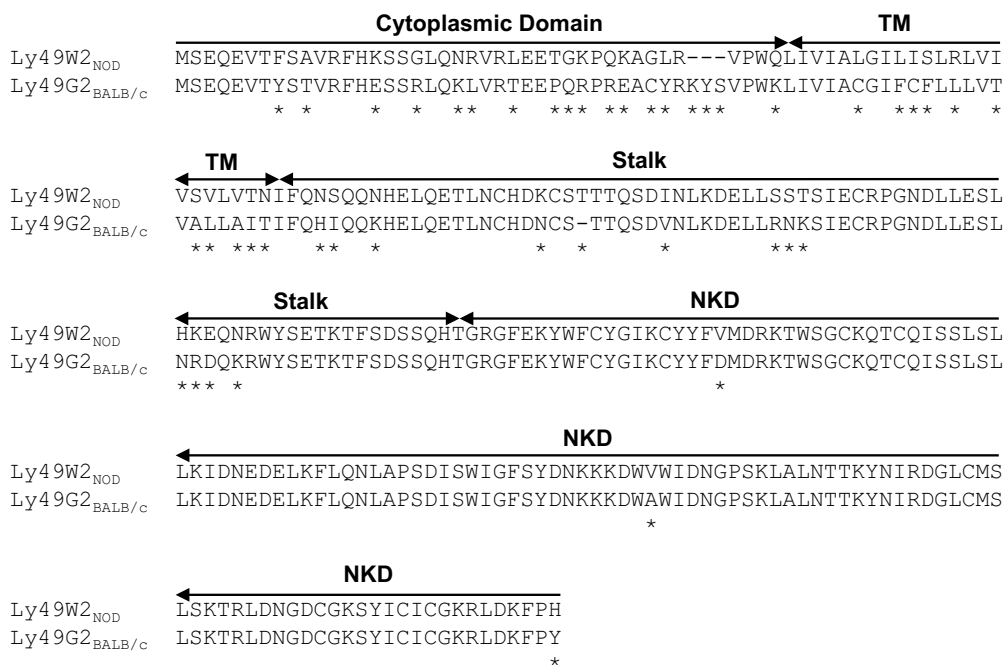


**Figure 5-8: Protein sequence alignment for the activating NOD mouse receptor Ly49W2 and inhibitory BALB/c receptor Ly49G2.** The protein sequence alignment for Ly49W2 and Ly49G2 (GI n°. 9965815 and 11935094, respectively) was executed using the online MAFFT sequence alignment tool (<http://www.ebi.ac.uk/Tools/msa/mafft/>). The various Ly49 structural domains are outlined (NOTE: *TM*=transmembrane domain; *NKD*=natural killer domain). An asterisk (\*) below the alignment denotes a different amino acid at the same location in both proteins. A dash (-) within a protein sequence denotes absent amino acids in the sequence at the particular location in comparison to the other receptor.

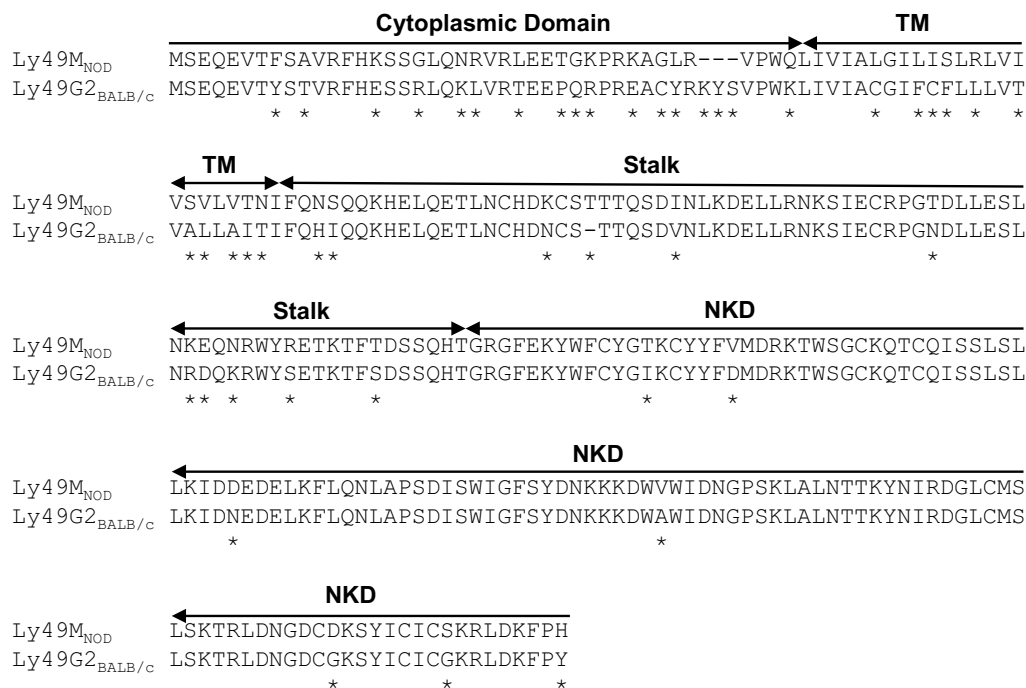


**Figure 5-9: Protein sequence alignment for the activating NOD mouse receptor Ly49M and inhibitory BALB/c receptor Ly49G2.** The protein sequence alignment for Ly49M and Ly49G2 (GI n<sup>o</sup>. 13021834 and 11935094, respectively) was executed using the online MAFFT sequence alignment tool (<http://www.ebi.ac.uk/Tools/msa/mafft/>). The various Ly49 structural domains are outlined (NOTE: *TM*=transmembrane domain; *NKD*=natural killer domain). An asterisk (\*) below the alignment denotes a different amino acid at the same location in both proteins. A dash (-) within a protein sequence denotes absent amino acids in the sequence at the particular location in comparison to the other receptor.

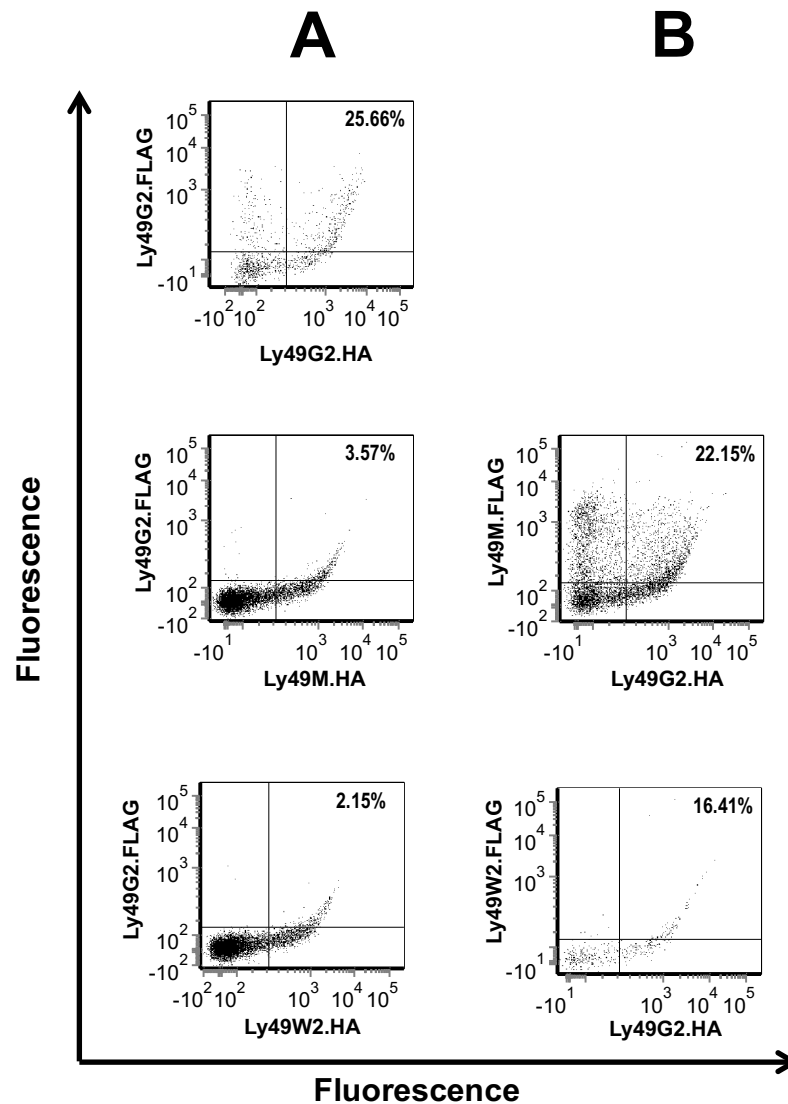


**Figure 5-10: Transfection of COS-7 cells with activating and inhibitory mouse receptors.**  $1 \times 10^6$  COS-7 cells were transfected with different combinations of Ly49 receptors along with mouse DAP12 (mDAP12) using the Amaxa<sup>®</sup> Nucleofector<sup>®</sup> kit for COS-7 cells. For each plot, the Ly49 receptors (and their respective tags – HA or FLAG) used for the transfection are displayed on the x-axis and y-axis. At 48-hours post transfection, receptor expression was assessed via flow cytometry. The analysis is gated on live cells. The percentage of gated cells expressing both of the receptors outlined for each plot is displayed at the top right hand corner. Data is representative of two independent experiments.

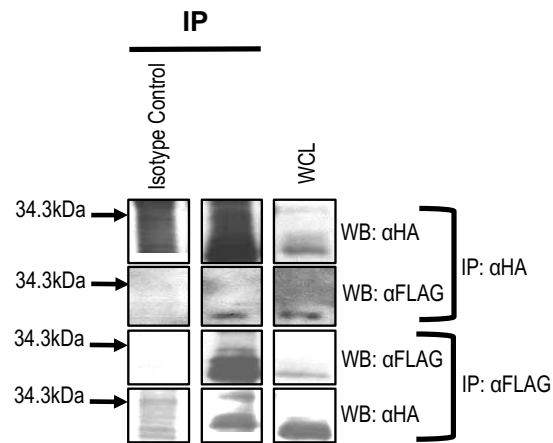


**Figure 5-11: The inhibitory Ly49G2.HA and Ly49G2.FLAG receptors associate, possibly forming homodimers.** Whole cell lysates of transfected COS-7 cells with Ly49G2.HA and Ly49G2.FLAG were immunoprecipitated (IP) with anti-HA antibody or with an isotype control antibody (*top 2 blot panels*) and ran on a 15% reducing SDS-PAGE gel. Immunoblotting (WB) for HA-tagged receptors was executed (*first panel*), followed by sequential probing for FLAG-tagged Ly49s (*second panel*). The reverse immunoprecipitation of FLAG-tagged Ly49 receptors, as well as for the respective isotype control, was then performed (*bottom two panels*). Immunoblotting for FLAG-tagged Ly49 receptors (*third panel*), followed by probing for HA-tagged receptors (*fourth panel*) was carried out. Non-immunoprecipitated WCL samples of each transfection reaction are also displayed. Data is representative of two independent experiments.

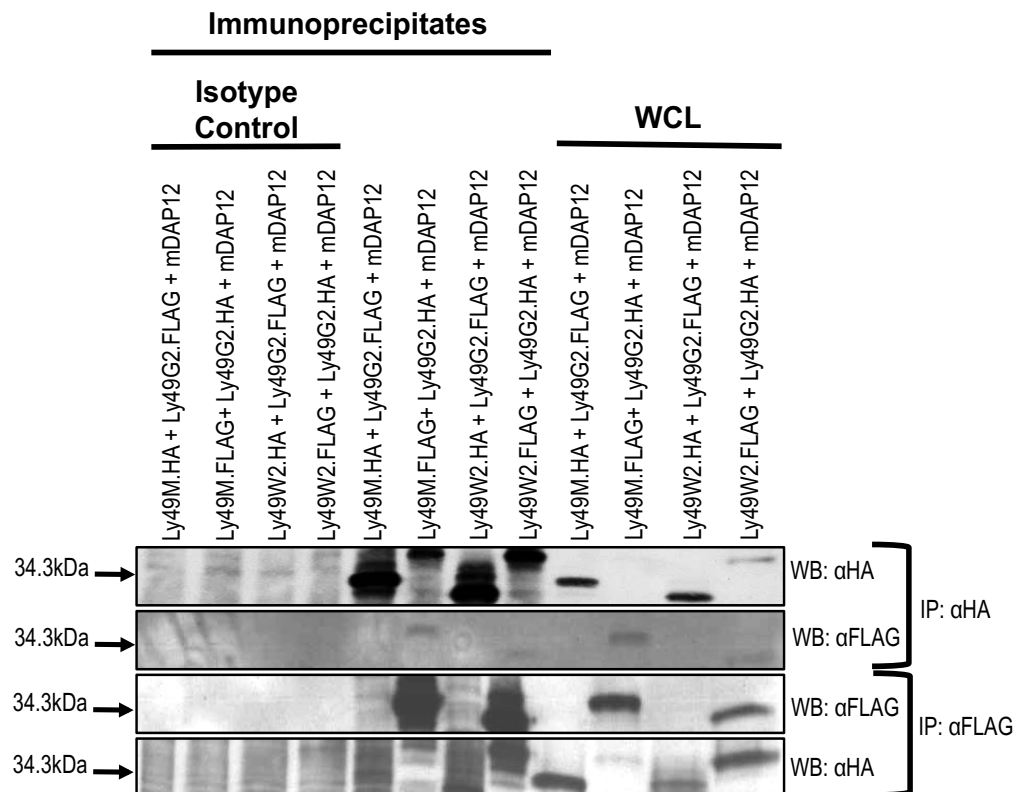


**Figure 5-12: The activating NOD mouse receptors Ly49M and Ly49W2 associate with the inhibitory BALB/c mouse receptor Ly49G2.** Whole cell lysates of transfected COS-7 cells with the following combinations (Ly49M.HA, Ly49G2.FLAG, and mDAP12; Ly49M.FLAG, Ly49G2.HA, and mDAP12; Ly49W2.HA, Ly49G2.FLAG, and mDAP12; Ly49W2.FLAG, Ly49G2.HA, and DAP12) were immunoprecipitated (IP) with anti-HA antibody or with an isotype control antibody (*top 2 blot panels*) and ran on a 15% reducing SDS-PAGE gel. Immunoblotting (WB) for HA-tagged receptors was executed (*first panel*), followed by sequential probing for FLAG-tagged Ly49s (*second panel*). The reverse immunoprecipitation of FLAG-tagged Ly49 receptors, as well as for the respective isotype control, was then performed (*bottom two panels*). Immunoblotting for FLAG-tagged Ly49 receptors (*third panel*), followed by probing for HA-tagged receptors (*fourth panel*) was carried out. Non-immunoprecipitated WCL samples of each transfection reaction are also displayed. Data is representative of two independent experiments.



## **CHAPTER VI: DISCUSSION AND CONCLUSION**

### **6.1 OVERVIEW OF THESIS**

The studies outlined in this thesis are aimed at further elucidating the fundamental requirements of natural killer (NK) cell Ly49 receptors for ligand recognition and self-assembly. Tasked with distinguishing healthy cells from virus infected or transformed cells, the NK cell Ly49 receptors are capable of such discrimination by engaging with MHC class I molecules. The interaction involves three distinct sites on the MHC class I molecule and three loop regions of the Ly49 NKD region. Any alteration could disrupt the interaction, affecting the recognition of the ligand by the receptor. The outcome of the interactions between the Ly49 receptors and the MHC class I molecules ultimately affect the effector functions of the NK cell. With the collective studies presented in this thesis, I sought to advance our current understanding of Ly49 receptors. Firstly, I identified a critical role for the L3 loop, and possibly the L6 loop of the inhibitory rat receptor Ly49i2 during engagement with its cognate ligand, the MHC class I molecule RT1-A1<sup>c</sup>. Then, I established a process to express Ly49 receptors on the cell surface of RNK-16 cells in a time efficient manner resulting in a high transfection efficiency rate. Lastly, I provide evidence of the association between monomers of different mouse Ly49s belonging to the same group of receptors, possibly forming heterodimers. Together, these studies provide insight into the fundamental nature of Ly49 receptors that allows them to function as critical members of the NK cell.

### **6.2 ANALYSIS OF THESIS STUDIES**

Natural killer cells are innate sentinels tasked with the crucial function of detecting and eliminating virus infected or cancerous cells [4]. The responsibility of surveying host cells and determining if they have been compromised lies with the vast array of receptors expressed at the surface of NK cells. Such a group includes the Ly49 receptors expressed on the surface of mouse and rat NK cells. Ly49 receptors are

functionally analogous to the human killer-cell immunoglobulin-like receptors (KIRs), yet structurally distinct [168]. Ly49s are type II transmembrane glycoproteins expressed as the cell surface of NK cells as disulfide-linked homodimers [169, 170]. The dimer structure of Ly49s is required for engagement with their ligands, MHC class I molecules [188, 189]. Ly49 receptors have been the subject of extensive numbers of investigations, thus have been extensively characterized in the mouse, and to a much lesser degree in the rat. Mice and rats are extensively used as models of human disease, hence understanding the structure and function of evokers of effector responses is of great importance. Ly49 receptors are crucial mediators of NK cell function, therefore, elucidating the requirements for ligand recognition, as well as the requirements for the assembly of Ly49 dimers, is the focus of this collective body of work.

### ***6.2.1 STRUCTURAL SPECIFICITY DETERMINANTS OF THE Ly49i2 RECEPTOR FOR ITS COGNATE LIGAND RT1-A1<sup>c</sup>***

#### ***Summary of Contributions***

The engagement and interaction between Ly49 receptors and MHC class I ligands occurs in a furrow below the peptide binding groove [188, 189]. The interaction for ligand recognition requires contact between three subsites on the MHC class I molecule with three loop regions within the ligand-interacting region of the receptor, the natural killer domain (NKD) [187, 190-193]. Understanding the contribution made by each Ly49 loop region to MHC class I recognition is of great importance in elucidating triggers of NK cell activation.

The interaction between rodent Ly49 receptors and MHC class I molecules involves the MHC class I  $\alpha 1$  and  $\alpha 2$  domains, as well as the  $\alpha 3$  domain and  $\beta_2m$  designated as subsites B, F, and C, with the Ly49 receptor NKD loop regions L3, L5, and L6, respectively [187-189, 192]. This interaction is required for ligand recognition and allele specificity of MHC class I. The rat Ly49 receptors exhibit significant polymorphism in the L3 loop, and a more conserved L5 and L6 loop (Figure 1-5 B). In mice, Ly49 receptors display a much more variable L6 loop and more conserved L3 loop (Figure 1-5 A). Interestingly, the sequence of the L5 loop is highly conserved amongst

both mouse and rat Ly49 receptors (Figure 1-5). Given the diversity between mouse and rat Ly49 receptors, specifically within the L3 and L6 loop regions, it is important to understand the mechanism of ligand recognition as it likely varies between both species. The polymorphic differences observed in the various loops may be relevant to the recognition of MHC class I, as well as to its allele specificity.

In Chapter III, I sought to elucidate the role of the L3, L5, and L6 loop regions in the rat. Specifically, I was interested in determining the impact of the interaction between the inhibitory rat Ly49i2 receptor and its ligand, the rat MHC class I molecule RT1-A1<sup>c</sup>. By using surface plasmon resonance (SPR), I quantitatively assessed the binding interactions between various Ly49i2 chimeric receptors and the MHC class I ligand to determine the significance of each loop region for ligand recognition. To execute SPR studies, properly folded protein is required. To assess the folding of each Ly49i2 mutant, I assessed the interaction between the Ly49i2 receptors and the antibody STOK2, an antibody that recognizes properly folded Ly49i2 [281, 282]. Firstly, I determined that the affinity between wildtype Ly49i2 and RT1-A1<sup>c</sup> is much greater as compared to the affinity between inhibitory mouse Ly49 receptors and their MHC class I ligands [371]. This observation is supported by previous work performed in the laboratory. By mutagenesis of the mouse H-2D<sup>d</sup>, recognition by the Ly49G receptor was disrupted by a single point mutation at any of the MHC class I subsites; whereas, disruption of the interaction between Ly49i2 and RT1-A1<sup>c</sup> required either a mutation at minimum of two subsites, or double mutations at each subsite [192]. This suggested that Ly49i2 likely engages and interacts with its MHC class I ligand, RT1-A1<sup>c</sup> with a greater overall affinity as compared to its mouse counterpart(s). Given the dissociation constants ( $K_D$ ) reported for mouse Ly49 receptors and their respective MHC class I ligands (Table 4-1), the affinity between Ly49i2 and RT1-A1<sup>c</sup> is between 2580-3290-fold higher when compared to the mouse inhibitory Ly49C receptor and H-2K<sup>b</sup> [187, 189]; a 1500-fold increase in affinity as compared to Ly49G2 and H-2D<sup>d</sup> [371]; and between 58-142-fold increase in affinity as compared to Ly49A and H-2D<sup>d</sup> [187, 370].

To define the role of the L3, L5, and L6 loop of Ly49i2 in the recognition of RT1-A1<sup>c</sup>, I generated chimeric receptors for each loop aimed at possibly disrupting recognition, or even lowering the affinity between the chimeric Ly49i2 receptor and

RT1-A1<sup>c</sup>. I relied on the  $K_D$  I had determined for Ly49i2:RT1-A1<sup>c</sup> as a base for comparison. Overall, I was able to demonstrate a vital role for the L3 loop of Ly49i2 for recognition of RT1-A1<sup>c</sup>. By exchanging the L3 loop in Ly49i2 for L3 loops found in other rat Ly49 receptors (Ly49i5, Ly49s5, and Ly49s3) that do not recognize RT1-A1<sup>c</sup>, I was able to completely disrupt the interaction between the receptor and the ligand as measured by SPR. Furthermore, I was able to partially restore recognition of RT1-A1<sup>c</sup> when the L3 loop of Ly49i2 was placed in Ly49i5. Although the partial restoration in ligand recognition was 90-fold less in affinity as compared to wildtype Ly49i2, the resulting  $K_D$  was still comparable to what has been observed between the mouse Ly49A receptor and H-2D<sup>d</sup>, as well as the human KIR2DL3 receptor with the human MHC class I molecule HLA-C (Table 3-1) [187, 370, 374]. The other rat Ly49 receptors, Ly49i5, Ly49s5, and Ly49s3, all share complete protein sequence identity with the Ly49i2 L5 and L6 loop, with the exception of two residues within Ly49s3, S<sup>240</sup> in the L5 loop and Y<sup>251</sup> in the L6 loop (Table 3-1). Given the highly conserved sequence identity in the L5 and L6 loop, as well as the complete disruption of binding between the receptor and the ligand, it is likely that allele specificity for RT1-A1<sup>c</sup> lies within the L3 loop of Ly49i2.

The L6 loop, as we have previously shown, may be significant in MHC class I recognition [190, 288]. In Chapter III, I designed two Ly49i2 chimeric receptors targeting the L6 loop by altering the conserved DCGK sequence normally encoded in Ly49i2. The Ly49i2 L6 loop is predicted to engage with RT1-A1<sup>c</sup> at subsite C. Specifically, Ly49i2 D<sup>249</sup> and K<sup>252</sup> may interact with the conserved  $\alpha$ 3 domain residues E<sup>232</sup> and K<sup>243</sup> of RT1-A1<sup>c</sup> [192]. By mutating the two Ly49i2 contact residues to Ala, the interaction between the receptor and the ligand was altered. The affinity between the chimeric Ly49i2 receptor and RT1-A1<sup>c</sup> was reduced 224-fold as compared to the wildtype receptor. Moreover, the mutant Ly49i2 receptor was recognized by the STOK2 antibody, therefore the outcome from the interaction between the mutant receptor and RT1-A1<sup>c</sup> implies a potential role for the L6 loop in ligand recognition. Both D<sup>249</sup> and K<sup>252</sup> are charged residues, thus the D249A and K252A substitutions in the DCGK L6 loop sequence likely neutralized the L6 loop and disrupted the interaction and potential binding between the receptor and the ligand. To further corroborate the importance of the L6 loop, I also generated a Ly49i2 mutant where the DCGK sequence of the L6 loop

was completely exchanged for the sequence NCDQ. The latter sequence is found in the mouse Ly49A and Ly49P receptors (Figure 1-5 A). We had previously shown that by exchanging the NCDQ sequence in Ly49P for the DCGK sequence found in several receptors, including the mouse Ly49W, recognition for the mouse MHC class I molecule H-2D<sup>k</sup> was conferred to Ly49P, a receptor that does not recognize H-2D<sup>k</sup> [190]. By exchanging DCGK in the L6 loop of Ly49i2 for NCDQ we were able to show that the interaction between the Ly49i2 chimeric receptor and RT1-A1<sup>c</sup> was completely disrupted. The STOK2 antibody, however, did not recognize the mutant Ly49i2 receptor. The epitope of the STOK2 antibody has not been mapped, thus the antibody-binding site may lie in the L6 loop or in near proximity. By mutating the DCGK sequence, complete loss of antibody binding occurred, whereas Ala mutations to two L6 loop residues did not inhibit the binding of the STOK2 antibody. The Ala mutations may have only slightly distorted the loop, while the presence of NCDQ altered the epitope sufficiently to hinder binding of the antibody to the chimeric receptor. Regardless, the complete loss of binding between the Ly49i2 mutant bearing the NCDQ sequence and RT1-A1<sup>c</sup> may be due to improperly folded protein impeding the interaction with RT1-A1<sup>c</sup>. Conversely, the Ly49i2 mutant may have been folded properly, which may signify that the binding interaction was completely disrupted. By analyzing the putative L6 loop bearing the NCDQ sequence (Figure 3-23), the biggest alteration appears to be the orientation of the D<sup>251</sup> and Q<sup>252</sup> compared to G<sup>251</sup> and K<sup>252</sup>. Both D<sup>251</sup> and Q<sup>252</sup> are oriented differently, in the opposite direction of G<sup>251</sup> and K<sup>252</sup>. This alteration in configuration may be sufficient to alter the binding residues and ultimately disrupt the interaction.

Lastly, I was unable to conclusively demonstrate a role for the L5 loop in Ly49i2 recognition of RT1-A1<sup>c</sup>. The L5 loop contains highly conserved residues amongst mouse and rat Ly49 receptors, S<sup>241</sup> and T<sup>243</sup> (Figure 1-5). The L5 loop of Ly49 receptors likely engages with subsite F of RT1-A1<sup>c</sup>. To assess the significance of the L5 loop, I generated mutants of the L5 loop by mutating S241A and T243A, either together, or separately. The STOK2 antibody did not recognize any of the three mutants. As stated earlier, the epitope for the STOK2 antibody is unknown, therefore, it is plausible that it is located near or at the L5 loop of Ly49i2. If this is the case, then the L5 loop mutants may have been folded properly, just not recognized by STOK2. Alternatively, the mutants

may not have folded appropriately, hence the lack of binding by the antibody. The SPR study to assess the binding interaction between the L5 loop Ly49i2 mutants and the ligand did not result in any detectable association. This result is difficult to interpret due to the lack of the STOK2 antibody binding profile with the mutants. The L5 loop of Ly49 receptors engages with subsite F on MHC class I, acting in both species likely as an anchor point for the receptor and the ligand through the interactions between the highly conserved L5 loop and the peptide C-terminal anchor residue-binding F pocket in the peptide binding groove of MHC class I [192]. Based on the putative L5 loop structure of Ly49i2 (Figure 3-24), the Ala substitutions may have been sufficient to disrupt the anchoring of the receptor to MHC class I. Both Ser and Thr are polar residues, thus hydrophilic. Ala, being a hydrophobic residue, would possibly alter the configuration of the loop in the opposite direction, away from exposure to any aqueous environment. Due to the inability to confirm that the L5 loop mutants properly folded, the L5 loop results are inconclusive.

Overall, apart from the non-interpretable results for the L5 loop binding studies, Chapter III illustrates a crucial role for the L3 loop of Ly49i2 during interaction with the MHC class I molecule, RT1-A1<sup>c</sup>. Furthermore, the L6 loop may also be required for the engagement between the receptor and the ligand.

### ***Discussion & Future Directions***

The function of NK cells is dependent on the activating or inhibitory signals received from the cell surface receptors upon engagement with their respective ligands. The interaction between the NK cell receptors and the ligands is therefore a crucial component during a potential immune response. The studies in Chapter III have further elucidated our understanding of immune recognition of the MHC class I molecule RT1-A1<sup>c</sup> by the inhibitory receptor Ly49i2. To overcome the potential lack of binding by the STOK2 antibody to Ly49i2 mutant receptors for assurance of properly folded protein, each of the mutants described in Chapter III can be assessed for their interaction with the ligand RT1-A1<sup>c</sup> by MHC tetramer staining. This technique would allow for the detection and quantification of Ly49i2 receptors that recognize and bind RT1-A1<sup>c</sup>.

The role of the L3, L6, and L5 loop regions of Ly49i2 need to be further assessed. The binding interaction studies of Chapter III provide some insight as to the importance of each loop region. Ultimately, however, the role of each loop requires a functional assessment to ultimately define the NK cell response upon interaction of RT1-A1<sup>c</sup> with Ly49i2. A <sup>51</sup>Cr release assay should be executed, relying on transduced RNK-16 cells as the effector cells, and YB2/0 cells transfected to express RT1-A1<sup>c</sup> at their cell surface would serve as target cells. Transduction of the RNK-16 cells could rapidly be executed using the method described in Chapter IV. Given the quantity of receptors required to assess the role of the L3, L5, and L6 loop regions, the lentivirus transduction system described in Chapter IV would significantly economize the time required to express the mutants on the cell surface of the effector RNK-16 cells.

The L3 loop analysis involved exchanging the L3 loop of Ly49i2 for the L3 loop of three receptors that do not recognize RT1-A1<sup>c</sup>, Ly49i5, Ly49s5, and Ly49s3. Upon complete loss of binding between the Ly49i2 chimeric receptor bearing the L3 loop of all three receptors, individually, I observed partial restoration of RT1-A1<sup>c</sup> recognition by incorporating the Ly49i2 L3 loop into the Ly49i5 receptor. It would be of interest to determine if partial or full restoration of RT1-A1<sup>c</sup> binding occurs with Ly49s5 and Ly49s3 also bearing the L3 loop of Ly49i2. The outcome would ascertain the critical role of the L3 loop.

The recognition of MHC class I is not always species specific. Recognition of xenogenic ligands has been previously reported for mouse Ly49 receptors [243, 288, 383, 384]. Amongst those studies, our laboratory has demonstrated that the activating Ly49W and inhibitory Ly49G receptors in the mouse both recognized the RT1-A1<sup>c</sup> as a xenogeneic MHC class I ligand [288]. While both the NOD mouse Ly49W activating receptor and the BALB/c Ly49G2 inhibitory receptor has been shown to recognize H-2D<sup>d</sup> and H-2D<sup>k</sup>, Ly49W further recognizes H-2K<sup>k</sup>, and Ly49G2 additionally recognizes H-2L<sup>d</sup> [242, 371]. Furthermore, Ly49W and Ly49G2 share 100% amino acid sequence identity in the L3, L5, and L6 loops (Figure 1-5 A). Ly49i2 shares 100% protein sequence identity with Ly49W and Ly49G2 in the L5 and L6 loops, yet great variability in the L3 loop (Figure 1-5). It would be of interest to examine of the ability of Ly49i2 to bind and recognize the mouse MHC class I ligands recognized by both Ly49G2 and Ly49W via

SPR analysis and/or  $^{51}\text{Cr}$  release assay. By performing the reciprocal study, the potential identification of new xenogeneic ligands may provide additional insights into Ly49 receptor ligand recognition. Depending on the outcome, subsequent analyses of the residues within the ligand interacting L3, L5, and L6 loops, may allow for further investigation into the allele specificity requirement of RT1-A1<sup>c</sup> recognition by Ly49i2. Not only could the xenogeneic ligand assessments further elucidate the requirements for receptor-ligand interaction, it could also provide insight into the potential use of NK cells in xenotransplantation tolerance [288].

Engagements between NK cells receptors and their ligands, such as the interaction between the Ly49i2 receptor and the MHC class I molecule RT1-A1<sup>c</sup>, ultimately dictates the functional output of the NK cell. The ability to distinguish self from non-self is a task that requires precise molecular interactions between specific sites and residues on both the ligand and the receptor. The engagement of the L3, L5, and L6 loops of Ly49i2 with RT1-A1<sup>c</sup> subsites B, F, and C, respectively (Figure 6-2), may involve a hierarchy. From the data in Chapter III, it appears that the L3 loop is critical for RT1-A1<sup>c</sup> recognition. Any alteration in the L3 loop may not be tolerated by the associating receptor:ligand complex. Furthermore, L5 and L6 may be required, but not crucial for conferring ligand recognition by Ly49i2. The proposed studies, together with the data presented, will allow us to define the role of each loop region in ligand recognition, and maybe even in the requirements for allele specificity of MHC class I.

## ***6.2.2 LENTIVIRAL-MEDIATED EXOGENOUS GENE EXPRESSION IN RNK-16 CELLS***

### ***Summary of Contributions***

Several groups, including our laboratory, rely on the rat leukemic cell line, RNK-16, for NK cell functional assays. The expression of exogenous Ly49 receptors on the surface of RNK-16 cells via electroporation has allowed for extensive NK cell functional studies [190-192, 243, 264-267, 273, 286-291]. Transfection of RNK-16 cells, however, is a difficult and tedious task that requires a considerable amount of time, usually resulting in low transfection efficiencies. To date, electroporation has been the only

transfection method possible for the expression of exogenous genes in RNK-16 cells. A major focus of our laboratory is defining and further elucidating the functions of NK cell receptors. Therefore, the development of a transfection method that would allow us to express NK cell receptors on the surface of RNK-16 cells for functional assessments in a more time efficient manner, resulting in higher transfection efficiencies was worth the investment.

Natural killer cells are resistant to exogenous gene transfers [268-271]. Hence, various attempts to successfully transfect NK cells with methods that did not involve electroporation, overall deemed unsuccessful [269, 270, 292-295, 298, 299, 302, 303]. Lentivirus transduction systems, however, have proven efficacious for the expression of exogenous genes in cells that are difficult to transfect, such as NK cells, as well as in non-dividing cells [268, 306, 307]. Furthermore, successful transgene expression in primary mouse NK cells by lentivirus transduction did not alter the viability, the function, or the phenotype of the NK cells [268]. Together, these reported results led us to pursue the possibility of expressing foreign genes in RNK-16 cells by lentivirus transduction.

For the expression of exogenous genes in RNK-16 cells, I assessed various lentivirus transduction system options. Expression of the transgene is dependent on the promoter encoded by the lentivirus plasmid. Firstly, I explored expressing the rat inhibitory receptor Ly49i2 on the surface of RNK-16 cells under the control of the CMV promoter. By using commercially available kits for lentivirus transduction, all the required components and instructions were provided. Moreover, should the CMV promoter successfully induce the expression of Ly49i2 in RNK-16 cells, the transfection process would have been quite fast. The CMV promoter, however, was unable to drive the expression of Ly49i2 in the RNK-16 cells. These results had been similarly observed in human NK cells [295]. Although the exact mechanism is unknown, DNA methylation and histone deacetylation are believed to cooperate and silence the CMV promoter in human and rodent cells [348, 350, 353, 354]; a concept supported by the gain of function by the re-activated CMV promoter upon the inhibition of both DNA methylation and histone deacetylation [349, 355, 356]. Likely, the CMV promoter is silenced in RNK-16 cells, thus rendering this approach unusable.

In cell types where the CMV promoter has been less successful, as well as cells

that are difficult to transfect, the EF-1 $\alpha$  promoter has proven successful in transgene expression [325, 338-342]. I decided to explore an alternate transduction method reliant on the EF-1 $\alpha$  promoter for expression of Ly49i2 on the surface of RNK-16 cells. For this approach, I did not depend on commercially available systems; instead, I relied on developing a method using a lentivirus vector and packaging plasmids generously provided by Dr. Troy Baldwin (Department of Medical Microbiology & Immunology; University of Alberta). I proceeded to generate infectious lentivirus particles using the method described by The RNAi Consortium laboratory protocol. For the transduction of RNK-16 cells, I explored various methods. Ultimately, successful expression of Ly49i2 resulted when RNK-16 cells were infected with lentivirus following an optimized protocol (Figure 6-1).

To date, use of RNK-16 cells for transgene expression has only been possible by electroporation. In Chapter IV, I described the development of a transduction protocol that allows for the efficient transfection of RNK-16 cells resulting in high expression levels of Ly49i2. Furthermore, in comparison to electroporation, the described protocol requires much less time for gene expression in most cells, allowing for the transduced RNK-16 cells to be available for subsequent studies much quicker.

### ***Discussion & Future Directions***

RNK-16 cells are pivotal for NK cell activation studies. Although electroporation was the only method relied upon for successful exogenous gene expression in RNK-16 cells, the process was extremely time consuming and cumbersome. For each protein, an average of 6–8 months was required for the generation of stable transfectants with electroporation. The method described in Chapter IV allows for stable transductants to be generated within 2-3 weeks, from start to finish. This will allow us to screen multiple receptors for ligand interaction studies within a short period of time.

Our laboratory is focused on understanding the role of NK cell receptors on NK cell function. We typically rely on <sup>51</sup>Cr release assays for our NK cell functional studies. Employing the protocol described in Chapter IV for transgene expression in RNK-16 cells can allow us to conduct functional studies with either transient or stable

transductants.  $^{51}\text{Cr}$  release assays require approximately 1 working day for functional readout results, thus complete NK cell functional studies can be accomplished much more rapidly.

Before our laboratory can begin using this method for the generation of RNK-16 transductants, a functional assessment of the transduced RNK-16 cells is required. RNK-16 cells recognize NK cell tumor targets such as the rat YB2/0 cells, rapidly killing them [263, 272]. We have successfully used YB2/0 cells as targets during  $^{51}\text{Cr}$  release assays with electroporated RNK-16 cells as effectors [191, 192, 243, 267, 288]. To ensure the lentivirus transduction protocol described in Chapter IV does not alter the function or phenotype of RNK-16 cells, a  $^{51}\text{Cr}$  release assay should be carried out with RNK-16 transductants expressing Ly49i2 as the effector cells, and YB2/0 cells transfected with RT1-A1<sup>c</sup> as the target cells. Furthermore, the outcome of the  $^{51}\text{Cr}$  release assay should then be compared to results from a parallel  $^{51}\text{Cr}$  release assay relying on electroporated RNK-16 cells expressing the same receptor engaging with the same target cells expressing the same ligand. Once it has been ascertained that lentivirus transduction of RNK-16 cells does not alter their function, the method outlined in Chapter IV could then be employed ongoing for transgene expression in RNK-16 cells.

### ***6.2.3. DIMERIZATION OF Ly49 RECEPTORS***

#### ***Summary of Contributions***

Natural killer cell Ly49 receptors are expressed as homodimers at the cell surface [169, 170]. The Ly49 subunits are linked via disulfide bonds and work in concert to execute their function. The NKD is the ligand-interacting domain of the Ly49 receptor. The stalk region not only anchors the receptor to the cell membrane, it interacts with the NKD monomers to provide stability and flexibility to the entire receptor as it interacts with its ligand. Ly49 receptors recognize their MHC class I ligands in an allele specific manner; thus both NKD are capable of recognizing the same ligand(s). The engagement between Ly49 receptors and MHC class I molecules is crucial to the overall function of

the NK cell given that this association ultimately dictates the response of the NK cell. Fundamentally, the distinction between “self” and “non-self” is dependent on the interaction between Ly49 receptors and MHC class I molecules [230]. Although heterodimeric Ly49 receptors have not been reported, the fundamental concept of their potential is worth exploring. Understanding the molecular specificity for homodimer formation between Ly49 receptors, as well as the requirements for dimer assembly may allow for the manipulation of Ly49s that could impact NK cell function.

In Chapter V, I sought to assess heterodimer formation between different mouse Ly49 monomers. By flow cytometry and biochemical assays, I was able to demonstrate that Ly49 receptors within the same receptor group associate together, potentially as heterodimers. Firstly, I assessed the ability of activating receptors to engage and associate. Ly49M, Ly49W2, and Ly49P1 are all activating receptors of the NOD mouse and all members of group II (figure 1-5 *A*). Ly49M and Ly49W2 are members of subgroup IIb, while Ly49P1 is a member of subgroup IIa. Protein sequence alignments revealed that Ly49M and Ly49W2 share almost identical protein sequence identity, while in alignment with Ly49P1, they share much less. Despite some differences in sequence identity, I was able to demonstrate the receptors associated together in pairs. Furthermore, the evidence strongly suggests the association between the receptors is likely as heterodimers.

Subsequently, I sought to determine if dimer formation between an inhibitory receptor and an activating receptor was possible. I demonstrated that the inhibitory Ly49G2 BALB/c mouse receptor, which displays greater sequence identity with both Ly49M and Ly49W2 in the extracellular regions versus the transmembrane and cytoplasmic tail, also associates with Ly49M and with Ly49W2. The data further support the formation of heterodimers between the activating receptors Ly49M and Ly49W2 with the inhibitory receptor Ly49G2. Both Ly49G2 and Ly49W2 recognize the MHC class I molecules H-2D<sup>d</sup> and H-2K<sup>k</sup> [243, 289, 381], with similar binding affinities [371]. Therefore, it is not surprising that these two receptors associate, potentially as heterodimers. With the association and possible heterodimer assembly observed between Ly49M and Ly49W2, as well as the comparable sequence identity between Ly49W2 with Ly49G2 and Ly49M with Ly49G2, the association between the latter pair was also

expected. The evidence further implies that Ly49M and Ly49W2 form heterodimers with Ly49G2.

In Chapter V, I report the first potential heterodimer formation between Ly49 receptors. The data in this chapter is the foundation to elucidating the fundamental nature of Ly49 dimer assembly. Furthermore, Ly49 heterodimerization may have implications in ligand-binding interactions, ultimately affecting NK cell function.

### ***Discussion & Future Directions***

The function of mouse and rat NK cells is, in part, regulated by the Ly49 recognition of MHC class I molecules, requiring the engagement of the Ly49 homodimer with the ligand. The ligand-interacting region of the Ly49 receptor, the NKD, is responsible for distinguishing MHC class I alleles, thus possesses the ability to recognize self from non-self. Both of the Ly49 monomers display the same MHC class I allele specificity, thus are limited to their recognition spectrum. Entertaining the alternative possibility, Ly49 heterodimers, has been previously attempted; however, unsuccessfully [378, 379].

In Chapter V, the evidence not only suggests heterodimer formation amongst mouse activating receptors, but it also implies heterodimeric assembly amongst activating and inhibitory mouse receptors. The concept of bifunctional Ly49 receptors is already displayed in the rat, where 5 bifunctional receptor genes have been identified (*Ly49si1* – *Ly49si5*) [244]. The rat *Ly49si1* and *Ly49si2* have been shown to be differentially expressed in basal versus LPS-stimulated bone marrow-derived macrophages, and may also play a role in mediating glomerulonephritis susceptibility [385]. Furthermore, genetic mapping studies in an experimental autoimmune encephalomyelitis (EAE) rat model indicate a possible protective role for *Ly49si1* and *Ly49si3* [386]. The functional significance of bifunctional Ly49 receptors may not have been fully characterized; however, these receptors may prove vital in the resistance against disease. Therefore, the ability to generate bifunctional, heterodimeric Ly49 receptors should be explored.

Monofunctional, heterodimeric Ly49 receptors may also alter the dynamics of ligand recognition. The Ly49C:H-2K<sup>b</sup> co-crystal structure reveals a symmetrical

association of Ly49C with its ligand, where each Ly49C monomer binds one H-2K<sup>b</sup> molecule [189]. Conversely, the co-crystal structure of the mouse Ly49A with H-2D<sup>d</sup> revealed an asymmetrical conformation whereby the Ly49A homodimer binds one H-2D<sup>d</sup> [188]. An alternative engagement conformation, similar to that observed for Ly49C:H-2K<sup>b</sup>, has also been reported for Ly49A, where a solution nuclear magnetic resonance study of unbound Ly49A revealed that unligated Ly49A can also adopt a symmetric homodimer conformation, whereby each monomer engages an MHC class I molecule [387]. The differential engagement states observed for Ly49A are likely due to *cis* versus *trans* interactions between the receptor and the ligand resulting in an asymmetrical Ly49 conformation, or symmetrical Ly49 conformation, respectively ([387]. Given the possibility of each monomer engaging its own MHC class I molecule, Ly49 heterodimeric engagement with two different MHC class I allele products may allow for improved “self-screening”, resulting in quicker detection of altered self, ultimately, impacting NK cell function.

The data presented in Chapter V all support heterodimer assembly between various Ly49 receptors. I had hypothesized that Ly49M and Ly49W2 would not dimerize with Ly49P1; given the association observed for these receptors, the study requires a negative control. As a continuation to the study, receptors of another group should be introduced as potential negative control for heterodimer assembly. Others inquired about the possible heterodimer association between the inhibitory Ly49C, a group I member, and the inhibitory Ly49A, a member of group II; however were unsuccessful [379]. Group I receptors, like the inhibitory receptor Ly49C and the activating receptor Ly49H, display great variability in sequence identity compared to group II members, including the presence of an  $\alpha$ -helix within the L3 loop region, lacking in group II (Figure 1-5 A). Furthermore, within the  $\alpha_3$  helix, group I members encode either Asp or Glu, negatively charged residues, at position 125, yet group II members encode Asn or Lys (Figure 5-13). Asn is a polar residue and Lys is a positively charged residue, both with opposite properties in comparison to Asp and Glu. Moreover, within the L<sub>5</sub> loop, group I members contain Asp, a negatively charged amino acid, and group II members contain the positively charged His amino acid at position 140 (Figure 5-13). These opposing charges between the two groups may be what dictates heterodimer

assembly within a group, but not between groups. Thus, these differences may have contributed to the reported impediment of dimer assembly between Ly49A and Ly49C, resulting in the unlikely association between group I and group II members. Therefore, the flow cytometry and biochemical assays utilized in Chapter V should also be relied upon for dimer assembly queries between Ly49C and/or Ly49H with any or all of the group II members used in this study: Ly49M, Ly49W2, Ly49P1, and Ly49G2.

Immunoprecipitation followed by Western blotting are highly sensitive biochemical assays that allow for the detection of two proteins that associate together [388]. In Chapter V, the evidence for the detected association between the various Ly49 receptors strongly suggests that the Ly49 receptors are likely associating as heterodimers. To further corroborate heterodimeric Ly49 assembly, 2-D gel electrophoresis under reducing and non-reducing conditions should be performed. This technique was successfully used to ascertain the heterodimeric assembly of the T-cell receptor (TCR) complex with the TCR- $\alpha$  and TCR- $\beta$  chains [389, 390]. Following the biochemical analyses, mass spectrometry analyses should also be performed to confirm the protein sequence of the Ly49 heterodimers. Taken together, these studies will provide strong evidence for the heterodimeric association of Ly49 receptors.

The ligand-interacting region of Ly49 receptors, the NKD, is linked to the transmembrane and cytoplasmic domains via a stalk region of approximately 70 residues [197]. As compared to other NK cell receptors, the Ly49 stalk is a long structure as compared to the twenty-residue stalk of NKG2A and 17-residue stalk in KIRs [194]. The Ly49 stalk is composed of three alpha helices, the membrane proximal  $\alpha_{1S}$ ,  $\alpha_{2S}$ , and membrane distal  $\alpha_{3S}$ , where  $\alpha_{3S}$  is then linked to the NKD via a loop ( $L_S$ ) [197]. In general, stalk regions are usually viewed as innocuous, simply required for linking the extracellular region(s) to the cell membrane [382]. Recently, however, this notion has been challenged, where an appreciation for the Ly49 stalk region has emerged. The structure of the stalk allows the Ly49 receptor flexibility for effective engagement with its ligand. One method NK cells regulate their cellular signaling is via *cis* and *trans* interactions between Ly49 receptors and their MHC class I counterpart. For example, *cis* engagements, which involve Ly49 interacting with MHC class I ligand on the same cell membrane, are crucial in regulating and accenting inhibitory signals [391]. Furthermore,

these are possible due to the long, flexible stalk region of Ly49s [197]. In an interesting twist, the stalk can also serve as the interacting domain during ligand contact. The mouse cytomegalovirus (MCMV) encodes the MHC class I mimic m157 for immunoevasion, which is recognized by the C57BL/6 mouse Ly49H activating receptor resulting in NK cell cytotoxicity [222]. Recently, it has been reported that m157 targets and binds to the stalk region of Ly49H, bypassing the NKD, a phenomenon previously not seen in Ly49-ligand engagements [382]. The stalk region, therefore, plays a more important role in innate immunity than previously thought.

The stalk of Ly49s may also contribute to the structural dynamic required for functionality. The assembly of the Ly49 dimers occurs cotranslationally [392, 393], and given the interchain disulfide linkage within the stalk region, the stalk may be one of the domains required for assembly of the Ly49 monomers [361]. The reported crystal and co-crystal structures of various mouse Ly49s has provided great insight as to not only the structure of Ly49s, but also to their interaction with their respective ligands, as well as the interaction between Ly49 monomers [187-189, 197, 361, 382]. All of the crystal structures, with the exception of the activating Ly49L receptor, are of the Ly49 NKD. The resolution of the several Ly49 NKD crystal structures revealed that the Ly49 monomers interact through the  $\beta_0$  strand [196]. Intriguingly, the crystal structure of the Ly49L NKD with the partial stalk region further elucidated the interactions between the two subunits. The stalk backfolds onto the NKD of the Ly49 receptor, allowing the membrane distal  $\alpha_3$  portion of the stalk, as well as the  $L_S$  loop to interact with numerous NKD residues [197]. Furthermore, of all the contact residues between the NKD and the stalk regions, eight residues are conserved amongst all Ly49 receptors, implying that the backfolded structure of the stalk onto the NKDs observed with Ly49L may be a universal configuration amongst all Ly49s [197]. Given the reliance of the stability of the Ly49 dimer on the engagement between the  $\alpha_3$  portion of the stalk and the  $L_S$  loop with the NKD, it is probable that the assembly of the Ly49 dimers requires the NKD and the stalk region. Therefore, it is of great importance to determine the role of the stalk and/or the NKD during dimer assembly. The Ly49s identified to date have been reported as homodimers; therefore, the interacting residues between the stalk and the NKD (Figure 5-13) are likely needed for dimer formation and should be assessed. To determine if the

Ly49 stalk and/or the NKD are required for dimer assembly, Ly49 chimeric receptors consisting of an Ly49 with the stalk region of another Ly49 that does not associate with it, likely two receptors from different groups, should be generated. Heterodimer formation would be assessed via the biochemical assays described in Chapter V and this Chapter, between the chimeric receptor and its wildtype form, as well as with the stalk-donor wildtype Ly49. Depending on the outcome, mutagenesis of point-mutants may then be required to identify the residue(s) responsible for dimer assembly.

Some of the interacting residues between the stalk and the NKD may also be required for the specificity that allows for only homodimer assembly. Several Ly49 receptors share a high degree of sequence identity, yet Ly49 heterodimers have not been reported. The activating receptors Ly49M and Ly49W2 share approximately 98% protein sequence identity and are both found in the NOD; yet these two receptors have not been detected as heterodimers. Understanding the molecular requirements for homodimer specificity is also of great importance. This will allow for the exploration of heterodimer assembly between Ly49W, Ly49M, Ly49P and Ly49G in NOD NK cells. Taken together, these findings would lay the foundation to further exploration of the functional significance of Ly49 heterodimers. The ability to manipulate Ly49 receptor recognition of, or even the distinction of allele specificity of MHC class I may allow for altered NK cell functions not yet explored.

### **6.3 CONCLUDING REMARKS**

This collective body of work has further elucidated the interaction and recognition of Ly49 receptors with MHC class I molecules. I have demonstrated the Ly49 loop regions required for the recognition of MHC class I. Additionally, I have also developed a method that will allow for rapid expression of Ly49 receptors required for functional assays. Lastly, I provided evidence for the heterodimer assembly of Ly49 receptors. The collective work presented in this thesis provides greater insight into the role of the Ly49 during ligand recognition, ultimately dictating the functional response of the NK cell.

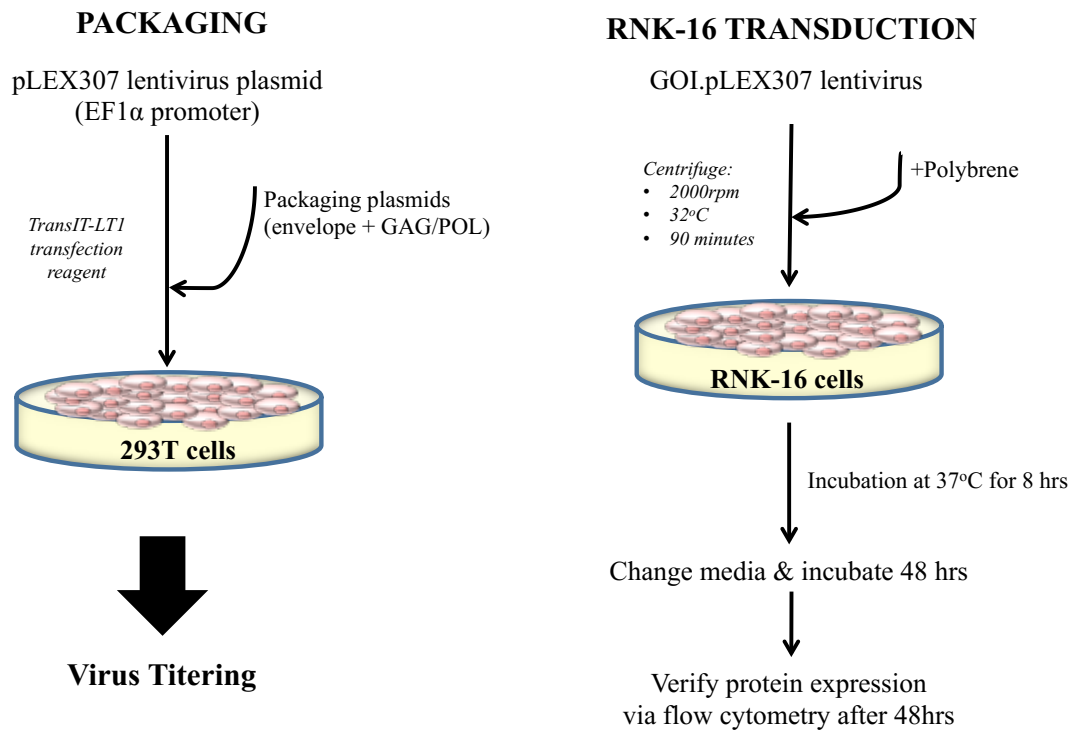


**Figure 6-1: Lentiviral-mediated exogenous gene expression in RNK-16 cells.** The outline for packaging lentivirus bearing the gene of interest for expression in RNK-16 cells is displayed (*left*). The gene of interest is cloned into pLEX307 via Gateway recombination and packaged in 293T cells. Upon virus titering, RNK-16 cells are transduced (*right*). RNK-16 cells are incubated with lentivirus particles and polybrene during a 90-minute spinfection at 2000rpm and 32°C. Cells are further incubated in an incubator for an additional 8 hours, after which fresh medium is introduced. RNK-16 cells are incubated for an additional 48 hours before cell surface expression of the gene of interest is assessed by flow cytometry.

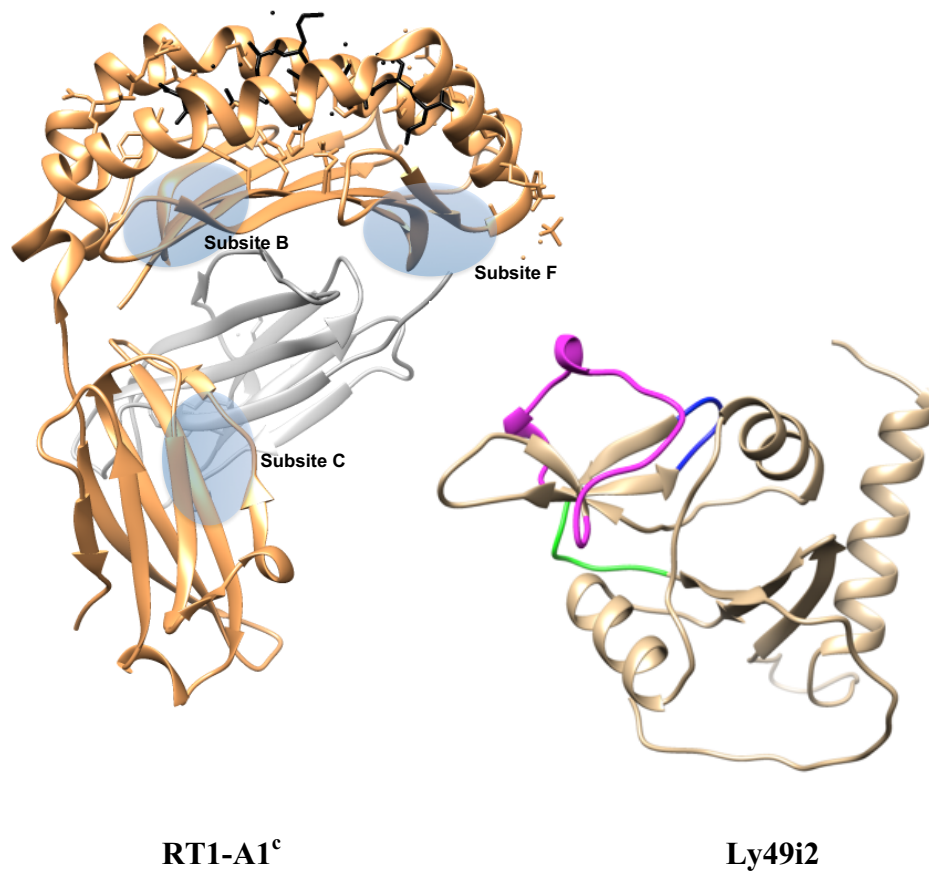


**Figure 6-2: The rat MHC class I molecule RT1-A1<sup>c</sup> and the putative inhibitory rat Ly49i2 receptor.** The rat inhibitory Ly49i2 receptor (*tan*) recognizes the MHC class I molecule, RT1-A1<sup>c</sup> (*gold*;  $\beta_2m$  in *grey*), as its cognate ligand. Putative MHC class I interaction sites with the Ly49i2 L3 (*magenta*), L5 (*blue*), and L6 (*green*) loop regions are designated as subsites B, F, and C, respectively. The putative structure of the inhibitory rat Ly49i2 receptor was predicted using the molecular modeling system Chimera (<http://www.cgl.ucsf.edu/chimera/>) with the graphical interface to Modeller (<http://www.salilab.org/modeller/>), relying on the structure of the mouse activating receptor Ly49L (PDB ID: 3G8L). RT1-A1<sup>c</sup> PDB ID: 1KJV.

## **BIBLIOGRAPHY**

1. Kiessling, R., et al., "Natural" killer cells in the mouse. II. Cytotoxic cells with specificity for mouse Moloney leukemia cells. Characteristics of the killer cell. *Eur J Immunol*, 1975. **5**(2): p. 117-21.
2. Kiessling, R., E. Klein, and H. Wigzell, "Natural" killer cells in the mouse. I. Cytotoxic cells with specificity for mouse Moloney leukemia cells. Specificity and distribution according to genotype. *Eur J Immunol*, 1975. **5**(2): p. 112-7.
3. Vivier, E., et al., *Innate or adaptive immunity? The example of natural killer cells*. *Science*, 2011. **331**(6013): p. 44-9.
4. Campbell, K.S. and J. Hasegawa, *Natural killer cell biology: an update and future directions*. *J Allergy Clin Immunol*, 2013. **132**(3): p. 536-44.
5. Reynolds, C.W., T. Timonen, and R.B. Herberman, *Natural killer (NK) cell activity in the rat. I. Isolation and characterization of the effector cells*. *J Immunol*, 1981. **127**(1): p. 282-7.
6. Gregoire, C., et al., *The trafficking of natural killer cells*. *Immunol Rev*, 2007. **220**: p. 169-82.
7. Orange, J.S. and Z.K. Ballas, *Natural killer cells in human health and disease*. *Clin Immunol*, 2006. **118**(1): p. 1-10.
8. Colucci, F., M.A. Caligiuri, and J.P. Di Santo, *What does it take to make a natural killer?* *Nat Rev Immunol*, 2003. **3**(5): p. 413-25.
9. Poli, A., et al., *Novel method for isolating untouched rat natural killer cells with higher purity compared with positive selection and fluorescence-activated cell sorting*. *Immunology*, 2010. **131**(3): p. 386-94.
10. Walzer, T., et al., *Natural killer cells: from CD3(-)NKp46(+) to post-genomics meta-analyses*. *Curr Opin Immunol*, 2007. **19**(3): p. 365-72.
11. Yu, J., A.G. Freud, and M.A. Caligiuri, *Location and cellular stages of natural killer cell development*. *Trends Immunol*, 2013. **34**(12): p. 573-82.
12. Boos, M.D., K. Ramirez, and B.L. Kee, *Extrinsic and intrinsic regulation of early natural killer cell development*. *Immunol Res*, 2008. **40**(3): p. 193-207.
13. Dubois, S., et al., *IL-15R $\alpha$  recycles and presents IL-15 In trans to neighboring cells*. *Immunity*, 2002. **17**(5): p. 537-47.
14. Becknell, B., et al., *Efficient infection of human natural killer cells with an EBV/retroviral hybrid vector*. *J Immunol Methods*, 2005. **296**(1-2): p. 115-23.
15. Grzywacz, B., et al., *Coordinated acquisition of inhibitory and activating receptors and functional properties by developing human natural killer cells*. *Blood*, 2006. **108**(12): p. 3824-33.
16. Kim, S., et al., *In vivo developmental stages in murine natural killer cell maturation*. *Nat Immunol*, 2002. **3**(6): p. 523-8.
17. Cooper, M.A., et al., *In vivo evidence for a dependence on interleukin 15 for survival of natural killer cells*. *Blood*, 2002. **100**(10): p. 3633-8.
18. Ranson, T., et al., *IL-15 is an essential mediator of peripheral NK-cell homeostasis*. *Blood*, 2003. **101**(12): p. 4887-93.
19. Trambas, C.M. and G.M. Griffiths, *Delivering the kiss of death*. *Nat Immunol*, 2003. **4**(5): p. 399-403.
20. Eischen, C.M. and P.J. Leibson, *Role for NK-cell-associated Fas ligand in cell-mediated cytotoxicity and apoptosis*. *Res Immunol*, 1997. **148**(3): p. 164-9.

21. Arase, H., N. Arase, and T. Saito, *Fas-mediated cytotoxicity by freshly isolated natural killer cells*. J Exp Med, 1995. **181**(3): p. 1235-8.
22. Kayagaki, N., et al., *Expression and function of TNF-related apoptosis-inducing ligand on murine activated NK cells*. J Immunol, 1999. **163**(4): p. 1906-13.
23. Screpanti, V., et al., *A central role for death receptor-mediated apoptosis in the rejection of tumors by NK cells*. J Immunol, 2001. **167**(4): p. 2068-73.
24. Wallin, R.P., et al., *Regulation of perforin-independent NK cell-mediated cytotoxicity*. Eur J Immunol, 2003. **33**(10): p. 2727-35.
25. Schoenborn, J.R. and C.B. Wilson, *Regulation of interferon-gamma during innate and adaptive immune responses*. Adv Immunol, 2007. **96**: p. 41-101.
26. Walzer, T., et al., *Natural-killer cells and dendritic cells: "l'union fait la force"*. Blood, 2005. **106**(7): p. 2252-8.
27. Maghazachi, A.A., *Role of chemokines in the biology of natural killer cells*. Curr Top Microbiol Immunol, 2010. **341**: p. 37-58.
28. Cudkowicz, G. and M. Bennett, *Peculiar immunobiology of bone marrow allografts. II. Rejection of parental grafts by resistant F 1 hybrid mice*. J Exp Med, 1971. **134**(6): p. 1513-28.
29. Cudkowicz, G. and M. Bennett, *Peculiar immunobiology of bone marrow allografts. I. Graft rejection by irradiated responder mice*. J Exp Med, 1971. **134**(1): p. 83-102.
30. Cudkowicz, G. and J.H. Stimpfling, *Hybrid Resistance to Parental Marrow Grafts: Association with the K Region of H-2*. Science, 1964. **144**(3624): p. 1339-40.
31. Lotzova, E. and G. Cudkowicz, *Hybrid resistance to parental NZW bone marrow grafts: association with the D end of H-2*. Transplantation, 1971. **12**(2): p. 130-8.
32. Yokoyama, W.M., *Hybrid resistance and the Ly-49 family of natural killer cell receptors*. J Exp Med, 1995. **182**(2): p. 273-7.
33. Oertel, M., et al., *Alloreactivity of natural killer cells in allogeneic liver transplantation*. Transplantation, 2001. **72**(1): p. 116-22.
34. Kitchens, W.H., et al., *The changing role of natural killer cells in solid organ rejection and tolerance*. Transplantation, 2006. **81**(6): p. 811-7.
35. McNerney, M.E., et al., *Role of natural killer cell subsets in cardiac allograft rejection*. Am J Transplant, 2006. **6**(3): p. 505-13.
36. van der Touw, W. and J.S. Bromberg, *Natural killer cells and the immune response in solid organ transplantation*. Am J Transplant, 2010. **10**(6): p. 1354-8.
37. Muntasell, A., et al., *Priming of NK cell anti-viral effector mechanisms by direct recognition of human cytomegalovirus*. Front Immunol, 2013. **4**: p. 40.
38. Martinez, J., X. Huang, and Y. Yang, *Direct TLR2 signaling is critical for NK cell activation and function in response to vaccinia viral infection*. PLoS Pathog, 2010. **6**(3): p. e1000811.
39. Bubic, I., et al., *Gain of virulence caused by loss of a gene in murine cytomegalovirus*. J Virol, 2004. **78**(14): p. 7536-44.
40. Dokun, A.O., et al., *Specific and nonspecific NK cell activation during virus infection*. Nat Immunol, 2001. **2**(10): p. 951-6.
41. Sun, J.C., J.N. Beilke, and L.L. Lanier, *Adaptive immune features of natural killer cells*. Nature, 2009. **457**(7229): p. 557-61.

42. Cooper, M.A., et al., *Cytokine-induced memory-like natural killer cells*. Proc Natl Acad Sci U S A, 2009. **106**(6): p. 1915-9.
43. O'Leary, J.G., et al., *T cell- and B cell-independent adaptive immunity mediated by natural killer cells*. Nat Immunol, 2006. **7**(5): p. 507-16.
44. Paust, S. and U.H. von Andrian, *Natural killer cell memory*. Nat Immunol, 2011. **12**(6): p. 500-8.
45. Sun, J.C., S. Ugolini, and E. Vivier, *Immunological memory within the innate immune system*. EMBO J, 2014. **33**(12): p. 1295-303.
46. Hughes, A.L. and M. Yeager, *Molecular evolution of the vertebrate immune system*. Bioessays, 1997. **19**(9): p. 777-86.
47. Kelley, J., L. Walter, and J. Trowsdale, *Comparative genomics of major histocompatibility complexes*. Immunogenetics, 2005. **56**(10): p. 683-95.
48. Hurt, P., et al., *The genomic sequence and comparative analysis of the rat major histocompatibility complex*. Genome Res, 2004. **14**(4): p. 631-9.
49. Rahim, M.M., et al., *Ly49 receptors: innate and adaptive immune paradigms*. Front Immunol, 2014. **5**: p. 145.
50. Fremont, D.H., et al., *Crystal structures of two viral peptides in complex with murine MHC class I H-2Kb*. Science, 1992. **257**(5072): p. 919-27.
51. Zhang, W., et al., *Crystal structure of the major histocompatibility complex class I H-2Kb molecule containing a single viral peptide: implications for peptide binding and T-cell receptor recognition*. Proc Natl Acad Sci U S A, 1992. **89**(17): p. 8403-7.
52. Bjorkman, P.J., et al., *Structure of the human class I histocompatibility antigen, HLA-A2*. Nature, 1987. **329**(6139): p. 506-12.
53. Rudolph, M.G., et al., *Crystal structures of two rat MHC class Ia (RT1-A) molecules that are associated differentially with peptide transporter alleles TAP-A and TAP-B*. J Mol Biol, 2002. **324**(5): p. 975-90.
54. Li, X.C. and M. Raghavan, *Structure and function of major histocompatibility complex class I antigens*. Curr Opin Organ Transplant, 2010. **15**(4): p. 499-504.
55. Peaper, D.R. and P. Cresswell, *Regulation of MHC class I assembly and peptide binding*. Annu Rev Cell Dev Biol, 2008. **24**: p. 343-68.
56. Rodgers, J.R. and R.G. Cook, *MHC class Ib molecules bridge innate and acquired immunity*. Nat Rev Immunol, 2005. **5**(6): p. 459-71.
57. Braud, V.M., D.S. Allan, and A.J. McMichael, *Functions of nonclassical MHC and non-MHC-encoded class I molecules*. Curr Opin Immunol, 1999. **11**(1): p. 100-8.
58. Beckman, E.M., et al., *Recognition of a lipid antigen by CD1-restricted alpha beta+ T cells*. Nature, 1994. **372**(6507): p. 691-4.
59. Skold, M. and S.M. Behar, *The role of group 1 and group 2 CD1-restricted T cells in microbial immunity*. Microbes Infect, 2005. **7**(3): p. 544-51.
60. Van Rhijn, I. and D.B. Moody, *CD1 and mycobacterial lipids activate human T cells*. Immunol Rev, 2015. **264**(1): p. 138-53.
61. Porcelli, S., et al., *Recognition of cluster of differentiation 1 antigens by human CD4-CD8-cytolytic T lymphocytes*. Nature, 1989. **341**(6241): p. 447-50.
62. Naper, C., et al., *The role of natural killer cells in the defense against Listeria monocytogenes lessons from a rat model*. J Innate Immun, 2011. **3**(3): p. 289-97.

63. Shegarfi, H., et al., *The rat NK cell receptors Ly49s4 and Ly49i4 recognize nonclassical MHC-I molecules on Listeria monocytogenes-infected macrophages.* J Leukoc Biol, 2011. **89**(4): p. 617-23.
64. Shegarfi, H., et al., *The activating rat Ly49s5 receptor responds to increased levels of MHC class Ib molecules on Listeria monocytogenes-infected enteric epithelial cells.* Eur J Immunol, 2010. **40**(12): p. 3535-43.
65. Shegarfi, H., et al., *The role of natural killer cells in resistance to the intracellular bacterium Listeria monocytogenes in rats.* Scand J Immunol, 2009. **70**(3): p. 238-44.
66. Andrews, D.M., et al., *Recognition of the nonclassical MHC class I molecule H2-M3 by the receptor Ly49A regulates the licensing and activation of NK cells.* Nat Immunol, 2012. **13**(12): p. 1171-7.
67. Alfonso, C. and L. Karlsson, *Nonclassical MHC class II molecules.* Annu Rev Immunol, 2000. **18**: p. 113-42.
68. Colten, H.R., *Structure organization and expression of the major histocompatibility class III genes.* Ann N Y Acad Sci, 1985. **458**: p. 269-76.
69. Deakin, J.E., et al., *Evolution and comparative analysis of the MHC Class III inflammatory region.* BMC Genomics, 2006. **7**: p. 281.
70. Biron, C.A., et al., *Natural killer cells in antiviral defense: function and regulation by innate cytokines.* Annu Rev Immunol, 1999. **17**: p. 189-220.
71. Pegram, H.J., et al., *Activating and inhibitory receptors of natural killer cells.* Immunol Cell Biol, 2011. **89**(2): p. 216-24.
72. Barrow, A.D. and J. Trowsdale, *You say ITAM and I say ITIM, let's call the whole thing off: the ambiguity of immunoreceptor signalling.* Eur J Immunol, 2006. **36**(7): p. 1646-53.
73. Lanier, L.L., et al., *Immunoreceptor DAP12 bearing a tyrosine-based activation motif is involved in activating NK cells.* Nature, 1998. **391**(6668): p. 703-7.
74. Cheent, K. and S.I. Khakoo, *Natural killer cells: integrating diversity with function.* Immunology, 2009. **126**(4): p. 449-57.
75. Wu, J., et al., *An activating immunoreceptor complex formed by NKG2D and DAP10.* Science, 1999. **285**(5428): p. 730-2.
76. Billadeau, D.D., et al., *NKG2D-DAP10 triggers human NK cell-mediated killing via a Syk-independent regulatory pathway.* Nat Immunol, 2003. **4**(6): p. 557-64.
77. Zompi, S., et al., *NKG2D triggers cytotoxicity in mouse NK cells lacking DAP12 or Syk family kinases.* Nat Immunol, 2003. **4**(6): p. 565-72.
78. Ono, M., et al., *Deletion of SHIP or SHP-1 reveals two distinct pathways for inhibitory signaling.* Cell, 1997. **90**(2): p. 293-301.
79. Binstadt, B.A., et al., *Sequential involvement of Lck and SHP-1 with MHC-recognizing receptors on NK cells inhibits FcR-initiated tyrosine kinase activation.* Immunity, 1996. **5**(6): p. 629-38.
80. Burshtyn, D.N., et al., *Recruitment of tyrosine phosphatase HCP by the killer cell inhibitor receptor.* Immunity, 1996. **4**(1): p. 77-85.
81. Olcese, L., et al., *Human and mouse killer-cell inhibitory receptors recruit PTP1C and PTP1D protein tyrosine phosphatases.* J Immunol, 1996. **156**(12): p. 4531-4.

82. Berg, S.F., S. Fossum, and E. Dissen, *NILR-1, a novel immunoglobulin-like receptor expressed by neutrophilic granulocytes, is encoded by a leukocyte receptor gene complex on rat chromosome 1*. Eur J Immunol, 1999. **29**(6): p. 2000-6.
83. Kim, J., et al., *Homology-driven assembly of a sequence-ready mouse BAC contig map spanning regions related to the 46-Mb gene-rich euchromatic segments of human chromosome 19*. Genomics, 2001. **74**(2): p. 129-41.
84. Wende, H., et al., *Organization of the leukocyte receptor cluster (LRC) on human chromosome 19q13.4*. Mamm Genome, 1999. **10**(2): p. 154-60.
85. Colucci, F., et al., *How does variability of immune system genes affect placentation?* Placenta, 2011. **32**(8): p. 539-45.
86. Trowsdale, J., et al., *The genomic context of natural killer receptor extended gene families*. Immunol Rev, 2001. **181**: p. 20-38.
87. Lebbink, R.J., et al., *Identification and characterization of the rat homologue of LAIR-1*. Immunogenetics, 2005. **57**(5): p. 344-51.
88. Lebbink, R.J., et al., *The mouse homologue of the leukocyte-associated Ig-like receptor-1 is an inhibitory receptor that recruits Src homology region 2-containing protein tyrosine phosphatase (SHP)-2, but not SHP-1*. J Immunol, 2004. **172**(9): p. 5535-43.
89. Meyaard, L., et al., *LAIR-1, a novel inhibitory receptor expressed on human mononuclear leukocytes*. Immunity, 1997. **7**(2): p. 283-90.
90. Lebbink, R.J., et al., *Collagens are functional, high affinity ligands for the inhibitory immune receptor LAIR-1*. J Exp Med, 2006. **203**(6): p. 1419-25.
91. Pessino, A., et al., *Molecular cloning of NKp46: a novel member of the immunoglobulin superfamily involved in triggering of natural cytotoxicity*. J Exp Med, 1998. **188**(5): p. 953-60.
92. Falco, M., et al., *Identification of the rat homologue of the human NKp46 triggering receptor*. Immunol Lett, 1999. **68**(2-3): p. 411-4.
93. Biassoni, R., et al., *The murine homologue of the human NKp46, a triggering receptor involved in the induction of natural cytotoxicity*. Eur J Immunol, 1999. **29**(3): p. 1014-20.
94. Narni-Mancinelli, E., et al., *Fate mapping analysis of lymphoid cells expressing the NKp46 cell surface receptor*. Proc Natl Acad Sci U S A, 2011. **108**(45): p. 18324-9.
95. Westgaard, I.H., et al., *Rat NKp46 activates natural killer cell cytotoxicity and is associated with FcepsilonRIgamma and CD3zeta*. J Leukoc Biol, 2004. **76**(6): p. 1200-6.
96. Cagnano, E., et al., *Expression of ligands to NKp46 in benign and malignant melanocytes*. J Invest Dermatol, 2008. **128**(4): p. 972-9.
97. Elboim, M., et al., *Tumor immunoediting by NKp46*. J Immunol, 2010. **184**(10): p. 5637-44.
98. Mandelboim, O., et al., *Recognition of haemagglutinins on virus-infected cells by NKp46 activates lysis by human NK cells*. Nature, 2001. **409**(6823): p. 1055-60.
99. Magri, G., et al., *NKp46 and DNAM-1 NK-cell receptors drive the response to human cytomegalovirus-infected myeloid dendritic cells overcoming viral immune evasion strategies*. Blood, 2011. **117**(3): p. 848-56.

100. Gur, C., et al., *The activating receptor NKp46 is essential for the development of type 1 diabetes*. Nat Immunol, 2010. **11**(2): p. 121-8.
101. Martin, A.M., et al., *Leukocyte Ig-like receptor complex (LRC) in mice and men*. Trends Immunol, 2002. **23**(2): p. 81-8.
102. Dennis, G., Jr., et al., *Characterization of paired Ig-like receptors in rats*. J Immunol, 1999. **163**(12): p. 6371-7.
103. Lepin, E.J., et al., *Functional characterization of HLA-F and binding of HLA-F tetramers to ILT2 and ILT4 receptors*. Eur J Immunol, 2000. **30**(12): p. 3552-61.
104. Navarro, F., et al., *The ILT2(LIR1) and CD94/NKG2A NK cell receptors respectively recognize HLA-G1 and HLA-E molecules co-expressed on target cells*. Eur J Immunol, 1999. **29**(1): p. 277-83.
105. Chapman, T.L., A.P. Heikeman, and P.J. Bjorkman, *The inhibitory receptor LIR-1 uses a common binding interaction to recognize class I MHC molecules and the viral homolog UL18*. Immunity, 1999. **11**(5): p. 603-13.
106. Kubagawa, H., P.D. Burrows, and M.D. Cooper, *A novel pair of immunoglobulin-like receptors expressed by B cells and myeloid cells*. Proc Natl Acad Sci U S A, 1997. **94**(10): p. 5261-6.
107. Takai, T., *Paired immunoglobulin-like receptors and their MHC class I recognition*. Immunology, 2005. **115**(4): p. 433-40.
108. Campbell, K.S. and A.K. Purdy, *Structure/function of human killer cell immunoglobulin-like receptors: lessons from polymorphisms, evolution, crystal structures and mutations*. Immunology, 2011. **132**(3): p. 315-25.
109. Guethlein, L.A., et al., *Evolution of killer cell Ig-like receptor (KIR) genes: definition of an orangutan KIR haplotype reveals expansion of lineage III KIR associated with the emergence of MHC-C*. J Immunol, 2007. **179**(1): p. 491-504.
110. Sambrook, J.G., et al., *Identification of the ancestral killer immunoglobulin-like receptor gene in primates*. BMC Genomics, 2006. **7**: p. 209.
111. Wilson, M.J., et al., *Plasticity in the organization and sequences of human KIR/ILT gene families*. Proc Natl Acad Sci U S A, 2000. **97**(9): p. 4778-83.
112. Welch, A.Y., M. Kasahara, and L.M. Spain, *Identification of the mouse killer immunoglobulin-like receptor-like (Kirl) gene family mapping to chromosome X*. Immunogenetics, 2003. **54**(11): p. 782-90.
113. Hoelsbrekken, S.E., et al., *Cutting edge: molecular cloning of a killer cell Ig-like receptor in the mouse and rat*. J Immunol, 2003. **170**(5): p. 2259-63.
114. Yokoyama, W.M. and B.F. Plougastel, *Immune functions encoded by the natural killer gene complex*. Nat Rev Immunol, 2003. **3**(4): p. 304-16.
115. Renedo, M., et al., *The human natural killer gene complex is located on chromosome 12p12-p13*. Immunogenetics, 1997. **46**(4): p. 307-11.
116. Dissen, E., et al., *An autosomal dominant locus, Nka, mapping to the Ly-49 region of a rat natural killer (NK) gene complex, controls NK cell lysis of allogeneic lymphocytes*. J Exp Med, 1996. **183**(5): p. 2197-207.
117. Yokoyama, W.M., et al., *cDNA cloning of mouse NKR-P1 and genetic linkage with LY-49. Identification of a natural killer cell gene complex on mouse chromosome 6*. J Immunol, 1991. **147**(9): p. 3229-36.
118. Giorda, R., et al., *NKR-P1, a signal transduction molecule on natural killer cells*. Science, 1990. **249**(4974): p. 1298-300.

119. Chambers, W.H., et al., *Monoclonal antibody to a triggering structure expressed on rat natural killer cells and adherent lymphokine-activated killer cells*. J Exp Med, 1989. **169**(4): p. 1373-89.
120. Kirkham, C.L. and J.R. Carlyle, *Complexity and Diversity of the NKR-P1:Clr (Klrbl:Clec2) Recognition Systems*. Front Immunol, 2014. **5**: p. 214.
121. Zhang, Q., et al., *Mouse Nkrp1-Clr gene cluster sequence and expression analyses reveal conservation of tissue-specific MHC-independent immunosurveillance*. PLoS One, 2012. **7**(12): p. e50561.
122. Lanier, L.L., C. Chang, and J.H. Phillips, *Human NKR-P1A. A disulfide-linked homodimer of the C-type lectin superfamily expressed by a subset of NK and T lymphocytes*. J Immunol, 1994. **153**(6): p. 2417-28.
123. Aldemir, H., et al., *Cutting edge: lectin-like transcript 1 is a ligand for the CD161 receptor*. J Immunol, 2005. **175**(12): p. 7791-5.
124. Rosen, D.B., et al., *Cutting edge: lectin-like transcript-1 is a ligand for the inhibitory human NKR-P1A receptor*. J Immunol, 2005. **175**(12): p. 7796-9.
125. Rosen, D.B., et al., *Functional consequences of interactions between human NKR-P1A and its ligand LLT1 expressed on activated dendritic cells and B cells*. J Immunol, 2008. **180**(10): p. 6508-17.
126. Fergusson, J.R., V.M. Fleming, and P. Klenerman, *CD161-expressing human T cells*. Front Immunol, 2011. **2**: p. 36.
127. Glimcher, L., F.W. Shen, and H. Cantor, *Identification of a cell-surface antigen selectively expressed on the natural killer cell*. J Exp Med, 1977. **145**(1): p. 1-9.
128. Ryan, J.C., et al., *Molecular cloning of the NK1.1 antigen, a member of the NKR-P1 family of natural killer cell activation molecules*. J Immunol, 1992. **149**(5): p. 1631-5.
129. Koo, G.C. and J.R. Peppard, *Establishment of monoclonal anti-Nk-1.1 antibody*. Hybridoma, 1984. **3**(3): p. 301-3.
130. Karlhofer, F.M. and W.M. Yokoyama, *Stimulation of murine natural killer (NK) cells by a monoclonal antibody specific for the NK1.1 antigen. IL-2-activated NK cells possess additional specific stimulation pathways*. J Immunol, 1991. **146**(10): p. 3662-73.
131. Hackett, J., Jr., et al., *Origin and differentiation of natural killer cells. II. Functional and morphologic studies of purified NK-1.1+ cells*. J Immunol, 1986. **136**(8): p. 3124-31.
132. Li, J., et al., *Expression cloning and function of the rat NK activating and inhibitory receptors NKR-P1A and -PIB*. Int Immunol, 2003. **15**(3): p. 411-6.
133. Ziegler, S.F., et al., *The mouse CD69 gene. Structure, expression, and mapping to the NK gene complex*. J Immunol, 1994. **152**(3): p. 1228-36.
134. Lopez-Cabrera, M., et al., *Molecular cloning, expression, and chromosomal localization of the human earliest lymphocyte activation antigen AIM/CD69, a new member of the C-type animal lectin superfamily of signal-transmitting receptors*. J Exp Med, 1993. **178**(2): p. 537-47.
135. Flornes, L.M., et al., *The complete inventory of receptors encoded by the rat natural killer cell gene complex*. Immunogenetics, 2010. **62**(8): p. 521-30.

136. Ziegler, S.F., et al., *Molecular characterization of the early activation antigen CD69: a type II membrane glycoprotein related to a family of natural killer cell activation antigens*. Eur J Immunol, 1993. **23**(7): p. 1643-8.
137. Borrego, F., et al., *CD69 is a stimulatory receptor for natural killer cell and its cytotoxic effect is blocked by CD94 inhibitory receptor*. Immunology, 1999. **97**(1): p. 159-65.
138. Zingoni, A., et al., *CD69-triggered ERK activation and functions are negatively regulated by CD94 / NKG2-A inhibitory receptor*. Eur J Immunol, 2000. **30**(2): p. 644-51.
139. Kelley, J., L. Walter, and J. Trowsdale, *Comparative genomics of natural killer cell receptor gene clusters*. PLoS Genet, 2005. **1**(2): p. 129-39.
140. Lazetic, S., et al., *Human natural killer cell receptors involved in MHC class I recognition are disulfide-linked heterodimers of CD94 and NKG2 subunits*. J Immunol, 1996. **157**(11): p. 4741-5.
141. Berg, S.F., et al., *Two genes in the rat homologous to human NKG2*. Eur J Immunol, 1998. **28**(2): p. 444-50.
142. Fossum, S., et al., *Paired opposing leukocyte receptors recognizing rapidly evolving ligands are subject to homogenization of their ligand binding domains*. Immunogenetics, 2011. **63**(12): p. 809-20.
143. Plougastel, B. and J. Trowsdale, *Cloning of NKG2-F, a new member of the NKG2 family of human natural killer cell receptor genes*. Eur J Immunol, 1997. **27**(11): p. 2835-9.
144. Kim, D.K., et al., *Human NKG2F is expressed and can associate with DAP12*. Mol Immunol, 2004. **41**(1): p. 53-62.
145. Huang, H., et al., *Up-regulation of NKG2F receptor, a functionally unknown killer receptor, of human natural killer cells by interleukin-2 and interleukin-15*. Oncol Rep, 2010. **24**(4): p. 1043-8.
146. Joly, E. and V. Rouillon, *The orthology of HLA-E and H2-Qa1 is hidden by their concerted evolution with other MHC class I molecules*. Biol Direct, 2006. **1**: p. 2.
147. Vance, R.E., et al., *Mouse CD94/NKG2A is a natural killer cell receptor for the nonclassical major histocompatibility complex (MHC) class I molecule Qa-1(b)*. J Exp Med, 1998. **188**(10): p. 1841-8.
148. Braud, V.M., et al., *HLA-E binds to natural killer cell receptors CD94/NKG2A, B and C*. Nature, 1998. **391**(6669): p. 795-9.
149. Lee, N., et al., *HLA-E is a major ligand for the natural killer inhibitory receptor CD94/NKG2A*. Proc Natl Acad Sci U S A, 1998. **95**(9): p. 5199-204.
150. Parker, K.E., et al., *The rat RT.BMI MHC class I cDNA shows a high level of sequence similarity to the mouse H-2T23d gene*. Immunogenetics, 1991. **34**(3): p. 211-3.
151. Houchins, J.P., et al., *DNA sequence analysis of NKG2, a family of related cDNA clones encoding type II integral membrane proteins on human natural killer cells*. J Exp Med, 1991. **173**(4): p. 1017-20.
152. Berg, S.F., et al., *Molecular characterization of rat NKR-P2, a lectin-like receptor expressed by NK cells and resting T cells*. Int Immunol, 1998. **10**(4): p. 379-85.

153. Diefenbach, A., et al., *Ligands for the murine NKG2D receptor: expression by tumor cells and activation of NK cells and macrophages*. *Nat Immunol*, 2000. **1**(2): p. 119-26.
154. Zhang, J., F. Basher, and J.D. Wu, *NKG2D Ligands in Tumor Immunity: Two Sides of a Coin*. *Front Immunol*, 2015. **6**: p. 97.
155. Srivastava, R.M., C. Varalakshmi, and A. Khar, *The ischemia-responsive protein 94 (Irp94) activates dendritic cells through NK cell receptor protein-2/NK group 2 member D (NKR-P2/NKG2D) leading to their maturation*. *J Immunol*, 2008. **180**(2): p. 1117-30.
156. Zhuo, M., et al., *Identification of the rat NKG2D ligands, RAE1L and RRLT, and their role in allograft rejection*. *Eur J Immunol*, 2010. **40**(6): p. 1748-57.
157. Bauer, S., et al., *Activation of NK cells and T cells by NKG2D, a receptor for stress-inducible MICA*. *Science*, 1999. **285**(5428): p. 727-9.
158. Cosman, D., et al., *ULBPs, novel MHC class I-related molecules, bind to CMV glycoprotein UL16 and stimulate NK cytotoxicity through the NKG2D receptor*. *Immunity*, 2001. **14**(2): p. 123-33.
159. Sutherland, C.L., et al., *UL16-binding proteins, novel MHC class I-related proteins, bind to NKG2D and activate multiple signaling pathways in primary NK cells*. *J Immunol*, 2002. **168**(2): p. 671-9.
160. Carayannopoulos, L.N., et al., *Cutting edge: murine UL16-binding protein-like transcript 1: a newly described transcript encoding a high-affinity ligand for murine NKG2D*. *J Immunol*, 2002. **169**(8): p. 4079-83.
161. Cerwenka, A., et al., *Retinoic acid early inducible genes define a ligand family for the activating NKG2D receptor in mice*. *Immunity*, 2000. **12**(6): p. 721-7.
162. Savithri, B. and A. Khar, *A transmembrane-anchored rat RAE-1-like transcript as a ligand for NKR-P2, the rat ortholog of human and mouse NKG2D*. *Eur J Immunol*, 2006. **36**(1): p. 107-17.
163. Trowsdale, J., *Genetic and functional relationships between MHC and NK receptor genes*. *Immunity*, 2001. **15**(3): p. 363-74.
164. Barten, R., et al., *Divergent and convergent evolution of NK-cell receptors*. *Trends Immunol*, 2001. **22**(1): p. 52-7.
165. Westgaard, I.H., et al., *Identification of a human member of the Ly-49 multigene family*. *Eur J Immunol*, 1998. **28**(6): p. 1839-46.
166. Barten, R. and J. Trowsdale, *The human Ly-49L gene*. *Immunogenetics*, 1999. **49**(7-8): p. 731-4.
167. Hao, L. and M. Nei, *Genomic organization and evolutionary analysis of Ly49 genes encoding the rodent natural killer cell receptors: rapid evolution by repeated gene duplication*. *Immunogenetics*, 2004. **56**(5): p. 343-54.
168. Abi-Rached, L. and P. Parham, *Natural selection drives recurrent formation of activating killer cell immunoglobulin-like receptor and Ly49 from inhibitory homologues*. *J Exp Med*, 2005. **201**(8): p. 1319-32.
169. Chan, P.Y. and F. Takei, *Molecular cloning and characterization of a novel murine T cell surface antigen, YE1/48*. *J Immunol*, 1989. **142**(5): p. 1727-36.
170. Yokoyama, W.M., et al., *A murine T lymphocyte antigen belongs to a supergene family of type II integral membrane proteins*. *J Immunol*, 1989. **143**(4): p. 1379-86.

171. Yokoyama, W.M., et al., *Chromosomal location of the Ly-49 (A1, YE1/48) multigene family. Genetic association with the NK 1.1 antigen.* J Immunol, 1990. **145**(7): p. 2353-8.
172. Morse, H.C., 3rd, F.W. Shen, and U. Hammerling, *Genetic nomenclature for loci controlling mouse lymphocyte antigens.* Immunogenetics, 1987. **25**(2): p. 71-8.
173. Ortaldo, J.R., et al., *The Ly-49 family: regulation of cytotoxicity and cytokine production in murine CD3+ cells.* J Immunol, 1998. **160**(3): p. 1158-65.
174. Skold, M. and S. Cardell, *Differential regulation of Ly49 expression on CD4+ and CD4-CD8- (double negative) NK1.1+ T cells.* Eur J Immunol, 2000. **30**(9): p. 2488-96.
175. Maeda, M., et al., *Regulation of NKT cells by Ly49: analysis of primary NKT cells and generation of NKT cell line.* J Immunol, 2001. **167**(8): p. 4180-6.
176. Denning, T.L., et al., *Mouse TCRalpha+CD8alphaalpha intraepithelial lymphocytes express genes that down-regulate their antigen reactivity and suppress immune responses.* J Immunol, 2007. **178**(7): p. 4230-9.
177. Aust, J.G., et al., *Mice lacking Ly49E show normal NK cell development and provide evidence for probabilistic expression of Ly49E in NK cells and T cells.* J Immunol, 2011. **186**(4): p. 2013-23.
178. Van Den Broeck, T., et al., *Differential Ly49e expression pathways in resting versus TCR-activated intraepithelial gammadelta T cells.* J Immunol, 2013. **190**(5): p. 1982-90.
179. Van Acker, A., et al., *Ly49E expression on CD8alphaalpha-expressing intestinal intraepithelial lymphocytes plays no detectable role in the development and progression of experimentally induced inflammatory bowel diseases.* PLoS One, 2014. **9**(10): p. e110015.
180. Chan, P.Y. and F. Takei, *Characterization of a murine T cell surface disulfide-linked dimer of 45-kDa glycopeptides (YE1/48 antigen). Comparison with T cell receptor, purification, and partial amino acid sequences.* J Immunol, 1988. **140**(1): p. 161-9.
181. Nylenna, O., et al., *The genes and gene organization of the Ly49 region of the rat natural killer cell gene complex.* Eur J Immunol, 2005. **35**(1): p. 261-72.
182. Faure, M. and E.O. Long, *KIR2DL4 (CD158d), an NK cell-activating receptor with inhibitory potential.* J Immunol, 2002. **168**(12): p. 6208-14.
183. Wilhelm, B.T., L. Gagnier, and D.L. Mager, *Sequence analysis of the ly49 cluster in C57BL/6 mice: a rapidly evolving multigene family in the immune system.* Genomics, 2002. **80**(6): p. 646-61.
184. Makrigiannis, A.P., et al., *A BAC contig map of the Ly49 gene cluster in 129 mice reveals extensive differences in gene content relative to C57BL/6 mice.* Genomics, 2002. **79**(3): p. 437-44.
185. Proteau, M.F., E. Rousselle, and A.P. Makrigiannis, *Mapping of the BALB/c Ly49 cluster defines a minimal natural killer cell receptor gene repertoire.* Genomics, 2004. **84**(4): p. 669-77.
186. Matsumoto, N., et al., *The lectin-like NK cell receptor Ly-49A recognizes a carbohydrate-independent epitope on its MHC class I ligand.* Immunity, 1998. **8**(2): p. 245-54.

187. Deng, L., et al., *Molecular architecture of the major histocompatibility complex class I-binding site of Ly49 natural killer cell receptors*. J Biol Chem, 2008. **283**(24): p. 16840-9.
188. Tormo, J., et al., *Crystal structure of a lectin-like natural killer cell receptor bound to its MHC class I ligand*. Nature, 1999. **402**(6762): p. 623-31.
189. Dam, J., et al., *Variable MHC class I engagement by Ly49 natural killer cell receptors demonstrated by the crystal structure of Ly49C bound to H-2K(b)*. Nat Immunol, 2003. **4**(12): p. 1213-22.
190. Ma, B.J., et al., *Reciprocal transfer of class I MHC allele specificity between activating Ly-49P and Ly-49W receptors by exchange of beta 4-beta 5 loop residues*. J Immunol, 2003. **171**(10): p. 5337-44.
191. Silver, E.T., et al., *Ly-49P activates NK-mediated lysis by recognizing H-2Dd*. J Immunol, 2000. **165**(4): p. 1771-81.
192. Lavender, K.J., H.H. Chau, and K.P. Kane, *Distinctive interactions at multiple site 2 subsites by allele-specific rat and mouse ly49 determine functional binding and class I MHC specificity*. J Immunol, 2007. **179**(10): p. 6856-66.
193. Matsumoto, N., et al., *The functional binding site for the C-type lectin-like natural killer cell receptor Ly49A spans three domains of its major histocompatibility complex class I ligand*. J Exp Med, 2001. **193**(2): p. 147-58.
194. Dimasi, N. and R. Biassoni, *Structural and functional aspects of the Ly49 natural killer cell receptors*. Immunol Cell Biol, 2005. **83**(1): p. 1-8.
195. Kane, K.P., E.T. Silver, and B. Hazes, *Specificity and function of activating Ly-49 receptors*. Immunol Rev, 2001. **181**: p. 104-14.
196. Li, Y. and R.A. Mariuzza, *Structural basis for recognition of cellular and viral ligands by NK cell receptors*. Front Immunol, 2014. **5**: p. 123.
197. Back, J., et al., *Distinct conformations of Ly49 natural killer cell receptors mediate MHC class I recognition in trans and cis*. Immunity, 2009. **31**(4): p. 598-608.
198. Back, J., et al., *Stable masking by H-2Dd cis ligand limits Ly49A relocalization to the site of NK cell/target cell contact*. Proc Natl Acad Sci U S A, 2007. **104**(10): p. 3978-83.
199. Lanier, L.L., *DAP10- and DAP12-associated receptors in innate immunity*. Immunol Rev, 2009. **227**(1): p. 150-60.
200. Anderson, S.K., J.R. Ortaldo, and D.W. McVicar, *The ever-expanding Ly49 gene family: repertoire and signaling*. Immunol Rev, 2001. **181**: p. 79-89.
201. Naper, C., et al., *Ly-49s3 is a promiscuous activating rat NK cell receptor for nonclassical MHC class I-encoded target ligands*. J Immunol, 2002. **169**(1): p. 22-30.
202. Smith, K.M., et al., *Ly-49D and Ly-49H associate with mouse DAP12 and form activating receptors*. J Immunol, 1998. **161**(1): p. 7-10.
203. Gibbs, R.A., et al., *Genome sequence of the Brown Norway rat yields insights into mammalian evolution*. Nature, 2004. **428**(6982): p. 493-521.
204. Hermsen, R., et al., *Genomic landscape of rat strain and substrain variation*. BMC Genomics, 2015. **16**: p. 357.
205. Atanur, S.S., et al., *The genome sequence of the spontaneously hypertensive rat: Analysis and functional significance*. Genome Res, 2010. **20**(6): p. 791-803.

206. Atanur, S.S., et al., *Genome sequencing reveals loci under artificial selection that underlie disease phenotypes in the laboratory rat*. *Cell*, 2013. **154**(3): p. 691-703.
207. Ma, M.C., et al., *Genomic structure of nucleotide diversity among Lyon rat models of metabolic syndrome*. *BMC Genomics*, 2014. **15**: p. 197.
208. Simonis, M., et al., *Genetic basis of transcriptome differences between the founder strains of the rat HXB/BXH recombinant inbred panel*. *Genome Biol*, 2012. **13**(4): p. r31.
209. Rat Genome, S., et al., *Combined sequence-based and genetic mapping analysis of complex traits in outbred rats*. *Nat Genet*, 2013. **45**(7): p. 767-75.
210. Guo, X., et al., *Whole-genome sequences of DA and F344 rats with different susceptibilities to arthritis, autoimmunity, inflammation and cancer*. *Genetics*, 2013. **194**(4): p. 1017-28.
211. Makrigiannis, A.P., et al., *Direct sequence comparison of two divergent class I MHC natural killer cell receptor haplotypes*. *Genes Immun*, 2005. **6**(2): p. 71-83.
212. Brown, M.G., et al., *A 2-Mb YAC contig and physical map of the natural killer gene complex on mouse chromosome 6*. *Genomics*, 1997. **42**(1): p. 16-25.
213. McQueen, K.L., et al., *Localization of five new Ly49 genes, including three closely related to Ly49c*. *Immunogenetics*, 1998. **48**(3): p. 174-83.
214. Depatie, C., et al., *Sequence-ready BAC contig, physical, and transcriptional map of a 2-Mb region overlapping the mouse chromosome 6 host-resistance locus Cmv1*. *Genomics*, 2000. **66**(2): p. 161-74.
215. Anderson, S.K., et al., *Complete elucidation of a minimal class I MHC natural killer cell receptor haplotype*. *Genes Immun*, 2005. **6**(6): p. 481-92.
216. Belanger, S., et al., *Ly49 cluster sequence analysis in a mouse model of diabetes: an expanded repertoire of activating receptors in the NOD genome*. *Genes Immun*, 2008. **9**(6): p. 509-21.
217. Bonazzi, M., M. Lecuit, and P. Cossart, *Listeria monocytogenes internalin and E-cadherin: from structure to pathogenesis*. *Cell Microbiol*, 2009. **11**(5): p. 693-702.
218. Lecuit, M., et al., *A single amino acid in E-cadherin responsible for host specificity towards the human pathogen Listeria monocytogenes*. *EMBO J*, 1999. **18**(14): p. 3956-63.
219. Lee, S.H., et al., *Susceptibility to mouse cytomegalovirus is associated with deletion of an activating natural killer cell receptor of the C-type lectin superfamily*. *Nat Genet*, 2001. **28**(1): p. 42-5.
220. Brown, M.G., et al., *Vital involvement of a natural killer cell activation receptor in resistance to viral infection*. *Science*, 2001. **292**(5518): p. 934-7.
221. Daniels, K.A., et al., *Murine cytomegalovirus is regulated by a discrete subset of natural killer cells reactive with monoclonal antibody to Ly49H*. *J Exp Med*, 2001. **194**(1): p. 29-44.
222. Adams, E.J., et al., *Structural elucidation of the m157 mouse cytomegalovirus ligand for Ly49 natural killer cell receptors*. *Proc Natl Acad Sci U S A*, 2007. **104**(24): p. 10128-33.
223. Arase, H., et al., *Direct recognition of cytomegalovirus by activating and inhibitory NK cell receptors*. *Science*, 2002. **296**(5571): p. 1323-6.

224. Smith, H.R., et al., *Recognition of a virus-encoded ligand by a natural killer cell activation receptor*. Proc Natl Acad Sci U S A, 2002. **99**(13): p. 8826-31.
225. Raulat, D.H., R.E. Vance, and C.W. McMahon, *Regulation of the natural killer cell receptor repertoire*. Annu Rev Immunol, 2001. **19**: p. 291-330.
226. Nash, W.T., et al., *Know Thyself: NK-Cell Inhibitory Receptors Prompt Self-Tolerance, Education, and Viral Control*. Front Immunol, 2014. **5**: p. 175.
227. Karre, K., et al., *Selective rejection of H-2-deficient lymphoma variants suggests alternative immune defence strategy*. Nature, 1986. **319**(6055): p. 675-8.
228. Ljunggren, H.G. and K. Karre, *In search of the 'missing self': MHC molecules and NK cell recognition*. Immunol Today, 1990. **11**(7): p. 237-44.
229. Karlhofer, F.M., R.K. Ribaldo, and W.M. Yokoyama, *MHC class I alloantigen specificity of Ly-49+ IL-2-activated natural killer cells*. Nature, 1992. **358**(6381): p. 66-70.
230. Sun, J.C., *Re-educating natural killer cells*. J Exp Med, 2010. **207**(10): p. 2049-52.
231. Raulat, D.H. and R.E. Vance, *Self-tolerance of natural killer cells*. Nat Rev Immunol, 2006. **6**(7): p. 520-31.
232. Kim, S., et al., *Licensing of natural killer cells by host major histocompatibility complex class I molecules*. Nature, 2005. **436**(7051): p. 709-13.
233. Yokoyama, W.M. and S. Kim, *Licensing of natural killer cells by self-major histocompatibility complex class I*. Immunol Rev, 2006. **214**: p. 143-54.
234. Brodin, P., K. Karre, and P. Hoglund, *NK cell education: not an on-off switch but a tunable rheostat*. Trends Immunol, 2009. **30**(4): p. 143-9.
235. Brodin, P., et al., *The strength of inhibitory input during education quantitatively tunes the functional responsiveness of individual natural killer cells*. Blood, 2009. **113**(11): p. 2434-41.
236. Joncker, N.T., et al., *NK cell responsiveness is tuned commensurate with the number of inhibitory receptors for self-MHC class I: the rheostat model*. J Immunol, 2009. **182**(8): p. 4572-80.
237. Chalifour, A., et al., *A Role for cis Interaction between the Inhibitory Ly49A receptor and MHC class I for natural killer cell education*. Immunity, 2009. **30**(3): p. 337-47.
238. Bessoles, S., et al., *Education of murine NK cells requires both cis and trans recognition of MHC class I molecules*. J Immunol, 2013. **191**(10): p. 5044-51.
239. Ebihara, T., A.H. Jonsson, and W.M. Yokoyama, *Natural killer cell licensing in mice with inducible expression of MHC class I*. Proc Natl Acad Sci U S A, 2013. **110**(45): p. E4232-7.
240. Elliott, J.M., J.A. Wahle, and W.M. Yokoyama, *MHC class I-deficient natural killer cells acquire a licensed phenotype after transfer into an MHC class I-sufficient environment*. J Exp Med, 2010. **207**(10): p. 2073-9.
241. Schenkel, A.R., L.C. Kingry, and R.A. Slayden, *The ly49 gene family. A brief guide to the nomenclature, genetics, and role in intracellular infection*. Front Immunol, 2013. **4**: p. 90.
242. Berry, R., J. Rossjohn, and A.G. Brooks, *The Ly49 natural killer cell receptors: a versatile tool for viral self-discrimination*. Immunol Cell Biol, 2014. **92**(3): p. 214-20.

243. Silver, E.T., et al., *Allelic variation in the ectodomain of the inhibitory Ly-49G2 receptor alters its specificity for allogeneic and xenogeneic ligands*. J Immunol, 2002. **169**(9): p. 4752-60.
244. Naper, C., et al., *Two structurally related rat Ly49 receptors with opposing functions (Ly49 stimulatory receptor 5 and Ly49 inhibitory receptor 5) recognize nonclassical MHC class Ib-encoded target ligands*. J Immunol, 2005. **174**(5): p. 2702-11.
245. van Hall, T. and S.H. van der Burg, *Mechanisms of peptide vaccination in mouse models: tolerance, immunity, and hyperreactivity*. Adv Immunol, 2012. **114**: p. 51-76.
246. Marques, A. and S. Muller, *Mouse models of autoimmune diseases*. Curr Drug Discov Technol, 2009. **6**(4): p. 262-9.
247. Cheon, D.J. and S. Orsulic, *Mouse models of cancer*. Annu Rev Pathol, 2011. **6**: p. 95-119.
248. Hall, A.M. and E.D. Roberson, *Mouse models of Alzheimer's disease*. Brain Res Bull, 2012. **88**(1): p. 3-12.
249. Wong, V.W., et al., *Surgical approaches to create murine models of human wound healing*. J Biomed Biotechnol, 2011. **2011**: p. 969618.
250. Dahlman, I., et al., *Quantitative trait loci disposing for both experimental arthritis and encephalomyelitis in the DA rat; impact on severity of myelin oligodendrocyte glycoprotein-induced experimental autoimmune encephalomyelitis and antibody isotype pattern*. Eur J Immunol, 1998. **28**(7): p. 2188-96.
251. Nordquist, N., et al., *Complex genetic control in a rat model for rheumatoid arthritis*. J Autoimmun, 2000. **15**(4): p. 425-32.
252. Lorentzen, J.C., et al., *Identification of rat susceptibility loci for adjuvant-oil-induced arthritis*. Proc Natl Acad Sci U S A, 1998. **95**(11): p. 6383-7.
253. Rao Sirasanagandla, S., et al., *Beneficial Effect of Cissus quadrangularis Linn. on Osteopenia Associated with Streptozotocin-Induced Type 1 Diabetes Mellitus in Male Wistar Rats*. Adv Pharmacol Sci, 2014. **2014**: p. 483051.
254. Wallis, R.H., et al., *Type 1 diabetes in the BB rat: a polygenic disease*. Diabetes, 2009. **58**(4): p. 1007-17.
255. Cui, S.L., J. Yu, and L. Shoujun, *Iodine Intake Increases IP-10 Expression in the Serum and Thyroids of Rats with Experimental Autoimmune Thyroiditis*. Int J Endocrinol, 2014. **2014**: p. 581069.
256. Sedgwick, J., S. Brostoff, and D. Mason, *Experimental allergic encephalomyelitis in the absence of a classical delayed-type hypersensitivity reaction. Severe paralytic disease correlates with the presence of interleukin 2 receptor-positive cells infiltrating the central nervous system*. J Exp Med, 1987. **165**(4): p. 1058-75.
257. Brostoff, S.W. and D.W. Mason, *Experimental allergic encephalomyelitis: successful treatment in vivo with a monoclonal antibody that recognizes T helper cells*. J Immunol, 1984. **133**(4): p. 1938-42.
258. Schulz, A., et al., *Genetic dissection of increased urinary albumin excretion in the munich wistar fromter rat*. J Am Soc Nephrol, 2002. **13**(11): p. 2706-14.
259. Etgen, G.J. and B.A. Oldham, *Profiling of Zucker diabetic fatty rats in their progression to the overt diabetic state*. Metabolism, 2000. **49**(5): p. 684-8.

260. Davies, R., et al., *Tamoxifen causes gene mutations in the livers of lambda/lacI transgenic rats*. *Cancer Res*, 1997. **57**(7): p. 1288-93.
261. Festing, M.F., *Fat rats and carcinogenesis screening*. *Nature*, 1997. **388**(6640): p. 321-2.
262. Szpirer, C., *Cancer research in rat models*. *Methods Mol Biol*, 2010. **597**: p. 445-58.
263. Ward, J.M. and C.W. Reynolds, *Large granular lymphocyte leukemia. A heterogeneous lymphocytic leukemia in F344 rats*. *Am J Pathol*, 1983. **111**(1): p. 1-10.
264. Nakamura, M.C., et al., *Mouse Ly-49A interrupts early signaling events in natural killer cell cytotoxicity and functionally associates with the SHP-1 tyrosine phosphatase*. *J Exp Med*, 1997. **185**(4): p. 673-84.
265. Houchins, J.P., et al., *Natural killer cell cytolytic activity is inhibited by NKG2-A and activated by NKG2-C*. *J Immunol*, 1997. **158**(8): p. 3603-9.
266. Ma, B.J. and K.P. Kane, *Recognition of class I MHC by a rat Ly49 NK cell receptor is dependent on the identity of the P2 anchor amino acid of bound peptide*. *J Immunol*, 2011. **187**(6): p. 3267-76.
267. Lavender, K.J. and K.P. Kane, *Cross-species dependence of Ly49 recognition on the supertype defining B-pocket of a class I MHC molecule*. *J Immunol*, 2006. **177**(12): p. 8578-86.
268. Tran, J. and S.K. Kung, *Lentiviral vectors mediate stable and efficient gene delivery into primary murine natural killer cells*. *Mol Ther*, 2007. **15**(7): p. 1331-9.
269. Savan, R., T. Chan, and H.A. Young, *Lentiviral gene transduction in human and mouse NK cell lines*. *Methods Mol Biol*, 2010. **612**: p. 209-21.
270. Grund, E.M. and R.C. Muise-Helmericks, *Cost efficient and effective gene transfer into the human natural killer cell line, NK92*. *J Immunol Methods*, 2005. **296**(1-2): p. 31-6.
271. Sutlu, T., et al., *Inhibition of intracellular antiviral defense mechanisms augments lentiviral transduction of human natural killer cells: implications for gene therapy*. *Hum Gene Ther*, 2012. **23**(10): p. 1090-100.
272. Ryan, J.C., E.C. Niemi, and M.C. Nakamura, *Functional analysis of natural killer cell receptors in the RNK-16 rat leukemic cell line*. *Methods Mol Biol*, 2000. **121**: p. 283-95.
273. Lavender, K.J. and K.P. Kane, *Determining ligand specificity of Ly49 receptors*. *Methods Mol Biol*, 2010. **612**: p. 299-311.
274. Rolstad, B., *The early days of NK cells: an example of how a phenomenon led to detection of a novel immune receptor system - lessons from a rat model*. *Front Immunol*, 2014. **5**: p. 283.
275. Jensen, F.C., et al., *Infection of Human and Simian Tissue Cultures with Rous Sarcoma Virus*. *Proc Natl Acad Sci U S A*, 1964. **52**: p. 53-9.
276. Gluzman, Y., *SV40-transformed simian cells support the replication of early SV40 mutants*. *Cell*, 1981. **23**(1): p. 175-82.
277. Lin, Y.C., et al., *Genome dynamics of the human embryonic kidney 293 lineage in response to cell biology manipulations*. *Nat Commun*, 2014. **5**: p. 4767.

278. Dull, T., et al., *A third-generation lentivirus vector with a conditional packaging system*. J Virol, 1998. **72**(11): p. 8463-71.
279. Naldini, L., et al., *Efficient transfer, integration, and sustained long-term expression of the transgene in adult rat brains injected with a lentiviral vector*. Proc Natl Acad Sci U S A, 1996. **93**(21): p. 11382-8.
280. Rasheed, S., et al., *Characterization of a newly derived human sarcoma cell line (HT-1080)*. Cancer, 1974. **33**(4): p. 1027-33.
281. Naper, C., et al., *Ly49i2 is an inhibitory rat natural killer cell receptor for an MHC class Ia molecule (RT1-A1c)*. Eur J Immunol, 2002. **32**(7): p. 2031-6.
282. Naper, C., et al., *Identification of an inhibitory MHC receptor on alloreactive rat natural killer cells*. J Immunol, 1998. **160**(1): p. 219-24.
283. Sastry, L., et al., *Titering lentiviral vectors: comparison of DNA, RNA and marker expression methods*. Gene Ther, 2002. **9**(17): p. 1155-62.
284. Ryan, J.C., et al., *NKR-P1, an activating molecule on rat natural killer cells, stimulates phosphoinositide turnover and a rise in intracellular calcium*. J Immunol, 1991. **147**(9): p. 3244-50.
285. Hesslein, D.G., et al., *Differential requirements for CD45 in NK-cell function reveal distinct roles for Syk-family kinases*. Blood, 2011. **117**(11): p. 3087-95.
286. Osman, M.S., D.N. Burshtyn, and K.P. Kane, *Activating Ly-49 receptors regulate LFA-1-mediated adhesion by NK cells*. J Immunol, 2007. **178**(3): p. 1261-7.
287. Osman, M.S., et al., *Epitope mapping of Ly-49G and G-like receptors: CK-1 antibody defines a polymorphic site of functional interaction with class I ligand*. J Leukoc Biol, 2005. **77**(5): p. 644-51.
288. Lavender, K.J., et al., *The rat RT1-A1c MHC molecule is a xenogeneic ligand recognized by the mouse activating Ly-49W and inhibitory Ly-49G receptors*. J Immunol, 2004. **172**(6): p. 3518-26.
289. Silver, E.T., et al., *Ly-49W, an activating receptor of nonobese diabetic mice with close homology to the inhibitory receptor Ly-49G, recognizes H-2D(k) and H-2D(d)*. J Immunol, 2001. **166**(4): p. 2333-41.
290. Daws, M.R., et al., *Identification of an MHC class I ligand for the single member of a killer cell lectin-like receptor family, KLRH1*. J Immunol, 2012. **189**(11): p. 5178-84.
291. Kveberg, L., et al., *Expression of regulator of G protein signalling proteins in natural killer cells, and their modulation by Ly49A and Ly49D*. Immunology, 2005. **115**(3): p. 358-65.
292. Tam, Y.K., et al., *Characterization of genetically altered, interleukin 2-independent natural killer cell lines suitable for adoptive cellular immunotherapy*. Hum Gene Ther, 1999. **10**(8): p. 1359-73.
293. Zhang, J., et al., *Characterization of stem cell factor gene-modified human natural killer cell line, NK-92 cells: implication in NK cell-based adoptive cellular immunotherapy*. Oncol Rep, 2004. **11**(5): p. 1097-106.
294. Zhang, J., et al., *Characterization of interleukin-15 gene-modified human natural killer cells: implications for adoptive cellular immunotherapy*. Haematologica, 2004. **89**(3): p. 338-47.
295. Trompeter, H.I., et al., *Rapid and highly efficient gene transfer into natural killer cells by nucleofection*. J Immunol Methods, 2003. **274**(1-2): p. 245-56.

296. Schoenberg, K., H.I. Trompeter, and M. Uhrberg, *Delivery of DNA into natural killer cells for immunotherapy*. *Methods Mol Biol*, 2008. **423**: p. 165-72.
297. Maasho, K., et al., *Efficient gene transfer into the human natural killer cell line, NKL, using the Amaxa nucleofection system*. *J Immunol Methods*, 2004. **284**(1-2): p. 133-40.
298. Goding, S., et al., *Targeting of products of genes to tumor sites using adoptively transferred A-NK and T-LAK cells*. *Cancer Gene Ther*, 2007. **14**(5): p. 441-50.
299. Goding, S.R., et al., *Cytokine gene therapy using adenovirally transduced, tumor-seeking activated natural killer cells*. *Hum Gene Ther*, 2007. **18**(8): p. 701-11.
300. Schroers, R., et al., *Gene transfer into human T lymphocytes and natural killer cells by Ad5/F35 chimeric adenoviral vectors*. *Exp Hematol*, 2004. **32**(6): p. 536-46.
301. Cardone, J., G. Le Friec, and C. Kemper, *CD46 in innate and adaptive immunity: an update*. *Clin Exp Immunol*, 2011. **164**(3): p. 301-11.
302. Burshtyn, D.N., et al., *Conserved residues amino-terminal of cytoplasmic tyrosines contribute to the SHP-1-mediated inhibitory function of killer cell Ig-like receptors*. *J Immunol*, 1999. **162**(2): p. 897-902.
303. Jiang, K., et al., *Syk regulation of phosphoinositide 3-kinase-dependent NK cell function*. *J Immunol*, 2002. **168**(7): p. 3155-64.
304. Uherek, C., et al., *Retargeting of natural killer-cell cytolytic activity to ErbB2-expressing cancer cells results in efficient and selective tumor cell destruction*. *Blood*, 2002. **100**(4): p. 1265-73.
305. Guven, H., et al., *Efficient gene transfer into primary human natural killer cells by retroviral transduction*. *Exp Hematol*, 2005. **33**(11): p. 1320-8.
306. Bukrinsky, M.I., et al., *A nuclear localization signal within HIV-1 matrix protein that governs infection of non-dividing cells*. *Nature*, 1993. **365**(6447): p. 666-9.
307. Freed, E.O. and M.A. Martin, *HIV-1 infection of non-dividing cells*. *Nature*, 1994. **369**(6476): p. 107-8.
308. Hartley, J.L., G.F. Temple, and M.A. Brasch, *DNA cloning using in vitro site-specific recombination*. *Genome Res*, 2000. **10**(11): p. 1788-95.
309. Katzen, F., *Gateway((R)) recombinational cloning: a biological operating system*. *Expert Opin Drug Discov*, 2007. **2**(4): p. 571-89.
310. Landy, A., *Dynamic, structural, and regulatory aspects of lambda site-specific recombination*. *Annu Rev Biochem*, 1989. **58**: p. 913-49.
311. Wu, W.Y., et al., *Self-cleaving purification tags re-engineered for rapid Topo(R) cloning*. *Biotechnol Prog*, 2010. **26**(5): p. 1205-12.
312. Esposito, D., L.A. Garvey, and C.S. Chakiath, *Gateway cloning for protein expression*. *Methods Mol Biol*, 2009. **498**: p. 31-54.
313. Lederberg, E.M. and J. Lederberg, *Genetic Studies of Lysogenicity in Escherichia Coli*. *Genetics*, 1953. **38**(1): p. 51-64.
314. Craig, N.L. and H.A. Nash, *The mechanism of phage lambda site-specific recombination: site-specific breakage of DNA by Int topoisomerase*. *Cell*, 1983. **35**(3 Pt 2): p. 795-803.
315. Lewis, J.A. and G.F. Hatfull, *Control of directionality in integrase-mediated recombination: examination of recombination directionality factors (RDFs) including Xis and Cox proteins*. *Nucleic Acids Res*, 2001. **29**(11): p. 2205-16.

316. Moitoso de Vargas, L., S. Kim, and A. Landy, *DNA looping generated by DNA bending protein IHF and the two domains of lambda integrase*. *Science*, 1989. **244**(4911): p. 1457-61.
317. Bernard, P. and M. Couturier, *Cell killing by the F plasmid CcdB protein involves poisoning of DNA-topoisomerase II complexes*. *J Mol Biol*, 1992. **226**(3): p. 735-45.
318. Papadakis, E.D., et al., *Promoters and control elements: designing expression cassettes for gene therapy*. *Curr Gene Ther*, 2004. **4**(1): p. 89-113.
319. Southern, J.A., et al., *Identification of an epitope on the P and V proteins of simian virus 5 that distinguishes between two isolates with different biological characteristics*. *J Gen Virol*, 1991. **72 ( Pt 7)**: p. 1551-7.
320. Follenzi, A. and L. Naldini, *Generation of HIV-1 derived lentiviral vectors*. *Methods Enzymol*, 2002. **346**: p. 454-65.
321. Durand, S. and A. Cimarelli, *The inside out of lentiviral vectors*. *Viruses*, 2011. **3**(2): p. 132-59.
322. Emi, N., T. Friedmann, and J.K. Yee, *Pseudotype formation of murine leukemia virus with the G protein of vesicular stomatitis virus*. *J Virol*, 1991. **65**(3): p. 1202-7.
323. Burns, J.C., et al., *Vesicular stomatitis virus G glycoprotein pseudotyped retroviral vectors: concentration to very high titer and efficient gene transfer into mammalian and nonmammalian cells*. *Proc Natl Acad Sci U S A*, 1993. **90**(17): p. 8033-7.
324. Davis, H.E., et al., *Charged polymers modulate retrovirus transduction via membrane charge neutralization and virus aggregation*. *Biophys J*, 2004. **86**(2): p. 1234-42.
325. Salmon, P., et al., *High-level transgene expression in human hematopoietic progenitors and differentiated blood lineages after transduction with improved lentiviral vectors*. *Blood*, 2000. **96**(10): p. 3392-8.
326. Uchida, N., et al., *HIV, but not murine leukemia virus, vectors mediate high efficiency gene transfer into freshly isolated G0/G1 human hematopoietic stem cells*. *Proc Natl Acad Sci U S A*, 1998. **95**(20): p. 11939-44.
327. Cire, S., et al., *Immunization of mice with lentiviral vectors targeted to MHC class II+ cells is due to preferential transduction of dendritic cells in vivo*. *PLoS One*, 2014. **9**(7): p. e101644.
328. VandenDriessche, T., et al., *Lentiviral vectors containing the human immunodeficiency virus type-1 central polypurine tract can efficiently transduce nondividing hepatocytes and antigen-presenting cells in vivo*. *Blood*, 2002. **100**(3): p. 813-22.
329. Sutton, R.E., et al., *Human immunodeficiency virus type 1 vectors efficiently transduce human hematopoietic stem cells*. *J Virol*, 1998. **72**(7): p. 5781-8.
330. Blomer, U., et al., *Highly efficient and sustained gene transfer in adult neurons with a lentivirus vector*. *J Virol*, 1997. **71**(9): p. 6641-9.
331. Kafri, T., et al., *Sustained expression of genes delivered directly into liver and muscle by lentiviral vectors*. *Nat Genet*, 1997. **17**(3): p. 314-7.
332. Farazmandfar, T., et al., *Use of integrase-minus lentiviral vector for transient expression*. *Cell J*, 2012. **14**(2): p. 76-81.

333. Uetsuki, T., et al., *Isolation and characterization of the human chromosomal gene for polypeptide chain elongation factor-1 alpha*. J Biol Chem, 1989. **264**(10): p. 5791-8.
334. Thiele, D., et al., *Elongation factor 1 alpha from Saccharomyces cerevisiae. Rapid large-scale purification and molecular characterization*. J Biol Chem, 1985. **260**(5): p. 3084-9.
335. Kim, D.W., et al., *Use of the human elongation factor 1 alpha promoter as a versatile and efficient expression system*. Gene, 1990. **91**(2): p. 217-23.
336. Miyajima, A. and Y. Kaziro, *Coordination of levels of elongation factors Tu, Ts, and G, and ribosomal protein S1 in Escherichia coli*. J Biochem, 1978. **83**(2): p. 453-62.
337. Mizushima, S. and S. Nagata, *pEF-BOS, a powerful mammalian expression vector*. Nucleic Acids Res, 1990. **18**(17): p. 5322.
338. Gopalkrishnan, R.V., et al., *Use of the human EF-1alpha promoter for expression can significantly increase success in establishing stable cell lines with consistent expression: a study using the tetracycline-inducible system in human cancer cells*. Nucleic Acids Res, 1999. **27**(24): p. 4775-82.
339. Wang, N., et al., *Comparison of transduction efficiency among various lentiviruses containing GFP reporter in bone marrow hematopoietic stem cell transplantation*. Exp Hematol, 2013. **41**(11): p. 934-43.
340. Wang, R., et al., *Promoter-dependent EGFP expression during embryonic stem cell propagation and differentiation*. Stem Cells Dev, 2008. **17**(2): p. 279-89.
341. Teschendorf, C., et al., *Comparison of the EF-1 alpha and the CMV promoter for engineering stable tumor cell lines using recombinant adeno-associated virus*. Anticancer Res, 2002. **22**(6A): p. 3325-30.
342. Chan, K.K., et al., *Generation of high-level stable transgene expressing human embryonic stem cell lines using Chinese hamster elongation factor-1 alpha promoter system*. Stem Cells Dev, 2008. **17**(4): p. 825-36.
343. Neumann, E., et al., *Gene transfer into mouse lymphoma cells by electroporation in high electric fields*. EMBO J, 1982. **1**(7): p. 841-5.
344. Wong, T.K. and E. Neumann, *Electric field mediated gene transfer*. Biochem Biophys Res Commun, 1982. **107**(2): p. 584-7.
345. Escors, D. and K. Breckpot, *Lentiviral vectors in gene therapy: their current status and future potential*. Arch Immunol Ther Exp (Warsz), 2010. **58**(2): p. 107-19.
346. Matrai, J., M.K. Chuah, and T. VandenDriessche, *Recent advances in lentiviral vector development and applications*. Mol Ther, 2010. **18**(3): p. 477-90.
347. Ramezani, A. and R.G. Hawley, *Overview of the HIV-1 Lentiviral Vector System*. Curr Protoc Mol Biol, 2002. **Chapter 16**: p. Unit 16 21.
348. Mehta, A.K., et al., *Epigenetic regulation of cytomegalovirus major immediate-early promoter activity in transgenic mice*. Gene, 2009. **428**(1-2): p. 20-4.
349. Choi, K.H., et al., *Activation of CMV promoter-controlled glycosyltransferase and beta -galactosidase genes by butyrate, tricostatin A, and 5-aza-2'-deoxycytidine*. Glycoconj J, 2005. **22**(1-2): p. 63-9.

350. Prosch, S., et al., *Inactivation of the very strong HCMV immediate early promoter by DNA CpG methylation in vitro*. Biol Chem Hoppe Seyler, 1996. **377**(3): p. 195-201.
351. Niller, H.H. and L. Hennighausen, *Formation of several specific nucleoprotein complexes on the human cytomegalovirus immediate early enhancer*. Nucleic Acids Res, 1991. **19**(13): p. 3715-21.
352. Curradi, M., et al., *Molecular mechanisms of gene silencing mediated by DNA methylation*. Mol Cell Biol, 2002. **22**(9): p. 3157-73.
353. Duan, B., et al., *Silencing of fat-1 transgene expression in sheep may result from hypermethylation of its driven cytomegalovirus (CMV) promoter*. Theriogenology, 2012. **78**(4): p. 793-802.
354. Skalamera, D., et al., *Generation of a genome scale lentiviral vector library for EF1alpha promoter-driven expression of human ORFs and identification of human genes affecting viral titer*. PLoS One, 2012. **7**(12): p. e51733.
355. Kia, A., et al., *Inhibition of histone deacetylation and DNA methylation improves gene expression mediated by the adeno-associated virus/phage in cancer cells*. Viruses, 2013. **5**(10): p. 2561-72.
356. Grassi, G., et al., *Inhibitors of DNA methylation and histone deacetylation activate cytomegalovirus promoter-controlled reporter gene expression in human glioblastoma cell line U87*. Carcinogenesis, 2003. **24**(10): p. 1625-35.
357. Goldman, L.A., et al., *Modifications of vectors pEF-BOS, pcDNA1 and pcDNA3 result in improved convenience and expression*. Biotechniques, 1996. **21**(6): p. 1013-5.
358. Sinici, I., et al., *Comparison of HCMV IE and EF-1 promoters for the stable expression of beta-subunit of hexosaminidase in CHO cell lines*. Biochem Genet, 2006. **44**(3-4): p. 173-80.
359. Chung, S., et al., *Analysis of different promoter systems for efficient transgene expression in mouse embryonic stem cell lines*. Stem Cells, 2002. **20**(2): p. 139-45.
360. Hanke, T., et al., *Direct assessment of MHC class I binding by seven Ly49 inhibitory NK cell receptors*. Immunity, 1999. **11**(1): p. 67-77.
361. Dimasi, N., et al., *Crystal structure of the Ly49I natural killer cell receptor reveals variability in dimerization mode within the Ly49 family*. J Mol Biol, 2002. **320**(3): p. 573-85.
362. Pattnaik, P., *Surface plasmon resonance: applications in understanding receptor-ligand interaction*. Appl Biochem Biotechnol, 2005. **126**(2): p. 79-92.
363. Stevens, J., et al., *Efficient generation of major histocompatibility complex class I-peptide complexes using synthetic peptide libraries*. J Biol Chem, 1998. **273**(5): p. 2874-84.
364. Stevens, J., et al., *Peptide specificity of RT1-A1(c), an inhibitory rat major histocompatibility complex class I natural killer cell ligand*. J Biol Chem, 2000. **275**(38): p. 29217-24.
365. Pyzik, M., et al., *Distinct MHC class I-dependent NK cell-activating receptors control cytomegalovirus infection in different mouse strains*. J Exp Med, 2011. **208**(5): p. 1105-17.

366. Toyama-Sorimachi, N., et al., *Ly49Q, a member of the Ly49 family that is selectively expressed on myeloid lineage cells and involved in regulation of cytoskeletal architecture*. Proc Natl Acad Sci U S A, 2004. **101**(4): p. 1016-21.
367. Toyama-Sorimachi, N., et al., *Inhibitory NK receptor Ly49Q is expressed on subsets of dendritic cells in a cellular maturation- and cytokine stimulation-dependent manner*. J Immunol, 2005. **174**(8): p. 4621-9.
368. Fee, C.J., *Label-free, real-time interaction and adsorption analysis 1: surface plasmon resonance*. Methods Mol Biol, 2013. **996**: p. 287-312.
369. Jason-Moller, L., M. Murphy, and J. Bruno, *Overview of Biacore systems and their applications*. Curr Protoc Protein Sci, 2006. **Chapter 19**: p. Unit 19 13.
370. Wang, J., et al., *Binding of the natural killer cell inhibitory receptor Ly49A to its major histocompatibility complex class I ligand. Crucial contacts include both H-2Dd AND beta 2-microglobulin*. J Biol Chem, 2002. **277**(2): p. 1433-42.
371. Ma, B.J., C.M. Craveiro Salvado, and K.P. Kane, *The activating Ly49W and inhibitory Ly49G NK cell receptors display similar affinities for identical MHC class I ligands*. Immunogenetics, 2014. **66**(7-8): p. 467-77.
372. Nei, M., P. Xu, and G. Glazko, *Estimation of divergence times from multiprotein sequences for a few mammalian species and several distantly related organisms*. Proc Natl Acad Sci U S A, 2001. **98**(5): p. 2497-502.
373. Stewart, C.A., et al., *Recognition of peptide-MHC class I complexes by activating killer immunoglobulin-like receptors*. Proc Natl Acad Sci U S A, 2005. **102**(37): p. 13224-9.
374. Frazier, W.R., et al., *Allelic variation in KIR2DL3 generates a KIR2DL2-like receptor with increased binding to its HLA-C ligand*. J Immunol, 2013. **190**(12): p. 6198-208.
375. Li, H., et al., *Kinetics of interaction of HLA-B2705 with natural killer cell immunoglobulin-like receptor 3DS1*. Protein Pept Lett, 2010. **17**(5): p. 547-54.
376. Vales-Gomez, M., et al., *Kinetics and peptide dependency of the binding of the inhibitory NK receptor CD94/NKG2-A and the activating receptor CD94/NKG2-C to HLA-E*. EMBO J, 1999. **18**(15): p. 4250-60.
377. Kaiser, B.K., et al., *Interactions between NKG2x immunoreceptors and HLA-E ligands display overlapping affinities and thermodynamics*. J Immunol, 2005. **174**(5): p. 2878-84.
378. Wang, L.L. and W.M. Yokoyama, *Regulation of mouse NK cells by structurally divergent inhibitory receptors*. Curr Top Microbiol Immunol, 1998. **230**: p. 3-13.
379. Brennan, J., et al., *Recognition of class I major histocompatibility complex molecules by Ly-49: specificities and domain interactions*. J Exp Med, 1996. **183**(4): p. 1553-9.
380. Tassi, I., et al., *DAPI10 associates with Ly49 receptors but contributes minimally to their expression and function in vivo*. Eur J Immunol, 2009. **39**(4): p. 1129-35.
381. Mason, L.H., et al., *Cloning and functional characteristics of murine large granular lymphocyte-1: a member of the Ly-49 gene family (Ly-49G2)*. J Exp Med, 1995. **182**(2): p. 293-303.
382. Berry, R., et al., *Targeting of a natural killer cell receptor family by a viral immunoevasin*. Nat Immunol, 2013. **14**(7): p. 699-705.

383. Furukawa, H., et al., *A ligand for the murine NK activation receptor Ly-49D: activation of tolerized NK cells from beta 2-microglobulin-deficient mice.* J Immunol, 2002. **169**(1): p. 126-36.
384. Nakamura, M.C., et al., *Natural killing of xenogeneic cells mediated by the mouse Ly-49D receptor.* J Immunol, 1999. **163**(9): p. 4694-700.
385. Maratou, K., et al., *Characterization of the macrophage transcriptome in glomerulonephritis-susceptible and -resistant rat strains.* Genes Immun, 2011. **12**(2): p. 78-89.
386. Thessen Hedreul, M., et al., *Combining genetic mapping with genome-wide expression in experimental autoimmune encephalomyelitis highlights a gene network enriched for T cell functions and candidate genes regulating autoimmunity.* Hum Mol Genet, 2013. **22**(24): p. 4952-66.
387. Dam, J., et al., *Variable dimerization of the Ly49A natural killer cell receptor results in differential engagement of its MHC class I ligand.* J Mol Biol, 2006. **362**(1): p. 102-13.
388. Trieu, E.P. and I.N. Targoff, *Immunoprecipitation: Western blot for proteins of low abundance.* Methods Mol Biol, 2015. **1312**: p. 327-42.
389. Haskins, K., et al., *The major histocompatibility complex-restricted antigen receptor on T cells. I. Isolation with a monoclonal antibody.* J Exp Med, 1983. **157**(4): p. 1149-69.
390. Allison, J.P., B.W. McIntyre, and D. Bloch, *Tumor-specific antigen of murine T-lymphoma defined with monoclonal antibody.* J Immunol, 1982. **129**(5): p. 2293-300.
391. Held, W. and R.A. Mariuzza, *Cis interactions of immunoreceptors with MHC and non-MHC ligands.* Nat Rev Immunol, 2008. **8**(4): p. 269-78.
392. Sawicki, M.W., et al., *Structural basis of MHC class I recognition by natural killer cell receptors.* Immunol Rev, 2001. **181**: p. 52-65.
393. Sullivan, L.C., et al., *The heterodimeric assembly of the CD94-NKG2 receptor family and implications for human leukocyte antigen-E recognition.* Immunity, 2007. **27**(6): p. 900-11.